U.S.NRC
United States Nuclear Regulatory Commission
Protecting People and the Environment

NUREG/CR-7178

Uranium Sequestration During Biostimulated Reduction and In Response to the Return of Oxic Conditions In Shallow Aquifers

Office of Nuclear Regulatory Research

AVAILABILITY OF REFERENCE MATERIALS IN NRC PUBLICATIONS

NRC Reference Material

As of November 1999, you may electronically access NUREG-series publications and other NRC records at NRC's Public Electronic Reading Room at http://www.nrc.gov/reading-rm.html. Publicly released records include, to name a few, NUREG-series publications; *Federal Register* notices; applicant, licensee, and vendor documents and correspondence; NRC correspondence and internal memoranda; bulletins and information notices; inspection and investigative reports; licensee event reports; and Commission papers and their attachments.

NRC publications in the NUREG series, NRC regulations, and Title 10, "Energy," in the *Code of Federal Regulations* may also be purchased from one of these two sources.

1. The Superintendent of Documents
   U.S. Government Printing Office
   Mail Stop SSOP
   Washington, DC 20402–0001
   Internet: bookstore.gpo.gov
   Telephone: 202-512-1800
   Fax: 202-512-2250
2. The National Technical Information Service
   Springfield, VA 22161–0002
   www.ntis.gov
   1–800–553–6847 or, locally, 703–605–6000

A single copy of each NRC draft report for comment is available free, to the extent of supply, upon written request as follows:

Address: U.S. Nuclear Regulatory Commission
Office of Administration
Publications Branch
Washington, DC 20555-0001
E-mail: DISTRIBUTION.RESOURCE@NRC.GOV
Facsimile: 301–415–2289

Some publications in the NUREG series that are posted at NRC's Web site address http://www.nrc.gov/reading-rm/doc-collections/nuregs are updated periodically and may differ from the last printed version. Although references to material found on a Web site bear the date the material was accessed, the material available on the date cited may subsequently be removed from the site.

Non-NRC Reference Material

Documents available from public and special technical libraries include all open literature items, such as books, journal articles, transactions, *Federal Register* notices, Federal and State legislation, and congressional reports. Such documents as theses, dissertations, foreign reports and translations, and non-NRC conference proceedings may be purchased from their sponsoring organization.

Copies of industry codes and standards used in a substantive manner in the NRC regulatory process are maintained at—

The NRC Technical Library
Two White Flint North
11545 Rockville Pike
Rockville, MD 20852–2738

These standards are available in the library for reference use by the public. Codes and standards are usually copyrighted and may be purchased from the originating organization or, if they are American National Standards, from—

American National Standards Institute
11 West 42nd Street
New York, NY 10036–8002
www.ansi.org
212–642–4900

Legally binding regulatory requirements are stated only in laws; NRC regulations; licenses, including technical specifications; or orders, not in NUREG-series publications. The views expressed in contractor-prepared publications in this series are not necessarily those of the NRC.

The NUREG series comprises (1) technical and administrative reports and books prepared by the staff (NUREG–XXXX) or agency contractors (NUREG/CR–XXXX), (2) proceedings of conferences (NUREG/CP–XXXX), (3) reports resulting from international agreements (NUREG/IA–XXXX), (4) brochures (NUREG/BR–XXXX), and (5) compilations of legal decisions and orders of the Commission and Atomic and Safety Licensing Boards and of Directors' decisions under Section 2.206 of NRC's regulations (NUREG–0750).

U.S.NRC
United States Nuclear Regulatory Commission
Protecting People and the Environment

NUREG/CR-7178

Uranium Sequestration During Biostimulated Reduction and In Response to the Return of Oxic Conditions In Shallow Aquifers

Manuscript Completed: February 2014
Date Published: December 2014

Prepared by:
C. C. Fuller[1], K. J. Johnson[1*], K. C. Akstin[1],
D. M. Singer[2], S. B. Yabusaki[3], Y. Fang[3],
M. Fuhrmann[4]

[1] U.S. Geological Survey, Menlo Park, CA
[2] Kent State University, Kent OH
[3] Pacific Northwest National Laboratory, Richland, WA
[4] U.S. Nuclear Regulatory Commission, Rockville, MD
[*] current address: MWH Global, Inc., Steamboat Springs, CO

Mark Fuhrmann, NRC Project Manager

NRC Job Code: N6651

Office of Nuclear Regulatory Research

Abstract

A proposed approach for groundwater remediation of uranium contamination is to generate reducing conditions by stimulating the growth of microbial populations through injection of electron donor compounds into the subsurface. Sufficiently reducing conditions will result in reduction of soluble hexavalent uranium, U(VI), and precipitation of the less soluble +4 oxidation state uranium, U(IV). This process is termed biostimulated reduction. A key issue in the remediation of uranium (U) contamination in aquifers by biostimulated reduction is the long term stability of the sequestered uranium. Three flow-through column experiments using aquifer sediment were used to evaluate the remobilization of bioreduced U sequestered under conditions in which biostimulation extended well into sulfate reduction to enhance precipitation of reduced sulfur phases such as iron sulfides. One column received added ferrous iron, Fe(II), increasing production of iron sulfides, to test their effect on remobilization of the sequestered uranium, either by serving as a redox buffer by competing for dissolved oxygen, or by armoring the reduced uranium. During biostimulation of the ambient microbial population with acetate, dissolved uranium was lowered by a factor of 2.5 or more with continued removal for over 110 days of biostimulation, well after the onset of sulfate reduction at ~30 days. Sequestered uranium was essentially all U(IV) resulting from the formation of nano-particulate uraninite that coated sediment grains to a thickness of a few 10's of microns, sometimes in association with S and Fe. A multicomponent biogeochemical reactive transport model simulation of column effluents during biostimulation was generally able to describe the acetate oxidation, iron, sulfate, and uranium reduction for all three columns using parameters derived from simulations of field scale biostimulation experiments.

Columns were eluted with artificial groundwater at equilibrium with atmospheric oxygen to simulate the upper limit of dissolved oxygen in recharge water. Overall about 9% of total uranium removed from solution during biostimulation was remobilized. Release of U during oxic elution was a continuous process over 140 days with dissolved uranium concentrations about 0.2 and 0.8 μM for columns with and without ferrous iron addition, respectively. Uranium remaining on the sediment was in the reduced form. The prolonged period of biostimulation and concomitant sulfate reduction appears to limit the rate of U(IV) oxidative remobilization in contrast to a large release observed for columns in previous studies that did not undergo sulfate reduction. Although continued sulfate reduction may cause decreased permeability from precipitation of iron sulfide, the greater apparent stability of the sequestered U(IV) provided by the sustained biostimulation should be considered in design of field scale remediation efforts.

Foreword

The Nuclear Regulatory Commission has received license applications and inquiries about the acceptability of in situ bioremediation (ISB) techniques for the cleanup of uranium contaminated aquifers. This technology is based on the stimulation of indigenous bacteria that catalyze reactions leading to the immobilization of uranium in the solid phase. Reduction of soluble hexavalent uranium, U(VI), to the much less soluble +4 oxidation state, U(IV), has been demonstrated to effectively remove uranium from solution. ISB has been considered for cleanup of shallow (less than 20 m depth) contaminated aquifers as well as the restoration of deep (greater than 150 m depth) in situ recovery sites from which uranium is commercially extracted.

In this document, staff from the U.S. Geological Survey and Pacific Northwest National Laboratory report the results of experiments and modeling studies investigating the processes that impact the use of bioremediation as it is applied to a shallow site. In another report (NUREG/CR-7167), the potential for ISB of uranium in situ recovery sites was assessed using similar experimental and modeling techniques.

Contents

List of Figures

List of Tables

Executive Summary

Uranium extraction and processing has resulted in contamination of groundwater and sediments at many locations worldwide. The high mobility of U(VI) under oxidizing conditions compared to the sparingly soluble +4 oxidation state, U(IV), can lead to dispersal of uranium contamination in groundwater and aquifer sediments. Traditional remediation methods of extraction and/or pump and treat are expensive and time consuming. Because of the ability of metal reducing microbes to chemically reduce dissolved U(VI), producing lower solubility U(IV), in situ stimulation of indigenous microbial populations in aquifers by electron donor addition has led to the concept of biostimulated reduction as a remediation strategy to immobilize uranium contamination. This topic has been the focus of many field and laboratory investigations over the past 20 years. A key issue for reduction based bioremediation of U(VI) is the stability of the solid phase reaction products over time. Remobilization of U(IV) through oxidation following cessation of electron donor addition remains a critical component in understanding the long term effectiveness of biostimulated reduction.

The focus of this study is to evaluate remobilization of U after biostimulation in response to the return to oxic conditions through long term (>100 pore volumes) column experiments using sediments from the Old Rifle site, a shallow aquifer contaminated from uranium ore milling and remediated through the Uranium Mill Tailings Remedial Action (UMTRA) program. The primary goal of this study was to evaluate the remobilization of U sequestered during biostimulated reduction under conditions in which biostimulation and concomitant U reduction extended well into sulfate reduction to enhance precipitation of reduced sulfur phases such as iron sulfides. Ferrous iron was added to the influent of one column during biostimulation to enhance the formation of iron sulfide. The intent of producing these reduced phases was to test their ability to inhibit remobilization of the sequestered uranium, either serving as a redox buffer by competing for dissolved oxygen, or by armoring the reduced uranium by precipitating an iron sulfide coating on mineral grains. Chemical analysis, X-ray absorption spectroscopy, micro-focused X-ray fluorescence mapping, and electron microscopy of sediments recovered from columns after biostimulation and after oxic elution were conducted to characterize the form of U on sediments and other solid phase constituents that may affect U remobilization, notably iron and sulfur. Reactive transport modeling of column effluent chemistry during biostimulation was conducted to understand uranium behavior in the context of 1) transient biostimulation with acetate electron donor, 2) functional indigenous microbial groups representing Fe(III)-reducing bacteria (FeRB) and sulfate-reducing bacteria (SRB) responding to the biostimulation, and 3) geochemical response to the biostimulation products.

During biostimulation of the ambient microbial population with acetate, the removal of dissolved U(VI) from the influent continued over 110 to 330 days of biostimulation, well after the onset of sulfate reduction at ~30 days. The concentration of dissolved uranium was lowered from the influent 10 μM to <4 μM. By day 60 of the reduction phase of the experiments, concentrations of uranium in the effluent of a column receiving Fe (II) in the influent, column C, were less than half of the other columns without Fe addition (A and B). The uranium sequestered during biostimulation was essentially all precipitated as U(IV) resulting in part from the formation of nano-particulate uraninite. The reduced U(IV) formed contiguous coatings on sediment grains with thicknesses of a few 10s of micrometers and was in association with S and Fe in some cases. Uranium spectra by Extended X-ray Absorption Fine Structure (EXAFS) of column sediments are consistent with U(IV) comprised of a mixture of both partially disordered nanoparticulate UO_2 and non-uraninite U(IV) species associated with biomass. The non-

uraninite U(IV)-bearing phase may exist separately from the partially polymerized nano-UO_2-like U(IV).

The multicomponent biogeochemical reactive transport model simulation of column effluents during biostimulation was generally able to describe the acetate oxidation, iron, sulfate, and uranium reduction for all three columns using parameters derived from simulations of field scale biostimulation experiments. Together, the effluent and solid phase measurements from columns during and after the biostimulation stage suggest that stimulation and growth of indigenous microbial population in the aquifer sediments from the Rifle site by addition of an electron donor and carbon source may be an effective means of removing dissolved uranium from contaminated groundwater, consistent with many field and laboratory studies.

Elution of bioreduced U(IV) associated with sediments from two columns (A and C) was conducted using artificial groundwater at equilibrium with atmospheric oxygen. This oxygen level was used to assess the upper limit of dissolved oxygen in recharge water. The difference between the two columns was the addition of 15 μM dissolved Fe(II) to column C during biostimulation to enhance formation of iron sulfides. Release of U during oxic elution was a continuous process over 120 to 140 days (300 to 350 PV). Remobilization of uranium was four times higher in column A compared to column C with effluent dissolved uranium concentrations approximately 0.8 and 0.2 μM for the column A and C, respectively. The effluent U concentration from column C decreased over time indicative of a decreasing re-oxidation rate. In contrast, uranium in the effluent from column A did not display this decreasing trend but was instead somewhat constant over 140 days. This suggests that the addition of Fe (II) to the influent and the subsequent precipitation of iron sulfide minerals may decrease the release of uranium. Overall, less than 9% of total uranium sequestered during biostimulation was remobilized. The limited oxidative remobilization of U(IV) in these column experiments is consistent with the decreased U remobilization where sulfate reduction occurred in contrast to the large release of U from columns reported in the literature which did not undergo sulfate reduction. Although continued sulfate reduction may cause a decrease in permeability from precipitation of iron sulfide, the greater apparent stability of the sequestered U(IV) provided by the sustained biostimulation could be considered in design of field scale remediation efforts. However, even with the greater uranium stability caused by iron sulfide precipitation the effluent uranium concentration of approximately 0.2 μM did exceed EPA's uranium MCL of 30 μg/L (0.126 μM). Advancement of biostimulated reduction strategies for remediation of groundwater uranium contamination could include additional field scale testing of the stability of bioreduced uranium to remobilization following the end of biostimulation.

Acknowledgments

We thank the following USGS scientists for their efforts on this study: Alex Blum for XRD analysis; Shelley Hoeft for assistance in HPLC measurements and guidance in microbial protocols; Steve Silva for total and isotopic composition of sulfur in sediments; Julie Kirshtein for microbial assay and providing a detailed report on the findings; and Larry Miller for many discussions on microbial and biogeochemical processes. Sam Webb and Ben Kocar of the Stanford Synchrotron Radiation Lightsource (SSRL) are acknowledged for assistance in micro-focused X-ray imaging. John Bargar of SSRL is thanked for providing uranium reference spectra and guidance in XAS data collection. Ken Williams of the Lawrence Berkeley National Laboratory is acknowledged for providing aquifer sediments from the Old Rifle site.

Portions of this research were conducted at the Stanford Synchrotron Radiation Lightsource, a national user facility operated by Stanford University on behalf of the US Department of Energy, Office of Basic Energy Sciences. The SSRL Structural Molecular Biology Program is supported by the Department of Energy, Office of Biological and Environmental Research, and by the National Institutes of Health, National Center for Research Resources, Biomedical Technology Program.

Massively parallel processing simulations were performed on the Chinook supercomputer at the Environmental Molecular Sciences Laboratory (EMSL), a national scientific user facility sponsored by the Department of Energy's Office of Biological and Environmental Research and located at Pacific Northwest National Laboratory.

We thank D.L. Stoliker, USGS, and K. Czyscinski, US EPA, for helpful reviews that improved this report. We also thank Earl Greene (USGS) and Thomas Nicholson (NRC) for their help with this work.

1 Introduction

1.1 Purpose and Scope

Uranium extraction and processing has resulted in contamination of groundwater and sediments at many locations worldwide. The high mobility of U(VI) under oxidizing conditions compared to the sparingly soluble +4 oxidation state, U(IV), can lead to dispersal of uranium contamination in groundwater and aquifer sediments. Development of effective strategies for remediation of uranium contamination in groundwater has focused largely on using in situ treatment processes because of higher costs associated with traditional pump and treat methods. Surface complexation of U(VI) on sediment surfaces maintains dissolved uranium concentrations. This greatly increases the time for flushing U contamination from an aquifer and limits the success of pump and treat or natural attenuation strategies. Because of the ability of metal reducing microbes to reduce dissolved U(VI) (Lovley *et al.*, 1991), in situ stimulation of indigenous microbial populations in aquifers by electron donor addition has led to the concept of biostimulated reduction as a remediation strategy to immobilize uranium contamination (Lovley and Phillips, 1992). This topic has been the focus of many field and laboratory investigations over the past 20 years.

A key issue for reduction based bioremediation of U(VI) is the stability of the solid phase reaction products over time (Yabusaki *et al.*, 2010). Remobilization of U(IV) through oxidation following cessation of electron donor addition remains a critical component in understanding the long term effectiveness of biostimulated reduction. Previous laboratory studies have shown that U(IV) produced during biostimulation is more stable and less prone to oxidative remobilization when biostimulation proceeds well into sulfate reduction compared to experimental systems with limited sulfate reduction (Komlos *et al.*, 2008b; Moon *et al.*, 2009). Enhanced stability of U(IV) has been attributed to iron sulfides produced during biostimulation (Abdelouas *et al.*, 1999). Evaluating the long term stability of bioreduced uranium in field scale biostimulation experiments has not been adequately addressed, in part because of the long time scales required. Laboratory studies allow evaluating stability over many pore volumes in a much shorter time scale than can be studied practically in field-scale studies and thus may help predict long term stability in a remediated aquifer.

The focus of this study is to evaluate remobilization of U(IV) after biostimulation in response to the return to oxic conditions through long term (> 100 pore volumes) column experiments using sediments from the Old Rifle site, a shallow aquifer contaminated from uranium ore milling and remediated through the UMTRA program. The site has been described in detail elsewhere (eg Anderson et al, 2003; Yabusaki et al, 2009). In these experiments, biostimulation was allowed to proceed for several months after the onset of sulfate reduction. Ferrous iron was added to the influent of one column during biostimulation to enhance the formation of iron sulfide to test its effect on oxidative remobilization of reduced uranium. Chemical analysis, X-ray spectroscopy, micro-focused X-ray fluorescence mapping, and electron microscopy of sediments recovered from columns after biostimulation and after oxic elution were conducted to characterize the form of U on sediments and other solid phase constituents that may affect U remobilization, notably iron and sulfur.

1.2 Bioremediation Processes

The high mobility of U(VI) under oxidizing conditions compared to the sparingly soluble +4 oxidation state, U(IV), has led to the concept of producing reducing conditions to immobilize U in situ as a remediation strategy. The demonstrated ability of microbes to either reduce U(VI) either directly through enzymatic processes (Lovley *et al.*, 1991) or indirectly through reaction byproducts of iron and sulfate reduction is the basis for in situ bioreduction of U(VI) and precipitation of U(IV) through stimulation of indigenous microbial populations through electron donor amendment as a remediation strategy. Numerous studies have evaluated the effectiveness of biostimulated reduction based immobilization of aqueous U(VI) in laboratory (Komlos *et al.*, 2008b; Moon *et al.*, 2007; Sharp *et al.*, 2011) and in field tests (Anderson *et al.*, 2003; Wu *et al.*, 2006; Williams *et al.*, 2011). The biostimulation approach is based on microbial mediated reduction and precipitation that enhances U(VI) immobilization over attenuation processes occurring under ambient groundwater conditions, such as reduction by pre-existing mineral phases. Considerable effort has been focused on identifying specific microbial populations responsible for U reduction. For example, a number of studies have identified the importance of *Geobacteraceae* during biostimulation for enhancing U immobilization through growth and concurrent reduction of both Fe(III) and U(VI), for example (Lovley *et al.*, 1991; Gorby and Lovley, 1992; Lovley and Phillips, 1992). The importance of the iron reducing bacteria *Geobacter* has been demonstrated in field biostimulation tests using acetate as an electron donor (Vrionis *et al.*, 2005; Williams *et al.*, 2011). The ability of sulfate reducing bacteria (SRB) to mediate reduction of uranium has also been observed. Sulfate reducing bacteria have been shown to reduce uranium directly through enzymatic mechanisms (Lovley *et al.*, 1993), and have been shown to be important in field scale biostimulation experiments using ethanol as an electron donor (Cardenas *et al.*, 2008; Luo *et al.*, 2007a). In contrast, no direct evidence has been found for U(VI) reduction by sulfate reducing bacteria (SRB) during biostimulation with acetate as an electron donor in field scale tests (Williams *et al.*, 2011).

In addition to direct enzymatic reduction by microbes, U(VI) reduction may also occur by abiotic reaction processes. Reduction of U(VI) by dissolved sulfide is thermodynamically favored but may be limited by the presence of elevated dissolved carbonate complexation of dissolved U(VI) (Sani *et al.*, 2005). Fe(II) can serve as an electron donor for abiotic U(VI) reduction (Campbell *et al.*, 2013), but is kinetically slow under pH and dissolved carbonate levels typical of many aquifers (Liger *et al.*, 1999). U(VI) reduction by Fe(II) sorbed to sediment surfaces has been observed and increases at higher sorbed Fe(II) concentrations (Fox *et al.*, 2013). Uranium reduction has been observed to occur by reaction with solid phases produced during microbial mediated reduction processes, such as iron sulfides (Veeramani *et al.*, 2013; Hyun *et al.*, 2012; Hua and Deng, 2008) and carbonate green rust, a mixed oxidation state iron mineral (O'Loughlin *et al.*, 2010). Although abiotic uranium reduction by the iron sulfide mackinawite has been demonstrated during field biostimulation experiments (Bargar *et al.*, 2013), the quantitative impact of abiotic uranium reduction has not been demonstrated in field studies.

1.3 Forms of U(IV) Produced by Bioreduction

Reduction of U(VI) and precipitation of U(IV) commonly forms uraninite (UO_2). The uraninite formed as the result of direct or indirect microbial processes has been shown to be nanoparticluate in size (Schofield *et al.*, 2008; Singer *et al.*, 2009; O'Loughlin *et al.*, 2010). This nanoparticulate biogenic uraninite has been found to be on the order of 3 nm in diameter and tends to form aggregates (Burgos *et al.*, 2008; Schofield *et al.*, 2008). Because of the small

particle size, Schofield *et al.* (2008) estimated that about 50% of the U is near the surface resulting in a lattice contraction compared to larger abiotic particles of bulk UO_2. Although the surface is distorted, the particle core remained highly ordered consistent with stoichiometric UO_2 (Burgos *et al.*, 2008; Schofield *et al.*, 2008; Singer *et al.*, 2009). The net effect, however, is that strain on the interior is negligible and likely does not enhance the solubility or stability (Schofield *et al.*, 2008). Nanoparticulate UO_2 has been shown to form aggregates, the size of which is, in some cases, due to the rate of U reduction (Burgos *et al.*, 2008; Senko *et al.*, 2002).

In addition, laboratory and field studies have shown that bioreduced U(IV) also forms complexes with microbial biomass binding to phosphate or carbon sites on cell biomass (Bernier-Latmani *et al.*, 2010; Sharp *et al.*, 2011; Boyanov *et al.*, 2011; Alessi *et al.*, 2012; Bargar *et al.*, 2013). These non-uraninite biogenic U(IV) species have been termed monomeric or molecular U(IV) and more recently have been referred to as “non-uraninite U(IV) species associated with biomass” or NUSAB (Stoliker *et al.*, 2013). NUSAB U(IV) may be more labile than uraninite and may have a higher susceptibility to oxidation than the biogenic nanoparticulate UO_2, but further characterization of its stability is needed. Thus, it is important to determine the forms of U(IV) produced during biostimulated reduction as part of evaluating the long term effectiveness of in situ bioremediation.

1.4 Stability of Bioreduced Uranium

A key issue for the success of in situ bioremediation of U(VI) is the stability of the solid phase reaction products over time. Remobilization of U through oxidation following cessation of electron donor addition remains a critical component in understanding the long term effectiveness of biostimulated reduction. Determining the stability of the bioreduced uranium that was formed during biostimulated reduction is needed to evaluate if the biostimulated reduction process would be an effective tool for long term remediation of U-contaminated shallow aquifers. Specifically, evaluation of oxidative remobilization in response to changes in groundwater chemistry after biostimulation has ceased, such as the return to oxic conditions, is required. Oxidative remobilization in shallow aquifers may also occur in response to recharge and flooding events, which increase groundwater dissolved oxygen concentrations (Yabusaki *et al.*, 2010).

The stability of bioreduced U(IV) following biostimulation is dependent both on the form of the bioreduced U(IV) and on the rate and extent of oxidation of the biogenic U(IV). Oxidation of U(IV) occurs primarily through abiotic processes by reaction with dissolved oxygen, nitrate, and Fe(III) solid phases. In contrast, biotic oxidation is limited particularly at the circum neutral pH of many aquifers (Campbell *et al.*, 2013). Similar rates of oxidation are reported for biogenic UO_2 and synthetic abiotic UO_2 on a surface area basis (Ulrich *et al.*, 2009). The susceptibility of nanoparticulate biogenic UO_2 to oxidation is thought to be controlled in part by the extent of aggregate formation that may offset the high surface area of nanoparticles (Burgos *et al.*, 2008; Senko *et al.*, 2007). Formation of strong complexes of U(VI) with dissolved carbonate present in most groundwater systems enhances U(VI) solubility, minimizing accumulation of oxidation products on UO_2 surfaces such that the oxidation reaction is rate limiting (Campbell *et al.*, 2013). Oxidation of biogenic UO_2 in the field under ambient geochemical and flow conditions was observed to be several orders of magnitude slower than laboratory rates (Campbell *et al.*, 2011).

Hydrologic, chemical and microbiological conditions expected at shallow, alluvial sediment sites will influence the stability of bio-reduced U(IV) and how it responds to the long-term re-introduction of oxidants to the system. The response of bio-reduced U(IV) during a return to oxidizing conditions has been the focus of several recent and ongoing research efforts (Moon *et al.*, 2007; Moon *et al.*, 2009; Komlos *et al.*, 2008b; Senko *et al.*, 2002; Zhong *et al.*, 2005). It has been shown that Fe, sulfate, and electron donor concentrations during the bio-reduction phase can largely influence both the bioreduction of U(VI) and the oxidative remobilization of U(IV) (Komlos *et al.*, 2008b; Moon *et al.*, 2007; Wan *et al.*, 2005; Zhong *et al.*, 2005). In column experiments, Komlos *et al.* (2008b) found that U(IV) re-oxidation readily occurs upon introduction of solutions containing atmospheric oxygen concentrations. However, Zhong *et al.* (2005) found that the addition of Fe(II) to an abiotic system containing biogenic U(IV) resulted in both a decrease in the extent of U(IV) re-oxidation and increased sorption of U(VI) to Fe(III) oxide phases formed during the re-oxidation process, thus retarding the mobility of uranium. Conversely, under certain conditions oxidation of U(IV) may occur by reaction with Fe(III) oxides produced from oxidation of Fe(II) phases produced during biostimulation following the reaction pathway described by Ginder-Vogel *et al.* (2010). (Abdelouas et al., 1999) and (Moon et al., 2009)) found that iron sulfides produced during biostimulation decreased the rate and extent of U(IV) re-oxidation upon introduction of oxidants to column influents (e.g., dissolved O_2, nitrate). However, the distribution of these secondary reduced Fe phases within the column sediments in relation to the distribution of reduced uranium was not determined. As a result, it is unclear if the decrease in U(IV) re-oxidation was the result of competition for oxidant (redox “buffering”), or armoring of biogenic U(VI) by iron sulfide precipitates. In addition, the presence of FeS along flow paths may limit transport of remobilized U(VI) through abiotic reduction (Hyun *et al.*, 2012; Gallegos *et al.*, 2013). Consumption of oxygen by biomass degradation also may affect the rate of uranium oxidation (Komlos *et al.*, 2008b).

1.5 Scope of Report

The intent of this report is to present the results of laboratory column experiments designed to investigate biostimulation and subsequent oxic elution of shallow aquifer sediments from the Old Rifle site in Colorado. The objectives of the study are to evaluate:

- the forms of reduced uranium precipitated during biostimulation
- biogeochemical processes occurring during biostimulation
- remobilization of bioreduced uranium upon return to oxic conditions following biostimulation
- the effect of ferrous iron added to the influent on uranium removal and subsequent remobilization.

In addition, the reactive transport model of Fang *et al*. (2009) developed for field scale biostimulation experiments is tested for its ability to simulate column effluent in response to biogeochemical processes likely occurring within the column during biostimulation.

Chapter 2 of the report provides a detailed description of the methods used for the column experiments and for characterization of sediments recovered from the columns.

Chapter 3 presents the results of the column experiments in the order of 1) effluent chemistry during biostimulation, 2) effluent chemistry during oxic elution, 3) solid phase analyses of

sediments after biostimulation reduction and after oxic elution; 4) X-ray spectroscopic and electron microscopy of column sediments, and 5) characterization of microbes involved in biogeochemical processes occurring in the columns.

Chapter 4 uses the findings of the various components of the results to discuss 1) the biogeochemical processes occurring during biostimulation resulting in uranium reduction and 2) the rates and extent of U remobilization observed in the two columns.

Chapter 5 describes reactive transport model simulation during biostimulation of the Rifle sediment column experiments. The approach couples process models to describe the interplay between the saturated flow, microbiology, and geochemistry during acetate biostimulation. The model is based on the reactive transport model developed to simulation field scale biostimulation experiments at the Old Rifle uranium mill site (Yabusaki *et al.*, 2007; Fang *et al.*, 2009). The modeling is intended to provide insight on the processes affecting uranium in the context of 1) transient biostimulation with acetate electron donors, 2) Fe(III)-reducing bacteria and sulfate-reducing bacteria responding to the biostimulation, and 3) geochemical response to the biostimulation products.

Chapter 6 summarizes the key findings of this study.

The laboratory column experiments and solid phase analysis were conducted at the U.S. Geological Survey. X-ray absorption spectroscopy and microfocused X-ray fluorescence measurements were collected at the Stanford Synchrotron Radiation Lightsource. Reactive transport modeling was conducted at Pacific Northwest Environmental Laboratory by Steve Yabusaki, who authored Chapter 5.

2 Experimental Methods and Approach

2.1 Artificial Groundwater Design and Composition

Artificial groundwater (AGW) used for column experiments was developed to simulate the average major ion chemistry of groundwater sampled at the Old Rifle site. AGW composition is shown in Table 1. The pCO_2 was fixed at 3.5% based on groundwater chemistry with dissolved calcium concentration iteratively adjusted in PHREEQC simulations to yield the desired pH of 7.0 for the column influent. The resulting calculated alkalinity of 6.6E-3 M was about a factor of 2 lower than groundwater from the field site (1.1E-2 to 1.3E-2 M). Both calcite and gypsum, phases present in the aquifer material, are slightly undersaturated in the AGW with log Saturation Index (SI) of -0.21 and -1.07, respectively. For the biostimulation stage of the column experiments, the AGW was amended with dissolved phosphate, ammonia, trace elements, and vitamins, as shown in Table 1. Dissolved uranium as U(VI) was added from a 1 mM stock solution prepared from dissolution of reagent grade UO_3 with sulfuric acid.

AGW for columns was prepared in 3.5 L batches in tared 5-L glass reservoirs (Kontes model KC14395 5000) fitted with 3-hole screw caps (Kontes 953930) that were threaded for gas inlet and outlet, and liquid outlet tubing fittings. Calcium sulfate was dissolved in 3 L deionized water, with appropriate volumes of concentrated salt solutions then added to yield desired final concentrations of all major ion components except for $NaHCO_3$ and U(VI). The reservoir was then sterilized by autoclave, along with inlet and gas purging tubing assemblies. After autoclaving, the reservoir was sealed until cooled. The remaining AGW components and amendments were then added through 0.22 μm filters to sterilize them. Reservoir weight was recorded after each addition, and after autoclaving. For the biostimulation stage, an electron donor was flowed continuously through the columns to stimulate the indigenous microbes to produce reducing conditions to immobilize dissolved uranium. Sodium acetate solution was added from a 1 M stock solution prepared from sodium acetate. This stock solution was filter sterilized and stored at 4° C in an autoclaved serum bottle flushed with nitrogen. Influent acetate was 10 mM for all of column A biostimulation and for the first 70 days of biostimulation of column B. Influent acetate was 8 mM for the remainder of column B and for all of the biostimulation period of column C. After addition of all components, the AGW reservoirs were flushed with 3.5% pCO_2 balance N_2 gas mixture for one hour at ~1 L/min through a gas dispersion stone. The inlet tubing apparatus was installed, and the reservoir was flushed for another 30 minutes before attaching to a column. A continuous flow of the gas mixture was bubbled through the reservoir at ~50 mL/min and vented through an airlock for the duration of the experiment.

Ferrous iron was added to the influent stream of column C throughout the biostimulation phase and to column B after 211 days of biostimulation. Iron addition was intended to produce additional iron sulfide to assess its effect on oxic remobilization of U that was reduced and precipitated during biostimulation. Iron was introduced to the influent from a second reservoir containing 150 μM ferrous iron from $FeCl_2$ adjusted to pH 4 with 4N HCl. This reservoir was prepared as outlined above by autoclaving the deionized water, purging with a CO_2/N_2 gas mixture, and then adding a 4 mM ferrous chloride solution that was sterilized by passing it through a 0.22 μm filter. Anoxic ferrous iron was mixed into the influent stream from the AGW reservoir through a three-way T-fitting about 40 cm before the column inlet to attain a 15 μM

ferrous iron concentration in the influent. The pH of the mixed influents was 7.0. Travel time for the Fe(II)-AGW mixture between the mixing T-fitting and the column inlet was about 4.5 minutes.

Table 1. Artificial groundwater composition

Constituent	with acetate moles/L	without acetate
Ca	**2.40E-03**	**2.40E-03**
Na	**1.84E-02**	**1.04E-02**
Mg	**4.00E-03**	**4.00E-03**
K	**4.00E-04**	**4.00E-04**
U	**1.00E-05**	**1.00E-05**
NH_4	**1.40E-04**	**0**
Cl	**3.00E-03**	**3.00E-03**
SO_4	**6.40E-03**	**6.40E-03**
Total CO_3	**7.79E-03**	**7.79E-03**
acetate	**8.00E-03**	**0**
PO_4	**7.14E-07**	**0**
pH	**7.0**	**7.0**
alkalinity	**6.56E-03**	**6.56E-03**
Trace elements, vitamins (biostimulation only)		
$CoCl_2 \bullet 6H_2O$	**8.0E-07**	
$MnCl_2 \bullet 4H_2O$	**5.1E-07**	
$ZnCl_2$	**5.1E-07**	
H_3BO_3	**9.7E-08**	
$Na_2MoO_4 \bullet 2H_2O$	**1.6E-07**	
$NiCl_2 \bullet 6H_2O$	**1.0E-07**	
$CuCl_2 \bullet 2H_2O$	**1.2E-08**	
$CoCl_2 \bullet 6H_2O$	**8.0E-07**	
p-amino-benzoic acid	**1.2E-08**	
biotin	**2.7E-09**	
folic acid	**1.5E-09**	
pyridoxine•HCl	**1.6E-08**	
thiamine•HCl	**5.0E-09**	
riboflavin	**4.4E-09**	
nicotinic acid	**1.4E-08**	
pantothenic acid	**3.5E-09**	
thioctic acid	**8.1E-09**	
vitamin B12	**2.0E-11**	

The AGW used for oxic elution of columns was prepared using the same procedure and recipe as AGW used for the biostimulation stage except no uranium, acetate, vitamins or nutrients were added. The suboxic AGW reservoir was purged with the desired gas mixture (see 3.2.3).

2.2 Column Apparatus and Operation

Three columns (A, B, and C) of identical dimensions were packed for this study. Two columns (B and C) had ferrous iron added during the biostimulation. All columns were subsampled at the end of the biostimulation stage and the recovered sediments used for geochemical and microbial analyses. After subsampling, the remaining sediment was removed, homogenized, and repacked into a new column for oxic elution. Remobilization of sequestered uranium (re-oxidation of U(IV) and desorption or dissolution of U(VI)) was tested in response to oxic conditions to simulate conditions in an aquifer following cessation of electron donor addition. This is termed the oxidation stage. A pulse of bromide tracer was passed through column C at the end of biostimulation, and through columns A and C at the end of oxic elution to determine column hydrodynamic parameters, and changes resulting from biostimulation and oxic elution. Because of clogging, column B was not used for oxic elution or bromide tracer tests.

2.2.1 Columns

Columns were Soil Moisture Equipment, Inc., 1400 Tempe pressure cells modified by using acrylic tubes of inner dimensions of 5.1 cm ID by 6 cm length. Flow dispersing end caps with glass fiber filters were used for both the column inlet and outlet. The column apparatus was sterilized prior to packing with sediment.

2.2.2 Plumbing and Pumps

Column inlet and outlet tubing was 1/16'' OD polypropylene with ¼"-20 flangeless fittings to connect to 4-way valves at about 12" from column inlet and outlet fittings. A pressure gauge was installed at a three-way (T-) fitting upstream of the inlet 4-way valve and downstream of the pump. All tubing from the reservoir cap to effluent collection outlet was encased within ¼" ID 1/8" wall Tygon R3607 tubing to jacket the influent and effluent tubing. The gas mixture was continuously flowed thought the jacketing to minimize gas exchange and oxygen contamination. Tygon tubing was attached to nylon T-connectors at each fitting and at the column inlet and outlet with a length of Tygon connecting adjacent T- connectors to provide a continuous purge of the entire length of influent and effluent tubing. The jacketing purge gas was flowed at 50 mL/min in the same direction as the AGW flow starting at the feed line from the reservoir to the column effluent outlet, bypassing the peristaltic pump, the pressure gauge, valves and the columns (Figure 1).

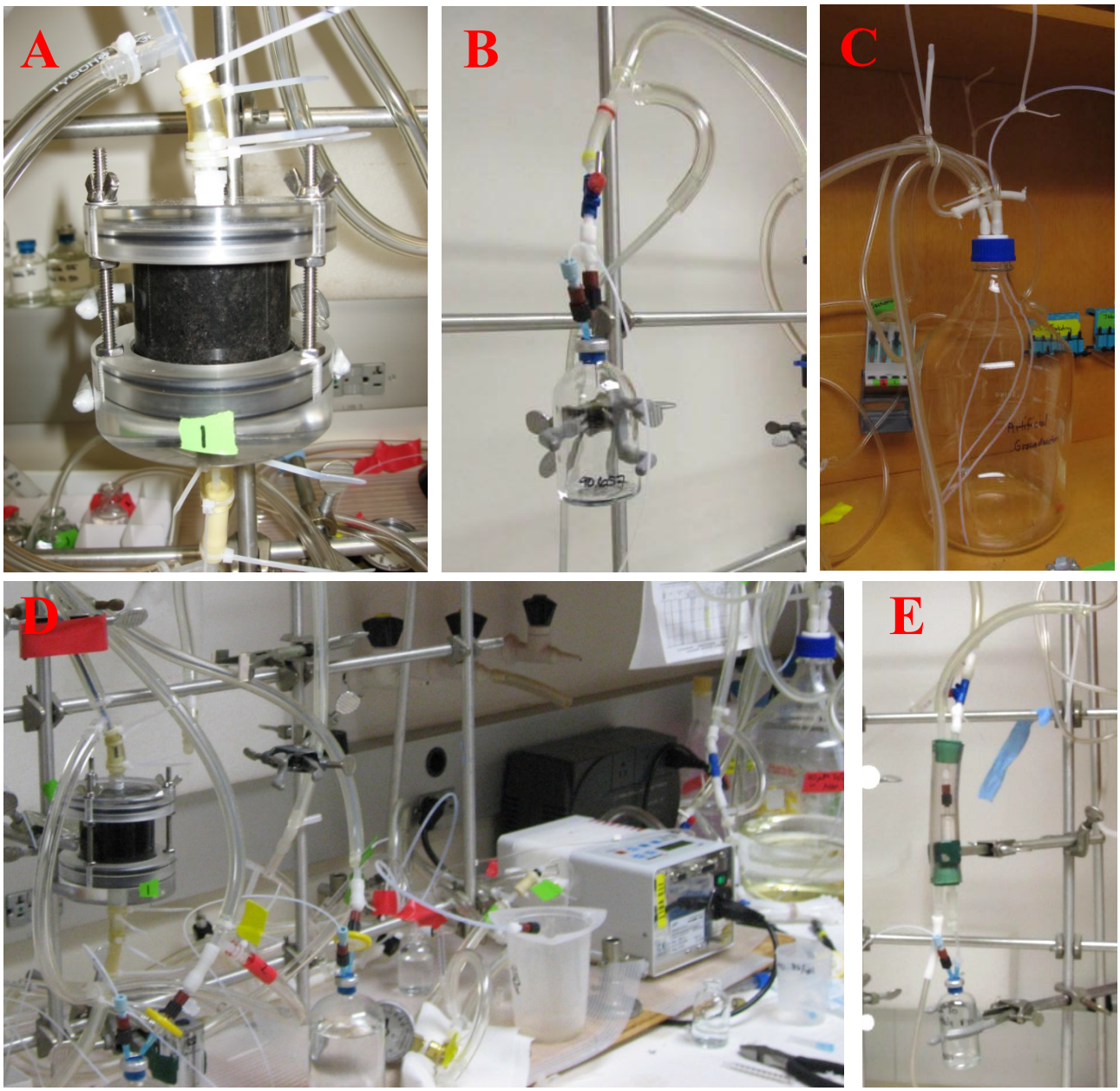

Figure 1. Column set up illustrating A) column, B) effluent tubing with gas purged jacketing to minimize oxygen invasion and effluent collection bottle, C) influent reservoir with gas mixture purge and outlet lines, D) influent lines with gas jacketing , E) Effluent filter for microbial assay, housed in gas jacketed housing. Photographs by C. Fuller.

The influent AGW was pumped from the reservoir through the columns using an ISMATEC 8-roller multi-channel pump fitted with 1.54 mm ID Tygon R3606 double stop tubing for pumping the AGW influent and with 0.44 mm ID tubing for the ferrous iron influent. Pump tubing was attached to jacketed reservoir and inlet tubing with nylon hose barbs. All tubing and fittings were autoclaved before use. Influent flow rates were 0.050 mL/min for the AGW and 0.005 mL/min for ferrous iron.

2.2.3 Gas Phase and Oxygen Control

Commercially-prepared, high-purity gas mixtures of 3.5% CO_2, 96.5% N_2 were used for the biostimulated reduction stage of the columns. An oxygen scrubber was fitted in line to remove residual oxygen in the commercial mixture. Reservoirs were continuously purged with the gas mixture at about 50 mL/min, after the initial flush, and vented through airlocks. Jacketed tubing (described above) also was continuously purged with this gas mixture. For the oxidation stage, a 3.5% CO_2, 20% O_2, 76.5% N_2 premixed gas was used. Because of gas exchange across pump tubing walls resulting from pressure from pump rollers, introduction of oxygen to the influent stream may have occurred during biostimulation. However, aerophyllic bacteria in the sediment likely consumed this oxygen at or near the upstream end of the column.

2.2.4 Column Packing

Sediments from the Old Rifle IFRC site were used for column biostimulation experiments. The sediment was provided by K. Williams (Lawrence Berkeley National Laboratory) that was collected from the aquifer from site BH-02. The site was located within the contamination zone from the Old Rifle uranium mill but not in areas of the aquifer where in situ biostimulation experiments have been conducted. The sediment was stored in a sealed jar until use, and was used as is. The sediment was described as a <2 mm grain size based on visual observation when collected. Instead, it is a silty sand which contains a significant fraction of coarser grains of up to ~8 mm diameter grains. No attempt was made to remove coarser material prior to the experimental study. Columns were packed with wet aquifer sediment in an anaerobic glove chamber. Starting and ending weights of the sediment container were recorded during column packing. Splits of the sediment were subsampled into tared glass vials to determine water content upon drying. Each column with its inlet and outlet fittings and tubing including 4-way valves at each end was weighed empty. Dead volumes of tubing, end caps and fittings were determined by weighing the column assembly full of deionized water and subtracting the empty weight.

An empty column cylinder with the inlet end cap, filter and fittings attached was mounted vertically with the inlet end down. Columns were oriented with outlet on top for upwards flow to minimize preferential flow paths. AGW was added through the inlet valve with a syringe until it was a few millimeters above the inlet bed support frit. The sediment mixture was added with a spatula to the column in increments of about 0.5 cm. A rubber policeman was used to move any sediment that adhered to column walls to the sediment bed. The column was tapped and sediment was allowed to settle for about 5 minutes before adding the next increment. AGW was added as needed to maintain a lens of water (1-2 mm) above the sediment. This process was repeated until the sediment was at the top of the acrylic cylinder. The sediment in the packed column was allowed to settle overnight. On the following day, any overlying water (~5 mL) was removed from the top of the sediment bed with an automatic pipette and retained in a tared vial to determine the mass of water and sediment removed. A second filter was placed on top of sediment and the outlet end cap and fittings were installed. Additional AGW was pushed through the column with a syringe until it flowed out of the outlet tubing. Inlet and outlet valves were then closed and the column was removed from the anaerobic chamber and weighed. Columns are mounted vertically with the outlet end up, and the influent and effluent plumbing attached to the appropriate 4-way valves. Flow of the gas mixture through the inlet and outlet tubing jackets was initiated. After one hour, flow of influent AGW containing dissolved U(VI), electron donor and other amendments, including ferrous iron for column C, was started.

Columns A and C were repacked after subsampling in the anaerobic chamber at the end of the biostimulation stage (see below). The remaining sediment in the column was removed and homogenized. A new column was repacked with this homogenized sediment following the method described above, with the exception that a ~0.5 cm layer of autoclaved Ottawa standard sand was added first to account for the volume of sediment removed for subsampling. The repacked columns were then used for oxidation stage of the experiment. Because of high back pressure due to clogging, column B was subsampled and repacked 10 days after addition of ferrous iron to the influent commenced. The biostimulation was continued using this repacked column. The remaining composited sediment not used for repacking was retained for solid phase analysis and stored as described below.

2.2.5 Column Physical Parameters

Measured dimensions and weights of the columns are shown in Table 2. Column pore volume and porosity were determined from total sediment weight used in packing the columns, total weight of column minus empty weight, and the dimensional volume minus volume of bed support fittings, inlet and outlet tubing. Pore volume and total dry sediment mass were similar in the three columns, which were intended to be identical.

Table 2. Column physical parameters

Value			Parameter
Biostimulation stage			
Column A	Column B	Column C	
5.13	5.13	5.13	Column diameter, cm
6	6	6	Column length, cm
267.3	262.296	258.97	Total sediment weight, wet, in column (g)
0.14	0.12	0.14	Fraction water in sediment
226.4	231.8	220.5	Dry sediment in column (g)
37.4	37.5	37.5	Water mass in column: ignores dead volume of inlet/outlet tubing (g)
4.0	2	1.20	Tubing dead volume (cm^3)
33.4	35.5	37.5	Pore volume (cm^3)
124.0	124.03	124.03	Total column volume (cm^3)
0.27	0.29	0.30	Porosity
2.50	2.62	2.55	Sediment density, rho (g/cm^3)
2	2	2	Flow rate pore volume/day
Oxic Elution (A and C); B repacking during biostimulated reduction			
Column A	Column B	Column C	
5.13	5.13	5.13	Column diameter (cm)
6	6	6	Column length (cm)
249.9	268.82	261.1	Total weight aquifer sediment and Ottawa sand, wet, in column (g)
0.13	0.12	0.14	Fraction water in sediment
177.4	183.6	168.0	Dry aquifer sediment in column (g)
40	45	48	Dry Ottawa sand (g)
1.1	1.3	1.4	Thickness Ottawa sand (cm)
23.5	26.3	28.1	Volume of Ottawa sand zone (cm^3)
9.2	10.3	11.0	Pore volume Ottawa sand, porosity 0.39
32.5	31.2	34.2	Water mass in column: ignores dead volume of inlet/outlet tubing (g)
4.0	3	4.0	Tubing dead volume (cm^3)
28.5	28.2	30.2	Pore volume (cm^3)
124.0	124.0	124.0	Total column volume (cm^3)
100.6	97.7	95.9	Geometric volume of sediment zone, 4.9 cm
0.28	0.29	0.31	Porosity of sediment zone
37.7	38.45	41.2	Total pore volume, sediment and Ottawa sand (cm^3)
0.30	0.31	0.33	Overall porosity, sediment and Ottawa sand zone
2.46	2.64	2.56	Sediment density, rho (g/cm^3)
2.4	2.46	2.46	Flow rate in sediment, pore volume/day

2.3 Column Effluent

2.3.1 Sampling

Samples of column effluent were collected continuously throughout the duration of the biostimulation stage of the column experiments into tared autoclaved serum bottles that were flushed with the 3.5% CO_2 balance N_2 gas mixture. The outlet tubing was fitted with a sterile 0.22-µm pore size 25-mm diameter sterile cartridge filter with an attached hypodermic needle that was inserted into a 1-cm thick butyl rubber serum bottle stopper. A second needle connected to an airlock was inserted that allowed the headspace of the bottle to vent during sample collection. This collection method was intended to maintain anaerobic conditions in the effluent sample bottle during collection and subsequent storage. Sample bottles were changed every 24 to 60 hours. Filters were replaced as needed with about three dead volumes allowed to flow through the filter and needle before being attached to the collection bottle. Sample volume was determined by the weight of effluent collected, and the flow rate from volume divided by the duration of sample collection. Typically, every other sample was acidified to 1% (v/v) with nitric acid for dissolved U and dissolved cation analyses. Samples were acidified at least 24 hours prior to subsampling and analysis, and may have been stored at room temperature for up to four weeks before subsampling. The other samples were stored under refrigeration and were not acidified. These unacidified samples were used for analysis of dissolved sulfate, headspace and total dissolved carbonate, and acetate. During the first 48 days of column A, subsamples for sulfate, acetate, and sulfide were taken for every tenth sample, the sample was then acidified for dissolved U and sulfate analyses. Headspace and total CO_2 measurements did not commence until 54 days (117 pore volumes) after the start of column A. Separate samples for dissolved sulfide analysis were collected periodically into 5-mL glass vacuvials previously flushed with the gas mixture and containing 1 mL 10% (wt/v) zinc acetate to preserve sulfide by precipitating as zinc sulfide. Sulfide samples were collected on a one to two week frequency during the biostimulation stage of columns A, B and C.

Influent reservoirs were sampled through the 4-way valve between the pump and the column when each new reservoir was installed.

2.3.2 Effluent Analyses

Dissolved U in effluent and batch samples was measured using a kinetic phosphorescence analyzer (KPA, Chemchek Instruments Model KPA1), following pretreatment of an aliquot of the acidified sample. The pretreatment consisted of drying on a hotplate in a glass scintillation vial, reconstituting in 1 mL of concentrated nitric acid, adding 7-10 drops of 30% H_2O_2, and heating to dryness. The dried sample was reconstituted in 0.1N HNO_3 and sonicated prior to KPA analysis. The pretreatment removes constituents (e.g. chloride, acetate) that quench uranium phosphorescence. KPA measures only U(VI), but in the unlikely event that any dissolved or colloidal U(IV)was present in the effluent samples it was likely oxidized to U(VI) during the pretreatment process and also measured as [U]. The KPA detection limit was 1E-9M with a precision of ±3%.

Dissolved cation concentrations (Fe, Ca, K, Mg, Mn, Na, etc) in effluent samples were measured by inductively coupled plasma optical emission spectrometry (ICP-OES) using Thermo Scientific iCAP6000. The ICP-OES also measures total dissolved sulfur which includes both sulfate and sulfide species. ICP-OES analyses required 10-fold sample dilution because of high dissolved Ca and Na. The detection limit for minor elements was higher as a result and was 3 μM for iron with a precision of ±3%. Dissolved sulfide concentrations were measured in preserved samples by the colorimetric method described by (Cline, 1969) using a Milton Rov Spectronic 21D spectrophotometer. Dissolved sulfide detection limit was 0.2 mM with a ±4% precision. Dissolved sulfate in the un-acidified samples was measured using a Dionex DX500 ion chromatograph, which had a detection limit of 0.05 mM and precision of ±2%. pH and alkalinity were calculated from the pCO_2 and total dissolved carbonate measured in the un-acidified samples. This method was used because acetate and sulfide contribute to acid neutralization during Gran titration. Headspace CO_2 of un-acidified samples was measured on a SRI 310C TCD detector gas chromatograph prior to other subsampling from these bottles. Subsequently a 5-mL aliquot of the effluent sample was transferred by syringe to a N_2 flushed serum bottle and acidified. The CO_2 evolved from dissolved carbonate was measured by GC. Alkalinity and pH were measured in influent AGW (without acetate) samples collected by the same method but directly from the pump outlet. These samples gave comparable values to pH measured by electrode and to alkalinity determined by Gran titration on separate aliquots of this AGW. Acetate in the un-acidified samples was measured using a Shimadzu SIL-10AF HPLC with a UV detector. The acetate analysis had a detection limit of 0.5 mM and precision of ±4%.

2.4 Solid Phase Sampling

2.4.1 Column Sectioning and Sediment Sample Preservation

Sediment samples were recovered from columns A, B and C at the end of the reduction stage and from columns A and C at the end of the oxidation stage for chemical analyses and microbial assay. Columns were dismantled and the sediment subsampled in the anaerobic glove chamber. Column outlet caps were removed. A cut-off 10 mL syringe barrel was used to core column sediment vertically from outlet to inlet at the end of the biostimulation stage (A and C), and after the clogging event of column B. The syringe barrel was pushed downwards to the inlet end while the plunger was held at the sediment surface. The sediment was extruded out of the syringe barrel column into ~1-cm sections with the length of the remaining sediment measured before and after each subsection was extruded. Each subsection was weighed and homogenized by mixing with a sterilized Teflon spatula. Each column subsection was about 4 to 5 grams of dry sediment. A split of sediment was taken to determine water content upon drying. A second split of about 1 g was transferred to a whirlpak bag for microbial assay. The remaining sediment was split between a 2-mL micro-centrifuge tube for gamma spectrometry, and a glass scintillation vial. These containers were double bagged in Mylar pouches containing oxygen scrubbers. The bags were heat sealed and stored at -80° C until analyzed. Column B was subsampled by removing five intervals with a spatula each about 1 cm thick starting from the outlet. The bottom interval subsampling was stopped when the Ottawa sand layer was reached. The Ottawa sand was retained as a subsample. Column C at the end of the oxidation stage was subsectioned by this method but with the addition of two smaller subsections that appeared more oxidized. Column A at the end of the oxidation stage was subsampled in more detail. Three syringe barrels were inserted for cores. Before removing the cores, sediments surrounding the syringe barrels were carefully removed using a spatula, with about 3 to 5 samples collected at about 1-cm depth increments while attempting to discriminate between

oxidized and reduced appearing sediments (see section 3.3.1). The syringe barrels were removed and subsampled as described above. A total of 26 subsamples were collected from column A after oxic elution, of which 23 were comprised of aquifer sediment. These samples ranged from 1.2 to 23.1 g of wet sediment.

2.4.2 Total U Screening by Gamma Spectrometry

Total uranium content of the column subsections and the pre-column sediment was determined by gamma spectrometry following the method outlined in (Fuller et al., 1999) The 63 KeV gamma emission of the ^{238}U daughter ^{234}Th was measured on a high resolution gamma spectrometer. This method assumes that the ^{234}Th daughter is in secular equilibrium. Because the column C samples were measured immediately at the end of the biostimulation reduction, they were likely were not in secular equilibrium, the total uranium of these samples measured by gamma spectrometry is considered a lower limit. These total uranium values were used primarily to determine which samples to use for X-ray adsorption spectroscopic measurements and as a guide for dilutions for chemical extraction analyses. Total uranium concentrations determined by hot nitric acid extraction were used for mass balance calculations and for comparison to loading calculated by integrating the difference between influent and effluent dissolved U.

2.4.3 Chemical Analyses

Two to five gram splits of recovered sediment from the columns were dried at room temperature in the anaerobic chamber for chemical analyses. The coarse fraction of sediments (>~2 mm) was removed from the dried sediment by hand in the anaerobic chamber. The small sample size was insufficient for separation by dry sieving. The coarse fraction was retained for analysis. The fine fraction of the dried sediment was homogenized and a 1-gram split was ground with an agate mortar and pestle for nitric acid extraction and total S measurement. The unground remainder was used for partial chemical extraction of ferric and ferrous iron, acid volatile sulfide, hot nitric acid dissolution, and total carbonate analysis. A split of the original BH-02 sediment, sieved to <2 mm, was also analyzed by the techniques outlined below to compare with this sediment following biostimulation reduction and suboxic elution. This material is referred to as the pre-column sediment.

2.4.3.1 Extractions

Hot nitric acid and peroxide extraction was used to determine total uranium and other constituents such as calcium and iron. This method is based on EPA method 3050 and dissolves most sedimentary phases except for silicates. Briefly, 0.1 gram of the dried, ground sediment was placed in a tared glass vial, 3 ml of concentrated HNO_3 was added and a glass reflux bulb placed on top of the vial. The sample was refluxed for 24 hours at 90°C. After cooling, 0.5 mL of 30% H_2O_2 was added and allowed to stand for 30 minutes. The reflux bulb was removed and the sample evaporated to dryness at 90°C. The dry weight was recorded and 10 mL of 0.1N HNO_3 added to reconstitute the sample. The sample was sonicated for 30 minutes and allowed to settle overnight. An aliquot of supernatant was removed with a syringe, passed through a 0.22 µm filter, and diluted appropriately for analysis by KPA for U and ICP. The U concentration determined using this hot nitric acid extraction and the gamma spectrometry total U measurement generally agreed within 10%. Extraction of replicate sample splits was not conducted.

Extractable ferrous iron (Fe(II)) and reducible iron were determined by separate 0.5 N HCl and 0.5 N HCl/0.25M hydroxylamine hydrochloride (HH) extractions of dried, unground <2 mm sediments. The difference between these two extractions has been defined operationally as the non-crystalline ferric iron oxides available for microbial reduction (Lovley and Phillips, 1987). The extractions were conducted in the anaerobic chamber on anaerobically preserved sediments. Briefly, 0.5 g of sediment was transferred to a tared polycarbonate Oak Ridge centrifuge tube and 30 mL of either 0.5 N HCl or 0.5N HCl/0.25 M hydroxylamine hydrochloride was added. Because of limited sample, duplicates were extracted on about every fifth sample, or a minimum of two per column. Tubes were mixed on an end over end shaker (12 RPM), and 3 mL of extraction solution recovered by filtering through 0.22 µm syringe filter. Extractions with 0.5 N HCl were sampled at 1 and 24 hours. HH extractions were sampled after 1 hour and 24 hours. Tubes were weighed after each subsample to account for the volume removed. Fe(II) concentrations in the HCl extraction solutions were determined by the ferrozine colorimetric method (Stookey, 1970) using a Milton Roy Spectronic 21D spectrophotometer. The total iron concentration in the 0.5 N HCl extraction solutions was determined by adding hydroxylamine hydrochloride to a separate aliquot of the filtered extraction solution to reduced dissolved Fe(III), and analyzed by the ferrozine method. Total Fe extracted by HH was determined directly by ferrozine since extraction reduces Fe(III). Extractable iron measurements of replicates agreed to within 10%.

2.4.3.2 Total carbonate, total sulfur and acid volatile sulfur

Total carbonate content of the pre-column sediments was determined by measuring the CO_2 evolved upon acidification. Briefly, 0.5 to 1.0 g splits of dried sediment were placed into 120 mL serum bottles which were sealed and flushed with N_2. Five mL of 2N HNO_3 were injected into the bottle after removing an equal volume of headspace. After mixing on an orbital shaker, a 60-mL syringe fitted with a 3-way valve and a needle was inserted into the stopper. The excess gas pressure was allowed to displace the plunger upwards and the volume of displacement recorded. After closing the valve and removing the syringe from the bottle, the syringe was connected to the injection loop of the TCD detector GC to measure CO_2 content of the gas phase. The percent carbonate in the solid was calculated by multiplying the gas phase CO_2 concentration by the sum of the bottle volume and syringe displacement and dividing by the initial sample weight. Post-biostimulation total carbonate was not determined on column sediments since the estimated mass of calcium carbonate precipitated based on the measured change in dissolved calcium would not be distinguishable above the carbonate of the pre-column sediments.

Total sulfur content and S isotope ratio of the dried, ground column sediment and pre-column material were measured using a Carlo Erba elemental analyzer (EA) coupled to a Micromass Isoprime mass spectrometer. This method provides a measure of all forms of S present in the sample. An increase in the % total S would reflect reduction of sulfate in the AGW during biostimulation and precipitation of reduced sulfur species, such as FeS. The S isotopic ratio, expressed as $\delta^{34}S$, can be used as an indicator of fractionation of S isotopes during microbial reduction of S (Habicht and Canfield, 1997), resulting in a lighter isotopic ratio (lower $\delta^{34}S$) of the reduced S. This fractionation results from the kinetic isotope effect in which the reaction rates for heavier isotopes (e.g ^{34}S) are slower resulting in a depletion of the heavier isotope in the product relative to the reactants. Briefly, 3 mg of the homogenized ground <2 mm sediment sample was weighed on a microbalance into tin capsules with approximately 2 mg of V_2O_5 added. The samples are combusted at 1000^0C. The EA traps water and separates the resulting CO_2 and N_2 from the SO_2 which is measured using an IR detector and then sent to the mass

spectrometer. The N_2 and CO_2 are vented. The samples are run in batches of 30 at 10 sample intervals. Each group of 10 samples was surrounded by four reference standards (NBS SRM bovine liver) run in a range of sizes to capture the range of S in the samples. A blank is included in the run. The standards were calibrated against Canyon Diablo Troilite (CDT) for $\delta^{34}S$. The ^{34}S isotope composition is expressed as a difference in the ratio relative to the CDT in parts per thousand or per mil (‰), termed $\delta^{34}S$.The $\delta^{34}S$ and %S values were corrected for instrumental drift. $\delta^{34}S$ values were also corrected for oxygen contribution. One standard deviation of the standards throughout a run was ± 0.5 per mil (‰) or better for $\delta^{34}S$, and 0.01 %S. Duplicates measured every fifth sample agreed within 0.05% S and within 0.5 per mil $\delta^{34}S$.

Acid volatile sulfur (AVS) content was measured on sediments recovered from the columns, and the pre-column sediment using a modified version of the diffusion method of (Hsieh and Yang, 1989). AVS is a measure of sulfide (S^{-2}) species in the sample such as FeS that are liberated upon acidification forming H_2S gas. The method used does not reduce more oxidized forms of S such as elemental sulfur or S^{-1} in FeS_2. In the anaerobic chamber, dried column < 2 mm sediment samples (0.3 g) are placed in 100 mL serum bottles along with 1 mL of 1 M ascorbic acid to eliminate oxidation of AVS by ferric minerals (Hsieh *et al.*, 2002). A 10 x 75 mm test tube containing 3 mL of alkaline zinc acetate (3% w/v zinc acetate in 2N NaOH) is placed in the serum bottle, with its' opening placed upwards and resting on the shoulder of the bottle. The alkaline zinc acetate solution traps the H_2S gas evolved on acidification forming a zinc sulfide precipitate. A 1-cm magnetic spin bar is placed in the bottom of the bottle. The serum bottles are then sealed and 10 mL of 6N HCl is injected through the serum bottle stopper with a syringe directly onto the sediment sample carefully avoiding contact with the zinc acetate solution. The bottles are removed from the anaerobic chamber and placed on a stir plate with gentle stirring. After 30 hours, the zinc acetate tubes are recovered. After weighing each tube, an additional 0.5 mL of 2N NaOH is added, and the tubes are stoppered, then sonicated for 30 minutes to disperse the ZnS precipitate. Weights are recorded at each step to determine actual volumes. The resulting suspension of zinc sulfide is subsampled and sulfide is determined colorimetrically (see section 2.2.2). The method was tested using a reference synthetic solid (70% FeS; 30% FeS_2). The measured AVS within 24 hours was equivalent to the S in the FeS component. No additional S was recovered after longer equilibration times consistent with previous studies that showed that acid without added reductants only volatilizes the S^{-2}, and not higher oxidation states such as S^- in FeS_2, or elemental S. Replicates of this reference sample agreed to within ± 5%, and duplicates of column samples agreed within ±10%. The detection limit for AVS by this method is estimated at 0.1 μmole per gram. The effect of CO_2 evolved from the carbonates present in the ISR samples during acidification on AVS recovery by alkaline zinc acetate was found to be negligible. Other treatments such as acidic Cr(II) to reduce higher oxidation states of S were not attempted. Instead, the difference between total sulfur increase (column minus pre-column total S) and the AVS is used as a measure of higher oxidation states of S precipitated during the biostimulated reduction stage of the column experiments. The coarse fraction (>2 mm) from selected column sediment subsamples also was analyzed for AVS. The entire >2 mm column subsample was used. Following recovery of AVS in the zinc acetate tube, a measured mass of the 6N HCl was recovered for analysis of U and cations. Because chloride quenches U phosphorescence in KPA analysis, the 6N HCl leachate required multiple drying steps with nitric acid to remove chloride by volatilization. No attempt was made to evaluate the effectiveness of the cold 6N HCl extraction relative to the hot concentrated HNO_3 digest used for the ground, <2 mm sediments.

2.4.4 Spectroscopic Measurements

Sediments recovered from sub-sectioning columns A, B and C were used for X-ray absorption spectroscopic (XAS) measurement to determine oxidation state and the local molecular structure of sequestered uranium. Column intervals for XAS measurement were selected based on the total U content and included samples from both the biostimulation and oxidation stages of the column experiments. The pre-column material was not measured because its total U was too low for collection of usable XAS spectra.

2.4.4.1 Bulk XAS

X-ray absorption near edge spectroscopy (XANES) and Extended X-ray Absorption Fine Structure (EXAFS) measurements were made at the Stanford Synchrotron Light Source (SSRL) beam lines (BL) 4-1 and 11-2 on anaerobically stored sediments recovered from the columns. Analysis of XANES spectra is used to provide a quantitative measure of the different oxidation states of an element in a sample. EXAFS spectra are used to derive the local atomic structure surrounding the element of interest in the sample by fitting the spectra based on spectra and structure of reference or model compounds spectra to determine the molecular scale speciation. Bulk XAS measurements provide information on the entire mass of the element of interest in the portion of sample illuminated by the X-ray beam. Beam size was typically 1 mm high by 8 mm wide with the sample placed at a 45° angle to the incoming X-ray beam, which resulted in an illumination area of 1 x 11.3 mm for the 1.2 mm thick sample.

Un-dried samples were ground with agate mortar and pestle in the anaerobic chamber, with AGW added to facilitate grinding. The larger grains were removed prior to grinding. The resulting paste of ground, wet sediment was packed into 1/32” thick polycarbonate holders with 10 mil Kapton tape windows. Uranium L_{II} and L_{III} edge fluorescence spectra were collected in an anaerobic stage to eliminate exposure to oxygen during sample collection.

For XANES, a minimum of three replicate scans of fluorescence spectra of each sample was collected across either the U-L_{II} or U-L_{III} edge using either a 30-element (BL 11-2) or 13-element (BL 4-1) germanium array detector. Internal calibration of the monochromator was made using either a Y or Mo foil placed on a second ion chamber “down-stream” of the sample stage, with foil edges collected at the start of each scan. The sample spectra were deadtime corrected and adjusted for drift of the monochromator prior to averaging. The averaged spectra were background subtracted and normalized using SIXPACK software (Webb, 2004). The resulting corrected spectra were fit to one or more reference U(IV) and U(VI) model spectra using the least squares fitting module in SIXPACK. Spectra of crystalline uraninite, andersonite, phosphuranylite and U(VI) sorbed to ferrihyrdrite provided by John Bargar, SSRL, were used for model compounds (personal communication). The model spectra were collected at other beam time sessions but also calibrated with internal reference foil for either the U-L_{II} or U-L_{III} edge. The least squares linear combination fitting (LC) procedure yields fractional components of U(IV) and U(VI) in the sample. The best fit was based on the lowest residual chi squared value. That is, the components that yielded the minimum difference between the sample spectra and the fit of the components.

Bulk U EXAFS spectra were collected on a limited number of samples because of availability of beam time. The low uranium concentration of the column samples limited the usable data collection range to about k of 10 at best. Up to 12 replicate scans were collected. Spectra were deadtime corrected and averaged as described above. Shell by shell fits of column sediment U

EXAFS spectra were performed to determine the speciation of sequestered uranium both at the end of biostimulated reduction and after oxic elution. Phase-shift and backscattering amplitude functions for quantitative EXAFS fitting were generated using FEFF 7.0 from the crystal structures of uraninite, liebigite, and autinite (Ankudinov and Rehr, 1997; Locock and Burns, 2003; Mereiter, 1982; Wyckoff, 1963). The phase shift and backscattering functions from models were used for shell by shell fits of sample EXAFS spectra. The spectra were fit over the k-range 3-9.5 $Å^{-1}$.

2.4.4.2 Microfocused synchrotron XRF and XAS

Thin sections of column sediment were prepared for imaging by microfocused synchrotron X-ray fluorescence (XRF) and for discrete point XANES at the SSRL BL 2-3 and BL 10-2 X-ray microprobes, which provide spatial resolution of 2 and 30 μm, respectively. The microfocused beam XRF (μXRF) provides elemental distributions or maps of elements in a thin section. The mapping can be conducted at several energies across the critical X-ray absorption edge of an element (e.g. U) of interest to provide maps of oxidation state for the area of interest (Mayhew *et al.*, 2011).

Petrographic thin sections of sediment recovered from columns were prepared by embedding the sediment in epoxy resin, then cut and polished to 30-μm thickness, and mounted on a quartz slide. Briefly, about 2 to 3 grams of the anaerobically stored sediment was dried by spreading into a thin layer on a 6-inch diameter paper filter in the anaerobic chamber. After drying, the sediment was transferred to a 10 mL polypropylene beaker with clumps gently broken up, as needed, if formed during drying. This made about a 0.5 cm thick layer in the beaker. Epotek 301 2-FL resin (Epoxy Technologies, Inc) that had been outgassed in the anaerobic chamber was mixed and poured onto the dried sediment covering the sediment with at least another 0.5 cm layer. The beakers were then placed in the anaerobic chamber airlock which was then evacuated to -10” Hg to remove any gas phase entrained within the dried sediment. The resin cured at room temperature over the next three days with additionally vacuum applied to maintain the desired pressure. After hardening, the resin pucks are removed from the beakers, labeled, and sealed in Mylar bags with oxygen scrubbers for shipment for thin section fabrication by Spectrum Petrographics (Vancouver, WA). Fabrication of thin sections entailed vertical slicing of the pucks and recast the slices into larger blocks using the same room temperature curing resin. Slices were cut from the block, mounted and polished using low oxygen and heat methods. Each thin section consisted of two slices or panels from the epoxy cast. The completed thin sections were transported in Mylar bags and stored in the anaerobic chamber until measured on the SSRL X-ray microprobes.

Thin sections were imaged using a flatbed scanner with the scanned image enlarged to provide a location map. The entire area of each thin section was mapped at SSRL BL10-2 using a 20-μm nominal beam size focused through a capillary tube using 30 μm steps and 50 msec dwell time. Fluorescence data were collected at each pixel as the sample was stepped under the beam at energies of 17,100 and 17,200 eV, below and above the U L_{III} edge. A difference map (above minus below the edge) was then constructed using the Microprobe Analysis Tool Kit (http://home.comcast.net/~sam_webb/smak.html) to remove the contribution of Rb fluorescence to the U fluorescence window. Single and multi-element XRF maps depicting relative concentration were then constructed for each thin section to depict the distribution of U, Fe, Ca and other elements of interest. These maps also are used to locate areas for more detailed mapping at BL 2-3.

Selected areas of thin sections with higher U concentration were imaged using the SSRL BL2-3 X-ray microprobe using a 1 μm focused monochromatic X-ray beam with fluorescence data collected at 50 to 200 msec dwell time as the sample was translated across the beam. The effective pixel size was 2 x 2 μm in most cases, and 5 x 5 μm for larger grains. The U enriched areas of the thin sections mapped with the X-ray microprobe were either individual grains or coatings on grain exteriors. Maps were collected at multiple energies across the U-L_{III} absorption edge at 17,170, 17,175, 17,178, and 17,190 eV. The resulting maps were processed using a least squares fitting routine in the SMAK software to calculate the fraction of U(IV) and U(VI) at each pixel based on the contribution of each component to the normalized fluorescence yield at these energies in XANES spectra of model U(IV) and U(VI) compounds. This XANES mapping routine is further described in previous studies (Mayhew *et al.*, 2011; Sharp *et al.*, 2011). U-L_{III} XANES and EXAFS spectra were then collected at specific points using a 1 μm beam spot size on thin sections that had sufficient U to provide usable data. These points were chosen based on apparent distribution of U(IV) and U(VI) from the XANES maps, and locations were optimized for maximum signal.

2.4.5 SEM-EDS Imaging

Carbon-coated epoxy-impregnated thin sections were analyzed by SEM-EDS using a JEOL 5600 full field emission scanning electron microscope operated at 15 keV. Selected thin sections were imaged using scanning electron microscopy both in secondary electron (SE) and back scatter (BSE) modes. Because of the presence of the epoxy impregnation, the vacuum in the electron microscope is unlikely to have induced morphological changes in the samples. Elemental compositions of the grain coatings and adjacent areas of U bearing grains were measured using electron stimulated energy dispersive spectroscopy (EDS) using X-ray fluorescence.

2.4.6 Microbial Assay

Microbial characterization of sediments and effluent filters were conducted by the USGS microbiology laboratory in Reston, VA. The general approach taken was to extract DNA, and perform bacterial Terminal Restriction Fragment Length Polymorphism (TRFLP) fingerprinting and quantitative Polymerase Chain reaction (qPCR) analyses of *Geobacter,* a and sulfate reducing bacteria (SRB) on all samples. In addition selected samples were further characterized by cloning *Geobacter* 16S rRNA gene, and/or *dsr*B gene coding for the dissimilatory sulfite reductase involved in sulfate reduction. The intent was to 1) gain an understanding of microbial dynamics in these experiments as biostimulation of U(VI) reduction occurred, as well as during potential remobilization of uranium, 2) to assess where in the column the microbial abundances were highest and relate that to chemistry and solid phase analyses, and 3) determine potentially important *Geobacter sp.* and sulfate reducing organisms involved in these processes in the column experiments.

2.4.6.1 Column sediments

Subsamples of sediments recovered from columns A, B and C at the end of the biostimulation stage, and from column A after the aerobic elution were processed for microbial characterization. Upon recovery from the column, about one gram of wet sediment was transferred to a whirl pak bag using a sterilized spatula. The sediment adhering to the filters on

the inlet (columns A, B,C) and outlet (column C) bed support also were assayed. The filters were folded into quarters and placed in a whirl pak bag. All samples were sealed in Mylar bags and frozen at -80°C. Samples were shipped on dry ice to the microbiology lab.

2.4.6.2 Effluent filters

Millipore Sterivex 0.2 µm filter capsules were installed in the column effluent line within a gas purged holder to limit exposure to oxygen (Figure 1E). The effluent was collected as described above, downstream of the Sterivex filter. Following the collection period, the filter capsules ports were sealed and the cartridge was stored at -80°C. Filter capsules and sediment samples were shipped on dry ice to the microbiology lab. Effluent filters for microbial assay were collected during the biostimulation stage: one for column B during sulfate reduction (days 113 to 121); two from column C during iron reduction (days 7 to 14) and at the onset of sulfate reduction (days 29 to 34). In addition, an effluent filter was collected from column A after cessation of acetate and U inflow but under anoxic conditions (days 179 to 188).

2.4.6.3 Measurement methods

DNA Extraction. The 0.5-1 g frozen sediment samples from the column experiments were thawed and then extracted using the MoBio ultraclean soil DNA megaprep kit according to manufacturer's instructions (MoBio, Inc., Carlsbad, CA). The solid from the flat end-cap filters was scraped then extracted by the same method. Sterivex capsule effluent filters were thawed and extracted as previously described using the Qiagen (Gentra) puregene kit with slight modifications. (Qiagen, Inc., Valenica, CA) (Ward *et al.*, 2007). Briefly, 0.9 mL of lysis buffer with 4.5 µL proteinase K was added to the filters and incubated with gentle rotation for 10 minutes at 80°C. Volumes of solutions used in subsequent protein precipitation and DNA precipitation steps were scaled up accordingly (3X) to reflect the 3X volume increase in lysis step compared to manufacturer's instructions (0.9 mL instead of 0.3 mL).

Bacterial 16S rRNA Gene PCR and TRFLP Fingerprinting. The polymerase chain reaction (PCR) technique was used to amplify bacterial DNA from samples, targeting the evolutionally conserved ribosomal RNA gene, 16S rRNA. This technique allows for the amplification of a specific segment of DNA of interest from the bulk DNA. Enough of the amplification product from PCR (amplicon) is produced such that it can then be detected and characterized further (cloning and sequencing or fingerprinting depending on the question being asked). PCR was performed as previously described using the 16S rRNA gene primers 46f-FAM and 519r (Jones *et al.*, 2006; Lane, 1991; Brunk *et al.*, 1996). A DNA fingerprinting method, the terminal restriction fragment length polymorphism (TRFLP) technique was also used to look at bacterial community differences between samples. This technique involves the enzymatic digestion of the PCR product, which has a fluorescent tag. The enzyme has a specific DNA recognition sequence and only cuts the DNA where that sequence exists. Therefore, depending on the PCR product's DNA sequences, enzyme digested products of varying size will be produced. The fragments from the end which contains the fluorescent tag can then be electrophoresed (size separated) and the fluorescence detected, generating a fragment size profile which is unique to that population of organisms with those sequences. This fingerprint can be compared to other samples to evaluate similarities and differences between the sample communities or within a community over time. TRFLP was performed as previously described (Jones *et al.*, 2006). Briefly, PCR amplicons were digested with Mn(II), precipitated, and electrophoresed on an ABI 310 genetic analyzer to generate fingerprint profiles. Fingerprint data were binned using the

software R, and imported into the SAS based JMP8 statistical package (SAS, Cary, NC) for clustering analysis.

Real time quantitative PCR (qPCR) for Geobacter and SRB. qPCR was performed on all samples for *Geobacter* using the 16S rRNA gene primers Geo494f and Geo825r (Anderson *et al.*, 1998; Holmes *et al.*, 2007), and for SRB using the functional gene *dsrB* primers drp-2060f and dsr4r (Wagner *et al.*, 1998; Geets *et al.*, 2006). The procedure including cycling temperatures and times are as previously published (Wilson *et al.*, 2010).

Clone Library Construction and Sequencing. Geobacter and SRB clone libraries were constructed for selected samples. PCR was performed using the Geobacter specific and SRB specific primer sets above. PCR conditions; Geobacter 30 cycles of 94°C (30 s), 53° C (30 s), and 72° C (30s) followed by a 7 minute 72°C extension incubation. SRB PCR was also 30 cycle and conditions were identical except the annealing temperature was 56°C rather than 53°C. Amplicons were purified by wizard prep (Promega, Madison, WI.), and cloned into TA vector according to manufacturer's instructions (Invitrogen, Carlsbad, CA). Single clones were picked and analyzed for insertion by PCR with M13f and M13r primers. PCR products were sequenced by single pass PCR sequencing (Beckman Coulter Genomics, Danvers, MA.).

Sequencing Analysis. Plasmid vectors were trimmed using the AWK program "vbgone" (Varnum Engineering, Seattle, WA). Sequences were oriented and aligned in Macvector 12 using ClustalW (MacVector, Cary, NC). Phylogenetic trees were built in MacVector12 using the Neighbor Joining method and TamuraNei distance with bootstrapping (1000 replicates) or BESTTREE. Representative sequences from each phylotype were checked for highest similarity to sequences in Genbank database using the Basic local alignment tool (Blast).

3 Results

3.1 Column Effluent: Biostimulation

3.1.1 Column A Effluent History during Biostimulated Reduction

Flow of anoxic AGW containing acetate and dissolved U through column A was initiated on July 7, 2009, at a flow rate of 0.05 mL/min. Using the sediment pore volume of 33.4 cm^3 (PV) calculated from the column weights (Table 2), this flow rate is equal to 2.16 pore volumes per day. Effluent acetate concentration equaled the influent (10 mM) over the first 17 days. A decrease in effluent acetate was measured starting at day 24 and continued to decrease through day 70, and subsequently changed little, averaging 1.5 mM (Figure 2) through day 111 when acetate was removed from the influent. Thus, acetate is not fully consumed but was utilized at a constant rate in the later stage of biostimulation.

Effluent dissolved iron increased from the onset of flow of acetate electron donor, reaching a maximum concentration by 15 days. Subsequently, effluent iron decreased to < 3 μM by day 25. Dissolved sulfide in the effluent was first measurable at day 32. Sulfide increased over the next 20 days and was then relatively constant throughout the remainder of acetate addition, averaging 2.2 mM between days 43 and 111. Effluent sulfate did not change measurably over the first 17 days, but began decreasing at day 24. By day 36 sulfate was below 3 mM and subsequently averaged 1.2 mM between days 43 and 111. The net loss of sulfate, the difference between influent and effluent sulfate (6.8 mM), during this period is about 3 times greater than the effluent sulfide concentration indicating precipitation and retention of reduced sulfur within the column.

Effluent carbonate alkalinity and pH measurements did not commence until day 53. At this time, effluent pH was 7.8, 0.8 pH units above the influent. Effluent pH decreased to about 7.7 by the end of the acetate amendment. Subsequently, effluent pH decreased to that of the influent. Alkalinity was also elevated between day 53 and 111, averaging 20.1±1.2 meq/L compared to influent alkalinity of 8 meq/L. Effluent alkalinity decreased to the influent level when acetate amendment was stopped.

Because of the low solubility of reduced U(IV), dissolved U, [U], is assumed to be all in the +6 oxidation state as U(VI). Dissolved U(VI) is dominated (>90%) by calcium uranyl carbonato complexes at the pH and composition of the influent and effluent. Effluent [U] increased over the first 3 days of the experiment to about the influent concentration. The lower effluent [U] during this initial period is consistent with U(VI) sorbing to aquifer sediments to attain surface complexation equilibrium. Effluent [U] began to decrease starting at day 10, and continued to decrease somewhat linearly throughout the biostimulation period. Effluent [U] was 3 μM at the end of biostimulation at day 111. The observed [U] decrease starting at day 10 slightly lagged the apparent onset of iron reduction and likely reflects microbial uranium reduction. Effluent [U] increased slightly from day 22 to day 30, after which it decreased through day 56 when another increase occurred. The first increase in [U] coincided with the onset of both decrease in effluent sulfate and increase in sulfide.

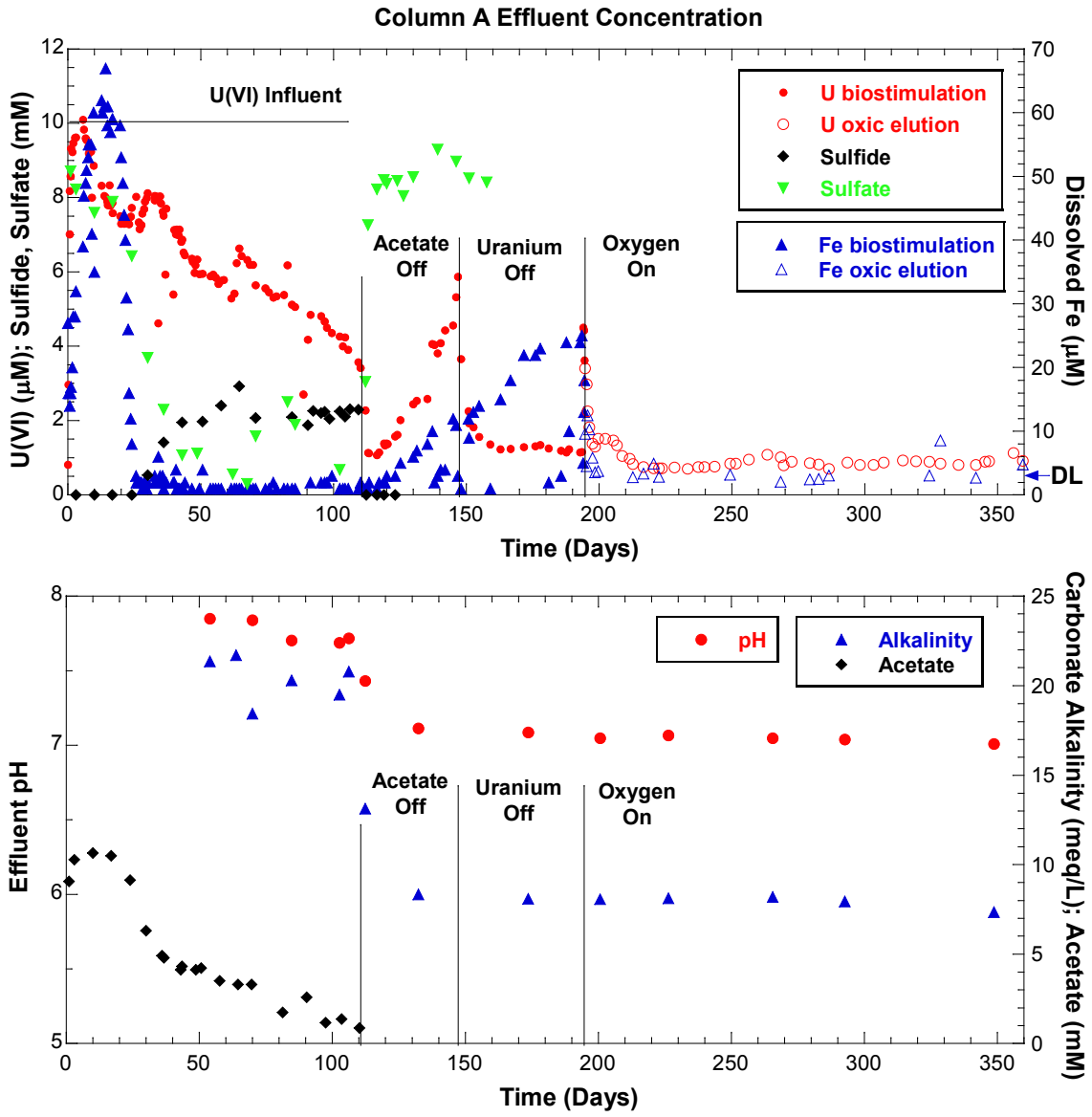

Figure 2. Effluent concentrations of (top) dissolved uranium, iron, sulfide and sulfate and (bottom) pH, carbonate alkalinity for column A during biostimulation and during oxic elution versus time from start of biostimulation. Iron concentrations below the 3μM method detection limit are plotted as the measured value.

Overall, the column A effluent profile displays the typical sequence of microbially mediated redox processes with iron reduction evidenced by the increase in effluent dissolved iron followed by the onset of sulfate reduction and the concomitant decrease in effluent Fe. It is unclear from effluent concentrations whether the resulting drop in effluent iron occurred because the pool of reducible iron was depleted or because sulfide production limited iron solubility.

Following cessation of acetate input at day 111, microbial activity decreased rapidly as indicated by the decrease in effluent sulfide to below detection, and the return of sulfate, pH and alkalinity to the influent levels. Effluent [U] immediately decreased to about 1 μM when acetate input stopped, then increased slowly approaching 5 μM [U] over the next 36 days, at which point U was removed from the influent. These data indicate sequestration of [U] continued after the acetate amendment was stopped. However, the rate of U uptake decreased during this period of anoxic influent containing U but not acetate. The possible processes that resulted in the continued U uptake after biostimulation ended are discussed below. Effluent dissolved Fe increased about 10 days after acetate inflow was stopped and was at 25 μM when the anoxic stage of the experiment was ended at day 194.

At day 148, anoxic AGW without U or acetate was passed through column A until day 194. During this time effluent [U] decreased from 5 to <2 uM over the first 10 days and was relatively constant averaging1.6 uM between day 158 and 194. At this point sediments from column A were subsampled and the remaining sediment homogenized and repacked into a new column for oxic elution with AGW.

3.1.2 Column B Effluent History during Biostimulated Reduction

Flow of acetate and uranium amended AGW through column B was started on Sept. 11, 2009. The same influent reservoir used for column A also was used to supply column B during its first 44 days of column B. The flow rate of 0.05 mL/min is equivalent to 2.02 pore volumes per day using the calculated pore volume of 35.5 cm^3 (Table 2). The general trends in effluent concentrations for column B prior to inclusion of 15 μM ferrous iron in the influent are similar to those in column A. The influent acetate was 10 mM over the first 70 days, then was lowered to the intended 8 mM influent concentration for the remainder of the biostimulation experiment. The decrease in effluent acetate was first observed at day 22 and continued to decrease through day 70 (Figure 3). Subsequently effluent acetate was relatively constant averaging 2.0±.05 mM through day 221.

Unlike column A, dissolved iron was not detected in the effluent until 5 days after the start of the acetate amendment of column B. Effluent iron then increased reaching a maximum concentration (~70 μM) at day 19. Subsequently, effluent [Fe] decreased to < 3 μM by day 28, and was low, averaging 2.5 μM, throughout the remainder of the biostimulation period prior to addition of ferrous iron to the influent. As observed in column A, the decrease in [Fe] from the maximum coincided with the onset of sulfate reduction and measurable effluent sulfide. Effluent sulfate began to decrease at day 22 from the influent concentration of 6.4 mM, and was 2 mM by day 70, after which it was relatively constant averaging 1.4±0.5 mM. Sulfide was measurable in effluent starting at day 25, and increased through day 70. Subsequently, effluent sulfide was somewhat constant, but varying irregularly, averaging 5.4±1.2 mM, through day 221. Although the effluent sulfate during this steady state period was comparable to column A, a factor of two higher steady state effluent sulfide was observed in column B compared to column A.

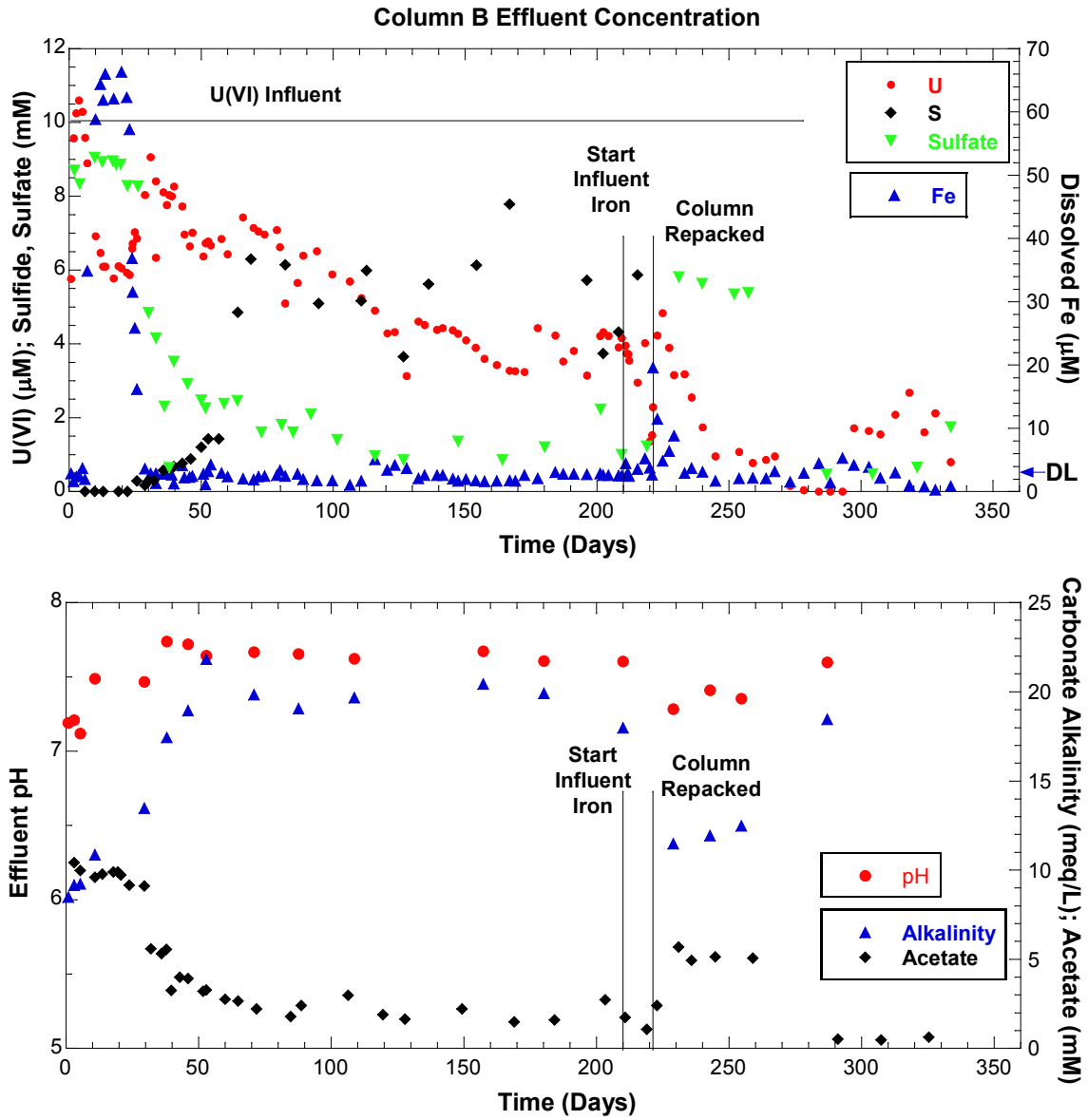

Figure 3. Effluent concentrations of (top) dissolved uranium, iron, sulfide and sulfate and (bottom) pH, carbonate alkalinity for column B during biostimulation elution versus time from start of biostimulation. Iron concentrations below the 3μM method detection limit are plotted as the measured value.

Effluent alkalinity increased from the influent level about 20% during the first 10 days followed by a further increase to about 20 meq/L by day 45. Alkalinity was relatively constant and averaged 19.7±1.1 meq/L from day 45 to day 221. Concurrently, effluent pH increased to 7.6 by day 38, 0.6 pH units above the influent. Effluent pH was relatively constant and averaged 7.65±0.04 from day 45 through day 221.

Effluent [U] increased to the influent concentration (10 uM) over the first three days of the experiment. [U] then decreased and was 6 μM by day 16. Effluent [U] then increased to about 8

μM by day 32. This increase coincided with the increases in pH and alkalinity during the onset of sulfate reduction. Subsequently, effluent [U] decreased slowly to 4 μM by day 211, although somewhat irregularly. By comparison, column A effluent [U] had decreased to 3 μM after 110 days.

Addition of 15 μM ferrous iron to the influent flow started on day 211. Within 10 days of the start of iron addition, the back pressure in column B had increased to above 30 PSI the limit for the apparatus. To resolve the back pressure, the column was subsampled in the anaerobic chamber, and the remaining sediment homogenized and repacked into a new column. The biostimulation experiment was then continued with 15 μM ferrous iron added to the acetate and U influent stream. Effluent [U], acetate and sulfate all increased to about half the influent concentration (Figure 3). During this period [U] steadily decreased while acetate and sulfate at these levels until 40 days later (day 260). Both subsequently decreased to <1 mM for the duration of the experiment. Effluent [Fe] increased for a short period of time, then was very low (<3 μM) for the remainder of the experiment. Effluent sulfide was not sampled until 50 days after repacking of column B; from this point it was about 4 mM for the remainder of the biostimulation experiment. Effluent [U] decreased from day 221 to about 1 μM by day 240, remained constant through day 270.

The column B experiment suffered from two inadvertent errors in influent preparation. First, the ferrous iron reservoir was replenished at day 267 but with a factor of ten lower concentration. This error was not corrected until day 328. Second, the AGW reservoir that also contains U and acetate was prepared with a much lower [U]. This lower [U] influent was used from day 273 to day 296, at which point it was restored to the intended 10 μM. This period coincided with near zero effluent [U]. Three days after the influent [Fe] was restored to the intended concentration on day 328, the column back pressure exceeded its limit again. The experiment was terminated and column sediments sampled in the anaerobic chamber for analysis. Column B thus underwent biostimulation with acetate for 211 days with 10 μM [U] added in the influent. The influent included 15 μM ferrous iron for 40 days during which time the column was repacked. The influent then had 1.5 μM ferrous iron for 61 days. Acetate and [U] input continued throughout this time but U input was much lower.

3.1.3 Column C Effluent History during Biostimulated Reduction

Flow through the third column, C, was started on March 5, 2010. This column was intended to be identical to columns A and B and thus its pore volume and flow rate were similar to the other columns (Table 2). Ferrous iron (15 μM) was added to the influent stream from the start of biostimulation of column C with the intent of producing additional iron sulfides to test their effect on U sequestration during biostimulation and on U remobilization during oxic elution.

The effluent profile for column C is similar to both columns A and B with respect to the timing of the onset of both iron and sulfate reduction. Acetate was near constant for the first 20 days during which time effluent [Fe] increased to 70 μM (Figure 4). Subsequently, both effluent acetate and [Fe] decreased. Effluent [Fe] decreased to <3 μM by day 40 at which time measurable sulfide was observed in the effluent. Effluent sulfate decreased from the influent concentration between days 24 and 31, and was <2 mM by day 60. Sulfate remained at about 2 mM though day 130. Sulfide increased to 3 mM by day 40. No effluent sulfide samples were collected between day 61 and day 132. Sulfide varied between 4 and 5 mM from day 132 to day 186.

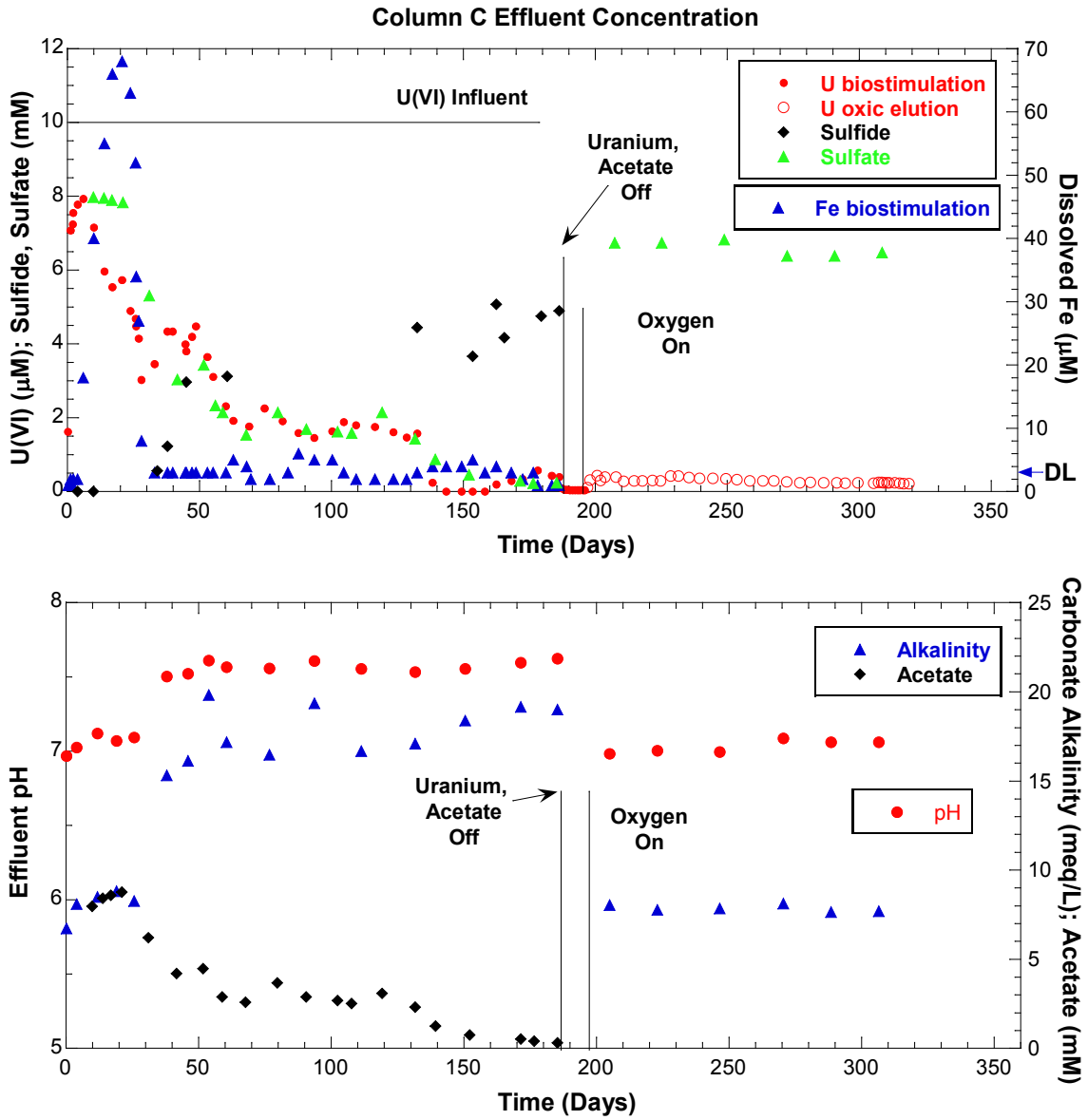

Figure 4. Effluent concentrations of (top) dissolved uranium, iron, sulfide and sulfate and (bottom) pH, carbonate alkalinity for column C during biostimulation and during oxic elution versus time from start of biostimulation. Iron concentrations below the 3μM method detection limit are plotted as the measured value.

Column C effluent pH and alkalinity began increasing on day 38 concurrent with the increase in sulfate reduction. pH varied little from this point through day 186 averaging 7.57±0.04. Effluent alkalinity also was elevated during this period, varied little and averaged 17.7±1.5 meq/L.

Effluent [U] increased through the first four days to 8 μM, 2 μM less than the influent concentration. Effluent [U] then decreased to 3 μM by day 28 followed by an increase to 4 μM during the onset of sulfate reduction and higher pH and alkalinity at about day 40. After 10 days, [U] decreased to 2 μM over the next 10 days, and subsequently varied little through day 132. At

this point [U] decreased to near zero at day 136 through day 159 as a result of the improper reservoir preparation described for column B. The biostimulation stage continued using the correct influent [U] from day 159 through day 186. As described for column B, column C also received the lower influent [Fe] starting at day132 through to the end of the biostimulation stage of the experiment at day 186.

3.1.4 Integrated Column Effluent Concentrations during Biostimulation

The overall characteristics of effluent profiles in all three columns indicate that the sequence of biogeochemical processes that occurred was the same and had similar timing. A more detailed comparison among columns is provided by estimating the extent of reactions from the effluent profiles of each column during biostimulation. The effluent water chemistry data were integrated to estimate total loading of uranium, reduction and dissolution of iron, loss of sulfate, production of sulfide, and production of total dissolved carbonate. Column B effluent changes were integrated to the start of ferrous iron addition. For U, sulfate, and acetate loss (or consumption) was calculated for each sample by subtracting the measured effluent concentration from the average measured concentrations in the influent reservoir. The change in concentration was then multiplied by the volume, in liters, of effluent sample collected. For total dissolved carbonate (TCO_2), the production during each sample collection period is the difference between the measured concentration and the average influent concentration measured in reservoirs multiplied by the volume of effluent collected for each sample. The change in concentration of samples not analyzed was set to the average of adjacent measured samples and then multiplied by its respective sample volume. The resulting change in each constituent in units of millimoles (micromoles for U) in each sample was then summed over the duration of the biostimulation. The integrated Fe release from column C is calculated both by assuming the Fe added to the influent is transported conservatively through the column, and by assuming the influent Fe was all retained in the column. The later provides an upper limit of total iron released from sediments and transported out of column C. The results of the total mass of production or loss of these constituents from the effluent integrations are summarized in Table 3. The uncertainty in these integrated changes is difficult to assess but likely is greater for constituents that were sampled or analyzed infrequently and at irregular intervals such as acetate, sulfide and sulfate.

The uptake of U during biostimulation was divided by the total dry mass of sediment in the column and plotted as micrograms U per gram solid versus time to illustrate the cumulative loading of U onto the sediments (Figure 5). Normalizing U uptake by total dry weight assumes uniform distribution of U uptake on the entire sediment mass in the column. The normalized cumulative U uptake in the three columns was similar over the first 20 days. Subsequently the rate of uptake in column A was greater than column B through 110 days despite the same influent amendments and nearly identical columns. Uranium uptake continued in column A after the acetate amendment was ended at 110 days, and occurred at a slightly greater rate. About one third (20.6 umol) of total U uptake in column A occurred after acetate amendment was halted (Table 3). Uranium input to column A ended at day 150, after which a decrease in calculated U loading was observed and equaled about 8% of the total U uptake. The total U uptake at the end of the biostimulation stage was about 62, 74, and 106 µmol in columns A, B and C, respectively, which equals retention of 52, 48 and 76% of the total U added to columns A, B and C, respectively (Table 3). The rate of U uptake for column C was substantially greater than column A or B after the first 20 days. The presence of 15 µM ferrous iron in the column C influent was the only difference in the three experiments.

Table 3. Integrated loss and gain from column effluent concentrations during acetate biostimulation. Units are millimoles except for uranium, which is in micromoles.

Constituent	A effluent	A sediment	B effluent[d]	B sediment	C effluent	C sediment
Total pore volumes	**315**		**415**		**401**	
U input	**118.3**		**154.8**		**137.0**	
U uptake	**61.6**[a]	**48.8**	**73.8**	**62.6**	**106**	**47**
U (μmol/g)[e]	**0.27**		**0.32**		**0.51**	**0.16**
% U retained	**52**		**48**		**76**	
U released (oxic)	**10.6**	**3.4**			**2.5**	**2.3**
Fe reduced	**0.084**	**9.1**	**0.110**	**9.5**	**0.081**[b] **0.110**[c]	**6.4**
Fe released (oxic)	**0.025**		**n.a.**		**n.m.**	
Acetate consumed	**46**		**85**		**71**	
Total CO_2 produced	**n.m.**		**160**		**120**	
Sulfate reduced	**33.2**		**64**		**78**	
Sulfide produced	**12.2**		**66**		**44**	
S retained		**5.7**		**8.3**		**7.8**

a. Total U uptake during biostimulation and after cessation of acetate. A total of 20.4 μmol U uptake occurred over 36 days (71 pore volumes) after acetate was removed from influent.
b. Integrated effluent iron corrected for the 15 μM influent Fe assuming that the influent Fe was transported through column without reactive loss.
c. Integrated effluent iron not corrected for 15 μM influent Fe.
d. Values for column B are prior to start of ferrous iron addition to influent.
e. Uranium uptake normalized to total dry mass of sediment in column.
n.m. and n.a. stand for not measured and not applicable, respectively.

Assuming effluent Fe is all Fe^{2+} released as a result of microbial iron reduction, the transport of iron out of the columns ranged from 0.8 to 0.11 mmoles, with greater amount for column B, which had a longer biostimulation period (Table 3). The peak of effluent Fe in the first 30 days accounted for 70 to 95% of the total effluent iron. This comparison for column C was made assuming the influent Fe was not transported out of the column. Effluent samples at or below the Fe detection limit (3 μM after dilution correction) were considered zero in these integrations.

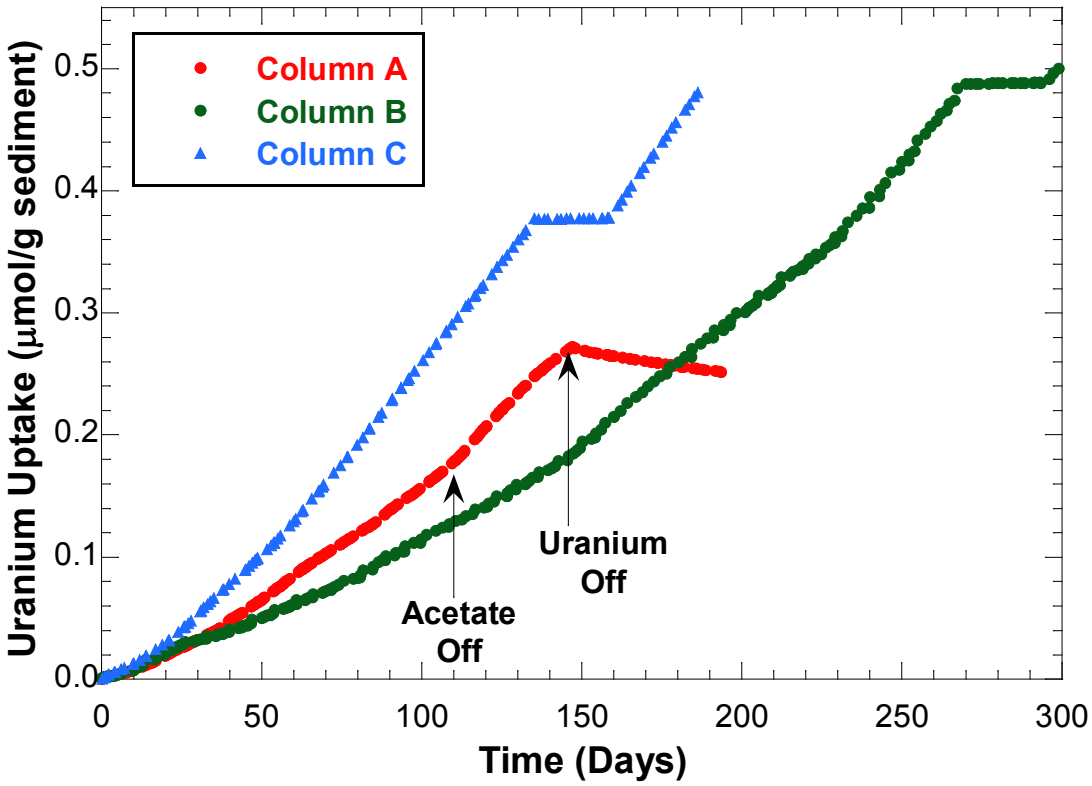

Figure 5. Cumulative uranium loading on column sediments during biostimulated reduction, in micromoles of uranium per gram of column sediment versus time.

Comparison of the integrated sulfate decrease with the integrated effluent sulfide transport out of the columns indicates the sulfate reduction was about equal (column B) or exceeded the integrated effluent sulfide by a factor of 2.7 and 1.7 for columns A and C, respectively (Table 3). This comparison does not include solid phase sulfide, such as FeS precipitation. Inclusion of solid phase sulfide measured in the sediment subsamples at the end of biostimulation does not close this balance for columns A and C (Section 4.1.1). There may be a component of colloidal iron sulfide in the effluent since it can be measured by the same method used here. However, the effluent stream passed through a 0.22 micron filter before entering the sample vial or bottle, so it is assumed that sulfide measured in the samples represent dissolved (<0.22 um) sulfide. Uncertainty in the integrated sulfate mass because of sampling infrequency and poorly constrained influent sulfate concentration likely contributed to this imbalance in columns A and C.

The integrated acetate consumption was greater as expected for the longer biostimulation period (Table 3). Oxidation of acetate to CO_2 has a 1:2 reaction stoichiometry. The molar ratio of total CO_2 produced to acetate consumed was 1.9 and 1.7 for columns B and C, respectively. Total CO_2 was not measured in column A effluent during the first half of the biostimulation period. Ratios lower than 2 may be the result of other microbial pathways of acetate consumption such as fermentation. Alternatively, these ratios may be the result of measurement and integration uncertainty. Assuming sulfate reduction is the dominant electron pathway for acetate oxidation, acetate consumption and sulfate reduction should be equivalent. The ratio of acetate consumed to sulfate reduced was 1.4, 1.3 and 0.9 for columns A, B and C, respectively. The contributions of iron and uranium reduction to electron balance are small. The deviation of

up to 40% from the balance between total sulfate reduction and acetate consumption from the inferred reaction stoichiometry (1:1) is attributed to the uncertainties in the integrated values resulting from sampling infrequency and uncertainty of the influent concentrations, but may also result from other pathways of acetate consumption.

3.2 Oxic Elution

The large extent of sequestration of dissolved uranium over the course of the biostimulation stage in all three columns suggests that stimulation of the ambient microbial population in the Old Rifle aquifer sediments may be an effective means of remediating dissolved uranium in groundwater at contaminated sites. The removal of dissolved uranium, which is in the +6 oxidation state, likely occurred predominantly by reduction to U(IV) and precipitation, since the +4 oxidation state has much lower solubility than U(VI) for the groundwater chemistry of the Old Rifle site. Measurement of the U oxidation state and characterization of the form of the U removed during biostimulation is presented in section 3.4.1. Determining the stability of the bioreduced uranium in response to changes in groundwater chemistry after biostimulation has ceased, such as the return to oxic conditions, is needed to evaluate if the biostimulated reduction process would be an effective tool for long term remediation of U-contaminated shallow aquifers. Elution of columns A and C sediment was conducted using AGW at equilibrium with atmospheric oxygen. This oxygen level was used to assess the upper limit of dissolved oxygen in recharge water.

Prior to oxic elution, sediments from both columns were subsampled, and the remaining sediment homogenized and repacked into new columns (see section 2.2.4). This sediment is subsequently referred to as the composite sediment. A layer of sterilized Ottawa sand was used at the inlet end (bottom) of the columns to account for mass of sediment removed during subsampling. The new columns had a uniform distribution of sequestered uranium prior to the start of oxic elution.

After repacking, anoxic AGW was flowed through column A for 1 day. Effluent [U] increased in the first 5 hours to 4.5 μM, well above the 1.2 uM at the end of the anoxic stage prior to repacking. Effluent [U] then decreased. The oxic gas mixture was introduced to the influent reservoir 24 hours after flow commenced through the repacked column. Effluent [U] decreased over the next 15 days to 1 μM, and subsequently varied little for the duration of the experiment averaging 0.85±0.11 μM (Figure 6). Effluent [Fe] decreased from 18 μM during the initial anoxic AGW flow through the repacked column then decreased further to <5 μM over the first 3 days of oxic AGW influent flow (Figure 2). Subsequently, [Fe] was at or near the 3 μM detection limit for the duration of the oxic elution stage. No measurable difference was observed between influent and effluent sulfate, pH, alkalinity or major cations throughout the oxic elution.

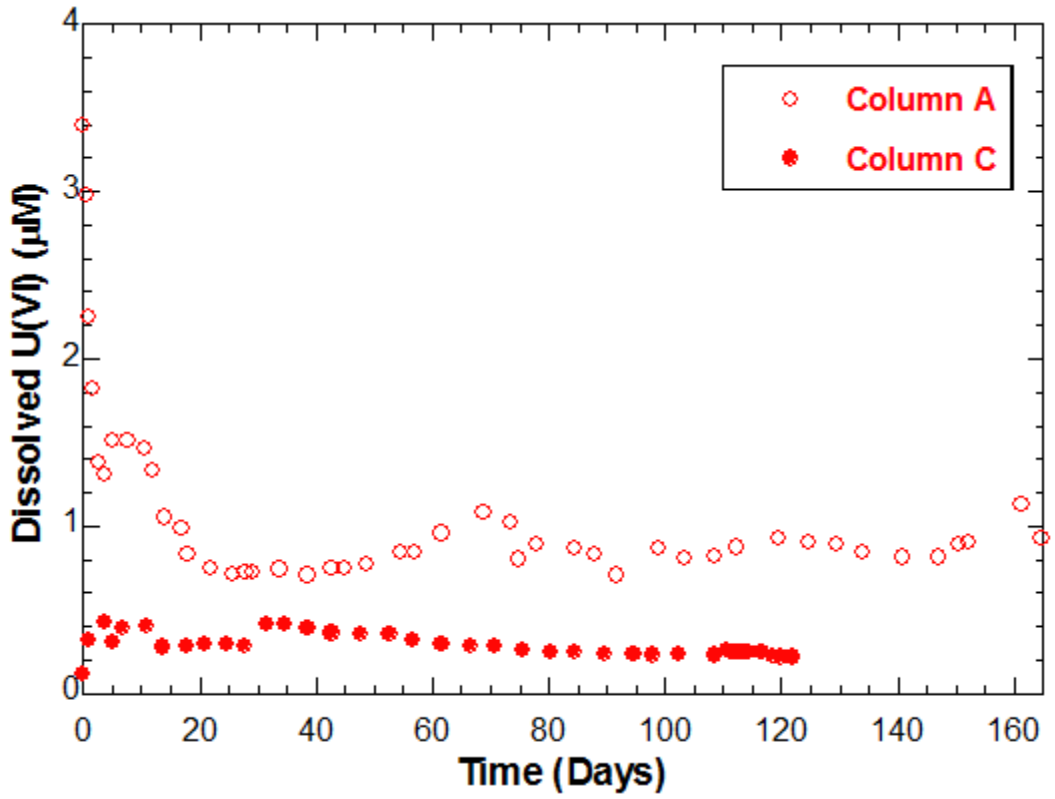

Figure 6. Effluent dissolved uranium from column A and column C during oxic elution versus days following introduction of dissolved oxygen to column influent.

Column C effluent had a much lower [U] (0.1 μM) during the first 24 hours of flow with anoxic AGW after repacking. Upon introduction of oxygen to the influent reservoir, effluent [U] increased to ~0.4 μM (Figure 6). Over the next 30 days of oxic elution effluent [U] varied slightly averaging 0.34±.07 μM. Subsequently, effluent [U] decreased gradually to 0.22 μM by the end of the experiment 86 days later. Effluent [Fe] was equal to or less than 3 μM throughout the oxic elution. No measurable difference was observed between influent and effluent sulfate, pH, alkalinity or major cations throughout the oxic elution of column C.

Overall, remobilization of uranium from column C during oxic elution resulted in about a factor of 4 lower integrated effluent dissolved [U] than was observed for column A. After 121 days of oxic elution, 2.5 μmol U, or about 3% of the total U uptake during biostimulation, was remobilized from column C. In contrast, 10.6 μmol, or 23% of the total U uptake, was released from column A over 161 days. Based on the integrated effluent, the total U uptake by column C (106 μmols) during biostimulated reduction was about a factor of two greater than for column A (62 μmols), in part because of the longer biostimulation period. In addition, the total U uptake in column C was substantially greater after 110 days of acetate and U(VI) inflow, 65 μmols, compared to 41 μmols U in column A at 110 days when acetate input was halted in column A. An additional 20 μmols of uranium uptake occurred in column A over the 36 days after the acetate amendment ended.

The release of uranium from sediments over time from the two columns is shown in Figure 7. These plots are based on incremental loss described by the mass of U measured in each effluent sample subtracted from the remaining sediment U mass at the start of each sampling

interval. The initial total sediment U concentration at the start of oxic elution was set at the measured total U in composite sediment used to repack the columns for oxic elution. In both columns the decrease in sediment loading occurred at near constant rates with the change in sediment U per gram versus time yielding release rates of 3.4E-9 and 1.2E-9 mol U/g sediment/day for columns A and C, respectively.

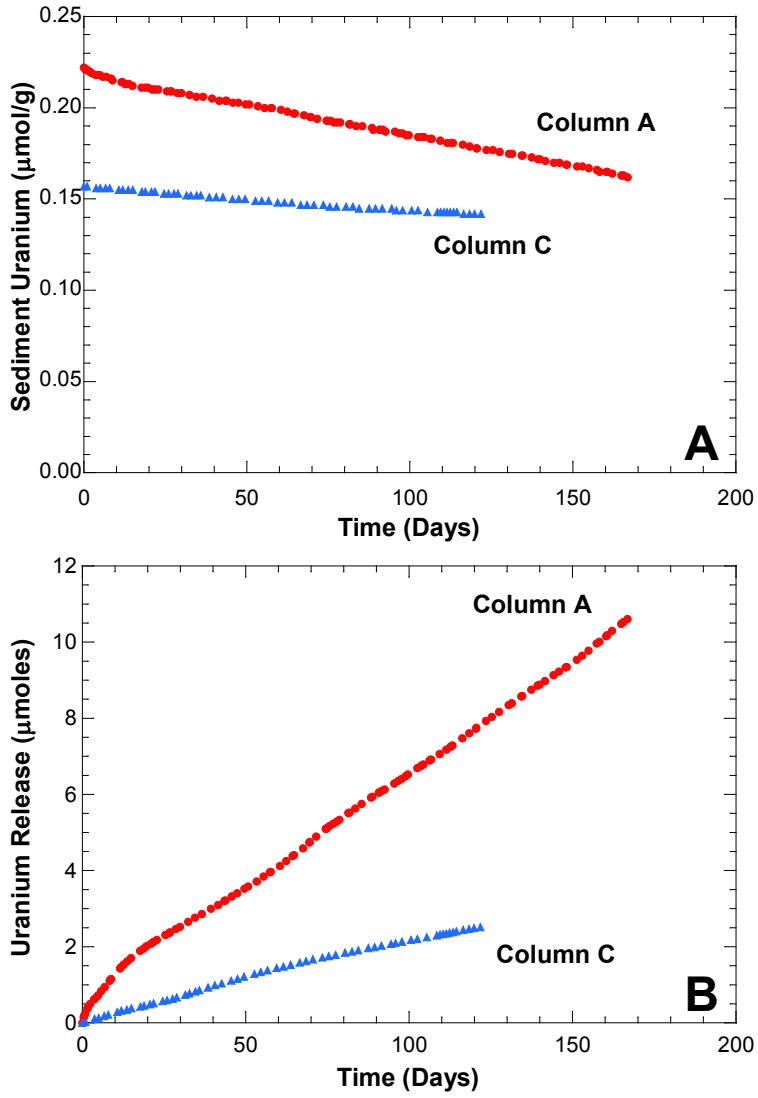

Figure 7. Change in sediment uranium concentration during oxic elution, plotted as (A) micromoles U per gram remaining on sediment versus days since the start of suboxic elution, and (B) cumulative mass of uranium release in micromoles versus time.

The cumulative release of U in micromoles versus time (Figure 7B) further illustrates the significantly greater remobilization rate of sequestered U from the column A sediments compared to column C. In both columns the release of U is a continuous process at near constant rates that continues for more than 120 days or 300 pore volumes. The primary difference between column A and C was the addition of 15 µM ferrous iron throughout the biostimulation period of column C. The ferrous iron may have contributed both to the greater sequestration of U through abiotic reduction of U(VI) by the additional FeS produced in column

C, and to limiting remobilization of U during oxic elution likely because of competition for oxygen, or by armoring of sequestered U shielding it from the solution phase.

3.3 Solid Phase Analyses

The BH-02 shallow aquifer sediment used for the column experiments consisted of a coarse sand with about a 20% coarser fraction (Table 4) despite being purported to be <2 mm. This sediment is referred to from here on as the pre-column sediment. This material also had a large component of silt and clay size sediment (<63 μm), 12% by weight. Grain size was determined by wet sieving to remove the fines (<63 μm), followed dry sieving of the remaining coarser material. The bulk sediment surface area determined by N_2-BET was 3.4 m^2/g. The <63 μm fraction accounted for about 60% of the surface area. Quantitative XRD analysis and chemical extractions of the pre-column sediment was conducted on the <2 mm fraction. The non-clay fraction of pre-column sediment is dominated by quartz (>50% by weight) with lesser amounts of feldspars (Table 5). Iron oxides comprised about 6%, and calcite 1.6%. Gypsum was not detected (<0.5%). Clays comprised about 7% of the sediment with muscovite the most abundant.

Total carbonate by CO_2 evolution on acidification was 1.6% as CO_3, or 2.7 % as $CaCO_3$, which is comparable to 1.6% calcite determined by XRD. The pre-column sediment total U was 1.7 μg/g or 0.007 μmol/g indicative of uncontaminated sediment. Extractable Fe and total S content are presented in Table 6 and discussed in relation to measurements of column sediment after biostimulated reduction and after oxic elution.

Table 4. Grain size distribution of Rifle BH-02 sediment used in column experiments, as determined by sieve analysis

Grain Size	Weight %	% finer	Surface Area	
			m^2/g	Fraction of surface area[a]
>2 mm	**18.5**	**81.5**	**n.m.**	
1 - 2 mm	**9.7**	**71.9**	**2.25**	**0.06**
0.5 - 1 mm	**30.8**	**41.0**	**1.60**	**0.14**
250 - 500 µm	**22.0**	**19.0**	**1.87**	**0.12**
125 - 500 µm	**3.1**	**15.9**	**2.20**	**0.02**
63 - 125 µm	**4.3**	**11.6**	**2.52**	**0.03**
<63 µm	**11.6**	**0**	**18.3**	**0.62**
Bulk sediment[b]			**3.43**	

a. calculated from weight % times surface area of fraction divide by bulk sediment surface area.

b. calculated from sum of measured surface area of grains size fractions times fraction of total mass

Table 5. Mineral weight percent of Rifle BH-02 sediment used in column experiments (pre-column) as determined by quantitative X-ray diffraction.

Mineral	Weight %
Non-Clays	
Quartz	**53.3**
Kspar (ordered Microcline)	**6.8**
Kspar (orthoclase)	**6.2**
Plagioclase (albite, var. cleavelandite)	**8.2**
Plagioclase (oligoclase; NC)	**3.2**
Plagioclase (oligoclase; Norway)	**1.5**
Plagioclase (andesine)	**5.2**
Plagioclase (anorthite)	**2.1**
Calcite	**1.6**
Ankerite	**0.7**
Magnetite	**0.6**
Hematite (fine grind)	**1.7**
Ferrihydrite (Humbug Creek)	**4.0**
Total non-clays	**95.0**
Clays	
Halloysite	**1.1**
Kaolinite	**0.7**
Biotite	**0.0**
Phlogopite	**0.3**
Muscovite	**5.5**
Total clays	**7.5**
Total	**102.5**

3.3.1 Column Sediment Subsamples Collected

At the end of biostimulation, column sediments appeared uniformly black, consistent with iron sulfide precipitation, in contrast to light brown color prior to biostimulation (Figure 8). During oxic elution, sediments changed from the black to brown.

Sediment samples recovered from the columns are listed in Tables 6, 7 and 8. Subsamples from columns A and C were collected after biostimulated reduction by coring the column down the center axis from the outlet end to inlet. Column B was also sampled by coring with a syringe barrel when it was disassembled to repack because of clogging shortly after the onset of ferrous iron input. Sediment surrounding the bottom of column B subcore near the inlet was collected. After removing the subcore, the remaining sediment was removed, subsampled, and then mixed to form the composite used for repacking for oxic elution. The excess composite was retained. Column B was sampled again at the end of biostimulation by removing the entire sediment in approximate 1 cm intervals until the Ottawa sand bed at the inlet end was reached. Column B sediment at the end of biostimulation appeared uniformly black in color.

Figure 8. Column A 26 days after the start of biostimulation (A), at the end of biostimulation (B), and after oxic elution (C). Photographs by C. Fuller.

During oxic elution the sediments of column A changed from black to brown with the transition proceeding from the inlet to the outlet in an irregular fashion suggesting preferential flow (Figure 8). Because of apparent channelized flow and distinct zones of oxidized and reduced sediment, twenty eight subsamples were recovered from column A after oxic elution. These included three syringe cores near the center of the column vertical axis starting from the outlet end (Figure 9). Cores were extruded in 5 intervals, each about 1 to 1.5 cm thick. The first ~1 cm of the subcores was in the Ottawa sand layer at the inlet end of the column. These sand intervals were not analyzed. Prior to removal of the cores, sediments surrounding the core barrels were removed in about 1-cm increments along the flow axis. These subsamples were chosen based on appearance to provide subsamples with differing apparent extent of oxidation (see Figure 9 and Table 6). A total of 28 sediment samples were recovered from column A following oxic elution, of which 23 were comprised of the aquifer sediment, with the remainder mostly Ottawa sand.

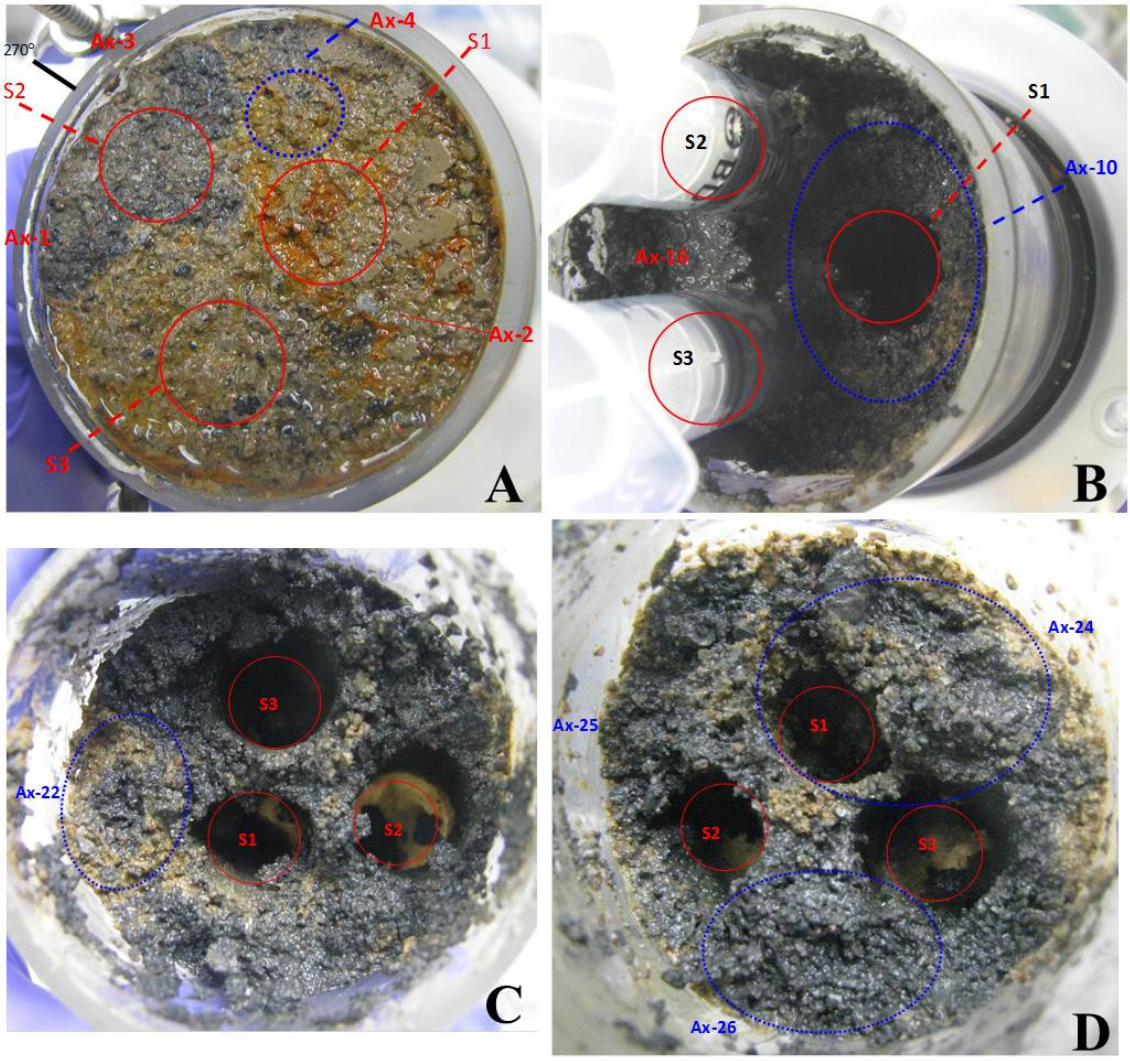

Figure 9. Column A sediments after oxic elution during subsampling depicting location of samples and variability in sediment appearance. (A) Column outlet end prior to subsampling. (B) After removal of syringe core S1 and ~1 cm of sediment. (C) After top 2 cm removed; note clockwise rotation of ~90 degrees. (D) After top 3 cm removed. Photographs by C. Fuller.

Column C after oxic elution was sampled using a spatula from the top downward in about 1 cm increments along the flow axis until the Ottawa sand layer was reached. The intervals sampled comprised the entire cross section of the column with the exception of the top interval. This interval was separated into two sections based on appearance. One portion, Cx-7, was brown suggesting more oxidation while the other, Cx-6, was black in color indicating it was still largely reducing (Figure 10). The brown portion spanned about 120 degrees of arc along the outside of the column and extended about 1.5 cm inwards in a wedge. The interval closest to the inlet also was brown. The other intervals were largely black.

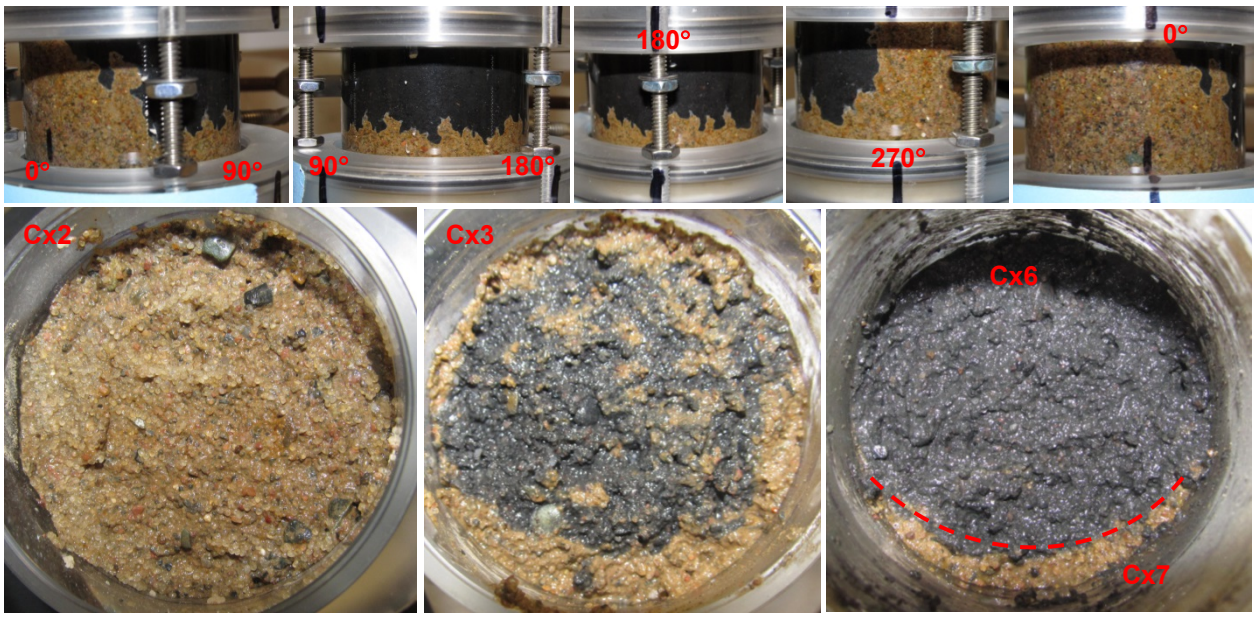

Figure 10. Column C at end of oxic elution, (Top) side view with degrees clockwise around column denoted (flow is from bottom to top); (bottom) surface of intervals view from inlet end prior to subsampling. Subsample IDs are shown in red. Photographs by C. Fuller.

3.3.2 Column A Sediment Chemistry after Biostimulated Reduction

Total U in the <2 mm fraction of the sediment at the end of the biostimulation stage of column A was much higher (0.30 μmol/g) in the first 1.5 cm interval of the syringe core compared to other subsamples (Figure 11). Sediment recovered from the inlet filter was almost a factor of two higher (0.54 μmol/g), suggesting most of the U sequestration occurred near the inlet end of the column. The sediment composited after the column was sub-cored, had a total U (0.26 μmol/g) almost as high as the core interval closet to the inlet (Figure 11; Table 6). The mass of U in each depth interval was calculated by multiplying the core interval sediment U concentration by the mass fraction of the column that depth interval represents times the total dry mass of the column. Summing total U of the intervals yields a whole column U content of 24 μmoles, which is more than a factor two lower than the whole column U mass of 57.7 μmoles based on the composite sediment U concentration. This difference indicates that after the first 1.5 cm of sediment, water largely by-passed the center of the column where the core was collected, and instead preferentially flowed around the outside of the center zone that was cored. The coarse grains (>2 mm), which were also black, contained 4 to 8% of the total U of the unfractionated sediment but account for 18.5% of the sediment mass. Based on the <2 mm composite sediment U concentration and accounting for the distribution among coarse and fine grain sediments yields a total column U uptake of 48.8 μmoles. This is about 20% lower than U uptake of 61 μmoles estimated by integrating the column effluent [U] (Table 3). About ~4 μmol were released during the period of flow without U or acetate in the influent, which is about one third of the difference between the two measurements of total U.

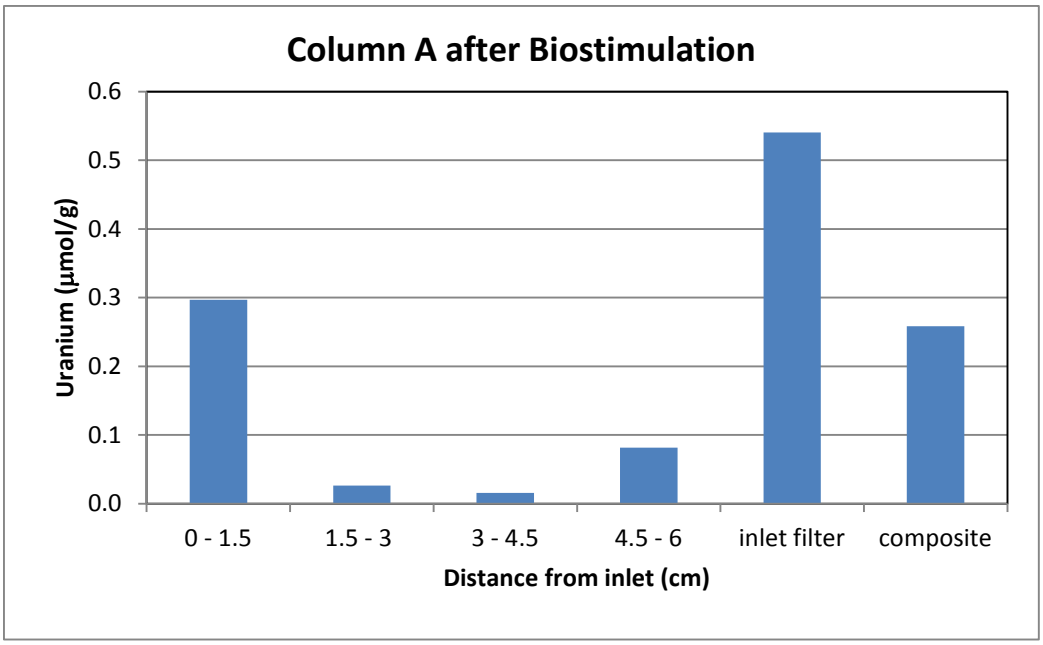

Figure 11. Total uranium concentration (µmol/g) of <2 mm sediment from column A after biostimulated reduction versus distance from inlet.

In column A, Fe(II) extracted by 0.5 N HCl for 1 hour increased during the biostimulation phase by 6 to 8-fold compared to the pre-column BH-02 sediment (Figure 12). This comparison is based on the <2 mm fraction. The extractable Fe(II) of coarser sediment was not measured but likely would not impact this trend. The composite sediment was higher than any of the subsamples but in most cases only by about 10%, which is the variability in extraction of replicate samples (Table 6). The whole column increase in Fe(II) was 6.6 mmoles using the mass weighted sum of the core intervals, or 9.1 mmoles using the composite Fe(II) concentration. Both are about two orders of magnitude greater than the integrated effluent iron indicating that a large majority of iron reduction resulted in iron sulfide precipitation or was Fe(III) in layer silicates reduced in place and not mobilized into solution. Reduction of Fe(III) in phyllosilicate minerals by dissimilatory microbial iron reduction can be significant in aquifer sediments (Wu *et al.*, 2012; Lee *et al.*, 2012; Komlos *et al.*, 2007). However, ferrous iron produced by reduction of Fe(III) silicates may not be quantitatively extracted by 0.5 N HCl since silicate phases are not dissolved by HCl. Thus, total iron reduction may be under estimated by an unknown amount. Total Fe (Fe(II) plus Fe(III)) in the 0.5N HCl extracts equaled the Fe(II) in the column sediments, whereas the pre-column sediment was about 20% Fe(III) (Table 3). This finding indicates the easily extractable Fe(III)in the pre-column sediment likely was reduced during biostimulation.

By the end of the biostimulation of column A, total sulfur increased about 3-fold from the pre-column sediment total S (Figure 13, Table 6) and averaged 0.031±.0004 mmol/g compared to 0.01 mmol/g for the pre-column. The increase in total S was slightly higher in the subsection closest to the inlet. Acid volatile sulfur (AVS) accounted for most of the increase in total S and was not detected in the pre-column sediment (< 0.001 mmol/g). AVS is a measure of sulfide (S^{-2}) species in the sample such as FeS that are liberated upon acidification forming H_2S gas.

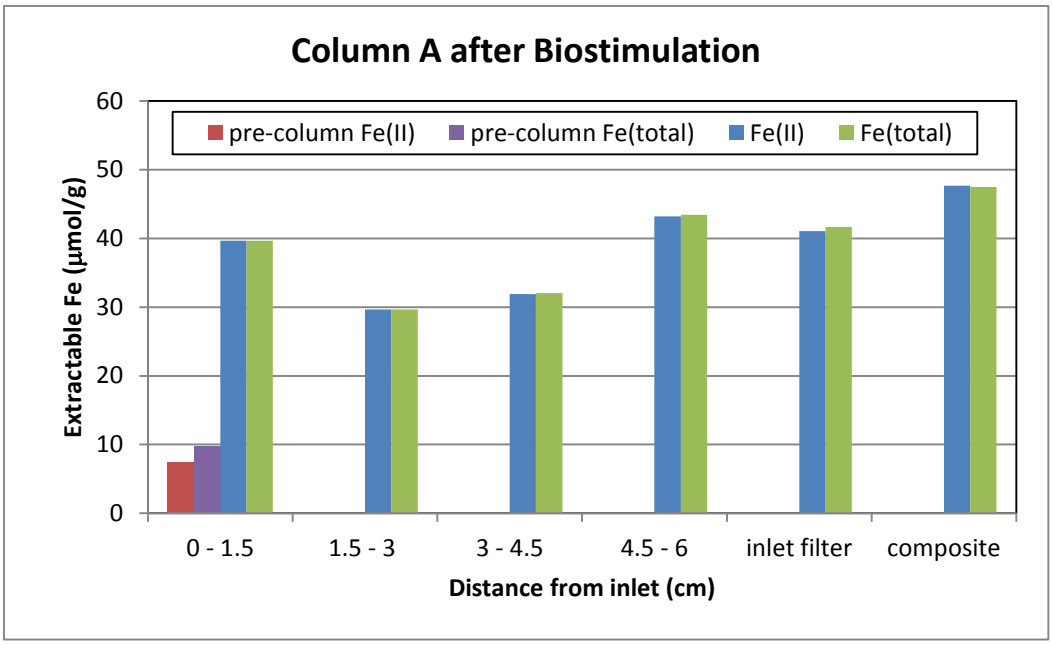

Figure 12. 0.5 N HCl extractable Fe(II) and total Fe (µmol/g) of <2 mm sediment from column A after biostimulated reduction versus distance from inlet.

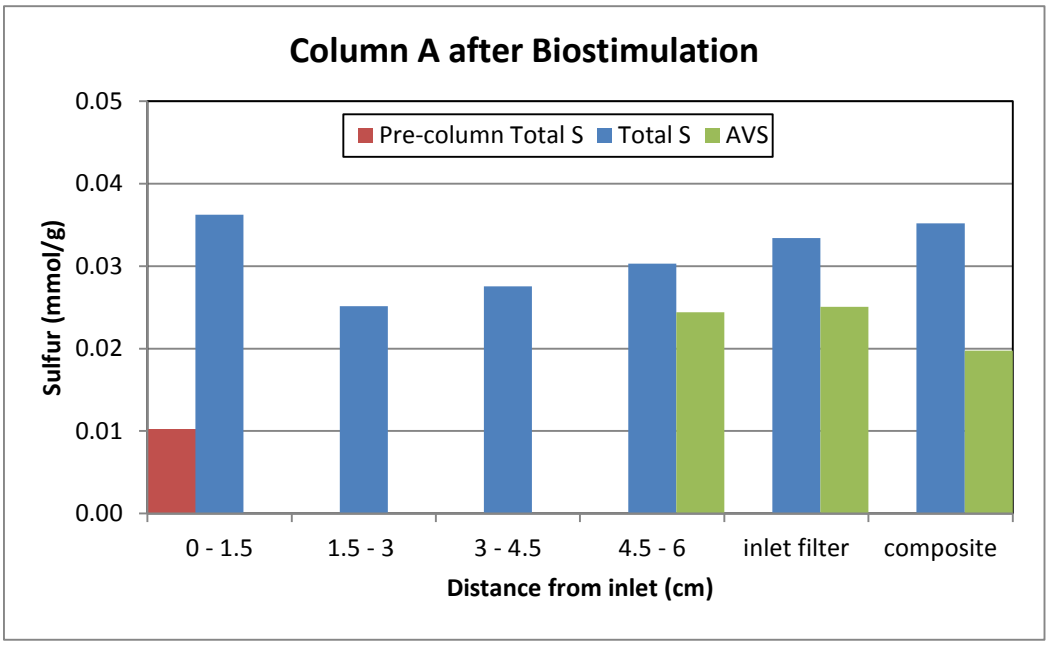

Figure 13. Total and acid volatile sulfur of <2 mm sediment from column A after biostimulated reduction versus distance from inlet. Pre-column is for total sulfur only; acid volatile sulfur not detected.

The method used does not reduce more oxidized forms of S such as elemental sulfur (S^o) or S^{-1} in FeS_2. For example, the column A composite sediment total S increased by 0.025 mmol/g after biostimulation and had an AVS of 0.019 mmol/g, which accounts for about 75% of the total S increase. The remaining S likely is in the form of elemental S or other less reduced sulfur species such as FeS_2. On a whole column basis, total S increased by 5.7 mmoles of which 4.4

mmoles were AVS. By comparison, the integrated effluent sulfide was 12.2 mmoles. Combined these yield a total sulfate reduction of 17.9 mmoles, which is significantly lower than the loss of sulfate (33.2 mmoles) calculated by integrating the change in effluent sulfate. Total S in the >2 mm sediment was not measured but AVS of the >2 mm accounted for about 20% of the unfractionated sediment AVS. Assuming a similar contribution of the >2 mm sediment to the total S would not increase the retained S sufficiently to close the difference between the two methods of estimating total S reduction during biostimulation. The increase in total S retained in the column (5.7 mmoles) is about 60% of the increase in extractable Fe(II), with AVS equal to about 50% of the increase in sediment Fe(II), suggesting about half of the ferrous iron increase is in the form of FeS. These processes are illustrated in the following reactions:

$$FeS + H_2S \leftrightarrow FeS_2 + H_2$$

Transformation of FeS to FeS_2 by reaction with H_2S is the primary pathway for pyrite formation under anaerobic conditions in groundwater systems (Maurer and Rittmann, 2004).

Stable sulfur isotopes measured during the total S analyses ranged from -1.14 to -3.18 per mil $\delta^{34}S$, which represents depletion in the heavier isotope, ^{34}S, of -0.74 to -2.78 per mil (‰) $\delta^{34}S$ relative to the pre-column sediment $\delta^{34}S$ of -0.40 ‰. The decrease in $\delta^{34}S$ is indicative of fractionation of S isotopes with the lighter isotope, ^{32}S, preferentially reduced and precipitated. The ^{34}S depletion was greater for samples which had the greatest increase in total S. The $\delta^{34}S$ of the S retained or precipitated in the column was calculated based on two component mass balance,

$$\delta^{34}S_{tot} * S_{tot} = \delta^{34}S_{ppt} * S_{ppt} + \delta^{34}S_{pre} * S_{pre},$$

where, $\delta^{34}S_{tot}$, $\delta^{34}S_{ppt}$, $\delta^{34}S_{pre}$ are the sulfur isotope ratios for the total S after biostimulation, the S precipitated in the column, and the S initially in the sediment prior to biostimulation, respectively, and S_{tot}, S_{ppt}, S_{pre} are the concentration of S in the sediment after biostimulation, S precipitated during biostimulation, and the initial total S in the sediment.

The $\delta^{34}S$ of the precipitated S calculated from this equation ranges from -1.59 to -4.45 per mil, which is a fractionation of about -1.4 to -4.3 per mil relative to the AGW sulfate $\delta^{34}S$ of 0.01 ‰. By comparison, the $\delta^{34}S$ of the total S of the column sediment would range from -0.10 to -0.15 per mil if no fractionation of the AGW sulfate S occurred during reduction. This was calculated using the above equation substituting the AGW sulfate $\delta^{34}S$ (0.01 per mil) for $\delta^{34}S_{ppt}$ and solving for $\delta^{34}S_{tot}$. Microbial sulfate reduction typically results in isotope fractionation on the order -20 or more ‰ $\delta^{34}S$ (Habicht and Canfield, 1997), but the extent of fraction is a function of reduction rate and availability of electron donor and sulfate (Sim *et al.*, 2011). In systems such as these column experiments where there is a continuous supply of both and neither is depleted or limiting, the fractionation factors are expected to be small. Thus, the observed S isotope fractionation, although low, is consistent with a microbial reduction process, which is expected in the biostimulation columns.

Table 6. Sediment chemistry for column A after biostimulated reduction and after oxic elution. Table continues on the following three pages.

Interval ID	Interval, cm from inlet	Description	Fraction of column[a]	Fraction >2 mm	U gamma[b] µmol/g	U <2 mm µmol/g	Interval U <2 mm µmol[c]	U >2 mm µmol/g	U total sediment µmol/g[d]	Interval total U µmol[e]
BH-02 pre-column sediment						0.007				
Column A Post Reduction		total dry sediment weight: 226.4 g								
Ar-1	0 - 1.5	syringe core interval	0.25	0.39	0.220	0.297	17.0			13.6
Ar-2	1.5 - 3	syringe core interval	0.24	0.26	0.163	0.026	1.4			1.2
Ar-3	3 - 4.5	syringe core interval	0.23	0.15		0.016	0.8			0.8
Ar-4	4.5 - 6	syringe core interval	0.28	0.16	0.159	0.082	5.1	0.025	0.073	4.5
Ar-5	inlet filter	inlet filter scrape		0.31	0.341	0.540		0.045	0.387	
Ar-6	composite[f]	remainder of column	1.00	0.21	0.254	0.258		0.087	0.222	
Total of core intervals[g]							24.4			20.1
Total from composite[h]							57.7			48.8

a. Fraction of whole column dry sediment mass contained in sample interval.
b. Total uranium by gamma spectrometry.
c. Total U, Fe, or S in an interval calculated from <2 mm fraction concentration times interval fraction of total dry sediment mass.
d. Total U concentration of sediment calculated from the U concentration of the <2 and >2mm fractions times their mass fraction.
e. Uranium of whole interval calculated from U concentration of the <2 mm and >2 mm fractions times interval fraction of total mass. The average ratio of >2 mm to <2 mm U concentration of all column samples is used to estimate the U contribution of the >2 mm fraction in cases where it was not measured.
f. Sediment remaining in column after syringe cores used to re-pack column for oxic elution.
g. Total mass of U, Fe or S in column calculated as the sum of the concentration measured in each interval times the interval sediment dry mass.
h. Total mass of U, Fe or S in column calculated from the concentration of the composite times the total sediment dry mass.
i. Fe(II) concentration of <2 mm size fraction extracted using 0.5N HCl for 1 hour.
j. One sigma standard deviation of the average of the analyses of replicate splits of sample.
k. Total Fe concentration of <2 mm size fraction extracted using 0.5N HCl for 1 hour.
l. AVS is acid volatile sulfur concentration of sediment.
m. Total AVS S concentration of sediment calculated from the AVS S concentration of the <2 and >2mm fractions times their mass fraction.

Table 6. continued.

Interval ID	Fe(II) <2 mm μmoles/g[i]	stdev[j]	<2mm interval total Fe(II) mmol[c]	Total Fe <2 mm μmoles/g[j]	stdev	Total S mmol/g	stdev[j]	Interval total S mmol	δ34S	stdev[j]	AVS S <2 mm mmol/g[l]	stdev[j]	AVS mmol/g >2 mm	AVS total sediment mmol/g[m]
BH-02	7.4	0.3		9.7	0.1	0.010	0.000		-0.40	0.21	<0.002			
Column A Post biostimulation														
Ar-1	39.6		2.3	39.6		0.036		2.08	-2.55					
Ar-2	29.7		1.6	29.7		0.025		1.37	-1.06					
Ar-3	31.9		1.7	32.0		0.028		1.44	-1.14					
Ar-4	43.2		2.7	43.4		0.030		1.90	-2.52		0.024	0.000	0.017	0.023
Ar-5	41.0			41.7		0.033			-3.18		0.025		0.019	0.023
Ar-6	47.7	3.8		47.5	4.7	0.035	0.000		-2.90	0.22	0.020	0.002	0.018	0.019
Total of core intervals[g]			8.3					5.65						
Total from composite			10.8					7.97						

Table 6. continued.

	Interval, cm from inlet	Description	Fraction of column[a]	Fraction >2 mm	U gamma[b] µmol/g	U <2 mm µmol/g	Interval U <2 mm µmol[c]	U >2 mm µmol/g	U total sediment µmol/g[d]	Interval total U µmol[e]
Post biostimulation composite				0.21	60	0.258		0.087	0.222	
Column A: Post oxic elution		total dry sediment weight: 177.4 g								
Ax-26	1 - 3	around syringe cores S2 and S3	0.076	0.2	0.152	0.194	2.6	0.108	0.177	2.4
Ax-24	1 - 3	1 - 3: around S1 towards S3	0.057	0.25	0.133	0.187	1.9			1.7
Ax-25	1 - 3	1 - 3: around S1 towards S3	0.034	0.25	0.073	0.093	0.6			0.5
Ax-12	1 - 2.3	S2 interval	0.025	0.17	0.085	0.232	1.0	0.113	0.211	0.9
Ax-18	1 - 2	S3 interval, browner on bottom	0.020	0.24	0.158	0.234	0.8	0.103	0.202	0.7
Ax-6	1 - 2.6	S1 interval	0.021	0.3	0.109	0.160	0.6			0.5
Ax-23	3 - 4	mostly black, mottled brown	0.127	0.24	0.142	0.226	5.1	0.024	0.177	4.0
Ax-22	3 - 4	around S1 and S3	0.066	0.24	0.072	0.109	1.3	0.233	0.139	1.6
Ax-19	2 - 3.3	S3 interval, mostly black	0.025	0.22	0.153	0.276	1.2			1.1
Ax-13	2.3 - 3.5	S2 interval	0.024	0.29	0.179	0.251	1.1	0.118	0.212	0.9
Ax-7	2.6 - 3.8	S1 interval	0.017	0.3	0.128	0.192	0.6			0.5
Ax-10	4 - 5	around S1	0.093	0.27	0.188	0.242	4.0	0.077	0.198	3.2
Ax-16	4 - 5	between S2 and S3	0.079	0.22	0.215	0.285	4.0	0.123	0.249	3.5
Ax-8	3.8 - 4.9	S1 interval	0.022	0.41	0.109	0.113	0.4			0.3
Ax-20	3.3 - 4.7	S3 interval	0.021	0.14	0.197	0.277	1.1			1.0
Ax-14	3.5 - 4.8	S2 interval	0.021	0.25	0.140	0.246	0.9	0.101	0.210	0.8
Ax-1	5 - 6	black below surface	0.070	0.19	0.188	0.244	3.0	0.085	0.214	2.6
Ax-2	5 - 6	top mottled orange; black below	0.079	0.24	0.195	0.366	5.1	0.117	0.306	4.3
Ax-3	5 - 6	between S1, S2:	0.063	0.23	0.197	0.288	3.2			2.8
Ax-4	5 - 6	between S1, S2: orange sediment	0.007		0.222	0.165	0.2			0.2
Ax-9	4.9 - 6	S1 interval	0.011		0.260	0.238	0.5			0.4
Ax-15	4.8 - 6	S2 interval	0.021	0.19	0.181	0.279	1.1			0.9
Ax-21	4.7 - 6	S3 interval	0.022	0.38	0.254	0.457	1.8			1.4
Total of intervals[g]							16.8			14.8

Table 6. continued.

Interval ID	Fe(II) <2 mm μmoles/g[i]	stdev[j]	<2mm interval total Fe(II) mmol[c]	Total Fe <2 mm μmoles/g[j]	stdev[j]	Total S mmol/g	stdev[j]	Interval total S mmol	δ34S	stdev[j]	AVS S <2 mm mmol/g[l]	stdev[j]	AVS mmol/g >2 mm	AVS total sediment mmol/g[m]
Composite	47.7	3.8		47.5	4.7	0.035	0.000		-2.90	0.22	0.020	0.002	0.018	0.019
Column A: Post oxic elution														
Ax-26	29.0		0.39	30.3		0.033		0.45	-2.33		0.010		0.016	0.012
Ax-24	31.7		0.32	31.7		0.027		0.27	-2.98					
Ax-25	24.3		0.15	25.7		0.021		0.13	-1.39					
Ax-12	31.6		0.14	32.2		0.031		0.13	-2.70		0.012		0.010	0.012
Ax-18	41.1		0.15	41.6		0.036		0.13	-3.17		0.014			
Ax-6	24.4		0.09	26.0		0.022		0.08	-1.87					
Ax-23	32.1	0.7	0.72	32.6	0.7	0.034	0.002	0.77	-3.00	0.05	0.010	0.001	0.009	0.010
Ax-22	26.1		0.31	27.5		0.023		0.27	-2.17		0.010		0.016	0.011
Ax-19	38.1		0.17	38.6		0.038		0.17	-3.95				0.023	
Ax-13	46.7		0.20	46.7		0.033		0.14	-2.57		0.020		0.010	0.017
Ax-7	26.0		0.08	28.1		0.026		0.08	-2.46					
Ax-10	34.9	1.5	0.57	35.6	1.0	0.032	0.001	0.53	-3.06	0.67	0.017	0.000	0.012	0.016
Ax-16	39.4		0.55	39.7		0.040	0.004	0.56	-5.09		0.019	0.000	0.014	0.018
Ax-8	18.3		0.07	21.8		0.020		0.08	-1.59					
Ax-20	42.0		0.16	44.4		0.046		0.17	-4.25					
Ax-14	39.0		0.15	39.4		0.041		0.15	-3.76				0.017	
Ax-1	32.7	0.3	0.40	33.1	0.1	0.030		0.37	-3.15		0.019	0.000	0.010	0.017
Ax-2	33.8	1.7	0.47	33.9	1.4	0.027		0.38	-2.45		0.016		0.009	0.014
Ax-3	32.2		0.36	30.8		0.030		0.33	-2.98					
Ax-4	33.6		0.04	33.2		0.022		0.03	0.27					
Ax-9	27.7		0.05	27.7		0.024		0.05	-2.60					
Ax-15	39.8		0.15	39.6		0.038		0.14	-3.07					
Ax-21	37.6		0.15	38.1		0.037		0.14	-4.95					
Total of intervals[g]			5.8					5.56						

Table 7. Sediment chemistry for column B during and after biostimulated reduction. See Table 6 for footnote description. Table continues on the following page.

Interval ID	Interval, cm from inlet	Description	Fraction of column[a]	Fraction >2 mm	U gamma[b] µmol/g	U <2 mm µmol/g	Interval U <2 mm µmol[c]	U >2 mm µmol/g	U total sediment µmol/g[d]	Interval total U µmol[e]
Column B: during biostimulation										
		total dry sediment weight: 231.8 g								
B1-5	0 - 0.2	~1 -2 mm on core hole bottom			2.27	n.a.				
B1-6	0 - 0.5	surrounding core hole ~ 5 mm		0.26	0.756	1.030				
B1-1	0 - 1.5	syringe core interval	0.28	0.34	0.102	0.085	5.6	0.032	0.067	4.4
B1-2	1.5 - 3	syringe core interval	0.26	0.19	0.024	0.030	1.8			1.6
B1-3	3 - 4.5	syringe core interval	0.22	0.22	0.019	0.024	1.2	0.009	0.021	1.0
B1-4	4.5 - 6	syringe core interval	0.24	0.21	0.043	0.072	4.1	0.029	0.063	3.6
B1-8	Composite[f]	surrounding core	1	0.28	0.202	0.331		0.055	0.261	
Total of core intervals[g]							12.6			10.6
Total from composite[h]							76.8			64.2
Column B: after biostimulation (end of experiment)										
		total dry sediment weight: 183.6 g								
Br-9	0 - 2	Ottawa sand: not analyzed	0.204							
B-F4	2 - 3	black sediment	0.172	0.19	0.350	0.353	11.2	0.127	0.310	9.8
Br-6	3 - 4	black sediment	0.208	0.25	0.298	0.510	19.5			16.4
Br-4	4 - 5	black sediment	0.171	0.26	0.251	0.351	11.0	0.125	0.292	9.2
Br-1	5 - 6	black sediment	0.245	0.14	0.354	0.390	17.6	0.178	0.361	16.2
B-F4 fines		fines separated from bulk				1.781				
Total of intervals[g]							59.2			51.6

Table 7. continued.

Interval ID	Fe(II) <2 mm μmoles/g[i]	stdev[j]	<2mm interval total Fe(II) mmol[c]	Total Fe <2 mm μmoles/g[j]	stdev[j]	Total S mmol/g	stdev[j]	Interval total S mmol	δ34S	stdev[j]	AVS S <2 mm mmol/g[l]	stdev[j]	AVS >2 mm mmol/g	AVS total sediment mmol/g[m]
Column B: initial subsampling during biostimulation														
B1-5	47.4			47.6										
B1-6	52.4			52.7		0.052			-2.86					
B1-1	42.3		2.78	42.5		0.037		2.44	-0.33		0.026		0.008	0.020
B1-2	40.3		2.40	40.3		0.036		2.17	-0.46					
B1-3	39.0		1.97	39.0		0.039		1.99	-0.49		0.028		0.015	0.025
B1-4	50.1		2.81	50.3		0.046	0.001	2.60	-1.40	0.04	0.032		0.021	0.029
B1-8	48.3	1.2		48.5	1.2	0.046					0.030	0.02	0.013	0.027
Total of core intervals[g]			10.0					9.2						
Total from composite			11.2					10.7						
Column B: after biostimulation (end of experiment)														
Br-9														
B-F4	51.9	1.1	1.64	52.1	0.0	0.056		1.78	-1.98		0.027	0.000	0.019	0.026
Br-6	50.6		1.93	51.2		0.070		2.65	-2.42		0.025		0.020	0.024
Br-4	49.9		1.56	49.7		0.052		1.64	-2.17		0.028			
Br-1	40.5		1.87	41.0		0.066	0.001	2.97	-2.17	0.01	0.029	0.001	0.011	0.026
B-F4 fines	142.6		7.0	143.9										
Total of all intervals[g]								9.0						

Table 8. Sediment chemistry for column C after biostimulated reduction and after oxic elution. See table 6 for footnote description. Table continues on the following page.

Interval ID	Interval, cm from inlet	Description	Fraction of column[a]	Fraction >2 mm	U gamma[b] µmol/g	U <2 mm µmol/g	Interval U <2 mm µmol[c]	U >2 mm µmol/g	U total sediment µmol/g[d]	Interval total U µmol[e]
Column C: Post Biostimulation		total dry sediment weight: 220.5 g								
Cr-4	0 - 1.7	syringe core interval	0.291	0.19	0.147	0.421	27.0	0.148	0.369	23.7
Cr-3	1.7 - 3.3	syringe core interval	0.218	0.24	0.039	0.011	0.5	0.010	0.011	0.5
Cr-2	3.1 - 4.4	syringe core interval	0.218	0.18	0.021	0.007	0.3	0.003	0.006	0.3
Cr-1	4.4 - 6	syringe core interval	0.273	0.20	0.041	0.077	4.6	0.021	0.066	4.0
Cr-5	0 - 1	surrounding core	0.167	0.18	0.406	0.580	21.3	0.346	0.538	19.8
Cr-6	1 - 2	surrounding core	0.167	0.18	0.126	0.183	6.7			6.0
Cr-7	2 - 5	surrounding core	0.500	0.25		0.143	15.8	0.006	0.109	12.0
Cr-8	composite[f]	composite of C5, C6, C7	1.000	0.27		0.213	47.0	0.005	0.157	34.6
Total of core intervals[g]							32.5			28.5
Total of C5, C6, C7							43.8			37.7
Total from composite[h]							47.0			34.6
Column C: Post oxic elution		total dry sediment weight: 167.8 g								
Cx-2	1.4 - 2.1	brown	0.086	0.32	0.054	0.046	0.7	0.015	0.036	0.5
Cx-3	2.1 - 2.9	black	0.214	0.23	0.148	0.190	6.8	0.069	0.162	5.8
Cx-4	2.9 - 3.8	black	0.259	0.27	0.171	0.194	8.4	0.053	0.156	6.8
Cx-5	3.8 - 4.8	black	0.194	0.20	0.187	0.207	6.7	0.036	0.173	5.6
Cx-6	4.8 - 6	black	0.197	0.26	0.194	0.176	5.8	0.084	0.152	5.0
Cx-7	5 - 6	oxidized wedge at outlet	0.051	0.28	0.060	0.045	0.4	0.022	0.039	0.3
Cx-6 fines		fines separated from bulk				0.965				
Total of intervals[g]							28.9			24.1

Table 8. continued.

Interval ID	Fe(II) <2 mm µmoles/g [i]	stdev[j]	<2mm interval total Fe(II) mmol[c]	Total Fe <2 mm µmoles/g[j]	stdev[j]	Total S mmol/g	stdev[j]	Interval total S mmol	δ34S	stdev[j]	AVS S <2 mm mmol/g[l]	stdev[j]	AVS >2 mm mmol/g	AVS total sediment mmol/g[m]
Column C: Post reduction														
Cr-4	50.8		3.26	51.1		0.039		2.52	-3.92		0.022		0.030	0.023
Cr-3	34.8		1.67	35.6		0.034		1.66	-0.08		0.012		0.019	0.014
Cr-2	38.8		1.87	39.0		0.030		1.43	-0.85		0.012		0.022	0.014
Cr-1	30.8		1.85	31.0		0.037		2.25	-2.34		0.019		0.031	0.021
Cr-5	36.3		1.33	36.3		0.037		1.35	-2.24		0.018		0.023	0.019
Cr-6	31.4		1.15	31.8		0.037		1.35	-2.37		0.019			
Cr-7	40.6		4.47	39.7		0.043		4.71	-2.36		0.025	0.000	0.018	0.023
Cr-8	36.6		8.06	39.4		0.046	0.003	10.08	-1.45	0.59	0.018	0.001	0.012	0.016
Total of core intervals[g]			8.7					7.9						
Total of C5, C6, C7			7.0					7.4						
Total from composite[h]			8.1					10.1						
Column C: Post oxic elution														
Cx-2	13.3		0.19	20.1		0.021		0.30	-0.72		0.001		0.007	0.003
Cx-3	43.4		1.56	43.0		0.045		1.63	-3.82		0.022		0.014	0.020
Cx-4	47.6	2.9	2.07	47.2	2.6	0.041	0.002	1.79	-3.54	0.11	0.020		0.012	0.018
Cx-5	43.5	3.3	1.41	44.0	3.3	0.039		1.25	-3.80		0.023	0.001	0.024	0.023
Cx-6	50.3		1.67	48.1		0.038		1.26	-3.43		0.016	0.001	0.025	0.018
Cx-7	16.3		0.14	29.0		0.021		0.18	-1.57		0.004		0.008	0.005
Cx-6 fines	165.3			168.3										
Total of intervals[g]			7.0					6.4						

3.3.3 Column B Sediment Chemistry after Biostimulation

Total U in column B sediments recovered after 221 days of biostimulation was 0.33±0.01 μmol/g in the <2 mm composite sediment (Figure 14A, Table 7). The syringe core intervals had much lower total U ranging from 0.02 to 0.09 μmol/g in the <2 mm sediment (Figure 14A). The sediment collected near the inlet (B1-5 and B1-6) had much higher U (Table 7). Uranium in the bulk sediment taken from within 0.2 cm of the inlet measured by gamma spectrometry was about 2.3 μmol/g. The >2 mm fraction accounted for 6 to 16% of the total U in all grain sizes. The whole column unfractionated sediment U is 62.6 μmol based on the composite sediment, which is comparable to the U uptake calculated from the integrated effluent, 73.8 μmol, given the uncertainty in integrating effluent.

Extractable Fe(II) increased during biostimulation by 5 fold or more compared to the pre-column sediment, and ranged from 39 to 52 μmoles/g. Negligible Fe(III) was extracted by the 0.5N HCl compared to 24% for the pre-column sediment (Table 7). Higher Fe(II) was measured both near the inlet and outlet (Figure 15A, Table 7). As measured for column A, the increase in extractable Fe(II) on a whole column basis was about two orders of magnitude greater than integrated effluent [Fe] transported out of the column (Table 3), consistent with retention of reduced iron either as sulfide or in another form such as reduction in place of Fe(III) silicates.

A 4 to 5-fold increase in total S was measured in column B sediments after 221 days of biostimulation (Table 7). AVS accounted for about 90% of the increase in total S. Higher total S was present in sediments closer to the column inlet and outlet (Figure 16A). Based on the composite sediment samples, the whole column total S increased by 8.3 mmoles of which 6.9 mmoles was AVS. Integrated effluent sulfide was 66 mmoles, yielding a combined measured total S reduction of 74 mmoles (Table 7). By comparison, integrated effluent sulfate loss was 64 mmoles. The increase in total S retained in the column (8.3 mmoles) is about 90% of the increase in extractable Fe(II), with AVS equal to about 70% of the increase in sediment Fe(II). The $\delta^{34}S$ of total S decreased relative to the pre-column sediment $\delta^{34}S$ by -0.33 to -2.86 ‰ with samples containing higher total S having a more negative $\delta^{34}S$. Calculated ^{34}S fractionation factors for sulfate reduction ranged of -0.2 to -3.4 ‰ based on the change in $\delta^{34}S$ of solid phase total S.

After repacking column B and continued biostimulation and U(VI) input for 110 days, sediment U concentration increased from 0.33 μmol/g in the composite used to repack the column to between 0.35 and 0.51 μmol/g for sediments recovered at the end of the experiment (Table 7, Figure 14B). Extractable Fe(II) did not increase significantly during the biostimulation after repacking suggesting that pool of reducible iron may have already been reduced prior to repacking (Table 7, Figure 15B). The total of the influent ferrous iron added to column B would result in a sediment concentration of 0.3 μmol/g, which is a small fraction of the measured extractable Fe(II) (39 to 50 μmol/g, Table 7). Total S increased about 15% during the second part of the biostimulated reduction while AVS did not change measurably from the composite used to repack the column (Table 7, Figure 16B). Total S $\delta^{34}S$ ranged from -1.98 to -2.42, and yielded ^{34}S fraction factors ranging from -2.3 to -2.7 ‰.

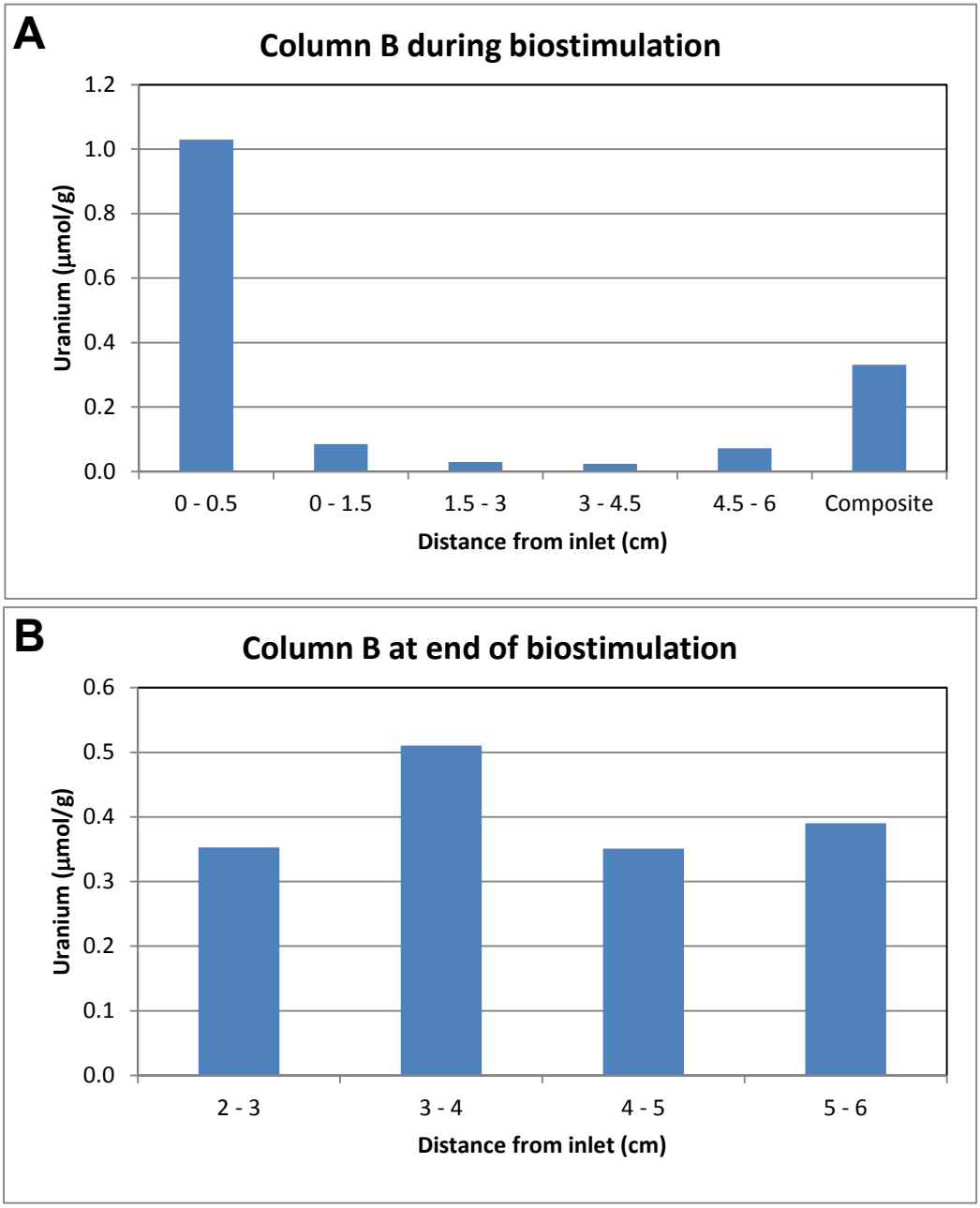

Figure 14. Total uranium concentration (µmol/g) of <2 mm sediment from column B after 221 days of biostimulated reduction stage prior to repacking versus distance from inlet. B. Total uranium in sediments at end of biostimulation experiment.

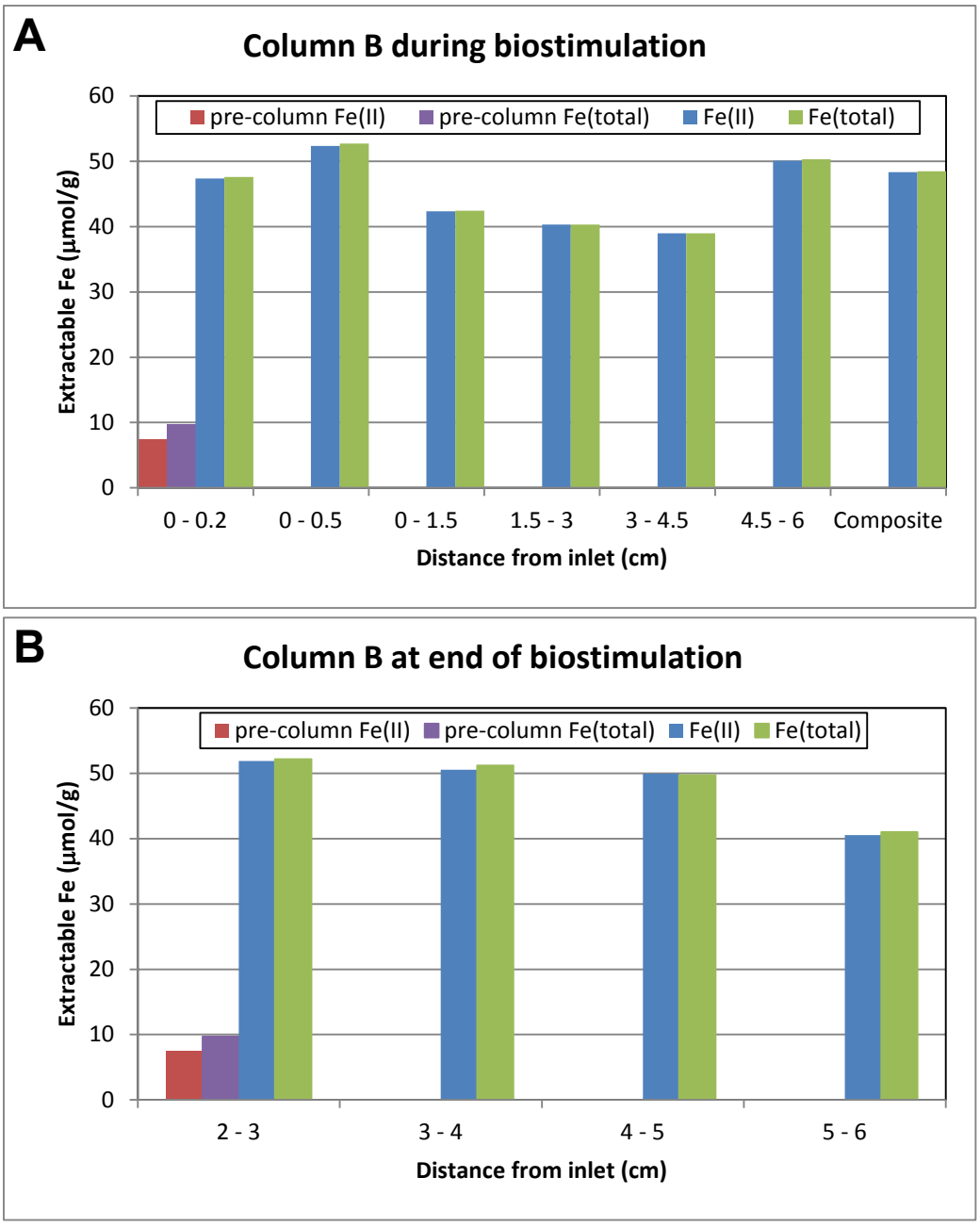

Figure 15. A. 0.5 N HCl extractable Fe(II) (µmol/g) of <2 mm sediment from column B after 221 days of biostimulated reduction stage prior to repacking versus distance from inlet. B. Extractable Fe(II) in sediments at end of biostimulation experiment.

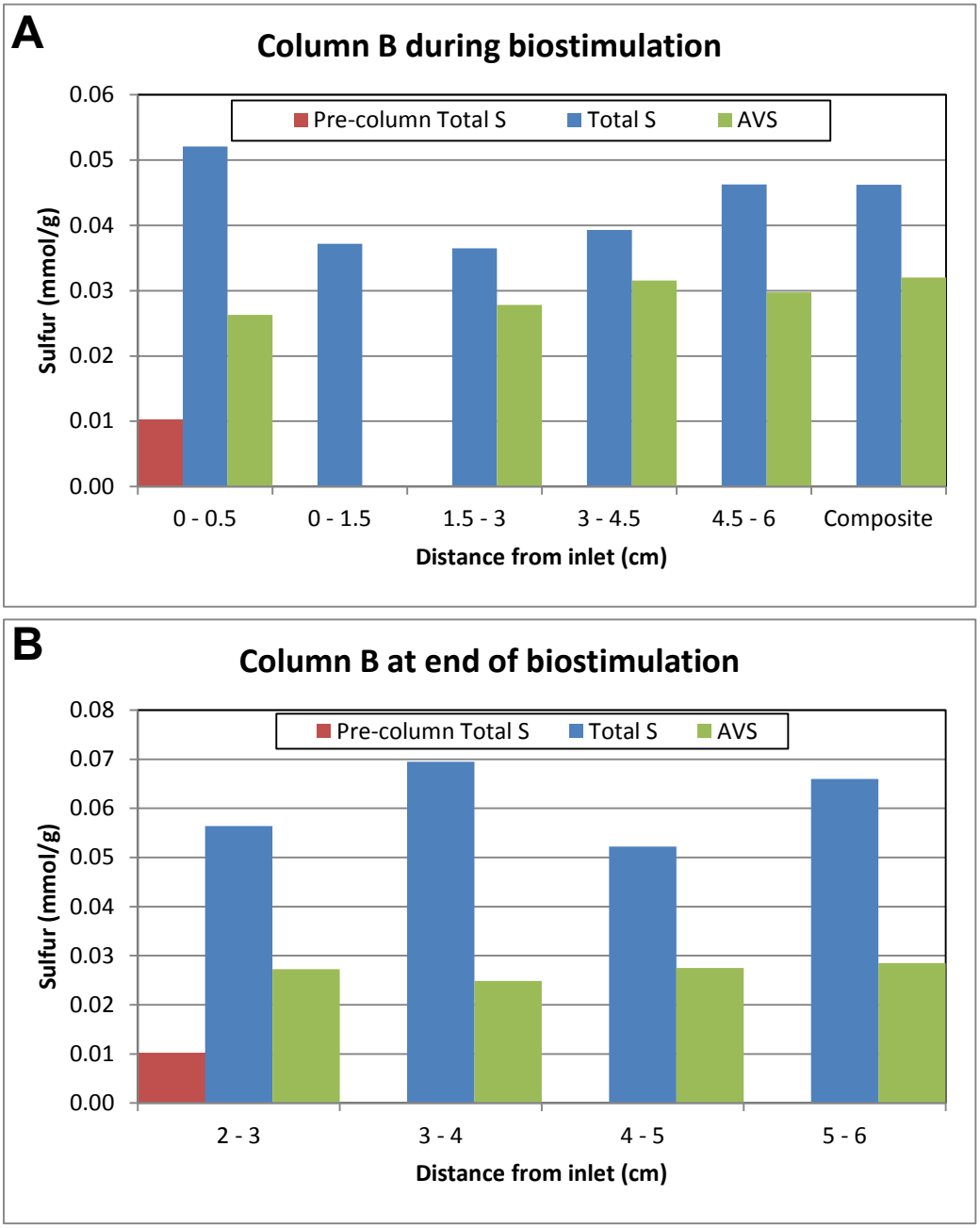

Figure 16. A. Total and acid volatile sulfur of <2 mm sediment from column B after 221 days of biostimulated reduction stage prior to repacking versus distance from inlet. B. Total and acid volatile sulfur in sediments at end of biostimulation experiment.

3.3.4 Column C Sediment Chemistry after Biostimulation

Total U in the <2 mm sediments recovered from column C at the end of the biostimulated reduction stage (186 days) ranged from the pre-column concentration (0.007 μmol/g) in the intermediate depth syringe core samples to 0.58 μmol/g in the sediment collected in the first 1 cm from the inlet (Table 8, Figure 17). The distribution of sequestered U within the column

indicates uptake occurred primarily near the inlet, but based on the composite sediment U concentrations also occurred away from the central axis of the column (Figure 17). Thus, flow may be preferential along the outer part of the column. The composite of the column sediment had a total U of 0.21 μmol/g, which equals a column sediment U uptake of 47 μmoles (Table 8) or less than half of estimated U uptake from integrating the effluent (Table 3). This calculation assumes that the >2 mm size fraction had the same U concentration as the <2 mm sediment. Accounting for the U in the >2 mm fraction and its mass contribution lowers this estimate slightly. The much lower total U uptake determined from sediment measurements indicates either 1) that the composite sediment did not include all sediment from the column (for example, the sediment closest to the inlet), 2) some fraction of U sequestration occurred on biomass adhering to the inlet filters, or 3) that some of the fine grain sediment was not included either in the composite or in its analysis. The sediment recovered from within 2 mm of the inlet in column B was a factor of 10 higher than the composite for this column (Table 7). The fines separated from the bulk sediment were also elevated 5-fold compared to the U of the bulk <2 mm sediment (Table 7 and 8). Fine grain sediments adhered to containers used for storing and drying sediments. In addition, fines were inadvertently loss lost during removal of coarse grains. Lastly, coarse sediments were separated from dried samples because of insufficient mass for wet sieving. As a result, an unknown but likely significant amount of fine grained material may have adhered to the coarse sediment.

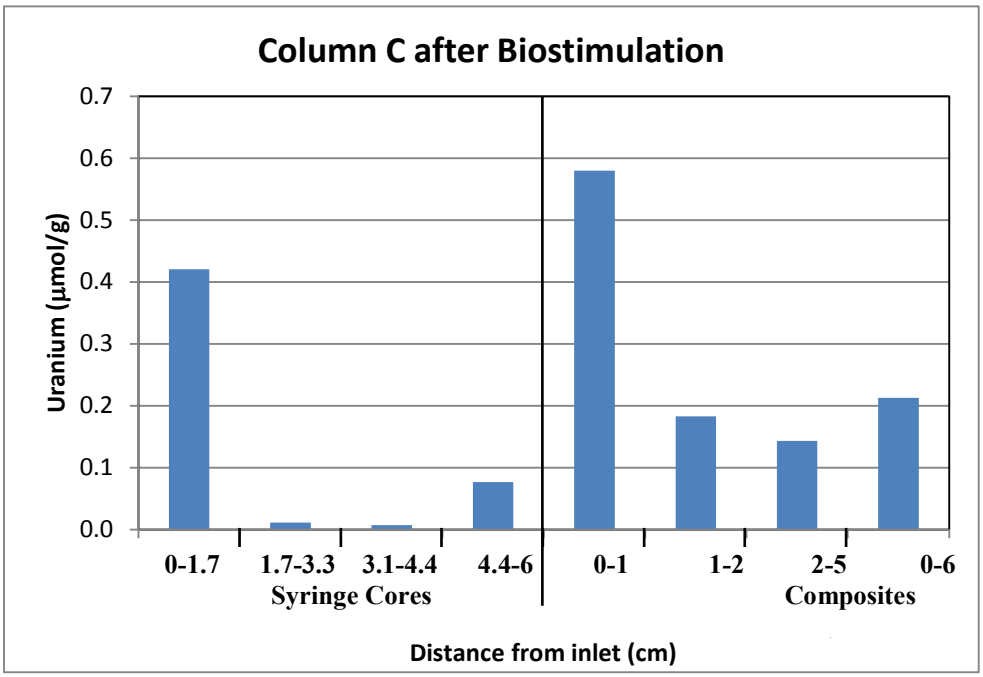

Figure 17. Column C total uranium concentration (μmol/g) of the <2 mm sediment after biostimulated reduction versus distance from inlet.

As observed in the other columns, extractable Fe(II) increased 5 to 7 fold during the biostimulation stage, with a negligible amount of Fe(III) extracted. Extractable Fe(II) was elevated near the inlet by 20 to 40% compared to other samples (Figure 18). Unlike U, this distribution suggests iron reduction occurs throughout the column, although somewhat enhanced near the inlet. The whole column increase in Fe(II) was 6.4 mmoles, which is nearly 2 orders of magnitude greater than the integrated effluent iron transported out of the column (Table 8). The Fe(II) added with the influent throughout the biostimulation was 0.14 mmoles, which is almost a factor two greater than iron exported from the column but small compared to the increase in sediment extractable Fe(II).

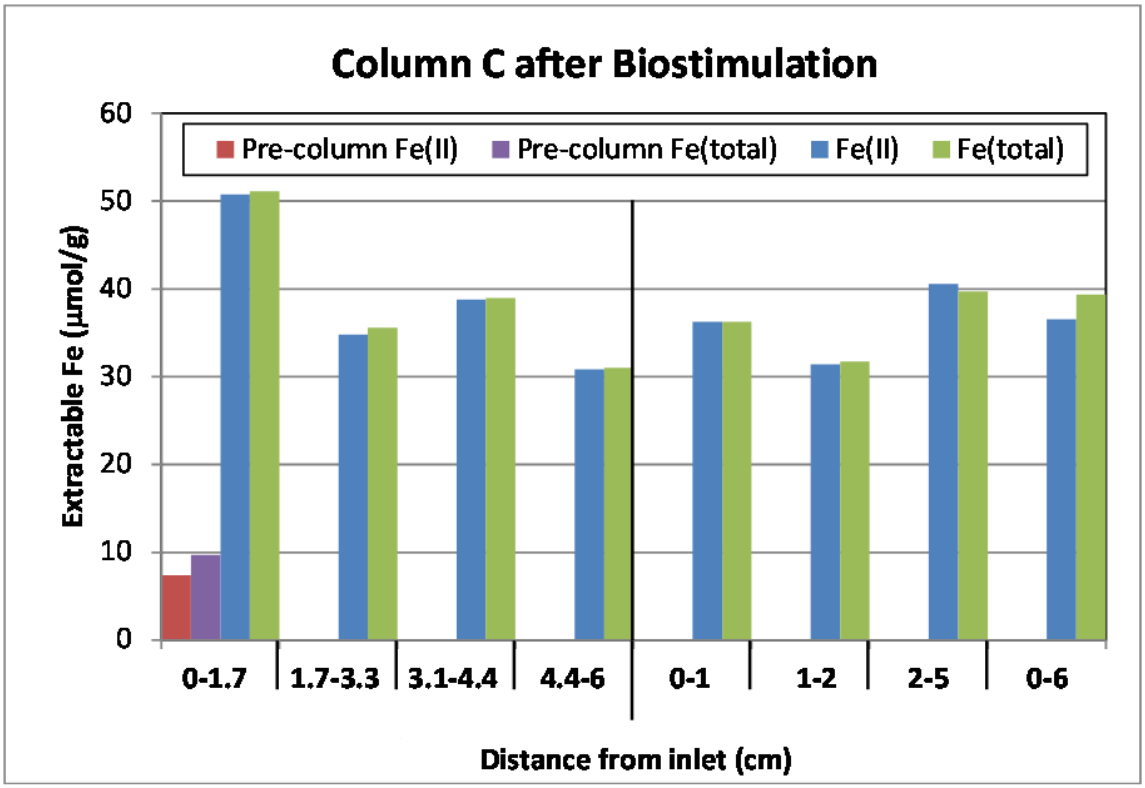

Figure 18. Column C sediment 0.5N HCl extractable Fe(II) and total Fe concentration (µmol/g <2 mm fraction) after biostimulated reduction stage versus distance from inlet. Extractable iron of sediment used to pack column shown for comparison and is denoted as pre-column.

Total S increased during biostimulation ranging from 3 to 4.5 times the pre-column S concentration (Table 8), with no obvious trend in position within the column (Figure 19). AVS accounted for 50 to 75% of the S increase. The total S increase on a whole column basis was 7.8 mmoles, which combined with the integrated sulfide exported from the column yields a total reduced S increase of 52 mmoles. By comparison, the estimated sulfate reduction from integrating the decrease in effluent sulfate was 78 mmoles. The increase in total S retained in the column (7.8 mmoles) is about 120% of the increase in extractable Fe(II), with AVS equal to about 60% of the increase in sediment Fe(II). The $\delta^{34}S$ of total S decreased relative to the pre-column sediment $\delta^{34}S$ with samples with higher total S having a more negative $\delta^{34}S$, ranging from -0.95 to -3.92‰. Calculated ^{34}S fractionation factors for sulfate reduction ranged of 0.2 to -5.1‰ based on the change in $\delta^{34}S$ of solid phase total S.

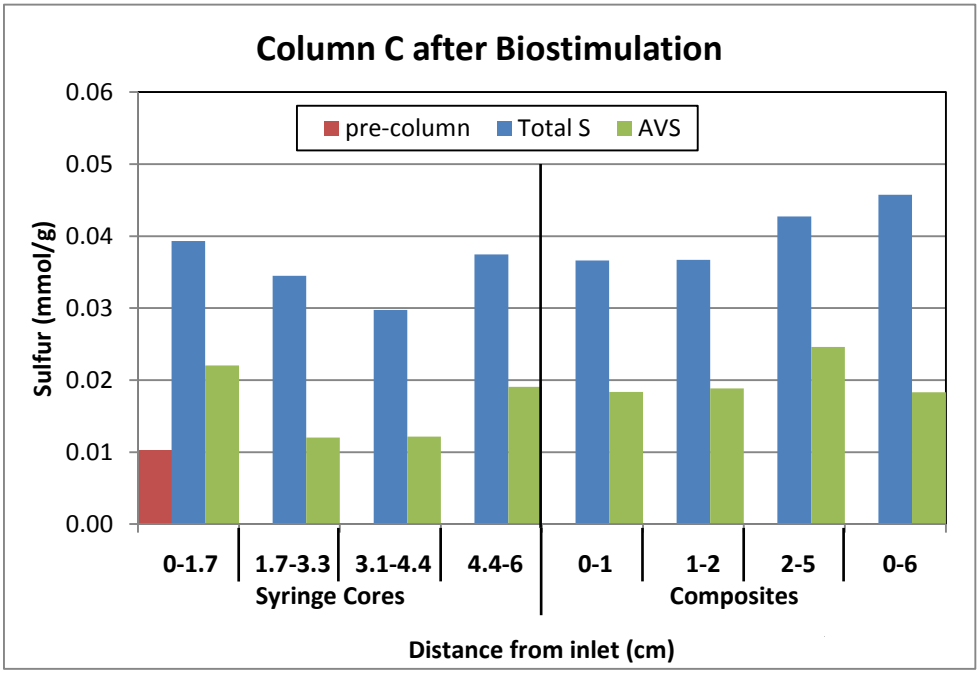

Figure 19. Column C sediment total and acid volatile sulfur following biostimulated reduction (mmol/g) versus distance from column inlet). Pre-column is for total sulfur only; acid volatile sulfur not detected.

3.3.5 Summary of Sediment U, Fe(II) and S during Biostimulation

Bioreduction resulted in precipitation and accumulation of U in each column, with between 62 and 104 µmoles retained on the columns. In all three biostimulation columns, U uptake occurred primarily at or near the inlet end of the column. In contrast, iron reduction as evidenced from the increase in extractable Fe(II) was relatively uniform over the entire column. Increases in extractable Fe(II) were about two orders of magnitude greater than the integrated effluent dissolved iron exported from the columns. The Fe(II) added to column C was about 2% of the extracted Fe(II). These findings indicate most of the iron reduced was retained within the column either as sulfide or as Fe(II) produced by in-place reduction of phyllosilicate Fe(III) (Komlos *et al.*, 2007). Total S increased 5-fold or more in all three columns with fully reduced S, measured as AVS (e.g. S^{-2}), contributing 50 to 75% of the total S increase. The total S increase ranged from 50 to 120% of increase in extractable Fe(II), with AVS equal to 50 to 70% of the sediment Fe(II) increase. Assuming the 0.5N HCl extraction recovers all iron reduced during biostimulation and that sulfur measured as AVS is all from FeS, between 30 and 50% of the reduced iron is in a form other than FeS. This likely includes other iron sulfides such as FeS_2, or iron reduced in place in iron silicate minerals. Precipitation of siderite ($FeCO_3$) is only favorable during the pulse of high effluent [Fe] prior to the onset of sulfate reduction, however, the kinetics of precipitation is slow (Jimenez-Lopez and Romanek, 2004). Small fractionation factors of -0.2 to -5.1‰ $\delta^{34}S$ were observed indicative of microbial sulfate reduction in systems where sulfate and electron donor are not limiting.

3.3.6 Sediment Chemistry after Oxic Elution

The sediment U concentration in column A after oxic elution had an overall trend of increasing from the inlet to the outlet end although some samples within each depth interval had up to 60% lower U than the composite used to repack the column for oxic elution (Figure 20). The apparent greater oxidative mobilization of U from those subsamples is likely the result of preferential flow paths. In contrast, a few subsamples near the outlet had U concentrations up to 77% higher than the composite, which represents the sediment U concentration throughout the column at the start of oxic elution. This increase may be due to uptake of the U released from sediments closer to the inlet. Sediment U decreased on a whole column basis by 3.9 μmols during oxic elution. This U loss was calculated by summing the U mass in the <2 mm sediments for each of the 23 subsamples and subtracting from the total U of the composite used to repack column A. Accounting for both the sediment mass and the U concentration of the >2 mm fraction results in a lower total U loss of 3.4 μmols. By comparison, a U release of 10.6 μmols was calculated by integrating the effluent [U] during oxic elution. The summed sediment U mass assumes that the entire sediment was recovered. About 58 grams of dry material that included the 40 g Ottawa sand was not analyzed. This unanalyzed sediment would account for an additional 4.7 μmols if all its U was remobilized and transported out of the column, partially closing the difference between sediment and effluent estimates of the total U remobilized from the column during oxic elution. Because of the uncertainty in sediment recovery and mass contributions to the whole column sediment, it is assumed that the integrated dissolved U in the effluent during elution, 10.6 μmols, is a better estimate of the overall U remobilization from column A.

Extractable Fe(II) was up to 50% lower than the composite (Figure 21; Table 6). The trend of lower Fe(II) among column A subsamples was similar to the trend in U concentration in that sediment with lower U generally had lower extractable Fe(II). The decrease in Fe(II) from the whole column was 2.6 mmol based on the sum of Fe(II) concentration of each of the 23 subsamples minus the initial Fe(II) of the composite sediment times the subsample mass fraction. The overall Fe(II) decrease represents about 30% of the Fe(II) increase during biostimulated reduction. The integrated effluent dissolved iron during oxic elution was 0.025 mmol (<1% of the decrease in Fe(II)), suggesting that nearly all of the Fe(II) decrease was by oxidation to Fe(III) which is retained in the column. The presence of ferric oxides was apparent in the sediment during sectioning of column A (Figure 9). Total iron (Fe(II) + Fe(III)) extracted by the 0.5N HCl increased up to 10% in some of the column A post oxic elution sediments with no increase observed in others indicating small increase in Fe(III) defined by this extraction. Iron extracted by 0.25 M hydroxylamine HCl at 50° C for 30 minutes ranged from 82 to 105 μmol/g compared to 96 μmol/g for the composite used to repack column A after biostimulation. Since this extraction is effective for dissolution of amorphous Fe(III) oxides (Chao and Zhou, 1983) as well as some Fe(II) phases, the small change from the composite indicates that iron that was oxidized and retained in the column during oxic elution is more crystalline and may include re-oxidation of iron in phyllosilicate phases. Komlos *et al.* (2007) observed that re-oxidation of bioreduced Fe(II) in phyllosilicates resulted in a large fraction of the Fe(III) retained in the silicate structure in the same form as the Fe(III) prior to bioreduction.

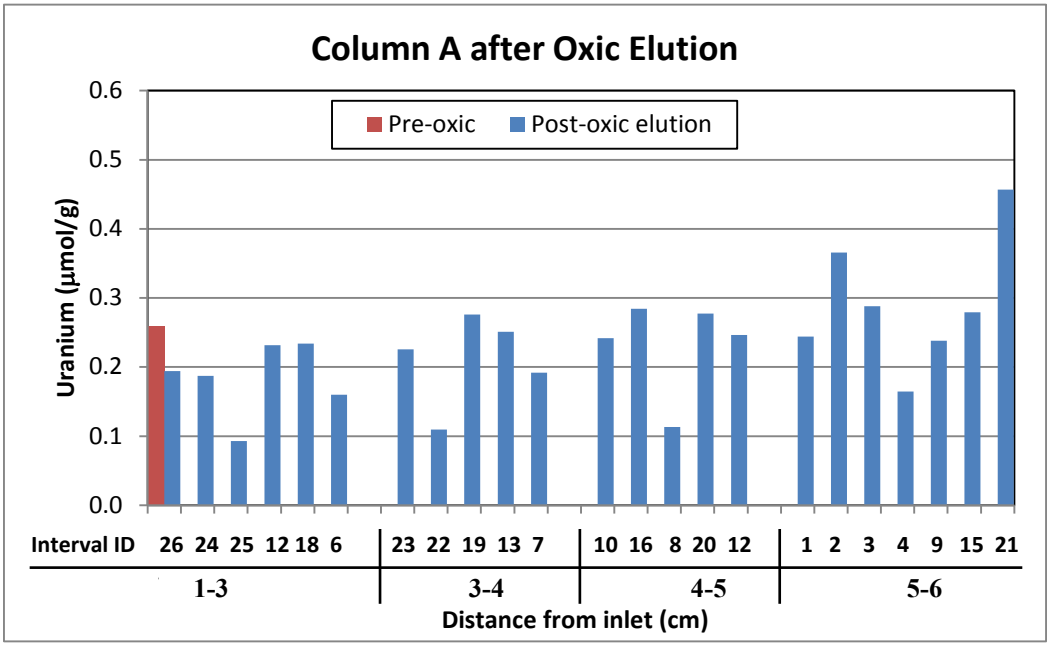

Figure 20. Total uranium concentration in sediments of column A (µmol/g <2 mm fraction) after oxic elution versus position in column.

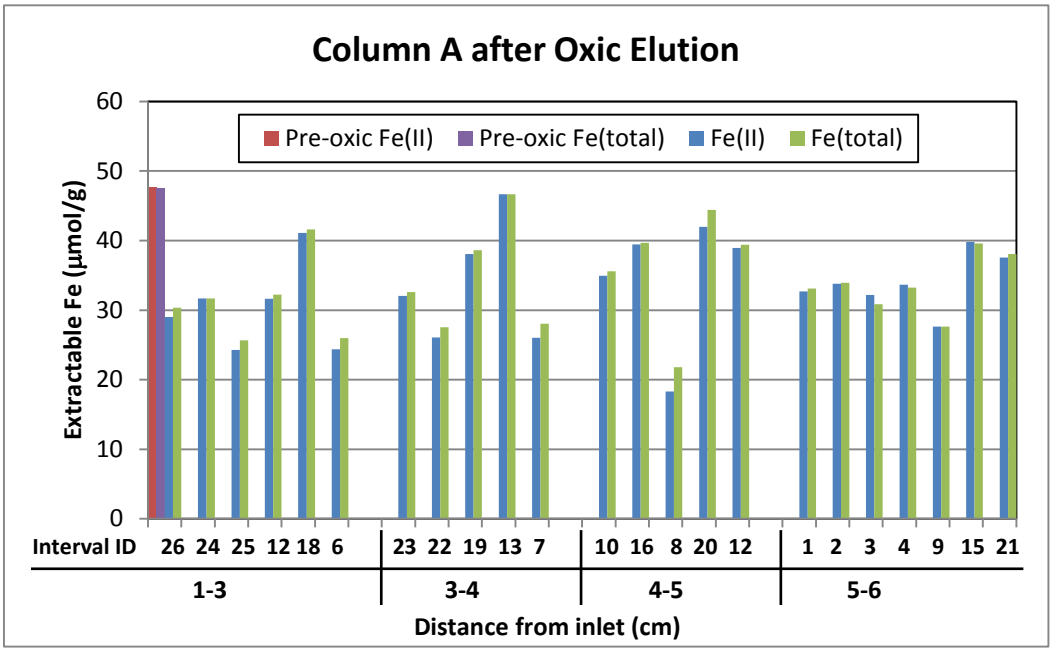

Figure 21. 0.5N HCl extractable Fe(II) concentration in sediments of column A (µmol/g <2 mm fraction) after oxic elution versus position in column. The composite sediment used to repack the column for oxic elution is plotted for comparison and noted as “pre-oxic”.

Total S decreased during oxic elution by 0.7 mmol (Figure 22) with a greater loss from subsamples that had a greater decrease in Fe(II) and U. Loss of total S was calculated by summing the product of the total S in each interval times its mass, and subtracting from the total S at the start of oxic elution defined by the composite sediment total S times the mass of sediment used to repack column A. The whole column loss of total S would result in an effluent sulfate concentration increase of 0.06 mM if the loss was uniform over the duration of oxic elution. This level of increase in effluent sulfate was too low to be measurable. After oxic elution AVS ranged from 0.010 to 0.020 mmol/g in the <2 mm fraction and averaged 26% less than the composite sediment (0.020 mmol/g) used to repack the column for oxic elution (Figure 22, Table 6). Because of insufficient sample to measure AVS on all sediment samples after oxic elution, the whole column mass and change in AVS could not be calculated. The ratio of AVS to total S corrected for pre-column sediment total S ranged from 43 to 96% and averaged 70%, compared to 79% for the composite. Thus, AVS decreased preferentially to total S during oxic elution. The oxidation of sulfide S to higher oxidation states and retention in the column cannot be determined from data collected.

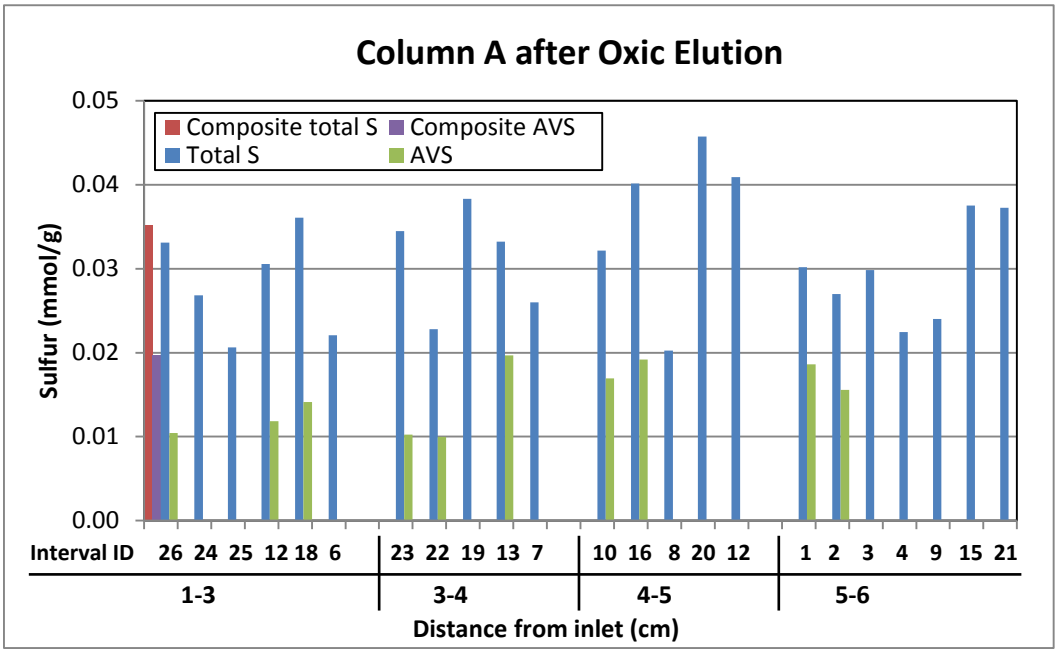

Figure 22. Column A <2 mm sediment total and acid volatile sulfur following oxic elution (millimoles per gram versus distance from column inlet. Composite is sediment used to pack column for oxic elution.

Total uranium remaining in column C sediment after oxic elution ranged from 0.08 to 0.21 μmoles/g compared to 0.21 μmoles/g in the composite used to repack the column for elution (Figure 23; Table 8). The largest decreases in U were in the interval nearest the inlet (Cx-2), and in a small section of column near the outlet (Cx-7; Figures 9, 23). Both of these samples appeared oxidized based on the transition in color from black, characteristic of sulfide in reduced sediment, back to the brown hues of the pre-column sediments. The net loss of U from the column is estimated from the difference between the measured sediment U concentration before and after elution. At the start of oxic elution the column had a total U of 26.4 μmol based on the composite post biostimulation sediment times the dry mass of sediment used to repack column C. The sum of the column C post oxic elution intervals (concentration times mass) is 24.1 μmols. The difference of 2.3 μmols is the U loss from the sediments. By comparison, 2.5 μmols of U remobilization was determined by integrating the effluent [U] during oxic elution.

Note that the net loss is in good agreement for the sediment and effluent based estimates, despite a factor of three higher integrated effluent U loading compared to the loading based on the measured U concentration of the composite sediment used to re-pack column C for oxic elution. The possible reasons for this difference are described in section 3.3.4.

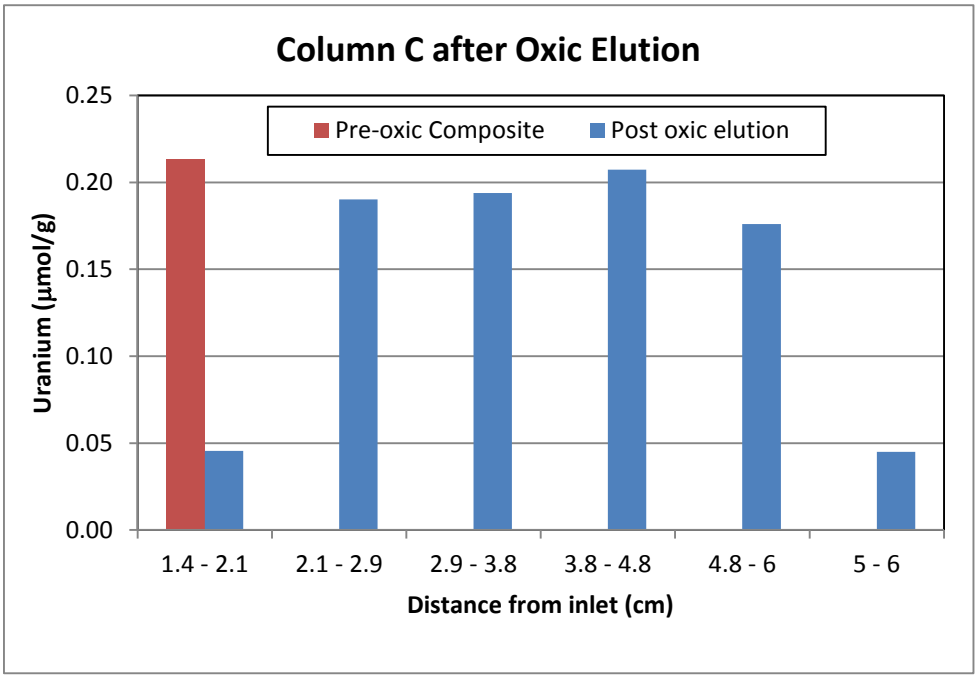

Figure 23. Column C sediment total uranium concentration (µmol/g <2 mm fraction) after oxic elution versus position in column. Pre-oxic composite represents sediment from biostimulation used to pack column for oxic elution.

A 3-fold decrease in 0.5N HCl extractable Fe(II) compared to the composite sediment was measured in the sediments from near the inlet and outlet that appeared oxidized (Figure 24; Table 8). The total Fe measured in these two samples by this extraction indicates about a third to half of the remaining Fe(II) was transformed to HCl extractable Fe(III). Because effluent [Fe] was not detected in column C during oxic elution, the decrease in total iron in these two samples (0.4 mmol) likely was due to transformation to a form not extracted by 0.5N HCl. Using the iron detection limit of 3 µM, the upper limit of iron transported out of the column during oxic elution is 0.02 mmol. All the other column samples had higher Fe(II) than the composite sediment at the start of the oxic elution, with Fe(II) comprising all of the total HCl extractable Fe indicating no measurable oxidation occurred in these intervals. The total increase in Fe(II) of these intervals compared to the composite (1 mmol) is greater than the loss of iron from the inlet-end interval (0.3 mmol). The reason for the difference is unknown since there was no source of Fe to the column during oxic elution. The fines (<63 µm) account for 14.3% of the <2 mm sediment mass but account for 60% of the extractable iron. To account for the apparent Fe increase in sample Cx-6, the composite would need to have a 35% lower mass fraction of the <63 µm sediments than this sample.

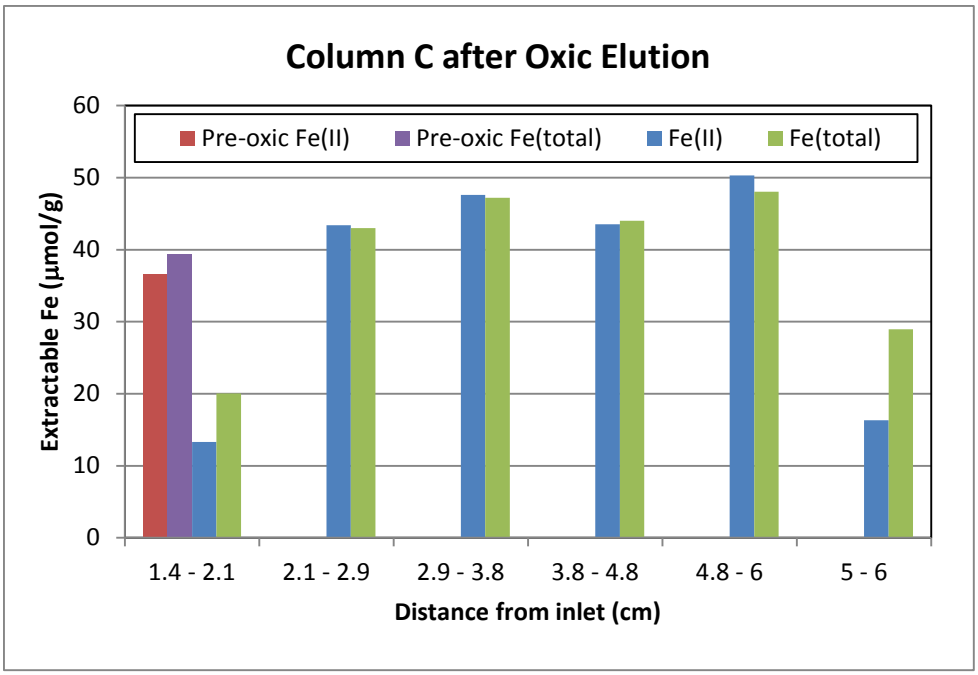

Figure 24. Column C sediment 0.5N HCl extractable Fe(II) and total Fe concentration (µmol/g <2 mm fraction) after oxic elution versus position in column. Sediment iron prior to oxic elution plotted for comparison.

Similar to extractable iron, total S decreased by more than a factor of two in the two oxidized intervals of column C sediments. The other intervals were similar in total S to the composite with a small decrease closer to the outlet (Table 8; Figure 25). AVS in the oxidized interval nearest the inlet (Cx-2) decreased by 95% during oxic elution. By comparison total S decreased 45% indicating loss of AVS accounts for about 70% of decrease in the total S. The decrease in total S was also about 45% in the oxidized interval near the outlet (Cx-7), with an 80% decrease in AVS. The proportion of AVS to total S in the other intervals was similar to the composite material used to pack the column for oxic elution. Thus, the loss of both total S and AVS occurred primarily in the two intervals that appeared more oxidized.

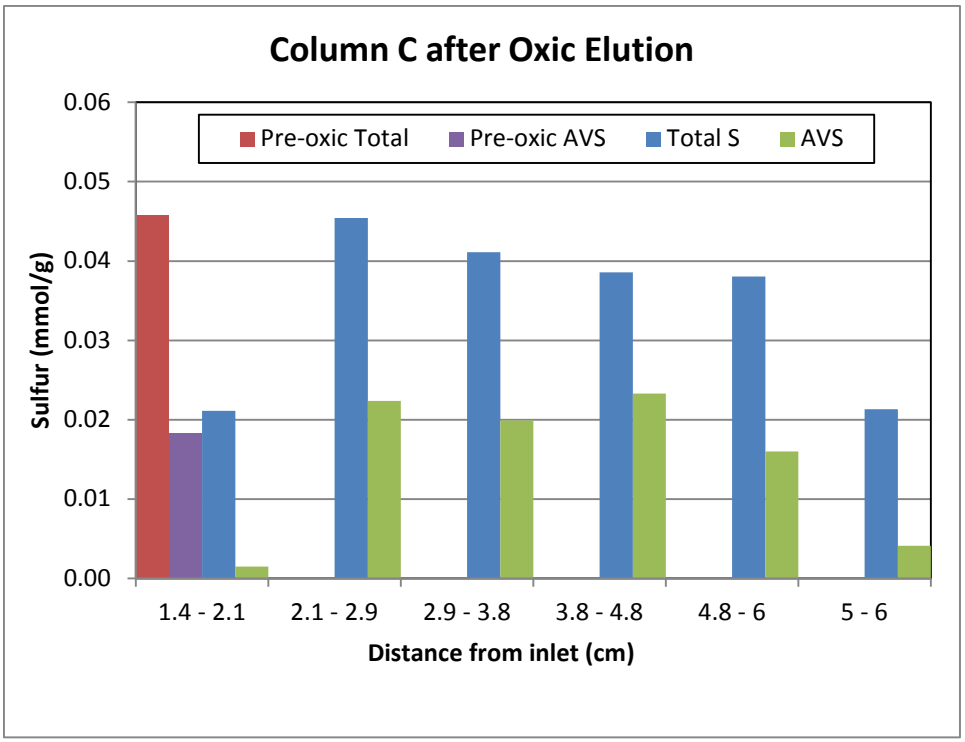

Figure 25. Column C sediment total and acid volatile sulfur following oxic elution (mmol/g vs distance from column inlet). Pre-oxic total and AVS represent sediment after biostimulation used to pack column for oxic elution.

3.4 X-ray Absorption Spectroscopy and Imaging

3.4.1 U Oxidation State

XANES spectra of uranium in column A, B and C sediments recovered at the end of the biostimulation period all are very similar to the XANES spectrum for U(IV) in the uraninite model compound (Figure 26). For example, both the energy of the absorption maxima and the shape of the near edge shoulder between 20960 and 20980 eV in U L_{II} spectra (Figure 26A) are consistent with U(IV). In contrast, for U(VI) the white line is at a higher energy and the post edge shoulder is significantly more pronounced, as illustrated by a spectrum for andersonite U(VI) model compound in Figure 26. The sediments recovered from columns A and C after oxic elution also are similar to the U(IV) model spectrum with the exception of the column C sample (Cx-7) near the outlet. This sample spectrum appears intermediate to the U(IV) and U(VI) model compounds based on a higher white line energy and a more prevalent post-edge shoulder than the other samples.

The oxidation state of uranium in the column sediments was quantified by linear combination fitting of the background corrected and normalized XANES spectra. The best fits were obtained using a synthetic crystalline uraninite for the U(IV) component and andersonite (a uranyl carbonate mineral) for the U(VI) component. Best fits were determined by the smallest residual chi squared (χ^2) value of the difference between the sample spectra and the linear combination fit of the components in the least squares fitting routine of SIXPACK software. The sum of the fractions of each component in the fits may not equal exactly one owing to uncertainty in the fit. Fitting of U XANES spectra typically can distinguish components to 5% at best (Singer *et al.*, 2009), such that a component ≤ 5% cannot be detected. Uncertainty in the fit fraction of U(IV) and U(VI) is estimated at 0.05.

The U was essentially all in the +4 oxidation state (U(IV)) in the column A and B sediments recovered during or after the biostimulation period (Table 9). The U in column C sediments recovered after biostimulated reduction were about 90% U(IV). Following elution with oxic AGW, the fraction of U(IV) ranged from 0.88 to 1.0 in column A sediments and 0.82 to 1.0 in column C sediments (Table 9). Sediments from column C that appeared more oxidized based on change in color from black to brown (Cx-2, Cx-7) had a greater U(VI) component than the other samples, which retained the black color through to the end of oxic elution. Column A sediments did not have any obvious trend in U oxidation state with visual changes in color. Overall, the U retained by the sediments and not remobilized was largely still reduced indicating that U oxidized during oxic elution was primarily transported out of the columns. Thus, little U(VI) was retained by surface complexation to sediment surfaces such as iron oxides. The fractions of U(IV) and U(VI) from post biostimulation and post oxic elution shown in Table 9 support this conclusion.

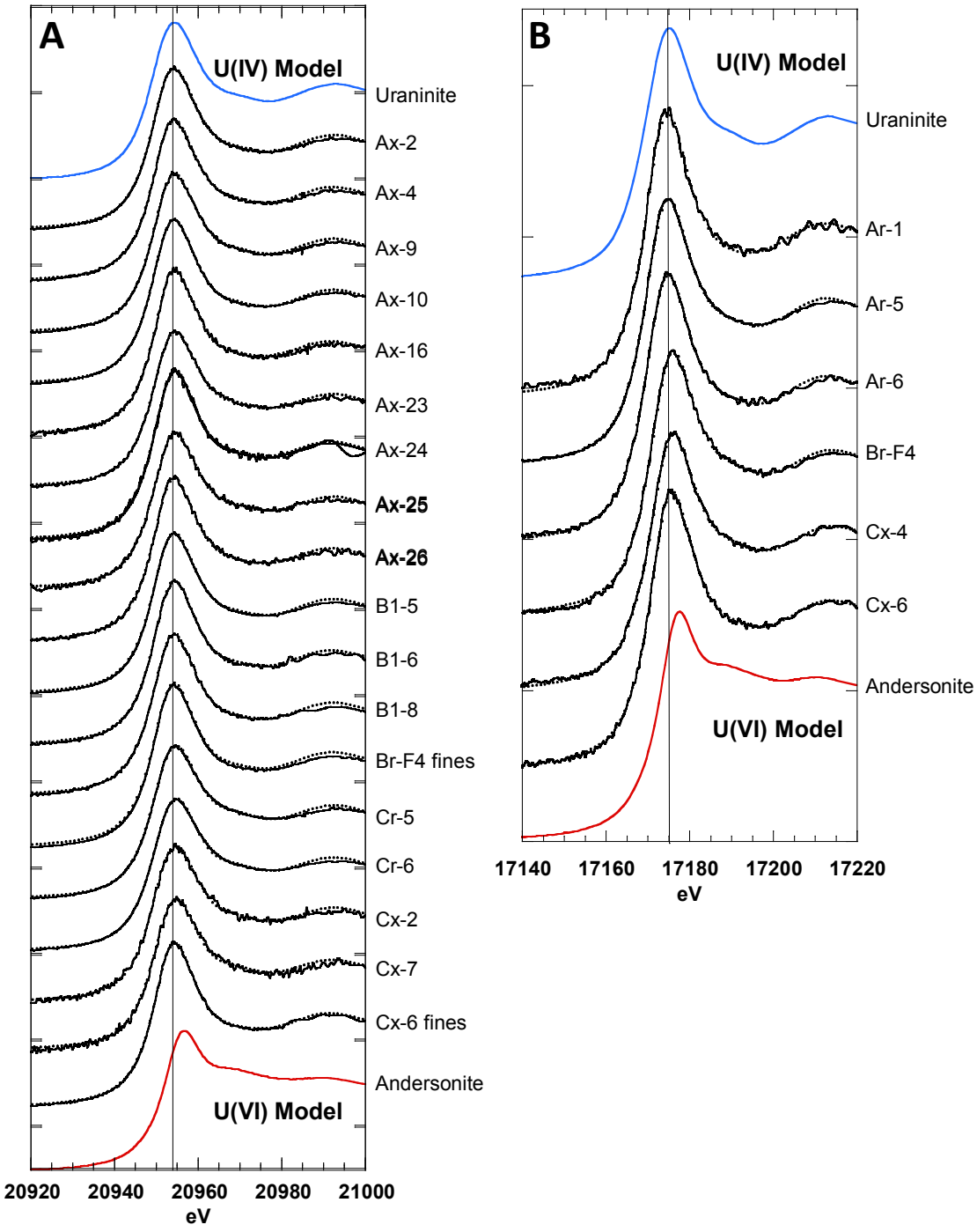

Figure 26. U-LII (A) and U-LIII (B) bulk XANES of column sediment samples. Sample IDs correspond to those listed in Tables 6, 7, and 8.

Table 9. Fraction of U(IV) and U(VI) of column sediments determined by linear combination fits to U-L_{II} and L_{III} bulk XANES spectra.

Sample	U μg/g[a]	U(IV)	U(VI)
Column A after biostimulated reduction			
Ar-1	71	1.00	0.00
Ar-5	129	0.97	0.03
Ar-6 composite	62	0.99	0.01
Column average		0.99	0.01
Column A Post-oxic elution			
Ax-24	44	0.88	0.12
Ax-25	17	0.88	0.12
Ax-26	36	0.95	0.05
Ax-23	34	0.88	0.12
Ax-10	45	0.94	0.06
Ax-16	51	0.92	0.08
Ax-2	46	1.00	0.00
Ax-4	53	0.99	0.01
Ax-9	62	0.93	0.07
Column average		0.93	0.07
Column C after biostimulated reduction			
Cr-4	100	0.84	0.16
Cr-5	138	0.86	0.14
Cr-6	44	0.99	0.01
Column average		0.90	0.10
Column C Post-oxic elution			
Cx-2	11	0.86	0.14
Cx-4	46	0.93	0.07
Cx-6	42	1.00	0.00
Cx-7	14	0.82	0.18
Cx-6 fines	230	0.94	0.06
Column average		0.91	0.09
Column B during reduction (before repack)			
B1-5	540	0.98	0.02
B1-6	246	0.96	0.04
B1-8	79	1.00	0.00
Column average		0.98	0.02
Column B after biostimulated reduction			
Br-F4	84	0.92	0.08
Br-F4 fines	424	0.99	0.01
Column average		0.95	0.05

a. U concentration determined by hot HNO_3 extraction.

3.4.2 Speciation of Sequestered Uranium

Extended X-Ray Absorption Fine Structure (EXAFS) spectra can provide information on the local bonding environment of an element through analysis of the spectrum and by comparison to model compounds. Shell by shell fits of column sediment U EXAFS spectra (Figure 27) were performed to determine the speciation of sequestered uranium both at the end of biostimulated reduction and after oxic elution. Phase-shift and backscattering amplitude functions for quantitative EXAFS fitting were generated using FEFF 7.0 from the crystal structures of uraninite, liebigite, and autinite (Ankudinov and Rehr, 1997; Locock and Burns, 2003; Mereiter, 1982; Wyckoff, 1963). The phase shift and backscattering functions from models were used for shell by shell fits of sample EXAFS spectra, with results shown in Table 10. The spectra were fit over the k-range 3-9.5 $Å^{-1}$.

Because linear combination fitting of the U L_{III}- and L_{II}-edge XANES spectra indicated that the samples are essentially 100% U(IV) (with an analytical error of 5%), no contribution from uranyl was considered in fitting the EXAFS spectra (Table 10). Further, the first shell of oxygen atoms at 2.36 Å in all spectra is consistent with the U(IV)-O interatomic distance, and not U(VI). The EXAFS spectra fits of the first four atomic shells are in agreement with recent results of U speciation in reduced sediments from Rifle (Stoliker *et al.*, 2013). The presence of a U-U pair correlation in the EXAFS spectra at 3.85 Å is consistent with the U-U interatomic distance in uraninite (O'Loughlin *et al.*, 2010; Schofield *et al.*, 2008; Singer *et al.*, 2009). This suggests that at least some polymerized U(IV) is present. However, the fit-derived coordination number is low (~ 3-7) compared to bulk UO_2 (12 U nearest neighbors) or nano-UO_2 (8-12 nearest neighbors) (O'Loughlin *et al.*, 2010; Schofield *et al.*, 2008; Singer *et al.*, 2009). As found by (Stoliker et al., 2013), the low coordination number and relatively high Debye-Waller factor of the first U-U pair is consistent with a small, partially disordered nano-UO_2-like cluster. However, in the current EXAFS analysis (excluding sample B1-5), a second uranium-uranium pair correlation was included at ~5.6 (± 0.3) Å, which is attributed to the second U-U interatomic distance in uraninite (5.45 Å). Excluding this pair-correlation resulted in an unaccounted contribution to the EXAFS spectra. This higher R shell has been previously included in the fits of EXAFS spectra of nanoparticulate UO_2 (Schofield *et al.*, 2008), and suggests that a higher degree of U(IV) polymerization is present in the current samples compared to sediments examined by Stoliker et al (2013). A multiple-scattering path (U-O-U-O) was included at 4.5 Å, and is consistent with previous fits of nano-UO_2 and partially polymerized U(IV) EXAFS spectra (Stoliker *et al.*, 2013; Schofield *et al.*, 2008; Singer *et al.*, 2009). The exclusion of this pair-correlation resulted in an unaccounted contribution to the EXAFS spectrum, and other single-scattering contributions at this distance could not reproduce this feature.

In addition to the nano-uraninite or partially polymerized uraninite, contributions from U(IV) in contact with organic matter were included in the fit. This contribution is similar to previously described “monomeric” U(IV) bound to organic matter (Bernier-Latmani *et al.*, 2010; Sharp *et al.*, 2011; Alessi *et al.*, 2012; Bargar *et al.*, 2013), and more recently referred to as “non-uraninite U(IV) species associated with biomass” or NUSAB (Stoliker *et al.*, 2013). For two of the samples (Ar-5 and Cx-4) a shell fit in the EXAFS spectra was modeled as ~3 carbon atoms at ~2.9 Å, typical of the observed U-C interatomic distance for U bonded to carbonate of 2.94 Å and for U(IV)-organic ligand moieties (Bernhard *et al.*, 2001; Kelly *et al.*, 2007; Singer *et al.*, 2012). Given that reducing conditions are strongly biologically-mediated through continuous input of acetate that stimulates microbial activity, it is not surprising that U(IV) is associated with organic carbon. The organic matter may bind to the reduced U(IV) and inhibit further polymerization to nanoparticulate UO_2, as suggested for monomeric U(IV) (Bernier-Latmani *et al.*, 2010; Sharp *et al.*, 2011; Alessi *et al.*, 2012; Bargar *et al.*, 2013). Three of the samples (Br-

F4, B1-5, and Br-F4_fines) were fit with ~3 phosphorus atoms at ~3.15 Å, in slight contrast to previous work that used two separate U-P distances (Bernier-Latmani *et al.*, 2010).Including two U-P distances in the EXAFS model resulted in poorer fits for this sample. Together, the U-P and U-U distance are consistent with previous work suggesting that partially polymerized U(IV) is bound to P in organic matter (Bernier-Latmani *et al.*, 2010; Sharp *et al.*, 2011; Alessi *et al.*, 2012; Bargar *et al.*, 2013). The fit quality obtained using either the C or P shells was similar; the reduced chi squared values were within 10% for each sample and each of the fits matched the EXAFS spectra well visibly. The atomic identification and coordination environment in Table 10 are for the fits which better modeled the second shell in the FT. Ultimately, it is not possible to distinguish between P and C coordination on the basis of EXAFS alone. Other backscattering atoms and combinations of atoms were attempted in the fit, including Al, Fe, S, Si, N, and Ca. Carbon or phosphorous (with only one shell, respectively) could fully account for this contribution to the EXAFS spectra. Fits with other backscatters in addition to, or replacing, C or P yielded fits with equivalent or worse reduced chi-squared values and were not statistically significant. Fits with equivalent reduced chi-squared values were with Si and S, and it is challenging to distinguish their x-ray scattering from C and P, respectively. High concentrations of aqueous Si during U(VI) reduction could result in the precipitation of coffinite ($USiO_4$), however the second U-U pair correlation in coffinite (~6.2 Å) is longer than the fit values which are consistent with UO_2. With respect to sulfur, a U(IV)-S mineral is unlikely, however, some U(IV) could be associated with S-bearing functional groups on organic matter.

Overall, the fitting results suggest a sediment containing only U(IV) as a possible mixture of both partially disordered nano-UO_2 and NUSAB associated with organic matter. This U(IV)-bearing phase could exist separately from the partially polymerized nano-UO_2-like U(IV) and/or the nano-UO_2 could exist as aggregates with organic matter. Ultimately, the fits of the EXAFS spectra indicate that some organic matter is intimately associated with U(IV); as potential NUSAB species do not have a U-U pair and dilute the signal from uraninite-like species. We could not successfully ascertain if both species were present as independent phases.

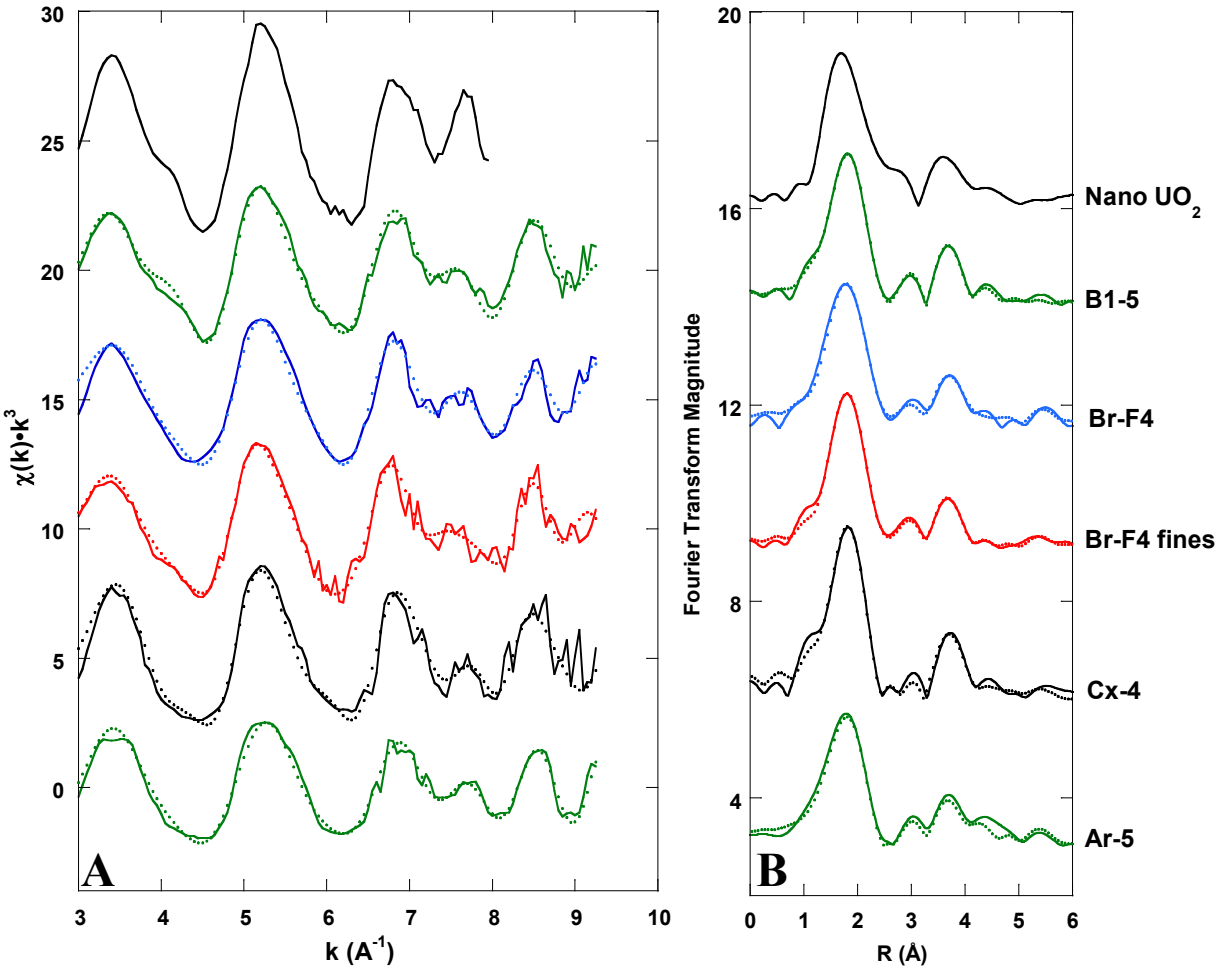

Figure 27. Bulk EXAFS (A) and (B) their Fourier transform of column sediment samples (lines) and best fit to spectra (dots). Sample IDs correspond to those listed in Tables 6, 7, and 8.

Table 10. EXAFS fitting parameters for column sediments. The estimated standard deviations are listed in parentheses, representing the errors in the last digit; values without reported errors were fixed during fitting. Scattering paths are derived from uraninite (U, O, and MS), and liebigite (C) calculated at the LII-edge.

Sample	Z	N [a]	R (Å) [b]	σ^2 (Å^2) [c]	ΔE^0 [e]	red. χ^2 [f]
Ar-5	O	8.2(5)	2.36(1)	0.011(2)	0.6(1)	18.9
	C	3(1)	2.97(1)	0.007(2)		
	U	4(1)	3.82(2)	0.007(2)		
	MS [d]	8(2)	4.7(1)	0.005(1)		
	U	4(2)	5.6(1)	0.008(2)		
Br-F4	O	7.9(4)	2.35(1)	0.012(2)	-0.5(1)	33.0
	P	3(1)	3.15(2)	0.010(5)		
	U	4(2)	3.81(2)	0.009(2)		
	MS	7(3)	4.6(1)	0.008(2)		
	U	5(2)	5.6(2)	0.007(3)		
Cx-4	O	8.4(5)	2.34(1)	0.013(1)	1.1(2)	6.5
	C	3(1)	2.93(4)	0.008(3)		
	U	4(1)	3.80(2)	0.009(2)		
	MS	12(3)	4.48(3)	0.008(4)		
	U	4(2)	5.6(3)	0.01(2)		
B1-5	O	8.6(3)	2.35(3)	0.011(1)	0.2(3)	8.3
	P	3(1)	3.16(2)	0.010(1)		
	U	7(1)	3.84(1)	0.015(1)		
	MS	18(7)	4.64(4)	0.017(3)		
Br-F4 fines	O	7.7(2)	2.34(1)	0.011(1)	-1.8(6)	3.0
	P	3(1)	3.14(2)	0.012(1)		
	U	3(1)	3.82(1)	0.009(2)		
	MS	6(3)	4.48(5)	0.010(1)		
	U	4(2)	5.64(3)	0.006(2)		

a. CN is Coordination number
b. R is Interatomic distance
c. σ^2 is theDebye-Waller factor
d. MS = multiple-scattering path: U–O–U–O
e. ΔE^0 is the difference in threshold Fermi level between data and theory
f. Reduced χ^2, a goodness-of-fit parameter

3.4.3 Distribution of Uranium on Sediments

Micro-focused synchrotron X-ray fluorescence (μXRF) was used to map the distribution of uranium and other elements in thin sections of column sediments recovered after biostimulation and after oxic elution. Thin sections of column sediments were mapped above and below the U L_{III} edge at 30 μm spatial resolution (SSRL beam line 10-2 X-ray microprobe) to locate areas or grains which were enriched in uranium. Selected areas or grains with elevated U were examined at higher resolution (2 μm step size, SSRL beam line 2-3 X-ray microprobe) to obtain higher spatial resolution elemental maps. The distribution of U oxidation states was mapped at selected locations using multi-energy imaging across the U L_{III} edge, or XANES imaging. U L_{III} edge XANES spectra were collected at specific points (μXANES) both to verify the XANES imaging approach and for comparison to bulk XANES measurements. The results of these measurements on three grains with U-rich coatings are described below as examples. Four other grains in sediments after biostimulated reduction and after oxic elution were also mapped by this technique and yielded comparable results.

Uranium in the pre-column sediment was not apparent in the 30-μm resolution XRF maps indicating that the background U is widely distributed throughout the sediment grains and not concentrated in grain coatings. In contrast, the 30-μm resolution μXRF maps of column sediment thin sections showed several grains with distinct areas of U. The U was present largely as discrete spots or as coatings on the exterior of grains. Examples are shown for column C composite sediment sample Cr-5 and column B interval Br-F4 along with optical scans of the thin sections (Figures 28 and 29). The range of sediment grain size is illustrated in the optical scans of the thin sections. Clusters of grains may, in part, be aggregates from drying or be natural aggregates of aquifer sediments. Some grains are rock fragments but can appear dominated by single minerals. Dark grains are typically iron bearing. The 30-μm resolution μXRF image of the Cr-5 thin section shows only one grain with a distinct U coating (Figure 28B, C). U in sample Br-F4 exists as coatings of varying intensity or concentration around several grains as well as smaller areas of one or two pixels (Figure 29). Some thin sections made from column intervals had no obvious areas of elevated U at the 30 μm map resolution. Fine grained sediments (<63 μm) are abundant (~12% by mass, Table 4) and contain 3 to 4 times higher U concentrations (Tables 7, 8). However, discrete particles of this size range are not evident at the 30-μm resolution μXRF mapping resolution. SEM images of U-bearing grain coatings do not appear to be comprised of fine grained sediments adhering to larger grains (Section 3.4.4).

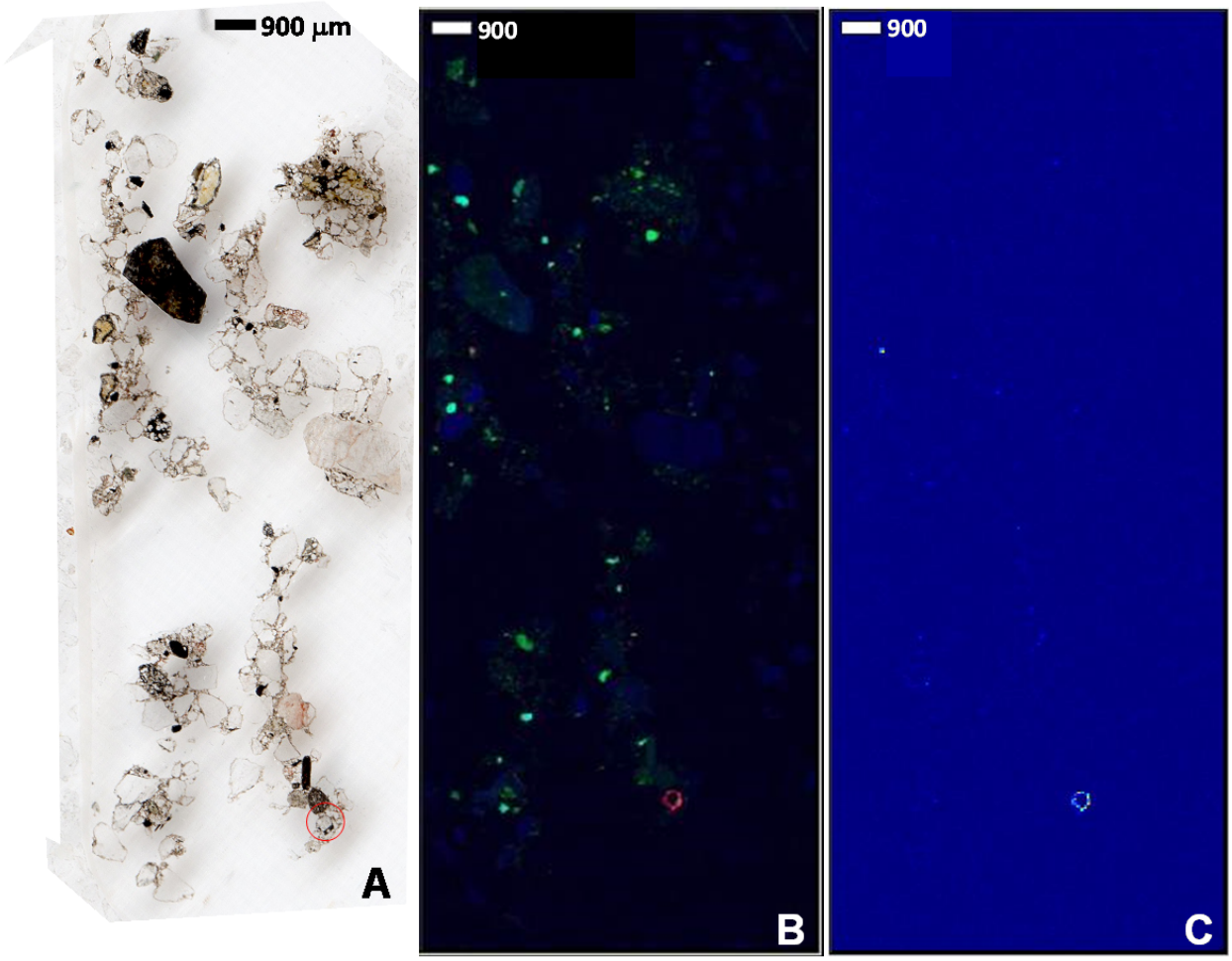

Figure 28. µXRF maps of post-biostimulation column sediment thin section of column C sediment sample Cr-5. (A) optical scan; (B) µXRF tricolor map of uranium (red), iron (green) and calcium (blue); and (C) µXRF map of uranium. The color intensity increases with relative concentration in the µXRF maps. Scale bars are in microns. Maximum counts in (A) are 587, 3753, and 630 for U, Fe and Ca fluorescence, respectively.

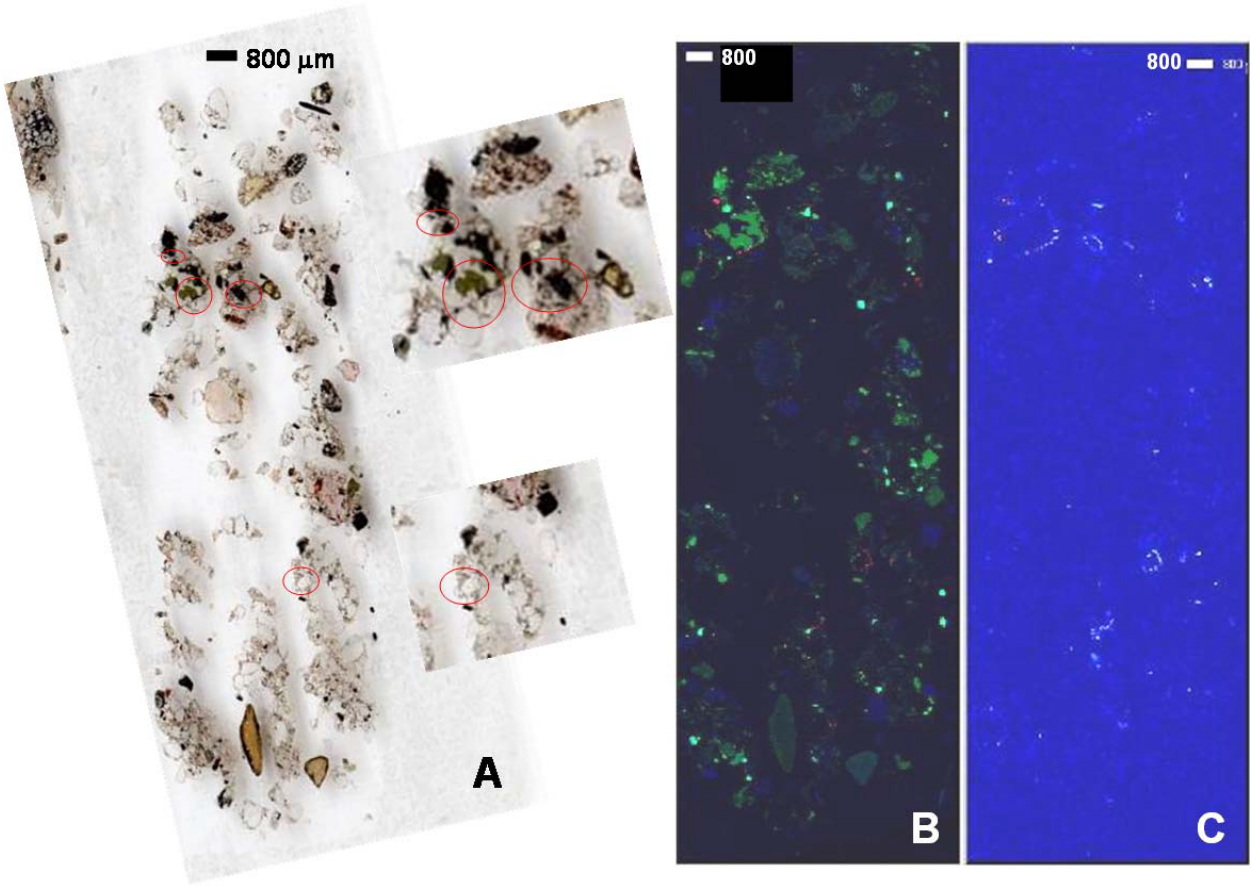

Figure 29. μXRF maps of post-biostimulation column sediment thin section of column B sediment sample Br-F4. (A) optical scan; (B) tricolor μXRF map of uranium (red), iron (green) and calcium (blue); and (C) μXRF map of uranium. The color intensity increases with relative concentration in the μXRF maps. Scale bars are in microns. Maximum counts in(A) are 1021, 3756, and 644 for U, Fe and Ca fluorescence, respectively.

The 2-μm resolution μXRF map of the U-coated grain in the column C thin section Cr-5 shows a near-contiguous coating of varying thickness ranging from 5 to 30 μm in thickness (Figure 30). This sediment sample was collected at the end of the biostimulation stage from near the inlet after removing the syringe core (Table 8). The underlying grain is a rock fragment with an iron rich zone. The multi-energy U XANES map, as well as point XANES spectra, shows that U is primarily U(IV). The U coatings overlay iron phases (Figure 30C) or possibly are intermixed with Fe. The coating also contains S intermixed with U. Locations of 1-μm (nominal beam size) point spectra for XANES and EXAFS are depicted in Figure 30. Spectra for points 2, 3 and 4 are shown in Figure 31 and the EXAFS spectrum of point 5 is shown in Figure 32. Linear combination fitting of spectra yields U(IV) fractions ranging from 0.61 to 0.78 and averaging 0.7 (Table 11), which is measurably less reduced in comparison to the XANES of the bulk sample (0.86 U(IV)). The lower fraction of U(IV) in the grain coating is attributed to calibration uncertainty in the μXANES spectra and partial oxidation of U(IV) during thin section fabrication instead of U(VI) sequestration in the coating. Multi-energy U XANES mapping conversely shows

U(IV) is dominant, comprising nearly all of the uranium in the coating with comparatively low and infrequent points of U(VI). The ratio of the sum of U(IV) in all pixels to the sum of the total U is 0.93, which is more in line with bulk XANES U(IV) fraction. Back scatter SEM imaging and EDS analysis of this grain are presented in section 3.4.4.

A near continuous coating of U was also present surrounding a large (~1 mm) grain in the thin section of sediment sample B-F4 (Figure 33) recovered from the first 1 cm near the inlet of column B at the end of the experiment. This sample is from the composite of column B after 221 days of biostimulation which was then packed into a new column and underwent 110 days of additional biostimulation with U(VI) inflow. The underlying grain has a mottled distribution of iron suggesting it is a rock fragment or an aggregate of smaller grains. The uranium coating ranged from <5 up to 30 μm thick and was dominated by U(IV) in the XANES map. The coating in part appears to have formed on Fe rich areas of the underlying grain and is largely comprised of U and S but little Fe, Ca or other elements evident within the coatings in the μXRF images (Figure 33E). The co-association of S with U may reflect U reduction by sulfides. Lower atomic number elements, notably carbon, cannot be detected by the BL2-3 X-ray microprobe. U(IV) from linear combination (LC) fits of the μXANES at individual points ranged from 0.74 to 0.90 and averaged 0.81±0.19 (Table 11; Figure 31). The individual points show a slightly lower U(IV) component (0.81) than the LC fit of bulk XANES of the column sediment sample (0.92). A U-L_{III} EXAFS spectrum was collected at one point (Figure 32).

A 200-μm diameter iron-bearing grain from column A subsample after oxic elution (Ax-23 grain 1) also has a near continuous coating of U of varying concentration. The coating ranges from a few microns to more than 30 microns (Figure 34). U(VI) is more abundant in this grain coating than in grain coatings from samples recovered after biostimulation. Based on total counts of the multi energy U XANES map, U(IV) comprises 65% of the total U counts. The thickest coating area near the top of the grain as shown in the μXRF maps appears more concentrated in U(VI) near the outside of the coating evidenced by the transition from red to green in the tri-color image in Figure 34C. Linear combination fits of XANES spectra from 5 points in the coating have U(IV) fractions ranging from 0.62 to 0.71, averaging 0.68±0.05 (Table 11; Figure 31). As noted for the other thin sections, the U in the Ax-23 thin section grain coating is more oxidized than determined from LC fit of the bulk XANES of the column sediment subsample (0.88 U(IV)). A U-L_{III} EXAFS spectrum was collected at one point (Figure 32). Little Fe or S was apparent in the coating imaged by μXRF.

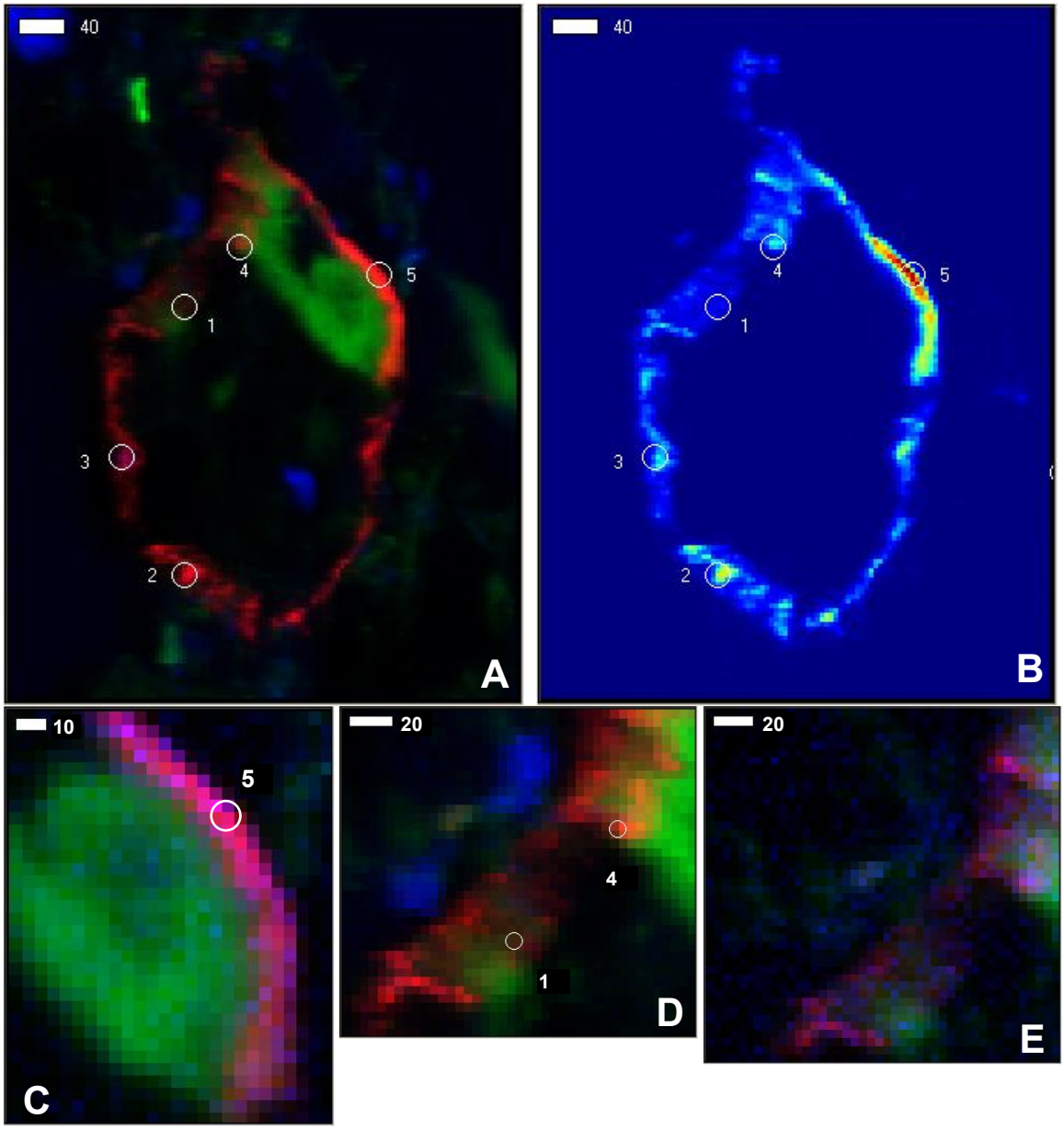

Figure 30. μXRF maps of column C sediment sample Cr-5 grain 1. (A) μXRF tricolor map of U(IV) in red, iron in green and calcium in blue; (B) μXANES map of U(IV); (C) zoom of area near point 5 in A showing of U(IV) in red, iron in green and sulfur in blue; (D) zoom of area near points 1 and 4 in A showing of U(IV) in red, iron in green and calcium in blue; (E) same area as D but showing of U(IV) in red, iron in green and sulfur in blue. The color intensity increases with relative concentration. Scale bars are in microns. Numbered points are locations of μXANES spectra. Maximum counts are 4018, 328, 4064, 828, and 30 for U(IV), U(VI), Fe, Ca and S fluorescence, respectively.

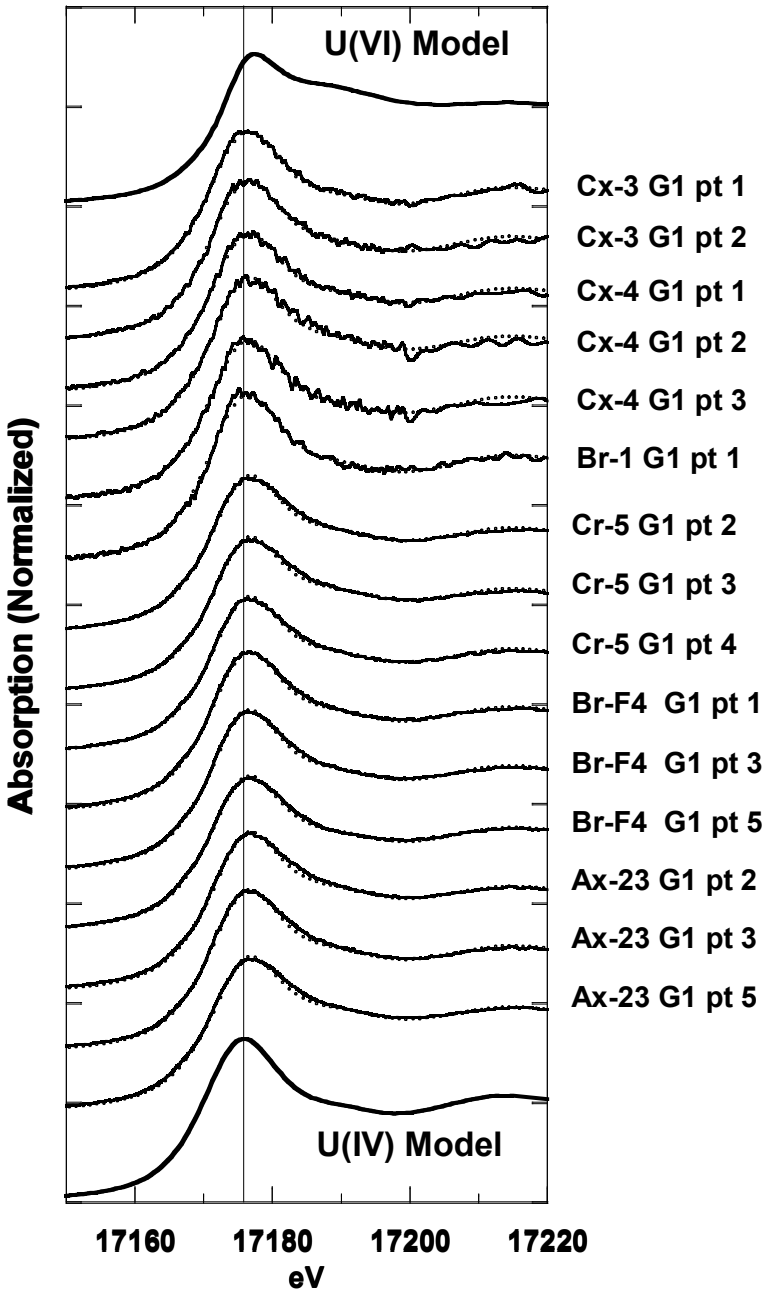

Figure 31. Micro-XANES of points on column sediment grain coatings. Sample IDs correspond to those listed in Table 11 and locations of points are depicted in Figures 30, 33 and 34.

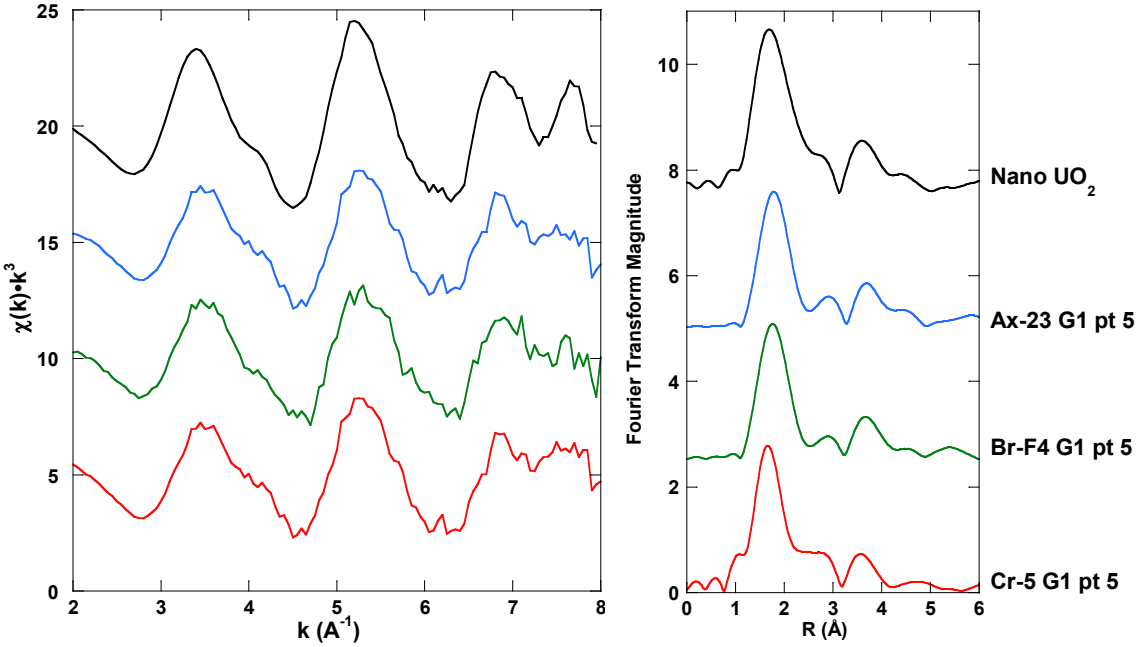

Figure 32. U-L_{III} µEXAFS of points on column sediment grain coatings. Sample IDs correspond to points depicted in Figures 30, 33, and 34.

Table 11. Fraction of U(IV) and U(VI) at thin section points column sediments determined by linear combination fits to U-L_{III} μXANES spectra.

Sample	U(IV)	U(VI)
Ax_23 pt 1 *	0.65	0.37
Ax_23 pt 2	0.66	0.34
Ax_23 pt 3 *	0.76	0.25
Ax_23 pt 4	0.71	0.31
Ax_23 pt 5 *	0.62	0.34
Ax_23 pt 5 EXAFS	0.69	0.28
average	0.68	0.32
standard deviation	0.05	0.04
Br-F4 pt 1 *	0.78	0.22
Br-F4 pt 2	0.81	0.19
Br-F4 pt 3 *	0.76	0.24
Br-F4 pt 4	0.85	0.17
Br-F4 pt 5 *	0.74	0.22
Br-F4 pt 6	0.9	0.13
Br-F4 pt 5 EXAFS	0.81	0.19
average	0.81	0.19
standard deviation	0.05	0.04
Br-F1 pt 1	0.95	0.09
Br-F1 pt 2	1.01	0.04
Br-F1 pt 3	0.93	0.12
average	0.96	0.08
standard deviation	0.04	0.04
Cr-5 pt 1	0.78	0.23
Cr-5 pt 2 *	0.68	0.3
Cr-5 pt 3 *	0.61	0.37
Cr-5 pt 4 *	0.7	0.27
Cr-5pt 5 EXAFS	0.69	0.28
average	0.69	0.29
standard deviation	0.05	0.06
BL 2-3 May 2012 U L-III		
Cx-3 g1 pt1 *	0.91	0.08
Cx-3 g1 pt2 *	0.83	0.18
average	0.87	0.13
standard deviation	0.06	0.07
Cx-4 g1 sp1 *	0.8	0.2
Cx-4 g1 sp2 *	0.75	0.29
Cx-4 g1 sp3 *	0.89	0.11
average	0.81	0.20
standard deviation	0.07	0.09

* denotes samples with spectra shown in Figure 31.

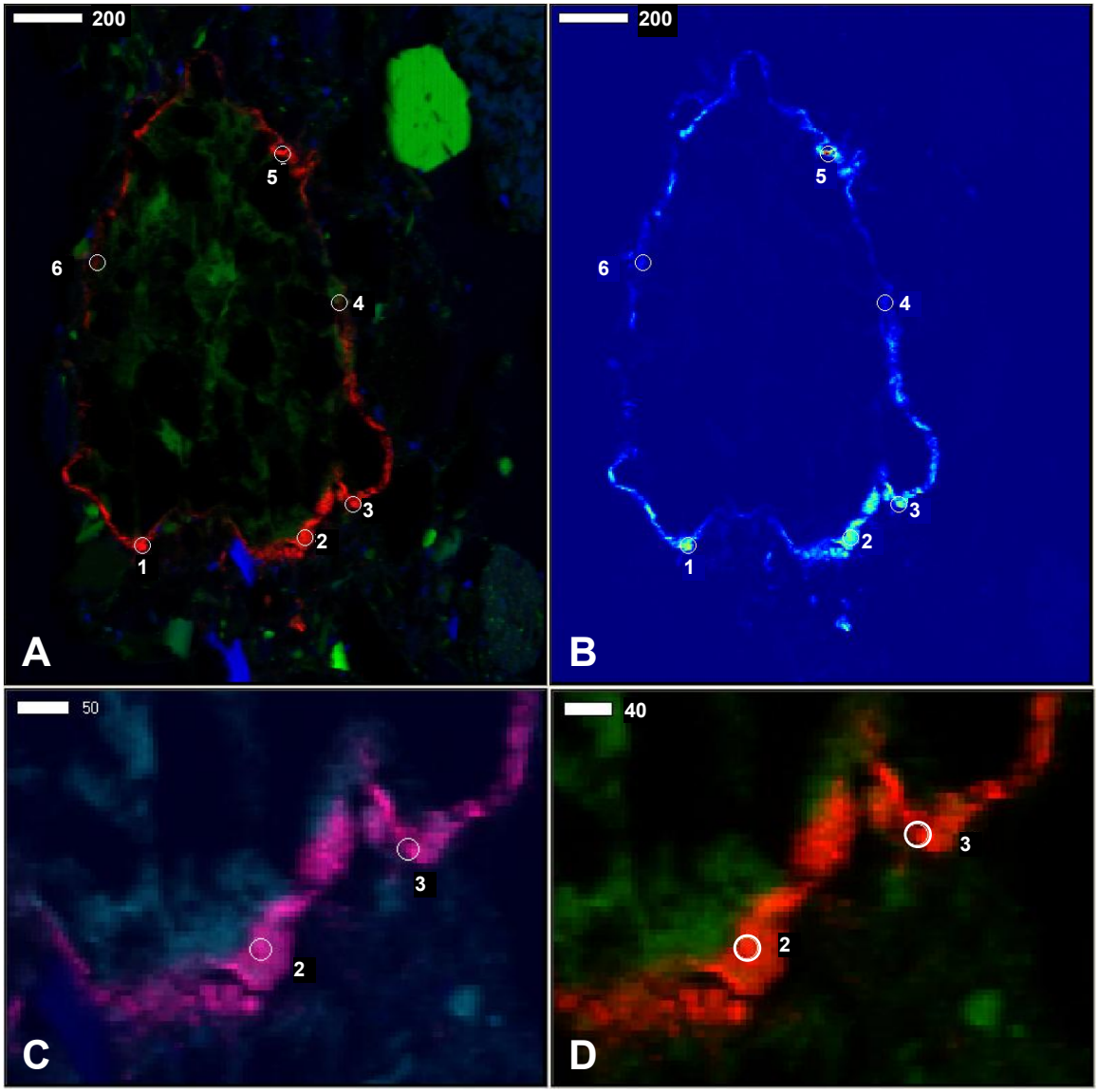

Figure 33. μXRF maps of column B sediment sample F4 grain 1. (A) μXRF tricolor map of U(IV) in red, iron in green and calcium in blue; (B) μXANES map of U(IV); (C) zoom of area near points 2 and 3 in A showing of U(IV) in red, iron in green and sulfur in blue; (D) zoom of area near points 2 and 3 in A showing of U(IV) in red, iron in green and calcium in blue. The color intensity increases with relative concentration. Scale bars are in microns. Numbered points are locations of μXANES spectra. Maximum counts are 3776, 116, 8521, 1126, and 51 for U(IV), U(VI), Fe, Ca and S fluorescence, respectively.

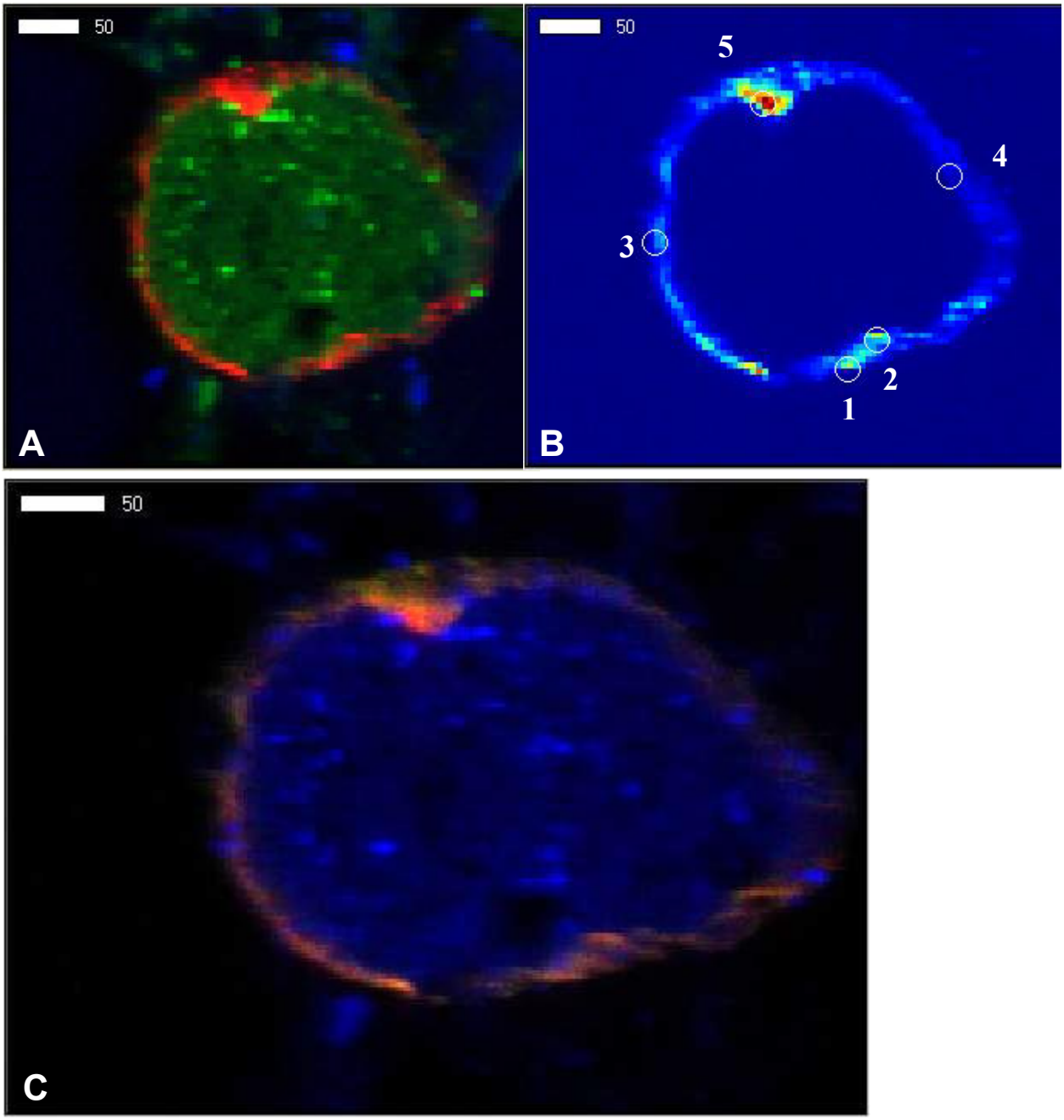

Figure 34. μXRF maps of column A sediment sample Ax-23 grain 1. (A) μXRF tricolor map of uranium in red, iron in green and calcium in blue; (B) μXRF map of uranium; (C) μXRF tricolor map of U(IV) in red, U(VI) in green and iron in blue. The color intensity increases with relative concentration. Scale bars are in microns. Numbered points are locations of μXANES spectra. Maximum counts are in (A) 2847, 3412, and 573 for U, Fe and Ca, respectively, and in (C) 2116, 881, and 3114 for U(IV), U(VI), an d Fe fluorescence, respectively.

Micro-focused U EXAFS spectra were collected at one point on each of the three grains described above (Table 11). The points with the highest U fluorescence count rate were chosen to provide best signal quality. The k-space k^3-weighted spectra of points in the U-rich grain coatings are similar to the nano-partculate uraninite reference spectrum (Figure 27) and to the bulk EXAFS of column sediments (Figure 32). In addition the Fourier transforms of the EXAFS also have peaks at distances similar to the U-O and U-U shells described for the bulk samples at 1.8 and 3.5Å, uncorrected for phase shift. Because of the significant fraction of U(VI) (0.19 to 0.28) present at these thin section grain points, shell by shell fits of the EXAFS were not possible because of the inability to accurately account for the contributions from U(VI) masking longer distance shells. Linear combination fits were not attempted because no suitable single component models exist for non-polymerized NUSAB U(IV). Nonetheless, qualitatively these spectra are consistent with a large component of nano-particulate uraninite in the coatings.

3.4.4 SEM-EDS Imaging of Column Sediments

Imaging of thin section grains was also conducted using back-scatter electron scanning electron microscopy (BSE-SEM). Because of its high atomic number, uranium has a much higher yield of back scattered electrons than lighter elements allowing qualitative identification of U-rich areas. However, because U in the column sediment thin sections was located in a relatively small number of grains, BSE-SEM was limited to U-rich grains previously identified in the 30-μm resolution μXRF maps. Energy dispersive X-ray spectral (EDS) analysis of elemental composition of selected points was conducted using a nominal 1 μm diameter beam size. Results of measurements of grains from column C recovered at the end of biostimulated reduction are presented below as examples.

The BSE-SEM image (Figure 35) of the entire grain of the column C sediment (Cr-5 thin section right panel grain 1) described above (Figure 30) has a bright white zone surrounding the grain. EDS analysis confirms that these bright regions have abundant U. Higher resolution images of areas containing U show a coating 1 to 5 μm in thickness on the grain exterior that fills embayment and voids in the sediment grain surface. The U coating consists of fibrous particles clustered or aggregated to form the coating, with other particles without U intermixed into the coating (Figure 30B) or adhering to the coating surface (Figure 30A). Uranium also extends up to 10 μm into cracks or fissures near the surface (Figure 30 area A). The U appears to follow the morphology of the underlying grain in the iron rich area of this grain (Figure 30C). Area A is near XANES point 4 depicted in Figure 30, and area C is near EXAFS point 5. EDS measurements of elemental abundances of selected points depicted in sub areas A and C of this grain confirm that the brighter areas have elevated U (Table 12). For example point A1 is 14 atomic % U, while an entrained grain (A2) has no measurable U but contains Fe and S. The EDS of the interior of the large grain at point A3 is consistent with quartz. The gray material, point A4, outside of the bright coating has lower U but contains elements common to aluminosilicate minerals such as clays that appear to be adhering to the coating on the larger grain. Point C2 within the grain in area C has detectable U, but elevated Fe and other elements indicating an iron silicate. Points C2 and C3 in the bright coating have high U, no Fe or S, and minor amounts of other elements. Both points have measurable P and point C2 has 22% C, which may be organic carbon since Ca and Mg, which are elements indicative of carbonate phases, are not present. EDS data was not collected in area B.

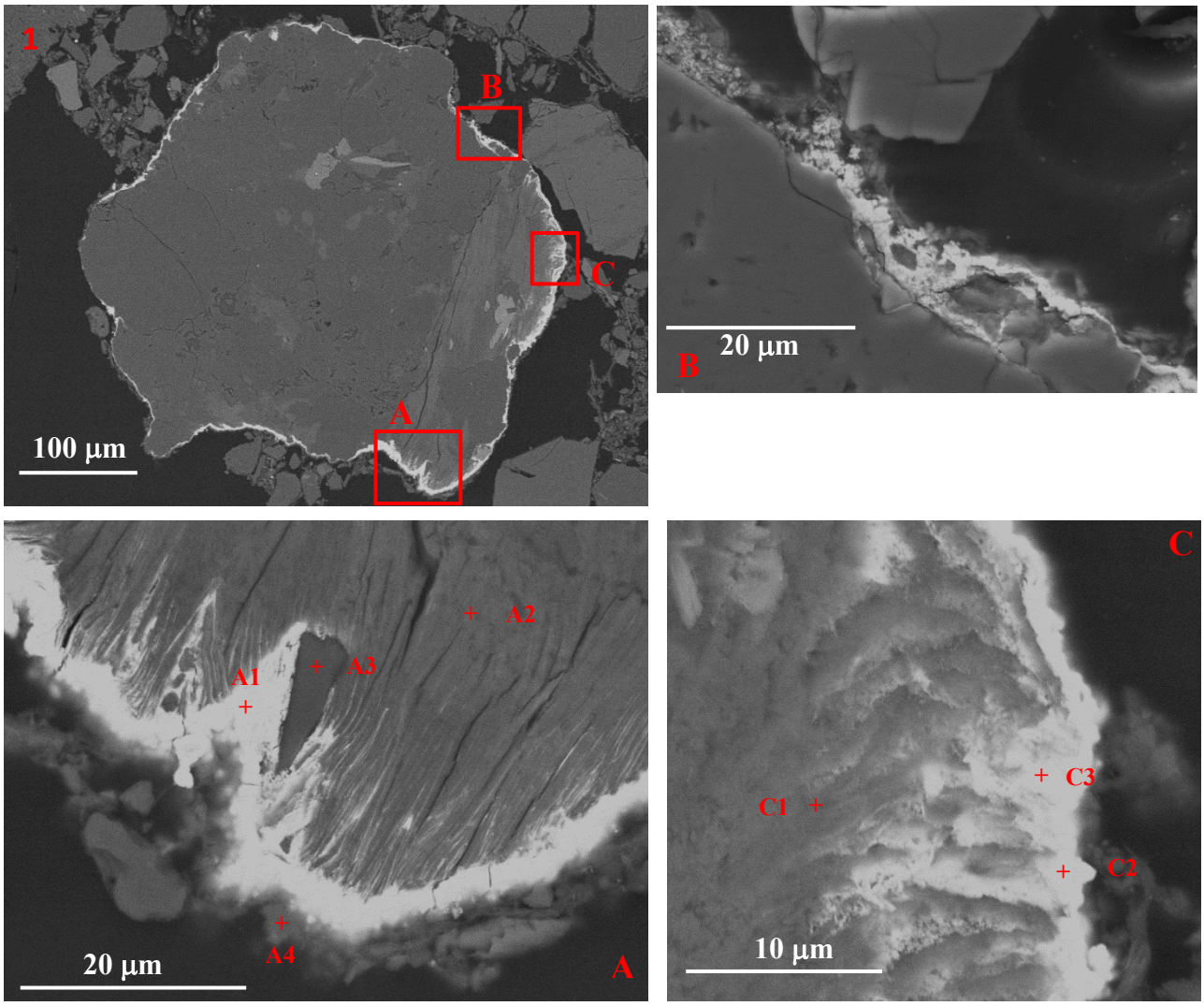

Figure 35. SEM-BSE images of column C after biostimulation interval 5 (Cr-5) thin section grain 1. Location of EDS spectra are shown in higher magnification images of areas A, B, and C outlined in red in the upper left image (1). µXRF images of this grain are shown in Figure 30.

Table 12. Atomic percent of elements detected in SEM-EDS points data from column C subsample Cr-5, thin section right panel, grain 1. See Figure 35 for location of EDS points.

Point	U[a]	Fe	S	C	O	Si	Al	Mg	Ca	K	P
A1	14.41				73.28	2.58	2.61		4.33		2.79
A2		8.22	1.11		62.59	10.96	8.02	9.11			
A3					68.64	31.36					
A4	2.3	2.04			66.50	16.34	8.13	1.42	1.65	1.61	
C1		8.59			62.26	10.97	7.82	8.53		1.85	
C2	9.32			21.9	61.68	1.95				2.9	2.25
C3	11.65				74.78	2.54	2.52			4.98	3.54

a. No value equals element below detection.

A small grain in column C thin section sample Cr-5 that had elevated U in the 30-μm resolution XRF map (not shown) was imaged using BSE-SEM with selected points measured by EDS (Figure 36; Table 13). The ~30 x 50 μm grain appears to be a cluster of smaller grains that includes bright U-rich areas near the exterior of the top and running vertically through the center of grain. The bright areas appear surrounded by a lighter gray material. Both zones have voids or dark areas throughout. Elevated U ranging from 4.3 to 7 atomic % was measured in the brightest areas (points A3, A8, B1, C4; Figure 36; Table 13). Points in the surrounding light gray areas had lower U (points A4, A6, A10, C2, C3 and C5). Points in darker areas or in obvious discrete grains had no measurable U (e.g B3, B4, C1). The light gray areas have high Fe and S. The high U points had lower, but measurable Fe and S. The S to Fe ratio in all the points in the bright and light area ranged from 0.6 to 1.2, consistent with the presence of iron sulfides. The U and the putative iron sulfides areas appear to be comprised of submicron particles or amorphous material. The high U areas appear to be forming on the iron sulfide material (e.g. area C). The nominal beam size of 1 μm diameter for EDS measurements limits resolving whether U is adjacent to or intermixed with iron sulfide areas. Combined, the BSE-SEM imaging and EDS measurements suggest that this particle is in part comprised of aluminosilicate material cemented by iron sulfides which have coatings or zones of U. These results are consistent with abiotic reduction of U by iron sulfides (Hyun *et al.*, 2012; Gallegos *et al.*, 2013). Points A3 and A4 have elevated carbon perhaps resulting from microbial biomass.

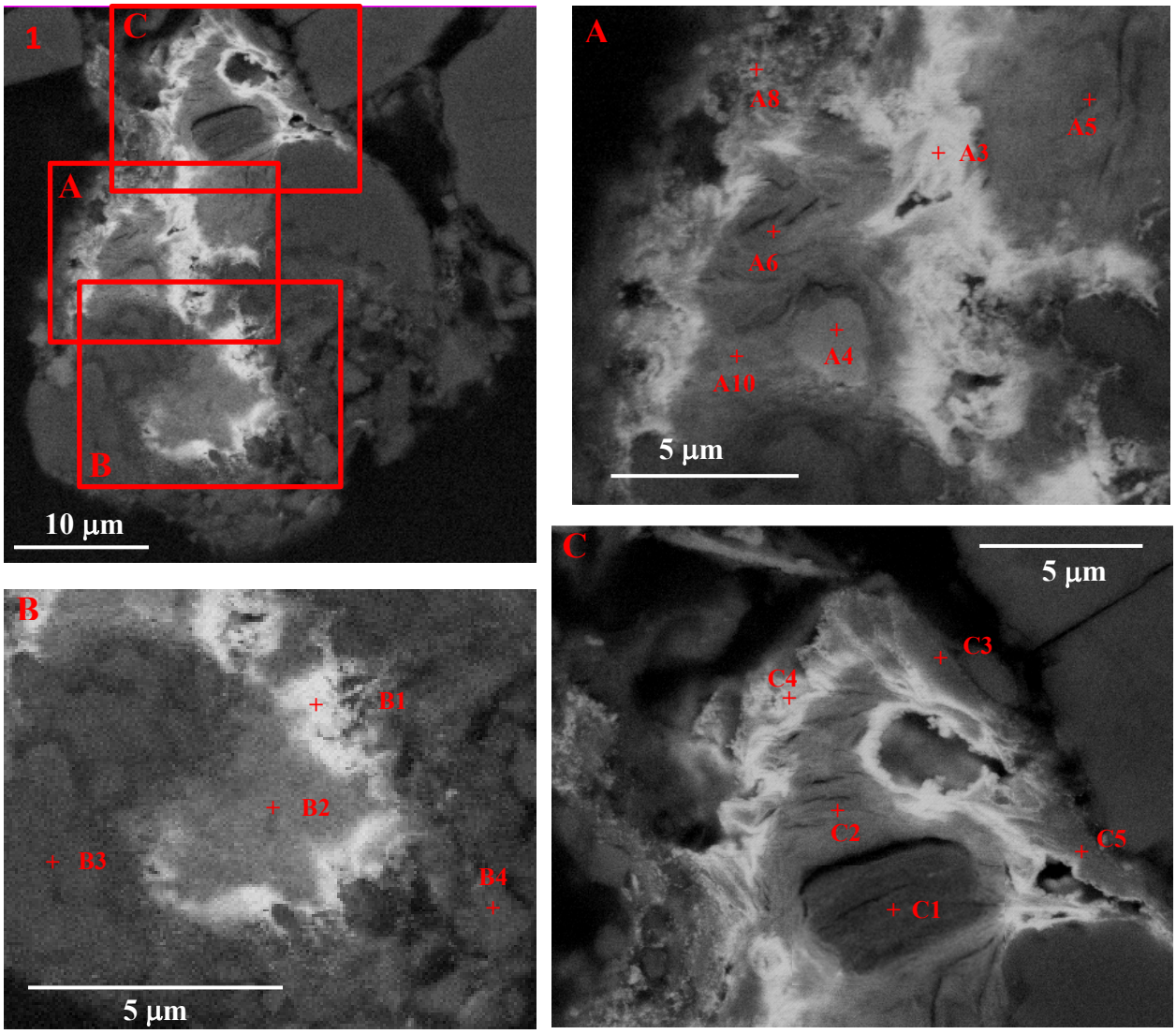

Figure 36. SEM-BSE images of column C interval 5 (Cr-5), grain 2 after biostimulation. Location of EDS spectra are shown in higher magnification images of areas outlined in red in the upper left image (1).

Table 13. Atomic percent of elements detected in SEM-EDS points data from column C post reduction, interval Cr-5 grain 2. Location of point spectra are shown in Figure 36.

Point	U[a]	Fe	S	S/Fe	C	O	Si	Al	Ti	Mg	Ca	K	P
A3	7.02	1.29	0.89	0.7	21.6	56.9	3.84	1.52		2.54	2.68		1.72
A4	0.79	3.57	4.34	1.2	9.79	58.44	3.77	1.6	15	2.23	0.46		
A5		15.7	17.35	1.1		46.68	10.46	3.49		6.32			
A6	0.48	9.52	10.38	1.1		55.26	10.69	4.78		8.22	0.67		
A8	4.32	2.48	1.27	0.5		63.97	14.78	7.88		3.27	2.03		
A10	1.3	14.48	13.28	0.9		48.66	12.16	4.38		5.75			
B1	6.13	1.31	0.94	0.7		56.88	27.9	1.19		1.52	2.55		1.57
B2		10.56	11.58	1.1		49.11	22.93	2.46		3.36			
B3						66.58	33.42						
B4		0.93				64.97	29.89	3.38				0.83	
C1		0.92	0.85	0.9		63.11	18.68	14.92				1.51	
C2	0.83	10.52	11.55	1.1		53.55	11.31	5.43		5.81	0.99		
C3	1.11	2.4	0.86	0.4		66.06	15.48	6.94		5.43	0.59	1.13	
C4	5.56	3.38	2.02	0.6		61.78	11.05	5.27		7.17	2.62		1.15
C5	1.61	3.03				63.83	15.09	7.68		4.58	1.43	1.7	1.06

a. No value equals element below detection.

3.5 Microbial Analysis

Biomass was generally plentiful in the sediment recovered at the end of the biostimulation stage and in effluent filter samples collected during biostimulation. In addition, sediments from column A after oxic elution had sufficient biomass for microbial assay. All of these samples were successfully amplified for Terminal Restriction Fragment Length Polymorphism (TRFLP) quantitative Polymerase Chain reaction analyses (qPCR) of the iron reducing bacteria *Geobacte*r and sulfate reducing bacteria (SRB).

3.5.1 TRFLP Fingerprinting

Figure 37 shows the cluster analysis of the bacterial TRFLP fingerprints for Rifle material. Samples from the same column generally grouped together, with some exceptions. Column A samples, for example, recovered after oxic elution all group together. Column B forms subclusters which include samples from column C. Both of these columns received input of ferrous iron; column B after 210 days of acetate and U input while column C had continuous ferrous iron input throughout acetate biostimulation. In addition, the effluent filter (taken from column C during the iron reduction phase, Cr-eff(1), Figure 37 and Table 14), clusters with the inlet and outlet filters of column B, as well as the outlet filters for column C. In contrast, the effluent filter taken during sulfate reduction (Cr-eff(2)), clusters more with sediment sections 1-4 of column C and some of the column C inlet filters.

Table 14. Column sediment microbial abundance data for sulfate reducing bacteria (SRB) and Geobacter (GEO).

Sample Name	Description	Sediment extracted (g)	SRB/μL	SRB/gram	GEO/μL	GEO/gram
Column A: after biostimulation						
Ar-1	syringe core	0.72	2.50E+05	1.74E+07	5.49E+05	3.81E+07
Ar-2	syringe core	0.96	1.38E+05	7.16E+06	4.46E+05	2.33E+07
Ar-3	syringe core	0.91	7.94E+04	4.36E+06	2.78E+05	1.53E+07
Ar-4	syringe core	0.85	1.60E+05	9.43E+06	2.08E+05	1.23E+07
Ar-f(out)	outlet end filter, scrape	0.57	2.15E+06	1.89E+08	7.25E+05	6.36E+07
Ar-f(out)	extract of outlet filter after scrape		1.52E+06		5.62E+05	
Ar-f(in) sed	sediment from inlet end filter	0.74	7.45E+05	5.03E+07	4.83E+05	3.26E+07
Ar-f(in)	inlet end filter, scrape	0.4	2.24E+05	2.80E+07	9.25E+04	1.16E+07
Ar-f(in)	extract of inlet filter after scrape		5.74E+05		1.78E+05	
Ar-eff-1	effluent filter day 179-186	0.69	8.03E+04	5.82E+06	1.94E+03	1.41E+05
Column A: after oxic elution						
Ax-2	column outlet end	1.02	1.58E+04	7.75E+05	6.43E+04	3.15E+06
Ax-23	mid-column lengthwise	0.65	6.37E+03	4.90E+05	3.26E+04	2.51E+06
Ax-26	column inlet end	0.62	2.39E+04	1.93E+06	1.28E+05	1.03E+07
Ax-f(out)	outlet end filter, scrapes	0.24	4.12E+03	8.58E+05	9.94E+03	2.07E+06
Column B: after biostimulation						
Br-eff-1	effluent filter day 113-121	0.584	4.95E+05	4.24E+07	2.26E+04	1.93E+06
Br-F1	sediment, 5-6 cm	0.53	8.84E+03	8.34E+05	1.04E+05	9.81E+06
Br-F3	sediment, 3-4 cm	0.46	4.37E+03	4.75E+05	5.77E+04	6.27E+06
Br-F4	sediment, 2-3 cm	0.64	3.88E+03	3.03E+05	6.93E+04	5.41E+06
Br-F5	sand pack; 0-2 cm	0.63	2.14E+04	1.70E+06	5.34E+04	4.24E+06
Br-f(in)	inlet end filter, scrapes	0.36	1.18E+04	1.64E+06	1.70E+03	2.36E+05
Br-f(out)	outlet end filter, scrapes	0.49	5.00E+03	5.10E+05	1.21E+03	1.23E+05
Column C: after biostimulation						
Cr-1	sediment, 4-5.5 cm	0.47	4.74E+02	5.04E+04	1.24E+05	1.32E+07
Cr-2	sediment, 2.8-4 cm	0.39	2.51E+02	3.22E+04	5.29E+04	6.78E+06
Cr-3	sediment, 1-2.8 cm	0.45	4.50E+02	5.00E+04	8.73E+04	9.70E+06
Cr-4	sediment, 0-1.6 cm	0.41	3.71E+03	4.52E+05	8.77E+04	1.07E+07
Cr-f(out) CN	outlet end filter, scrapes	0.23	3.54E+04	7.70E+06	1.69E+05	3.67E+07
Cr-f(out) GF	outlet end filter, scrapes	0.35	2.12E+03	3.03E+05	1.66E+03	2.37E+05
Cr-f(in) CN	inlet end filter, scrapes	0.20	1.22E+05	3.05E+07	1.62E+05	4.05E+07
Cr-6	sediment, composite	0.97	-	-	1.28E+04	6.60E+05
Cr-eff-1	effluent filter during iron reduction, day 7-14	0.52	3.81E+01	3.70E+03	6.61E+05	6.42E+07
Cr-eff-2	effluent filter during sulfate reduction, day 28-34	0.52	3.72E+04	3.61E+06	3.12E+05	3.03E+07

Samples in bold were characterized further with clone library analysis. Sample identification codes f(in), f(out), and eff refer to column inlet filter, outlet filter, and effluent filter, respectively; others as shown in Tables 6, 7, and 8. Volume filtered in liters is listed for effluent filters under sediment weight extracted, with SRB/L and GEO/L replacing per gram values for these samples.

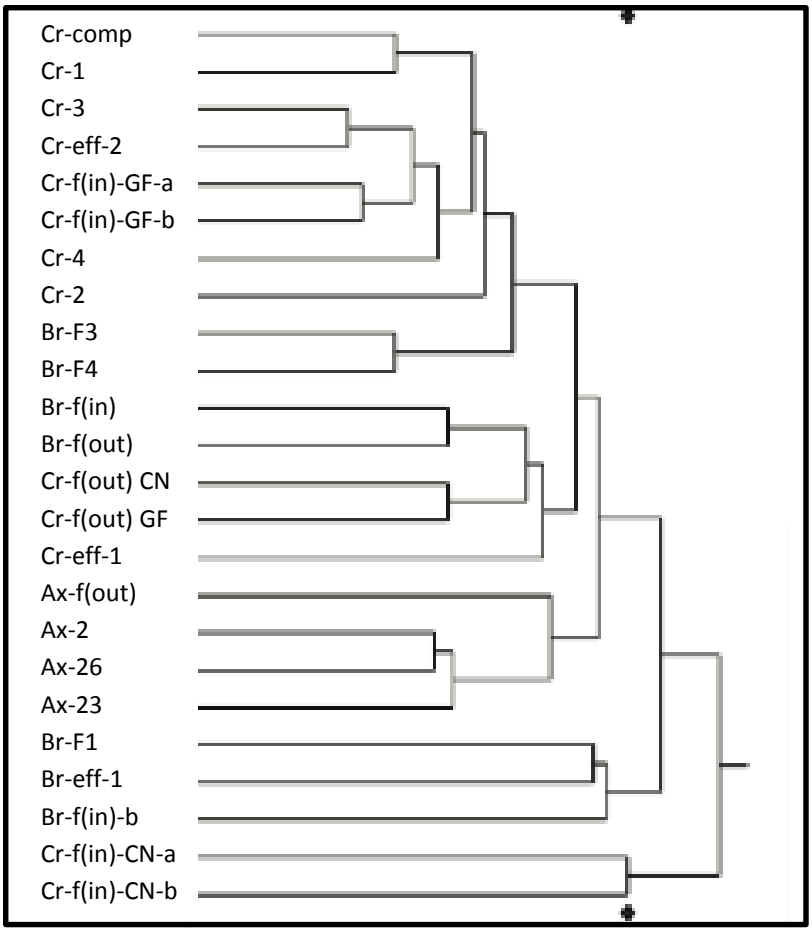

Figure 37. Cluster analysis for column sediments. See Table 14 for sample identification codes.

3.5.2 qPCR

Table 14 shows the abundance of dissimilatory sulfate reducing bacteria (SRB) and the iron reducing bacteria *Geobacter* 16sSrRNA gene expressed as copy number/g sediment or copy number/L filtered for effluent filters. The copy number is measured in the qPCR assay, and refers to the number of gene copies detected; this number relates to the cell number but is not equivalent to cell number, as copy number per cell depends on the gene and the organism. Typical SRB copies are 1-3 per cell, and Geobacter usually have 1-2 copies of 16SrRNA per cell.

Geobacter was higher in abundance than SRB in most samples. Column A, which was sampled during the reduction stage and later after oxic elution, showed decreases in both *Geobacter* and SRB abundances after oxic elution (Table 14). Figure 38 compares sediment abundances of the two groups for different locations within column A. *Geobacter* was in greater abundance than SRB in sediment samples for both reduction and oxidation stages. During reduction, SRB abundance was in the 1E7 copy/g range (4E6 to 1.7E7) in column sediments, with the highest abundance detected in filter scrapes from the effluent end of the column >1E8/g. *Geobacter* was in the 1 to 4E7 copy/g range in column sediments, with higher concentrations also observed in filters from the effluent end of the column. There were not large differences in

abundance among sediment samples, but the inlet end did contain higher abundances of both SRB and *Geobacter*. The trend of higher abundance of both in sediments near the inlet corresponds to higher sediment uranium measured near the inlet of the column. After oxic elution without electron donor amendment, abundances of both were much reduced compared to the reduction phase. SRB abundances had decreased to the 5E5 to 2E6 copy/g range, and *Geobacter* decreased to 2E6 to 1E7 copy/g range, with higher abundances present at the inlet end (Table 14).

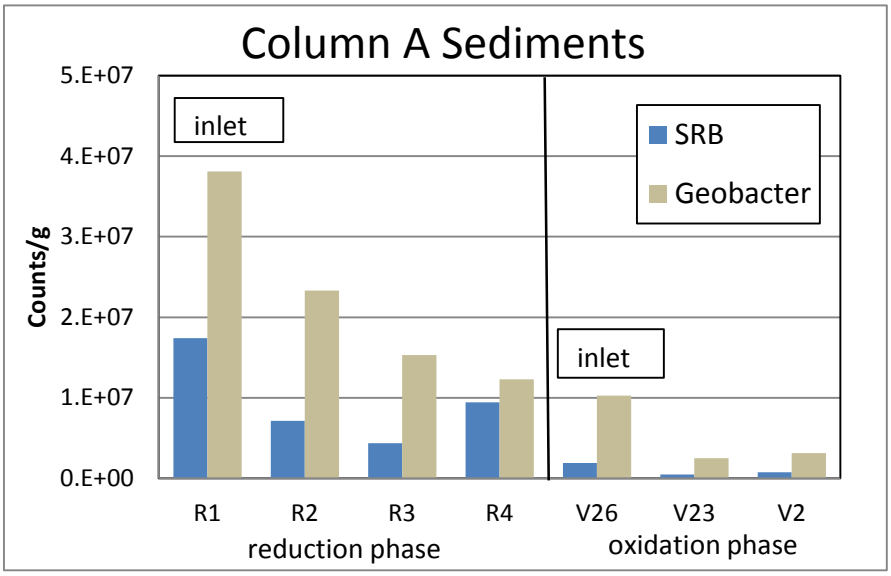

Figure 38. Abundances of sulfate reducing bacteria (SRB) and Geobacter in sediment of column A after biostimulated reduction and after oxic elution.

Microbial analysis of column B sediments was conducted on samples recovered at the end of the biostimulated reduction experiment. That is, sediments assayed were after 210 days of anaerobic artificial groundwater influent with U(VI) and acetate and an additional 120 day period of influent also containing ferrous iron. The range of SRB in column B sediment was 3E5 to 1.7E6 copies/g, and *Geobacter* was 4E6 to 1E6 copies/g. These abundances are lower than in column A sediments recovered at the end of the biostimulation stage despite a much longer biostimulation period. Column B sediments show that both SRBs and *Geobacter* abundances are lower at the inlet and highest at the outlet (Figure 39). It is important to note that column B was homogenized after 220 days of reduction stage (see section 3.1.2.) and that the sediments assayed were sampled after an additional 120 days of continued biostimulation. In addition, the sand pack at the inlet end of the column had substantially higher abundances (more than a factor of two) than adjacent column sediments. It appears that microbial activity and biomass growth was enhanced in the sand pack where electron donor first entered the column. Interestingly, although the *Geobacter* abundances were higher in the column sediments than SRB, the inlet and outlet filters had higher abundances of SRB (Table 14).

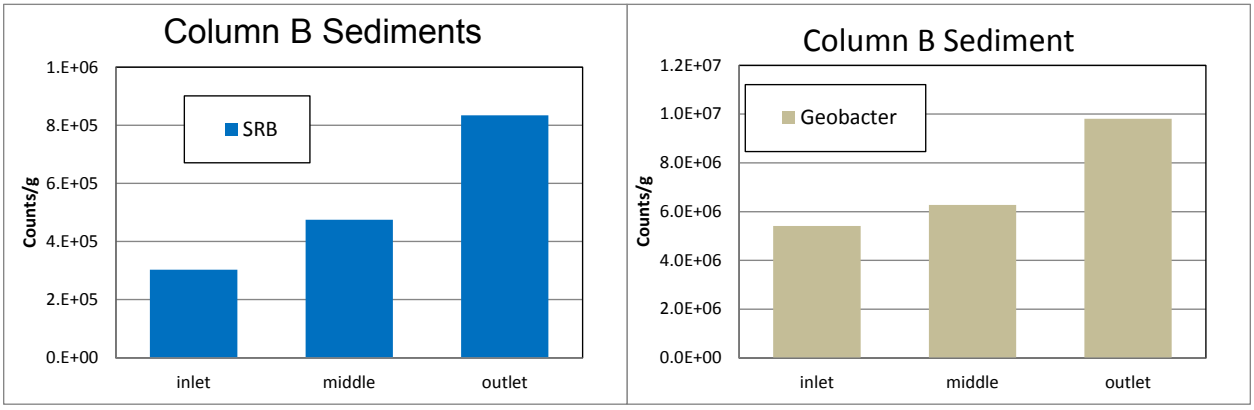

Figure 39. Comparison of abundances of sulfate reducing bacteria (SRB) and *Geobacter* in column B sediments.

Column C had simultaneous addition of ferrous iron, U(VI), and acetate for the entire 185 days of the biostimulation stage of the experiment. Column C sediments (Figure 40) showed the largest difference in abundance between SRB and *Geobacter* in sediments compared to the other columns, with *Geobacter* abundances 2 orders of magnitude greater than SRB. SRB was in the range of 3E4 to 4.5E5 copies/g, while *Geobacter* was in the range of 6.8E6 to 1.3E7 copies/g. Column C sediment SRB were highest nearest the inlet, an order of magnitude higher than the other column sediments, while there was little trend in *Geobacter* abundance within the column. Column C *Geobacter* sediment abundance was similar to column B, but substantially lower than column A (Table 14). SRB abundance in column C was up to a factor of 50 lower than column A. A large change in SRB, a 3 orders of magnitude increase, is observed between the filter samples taken during the Fe reduction stage and then at the sulfate reduction stage. A decrease of 6.4E7 to 3.0E7copies/L *Geobacter* abundance was observed during this transition.

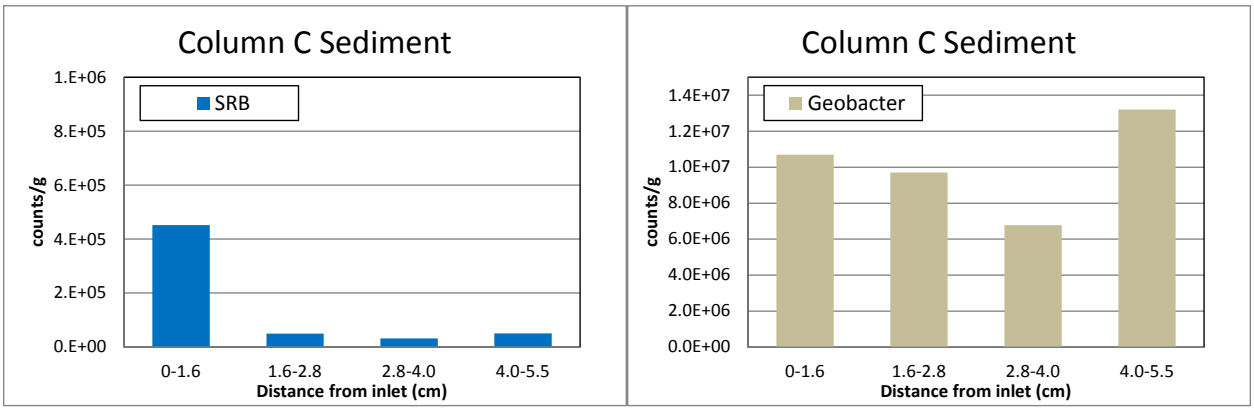

Figure 40. Comparison of sulfate reducing bacteria (SRB) and *Geobacter* abundance in column C sediment after biostimulated reduction.

Figure 41 shows abundances of *Geobacter* in sediment from all columns, including column A after 180 days of oxic elution. Figure 42 shows abundance of SRBs in the same samples. Abundance of *Geobacter* in column A during the biostimulation of column A is highest at the column inlet and decreases from there to the outlet. This is generally true for the SRBs as well. Column A sediments had a greater abundance of *Geobacter* by a factor of two or more than the

other columns. Abundances of SRB in sediments are up to a factor of 50 greater than in the other columns. Interestingly, column B and C had comparatively longer biostimulation periods, 334 and 186 days, respectively, versus 112 days for column A. The greater abundances in column A of both types were contrary to an expected increase in biomass growth in the other columns because of the longer period of continual addition of electron donor (acetate) and micronutrients. The primary difference between column A and the others is the absence of ferrous iron input to column A. It is unknown if the presence of dissolved iron limited growth of SRB. Additionally, column A had an extended period of 81 days anoxic influent in the absence of electron donor, which would be expected to result in limited increase in biomass. These results will be discussed further in relation to electron balance of likely microbial redox processes characterized by integrated effluent profiles and sediment chemical analyses.

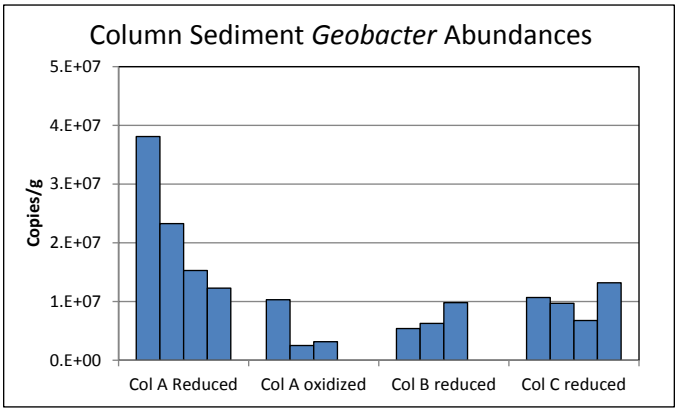

Figure 41. *Geobacter* abundances in columns A, B, C after biostimulated reduction, and after oxic elution (column A). Sample position in column from inlet to outlet is from left to right.

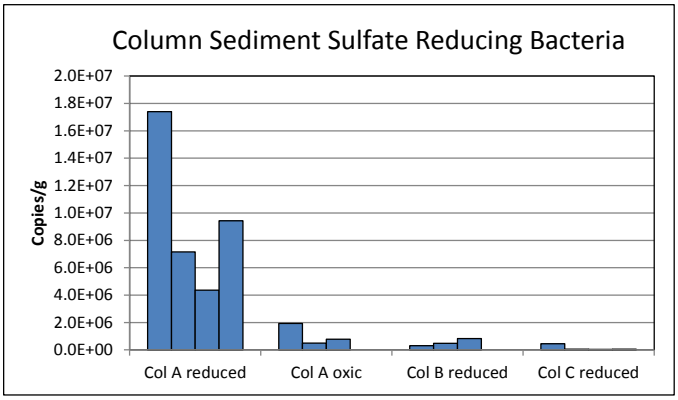

Figure 42. Abundance of sulfate reducing bacteria in column sediments. Sample position in column from inlet to outlet is from left to right.

3.5.3 Clone Library Analyses

Six samples were chosen for SRB cloning and sequencing, and 3 were chosen for *Geobacter* sequencing based primarily on cell abundance. Column A outlet filter at the end of biostimulation and the B effluent filter sampled in February 2010 during the biostimulated reduction stage were chosen for both SRB and *Geobacter* clone library construction. In addition, sediment from the outlet end of column A recovered after oxic elution and the column B inlet

filter after biostimulation were used for SRB clone library construction. From column C, the inlet end filter at the end of biostimulation and an effluent filter collected during sulfate reduction were chosen for SRB characterization by cloning. The column C effluent filter collected during the Fe reduction phase was chosen for *Geobacter* clone library analysis. These samples are denoted in Table 14.

Geobacter sequences were not very diverse and were dominated by those previously described as subsurface clade 1 of *Geobacteraceae*, believed to be important in U(VI) reduction in subsurface environments (Table 15). There are also a very few in the *D. acetoxidans* clade (Holmes *et al.*, 2007). The subsurface clade includes closely related sequences identified from water filtered from wells M16, M18, M21 at the Rifle site (Holmes *et al.*, 2007), as well as some *Geobacter* sequences found at other subsurface sites. Previously, these authors found the same trend at the Rifle site in their study of subsurface clade 1 domination with some other minor sequences such as the D. acetoxidans clade. The proportions of each sequence were not the same in each column, however. *Geobacter* prevalent at well M21 dominated in column A, and a sequence from well M16 was also prevalent representing 22% of the clones. The 3rd sequence found in column A, which was most closely related to "Riflegeoclone 4" from a previous study, represented 13% of the sequences in column A. However, this was the dominant sequence, representing 71% of the sequences in column B (Table 15). In addition, a sequence in the *D. acetoxidans* clade as described by (Holmes *et al.*, 2007) represents 14% of the sequences in column B. At the Rifle field site, M16 is a location closer to the acetate injection wells than M21. This suggests that M16 is more reducing than M18 which may be more reducing than M21. Thus the differences in sequences may represent different degrees of reducing conditions as a result of the concentration and input duration of acetate amendment.

Table 15. *Geobacter* clones from columns A outlet filter, Ar-f(out), and B effluent filter, Br-eff(1).

Phylotype Number	Relative abundance (%) Col A	Relative abundance (%) Col B	Closest Genbank relative (Blast)	Blast source description	Sequence similarity %
1	65	14	CP001661.1	Geobacter M21 from Rifle	100
2	22	0	EF668531.1	uncult Geo from M16 Rifle	100
3	13	71	EF668606.1	Riflegeoclone4	98
4	0	14	AJ271656.1	Pelobacter, Geothermobacter?	99

The column C effluent filter collected during the Fe(III) reduction phase, Cr-eff(2), was also mostly comprised of the subsurface clade 1 of Geobacteraceae. However, the M21 sequence was minor, representing 2% of the clone library. A sequence identical to a Rifle clone from M16 (Genbank accession #EF668531) was the dominant Geobacter representing 66% of the clones (accession #CP001661) with 15% of the clones related to Geobacter M18 (accession#CP002479), and 5% of the clones were most closely related to Pelobacter propionicus in the D. acetoxidans clade (accession # X70954). The rest of the clones, representing 12% of the sequences, were related to uncultured sequences from other environments, and do not appear to be part of the subsurface clade.

Table 16 summarizes SRB sequences found in each sample, the closest phylogenetic relatives based on BLAST searches, and the relative abundance in the clone library. The SRB sequences in column samples have relatively little diversity. For example, in column B effluent filter, Br-eff(1), collected well after the onset of sulfate reduction (day 113 to 121), only three

phylotypes were defined by SRB sequences. The two dominant phylotypes, representing 66% and 32% of the sequences, respectively, were most closely related to uncultured *dsr*B sequence obtained from a different uranium mill tailings site (AY015603), and a metal precipitation in groundwater experiment (AY731421) (Table M-3). The phylogenetic affiliations are *Desulfobulbaceae* and *Desulfobacteraceae*. The column A outlet filter recovered at the end of biostimulated reduction was dominated by the same type of *Desulfobulbaceae* organism (71% most similar to AY015603 from a uranium mill tailings site), but overall was more diverse than the column B sample, with 8 phylotypes (Table 16). The next most abundant sequence, representing 13% of the sequences retrieved from column A, was closest to an uncultured organism associated with steel corrosion in a French seaport (FR689663), and is in the *Syntrophobacteraceae*. This sequence identity has been found in many other Rifle samples, though never dominant. There are also representatives that group with *Desulfotomaculum* (*Peptococcaceae*), and *Desulfobactereaceae*.

The other column samples were low in diversity, typically with one or two dominant SRB, and several minor phylotypes. The column B inlet filter sample, Br-f(in) recovered at the end of biostimulated reduction contained 5 phylotypes, with 1 comprising 73% of the sequences (Table 16). This phylotype was most closely related to a SRB sequence retrieved from another uranium mill tailings site (AY015603), and is in the family *Desulfobulbaceae*. The next two dominant organisms corresponding to 10% of the sequences each are likely *Desulfotomaculum*, and *Syntrophobacteraceae.* This dominant sequence is the same as the effluent filter collected earlier from this column, but the *Desulfotomaculum* has decreased from 32% to 10% of the sequences, and the *Syntrophobacteraceae* have increased over time, from not detected on the effluent filter (day 113 to 121) to 10% of the population at the end of the biostimulation.

The SRB phyllotypes and abundances changed dramatically in column A as a result of oxic elution compared to during biostimulated reduction. Four phylotypes were measured after oxic elution, with the dominant sequence (73% of the clones) from a different organism, though still in the family *Desulfobulbaceae* (Table 16). Interestingly a group of *Syntrophobacteraceae* represent approximately the same percentage of SRB sequences as determined in the column outlet filter sample, Ar-f(out), but are a different *Syntrophobacteraceae* than observed earlier. No members of *Desulfotomaculum* or the *Desulobacteraceae* are evident in the samples collected after oxic elution.

Table 16. Sulfate reducing bacteria phylotypes, relative abundance, and closest BLAST Hits from column sediment samples recovered after biostimulated reduction and after oxic elution.

Group #[a]	#[b]	rel abund[c]	Closest Genbank relative (Blast)	% ID[d]	Source	Blast source Identification
Column A: Ar-f(out) outlet filter scrape						
1	**2**	**4.4**	**EF065046.1**	**81**	**landfill leachate**	**Desulfotomaculum? (Peptococcaceae)**
2	**1**	**2.2**	**DQ250766.1**	**95**	**landfill leachate**	**Syntrophobacteraceae**
3	**1**	**2.2**	**AM901668.1**	**96**	**freshwater grassland soil**	**Desulfosarcina? (Desulfobacteraceae)**
4	**1**	**2.2**	**FR689665.1**	**81**	**steel corrosion**	**Syntrophobacteraceae**
5	**6**	**13.3**	**FR689663.1**	**82**	**steel corrosion**	**Syntrophobacteraceae**
6	**32**	**71.1**	**AY015603.1**	**95**	**uranium mill tailings**	**Desulfobulbaceae**
7	**1**	**2.2**	**FR689616.1**	**85**	**steel corrosion**	**Syntrophobacteraceae**
8	**1**	**2.2**	**CP001720.1**	**87**	**isolate**	**Desulfotomaculum? (Peptococcaceae)**
Column A: sediment interval Ax-2						
1	**29**	**72.5**	**EF065041.1**	**87**	**landfill leachate**	**Desulfobulbaceae**
2	**6**	**15**	**AM901632.1**	**89**	**freshwater grassland soil**	**Syntrophobacteraceae**
3	**1**	**2.5**	**AM901621.1**	**90**	**freshwater grassland soil**	**Desulfobulbaceae**
4	**4**	**10**	**AY015603.1**	**86**	**uranium mill tailings site**	**Desulfobulbaceae**
Column B: Br-eff(1), effluent filter (day 113 to 121)						
1	**1**	**10.0**	**FR689629.1**		**landfill leachate**	**Desulfosarcina? (Desulfobacteraceae**
2	**25**	**72.5**	**AY015603.1**		**uranium mill tailings**	**Desulfobulbus?**
3	**12**	**5.0**	**AY731421.1**		**metal precipitation experiments, groundwater**	**Desulfobacteraceae**
Column B: Br-f(in), column inlet filter						
1	**4**	**10.0**	**AF334595.1**	**90**	**Desulfomonile tiedjei (Syntrophaceae)**	**Syntrophaceae**
2	**29**	**72.5**	**AY015603.1**	**94**	**uranium mill tailings site**	**Desulfobulbus?**
3	**2**	**5.0**	**AY929594.1**	**88**	**anaerobic sludge blanket**	**Desulfotomaculum?**
4	**4**	**10.0**	**AM901632.1**	**89**	**freshwater grassland soil**	**Desulfotomaculum?**
5	**1**	**2.5**	**AY929594.1**	**82**	**bioreacter granules, wastewater treatment**	
Column C: Cr-eff(2), column effluent filter during sulfate reduction (day 28 to 34)						
1	**13**	**37.1**	**AY015603.1**	**90**	**uranium mill tailings site**	**Desulfobulbaceae**
2	**21**	**61.8**	**AY015603.1**	**94**	**uranium mill tailings site**	**Desulfobulbaceae**
Column C: Cr-f(in), column inlet filter						
1	**14**	**37.8**	**AY015603.1**	**94**	**uranium mill tailings site**	**Desulfobulbaceae**
2	**1**	**2.7**	**AY015603.1**	**82**	**uranium mill tailings site**	**Desulfobulbaceae**
3	**22**	**59.5**	**FR689629.1**	**82**	**steel corrosion in port**	**Desulfobacteraceae**

a. Number of phylotypes

b. Number of clones

c. Relative abundance of clones

d. Sequence similarity

Two samples from column C were analyzed by clone library for SRB, and these samples were the least diverse for SRB of all of the samples examined. The effluent filter collected just after the onset of the sulfate reduction phase, Cr-eff(2), had two dominant groups, both in the *Desulfobulbaceae* and are most closely related to AY015603 from a uranium mill tailings site (Table 16). The column inlet filter, Cr-f(in), recovered at the end of biostimulated reduction also has lower diversity with two dominant groups observed (Table 16). One group is the same as the effluent filter sample and is most closely related to AY015603 from a uranium mill tailings site. It represents 39% of the clones. The other main phylotype represents 58% of the clones is dissimilar to most of in the database. It is closest to FR689629, which is only 82% similar (Table 16) and is in the phylotype *Desulfobacteraceae*.

3.5.4 Summary of Microbial Analyses of the Column Experiments

There was some structure in the columns in terms of abundances of *Geobacter* and SRB. In column A, which underwent a post reduction oxic elution, the abundances of SRB and Geobacter were highest in the outlet filter scrapes, but within the column itself, the highest abundances are towards the inlet end. Not surprisingly, the abundances of both *Geobacter* and SRB decreased between the biostimulated reduction phase and after oxic elution.

The distribution of SRB in column B was unlike column A. This is likely because sediments were homogenized when the column was repacked at day 220. However, the *Geobacter* abundances were actually higher at the outlet end of the column in this experiment. *Geobacter* may be more motile than SRBs and accumulated at the filter. Interestingly, although the *Geobacter* abundances were higher in the column sediments, the inlet and outlet filters had higher abundances of SRB.

Column C which had simultaneous addition of Fe(II), acetate and U(VI) throughout the biostimulated reduction stage of the experiment showed the largest difference in abundance between SRB and *Geobacter* compared to the other columns, with *Geobacter* abundances 2 orders of magnitude greater than SRB. This addition of ferrous iron throughout the experiment may have favored *Geobacter* over SRB. The abundances of *Geobacter* were similar throughout the column, suggesting the whole column was conducive to *Geobacter* growth. A small increase in SRB abundance (<20%) was observed in sediments near the inlet. A similar increase in total and acid volatile S was also observed in column C sediments. A 3-order of magnitude increase in SRB abundance in response to the onset of sulfate reduction was observed in the effluent filter compared to the filter collected before sulfate reduction during the Fe(III) reduction phase

The *Geobacteraceae* structure in clone libraries at Rifle are similar to those previously reported in this type of environment, dominated by subsurface clade 1 (Holmes *et al.*, 2007), and believed to be important in U(VI) reduction. Most of the sequences detected were either very similar or identical to those detected in other U(VI) remediation experiments performed at the Rifle site (Vrionis *et al.*, 2005). There were some differences in dominant *Geobacter* by column. For example a clone from Rifle site M16 was dominant in column C, whereas M21 was dominant in column A. The significance of these shifts is unknown, but likely reflects a differential response to the oxidation in column A for example, and to the continuous Fe addition in column C.

Sulfate reducing microbes were not very diverse in the column sediments. They were dominated by *Desulfobulbaceae* followed by *Desulfobacteraceae*, and to a lesser extent *Syntrophobacteraceae* , except in column C, where no *Syntrophobacteraceae* were detected. Generally only two to four phylotypes were observed, with the exception of the more diverse column A sample recovered at the end of biostimulated reduction, which had 8 phylotypes. In a

recent study, researchers investigated *dsr*AB transcript abundance during a U remediation experiment at the Rifle site and found these same 3 families to be dominant (Miletto *et al.*, 2011). They also found that *Desulfobacteraceae* appeared to respond most significantly to the acetate amendment. A fourth family, *Peptococcaceae*, also was found in columns A and C, though they were of much lower abundance. This group, which contains *Desulfotomaculum*, has also previously been found at a uranium contaminated site and is possibly important in the remediation (Chang *et al.*, 2005).

The abundance and diversity of SRB was lowest in column C, relative to columns A and B. Perhaps the competition with *Geobacter* allowed only a few groups of SRB to persist in the column. In column A, SRB changed dramatically after oxic elution compared to during reduction. The dominant sequence, representing 73% of the clones, is from a different organism, though still in the family *Desulfobulbaceae*. No members of *Desulfotomaculum* or the *Desulobacteraceae* are evident in the post oxidation sample, suggesting that they were sensitive to the oxic elution. An increase in sulfate reducers was found at the end of a field-scale remediation experiment at Rifle when mobilization of uranium was observed (Anderson *et al.*, 2003). Perhaps the sulfate reducing organism which became dominant was less oxygen sensitive than the other SRB, and possibly able to live under oxic conditions, and therefore outcompeted the other SRB.

4 Discussion of Column Experimental Results

4.1 Biostimulated Reduction

4.1.1 Electron Balance during Biostimulation

The integrated column effluent concentrations for acetate, total dissolved CO_2, sulfate, sulfide, iron, and uranium combined with "whole-column" changes in sediment content of iron, sulfur, and uranium (Table 3) provide insight on the relative importance of different biogeochemical processes occurring during the biostimulation period of the column experiments. These processes are incorporated into the reactive transport model simulation of biostimulated reduction presented in Chapter 5, specifically acetate oxidation and sulfate, iron and uranium reduction.

Acetate consumption was small during the first 20 days of biostimulation, but then increased throughout the remainder of the biostimulation period with effluent concentrations in column A and C showing near complete consumption of acetate by the end of the biostimulation period. The increase in acetate consumption starting at 30 days coincided with the increase in sulfate reduction as evidenced by the increase in effluent sulfide and decrease in effluent sulfate at this time. Oxidation of acetate by microbial processes requires equivalent reduction of other constituents to balance electron transfer from these electron donors. Likely terminal electron accepting processes (TEAP) under anaerobic conditions in aquifer sediments are sulfate, iron, manganese, and uranium reduction. An electron balance for electron donors (acetate oxidation) and TEAPs was constructed using the integrated column effluent data and solid phase analyses (Table 17). The total acetate consumption in columns B and C (85 and 71 millimoles, respectively) was greater than in column A (46 millimoles) consistent with the longer period of acetate amendment (Table 3). Oxidation of acetate to CO_2 produces 8 electrons. A net increase of 160 and 120 mmol total dissolved CO_2 was estimated for columns B and C, respectively, by integrating effluent sample concentrations (Table 17). Total consumption of acetate was 85 and 71 mmoles for columns B and C, respectively, which yields a ratio of acetate consumption to CO_2 production of 0.53 and 0.59, which are slightly higher than 0.5 for the 1:2 reaction stoichiometry for acetate oxidation to CO_2. The ratio of acetate consumption to CO_2 production for column A cannot be determined because total CO_2 was not measured in column A effluent samples during the first half of the biostimulation period.

Reduction of sulfate to sulfide (S^{-2}) requires an 8 electron transfer, 1 electron for reduction of Fe(III) to Fe(II), 2 electrons for U(VI) reduction to U(IV), and 2 electrons for Mn(IV) reduction to Mn(II) (Table 17). The sulfate reduction estimated from integrated loss of dissolved sulfate accounted for 72 to 110% of the electron transfer from acetate consumption. Total sulfate reduction also was estimated from the sum of the integrated effluent dissolved sulfide and the increase in solid phase S, assuming that solid phase S increase was all initially from complete reduction to S^{-2}. Subsequent partial oxidation of sulfide to S^{-1} forming FeS_2 or to S^o during reduction of Fe(III) phases by sulfide is thus accounted for by using the increase in total S. Total sulfur reduction from this estimate accounted for 39 to 87% of electron transfer from acetate oxidation (Table 17). Both of these estimates are consistent with sulfate reduction as the dominant TEAP process for oxidation of acetate for columns B and C. The comparison for column A indicates that the sulfate reduction TEAP accounts for 39 to 72% of the electron

transfer during acetate consumption. The discrepancy between the two estimates for column A likely is the result of error in the effluent dissolved sulfide since the solid phase measurements of S retained are in line with the other two columns given the duration of biostimulation of each.

Table 17. Summary of electron transfer during biostimulated reduction in columns A, B and C.

Constituent	Total mmoles			Electrons mmoles			Electrons donated (%)		
Column:	A	B	C	A	B	C	A	B	C
Electron donors:									
Acetate consumed[a]	**46**	**85**	**71**	**368**	**680**	**568**			
$C_2H_3O_2^- + 2H_2O \rightarrow 2HCO_3^- + 5H^+ + 8e^-$									
Electron acceptors:									
$SO_4^{-2} + 8e^- \rightarrow S^{-2}$ [b]	**33.2**	**64**	**78**	**-265.6**	**-512**	**-624**	**72.2**	**75.3**	**109.9**
Total sulfide[c]	**17.9**	**74.3**	**51.8**	**-143.2**	**-594.4**	**-414.4**	**38.9**	**87.4**	**73.0**
$Fe(III) + e^- \rightarrow Fe(II)$[d]	**9.2**	**9.6**	**6.5**	**-9.2**	**-9.6**	**-6.5**	**2.5**	**1.4**	**1.1**
$U(VI) + 2e^- \rightarrow U(IV)$[e]	**0.041**	**0.074**	**0.104**	**-0.082**	**-0.148**	**-0.208**	**0.02**	**0.02**	**0.04**
$Mn(IV) + 2e^- \rightarrow Mn(II)$	**0.059**	**0.045**	**0.048**	**-0.118**	**-0.09**	**-0.096**	**0.03**	**0.01**	**0.02**
Total TEAP				**-275**	**-522**	**-631**	**74.7**	**76.7**	**111.1**
Unaccounted e^-				**93**	**158**	**-63**			
Effluent Dissolved CO_2[f]	**n.m.**	**160**	**120**						
HCO_3^- produced[g]	**92**	**170**	**142**						

a. Acetate consumed is the integrated loss of acetate from difference between influent and effluent acetate over the duration of biostimulation.

b. Sulfate reduction determined by integrated effluent sulfate decrease over the duration of biostimulation. This measure of sulfate reduction is used in total TEAP estimate.

c. Total sulfide is the sum of the integrated effluent dissolved sulfide and the sum of the increase in total sulfur measured in each column sediment subsample times the samples mass fraction and the total sediment weight in the column.

d. Iron reduction is the sum of whole column increase in extractable ferrous iron and the integrated effluent dissolved iron.

e. Total uranium reduction is from the difference between integrated influent and effluent dissolved uranium during the period of acetate amendment.

f. Effluent Dissolved CO_2 is the integrated increase in effluent total dissolved CO_2.

g. HCO_3 produced is equal to two times acetate consumed.

Ferric iron reduction estimated from the integrated effluent iron and the increase in 1-hour 0.5N HCl extractable Fe(II) in column sediment accounts for 1.1 to 2.5% of electron transfer (Table 17), a small fraction of the electrons needed to balance acetate oxidation. Reduction of Fe(III) in phyllosilicate minerals by dissimilatory microbial iron reduction can be significant in aquifer sediments (Wu *et al.*, 2012; Lee *et al.*, 2012; Komlos *et al.*, 2007). However, it is unknown if Fe(II) produced by reduction of Fe(III) silicates is quantitatively extracted by 0.5 N HCl since silicate phases are not readily dissolved by HCl. As such, these estimates of iron reduction are likely lower limits. Reduction of uranium and manganese combined account for 0.6% of the electron transfer, at most. Combined, these terminal electron accepting processes account for 75, 77 and 110% of the electrons donated in column A, B and C, respectively (Table 17), with sulfate reduction the dominant TEAP. It is unknown if this disparity is the result of uncertainties in the estimated amounts of acetate consumption and reduction of S, Fe, U, and Mn, or if the unaccounted for electrons in columns A and B are the result of some other pathway of acetate consumption such as fermentation (Muyzer and Stams, 2008). Alternatively, the much higher microbial abundances in column A may account for part of the acetate balance assuming greater biomass growth. The biomass inferred from copy numbers in the qPCR analysis was greater for column A sediments than column B or C (Table 14).

4.1.2 Biogeochemical Processes during Biostimulated Reduction

The sequence of biogeochemical processes in the biostimulation stage of each of the three columns follows the expected sequence of iron reduction followed by sulfate reduction. The column effluent profiles overall are similar among the three biostimulation columns. The onset of iron reduction evidenced by the increase in effluent [Fe] occurred within 10 days of the start of the acetate inflow. Peak iron reduction based on maxima in effluent [Fe] occurred between 15 and 25 days in the three columns with effluent [Fe] maxima occurring later in columns B and C (Figure 43). Effluent [Fe] decreased to near the detection limit by 25 to 30 days, concomitant with the onset of sulfate reduction, based on the increase of effluent dissolved sulfide to measurable levels. The onset of U reduction occurred concurrent to iron reduction consistent with other lab (Komlos *et al.*, 2008a; Moon *et al.*, 2007) and field biostimulation experiments (Anderson *et al.*, 2003; Vrionis *et al.*, 2005; Williams *et al.*, 2011). The extent of U uptake increased overall throughout the duration of biostimulation (Figure 43) with the greatest uptake occurring during sulfate reduction. Uranium uptake was substantially greater in column C than in columns A and B throughout the biostimulation. The [U] effluent profiles for columns A and B show an increase in [U] starting at about day 25 concurrent with the onset of sulfate reduction. The effluent [U] increase likely is the result of the increase in bioreduction generating the higher pH and dissolved carbonate that increased U(VI) complexation in solution causing a decrease in the rate and extent of uranium reduction (Brooks *et al.*, 2003; Ulrich *et al.*, 2011) as well as enhancing U(VI) desorption. The increase in effluent [U] occurs later in column C, between day 40 and 50 days (Figure 43). The onset of sulfate reduction and the resulting pH and alkalinity increase also occurred later in column C (Figure 3, 4, and 5). Subsequently, the rate of uranium reduction increases in all columns. The increased reduction is evident from the decrease in effluent [U] to 4 μM by 110 days in columns A and B, and to 2 μM by 70 days in column C.

The enhanced U reduction in column C compared to columns A and B suggests either greater activity of metal reducing bacteria, or a greater component of indirect or abiotic reduction. The increased U removal is evident throughout the biostimulation period (Figure 43). Column C had continuous input of 15 μM Fe(II) throughout biostimulation, 1.5 times the influent [U]. Fox *et al*. (2013) showed that reduction of U(VI) can occur by electron transfer from Fe(II) sorbed to aquifer sediments at sorbed Fe(II) concentrations >20 μmol/g. This process may account for the difference in U reduction observed. However, the extractable Fe(II) concentrations in column C were similar to column A, so enhancement of U(VI) reduction by sorbed Fe(II) in column C is not expected. Alternatively, the sustained Fe(II) concentrations may result in ongoing formation of iron sulfides such as mackinawite during sulfate reduction providing additional sites for abiotic reduction of U(VI) (Veeramani *et al.*, 2013; Hyun *et al.*, 2012; Hua and Deng, 2008; Gallegos *et al.*, 2013).

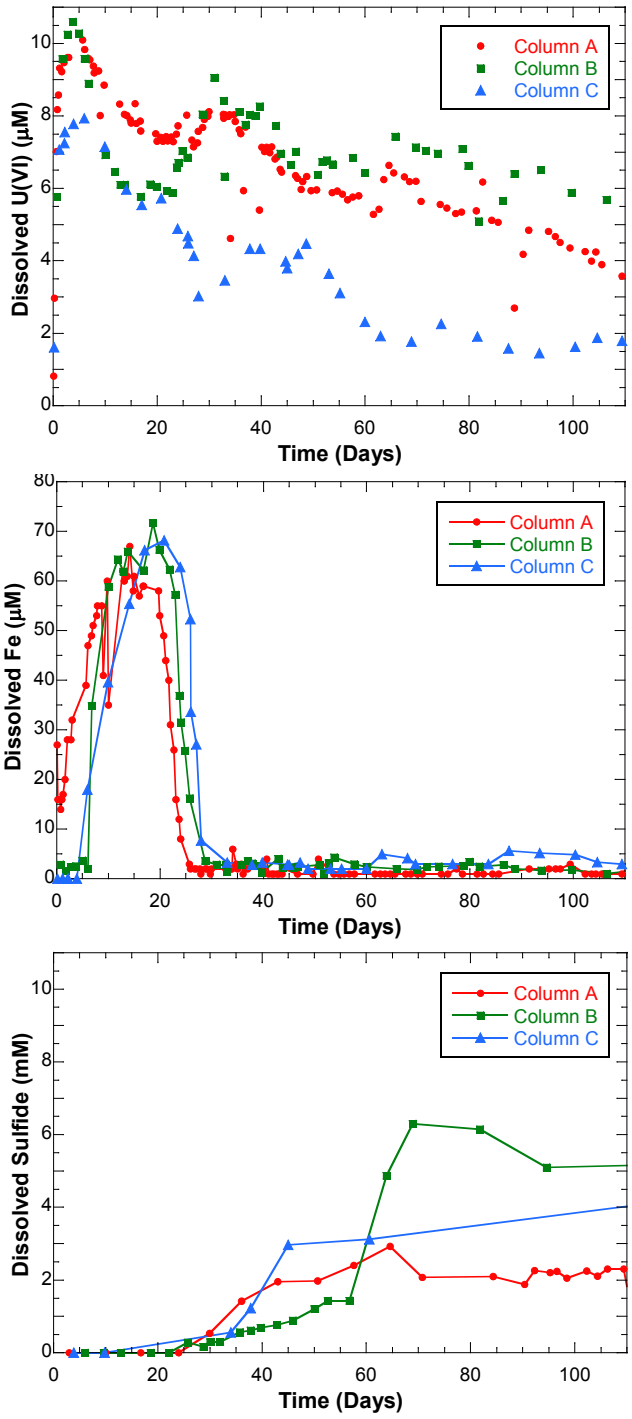

Figure 43. Comparison of effluent dissolved uranium (top), dissolved iron (middle), and dissolved sulfide (bottom) for columns A, B and C during biostimulation. The data are plotted for the duration of acetate addition to column A.

Sulfate reduction and retained S was greater in column C than column A (Table 17) consistent with enhanced U reduction by this abiotic process. Lastly, the abundance of *Geobacter* relative

to SRB was higher in column C (Figures 38, 40; Table 14). This observation suggests greater activity of metal reducing microbes in column C relative to sulfate reducers, perhaps resulting in the enhanced U(VI) reduction. However, the overall microbial abundances were substantially higher in the other columns. The processes contributing to the enhanced U(VI) uptake in column C cannot be constrained by the data collected.

The observed increase in uranium uptake during sulfate reduction contrasts with other studies that propose U reduction is greatest during iron reduction with acetate oxidizing sulfate reducing bacteria not as effective in uranium reduction (Anderson *et al.*, 2003; Yabusaki *et al.*, 2010) and field observations that show the greatest U(VI) reduction correlated with Fe(III) reduction and *Geobacter* abundance (Vrionis *et al.*, 2005). Additionally, field studies have observed that U(VI) removal is lower following the transition to sulfate reducing conditions, which has been attributed in part to less efficient uranium reduction by SRB relative to *Geobacte*r (Anderson *et al.*, 2003; Williams *et al.*, 2011). The observed increase in uranium reduction as sulfate reduction progresses in all three column experiments would require that dissimilatory metal reducing bacteria, such as *Geobacter*, are active and undergoing growth concurrent with sulfate reduction if these microbes are dominating uranium reduction. In field biostimulation experiments, groundwater and sediment chemistry data indicate simultaneous occurrence of iron and sulfate reduction where the electron donor was not limiting (Vrionis *et al.*, 2005). Williams *et al.* (2011) concluded that the availability of sufficient acetate to sustain metal-reducing microbes during sulfate reduction resulted in the ability of these microbes to control uranium removal from groundwater at the Rifle site. Because neither acetate, sulfate or reducible iron are depleted it is unlikely that the electron donor availability is limiting microbial processes in these columns, and thus competition between SRB and metal reducing microbes is not sufficient to diminish uranium reduction by metal reducing microbes. Similarly, Komlos *et al.* (2008a) observed that the rate of U(VI) reduction was unaffected by the sulfate reduction in biostimulation column experiments with Rifle sediment at low and high sulfate concentrations. In addition, these authors concluded that sulfate reduction commenced prior to depletion of reducible iron in part because electron donor was not limiting. Uranium reduction also could be the result of other microbial processes. For example, sulfate reducing bacteria have been shown to reduce uranium directly through enzymatic mechanisms using lactate and ethanol as electron donors (Lovley *et al.*, 1993; Luo *et al.*, 2007a), both of which can produce acetate during consumption.

In addition to direct enzymatic uranium reduction by microbes, U(VI) reduction has been shown to occur by abiotic reaction with products of other biotic reduction processes, such as iron sulfides (Veeramani *et al.*, 2013; Hyun *et al.*, 2012; Hua and Deng, 2008; Gallegos *et al.*, 2013). Association of U(IV) with reduced iron and sulfur has been observed in sediments recovered from in-situ columns exposed to groundwater during field-scale acetate biostimulation experiments at the Rifle site (Bargar *et al.*, 2013). These authors suggest a role of sulfides in ongoing sustained U(VI) reduction that has been observed in field biostimulation tests well after electron donor addition had been halted (Williams *et al.*, 2011). However, the importance of abiotic, non-enzymatic uranium reduction has not been conclusively demonstrated at the field scale. In the present experiments, continued U uptake was observed well after cessation of acetate inflow to column A (Figure 3). Over a 35 day period (74 pore volumes) under zero oxygen conditions and 10 μM U(VI) influent, effluent [U] remained low initially decreasing to <2 μM, then slowly rising (Figure 3). During this period of U(VI) input in the absence of acetate, a total uptake of 20.4 μmol was observed, which is about half of U uptake during acetate addition over 110 days (41.2 μmol). Analysis of XANES spectra of sediments recovered at the end of the anaerobic stage (after biostimulation, U inflow without acetate, and 45 days with no acetate or U(VI)), show that >97% of the U is U(IV) (Table 9). The U uptake after acetate cessation (20.4 μmol) is about one third of U uptake in the entire experiment, and is well above the ~5%

detection limit for U(VI). About 4.6 μmol of U was remobilized and transported out of the column over the 45 days of flow of AGW without acetate, U(VI), or dissolved oxygen (Figure 3). If this amount is assumed to be U(VI) that was sorbed (instead of reduced and precipitated as U(IV)) after acetate input ceased, it would equal to 22% of U uptake during this period. This percentage of U(VI) is readily detectable by XANES, but essentially only U(IV) was measured. This comparison indicates that significant U reduction continued after electron donor addition was halted. Since sulfate reduction decreased rapidly when acetate input ended as evidenced by sulfate returning to influent concentrations and effluent sulfide decreasing to below detection, SRB activity stopped, and likely other microbial activity decreased. We propose that the observed continued uranium uptake occurred largely by reduction by abiotic processes. The increase of Fe(II) and reduced S in sediments are consistent with U reduction by interactions with iron sulfides (Veeramani *et al.*, 2013; Hyun *et al.*, 2012; Hua and Deng, 2008; Gallegos *et al.*, 2013). Additionally, the co-association of U(IV) with Fe and S in some grain coatings (e.g. Figures 30, 33 and 36) support this conclusion. Abiotic U(VI) reduction may also occur by electron transfer from other forms of Fe(II), such as sorbed to sediment surfaces (Fox *et al.*, 2013). A component of sorbed Fe(II) is possible since effluent [Fe] increased during the period after acetate input was halted when sulfate reduction ended (Figure 3). This effluent [Fe] increase may be in part from desorption of Fe(II) or dissolution of reduced iron phases, both of which would be more favorable in the absence of dissolved sulfide.

In contrast to the continuously decreasing [U] in the effluent throughout the acetate addition, effluent Fe decreased substantially after 15 to 20 days, and reached a low level by 30 days that persisted for the duration of the biostimulation. The comparison of integrated effluent [Fe] with the increase in extractable Fe(II) in sediments recovered from columns after biostimulation shows that a large majority of reduced iron remained in the column. The increase in effluent sulfide following the iron effluent peak limited ferrous iron solubility and thus decreased dissolved iron transport out of the columns. In addition, previous studies have observed that only a small amount of the Fe(II) produced by biogenic reduction of phyllosilicate iron is solubilized with most of Fe(II) remaining in the silicate layer structure (Komlos *et al.*, 2007). Although its unknown if iron reduction continued throughout the biostimulation period, the availability of electron donor in excess of sulfate reduction throughout the biostimulation period and the abundance of metal reducing microbes measured in the sediments at the end of biostimulation suggest that iron reduction is likely occurring for the entire duration of electron donor addition. Poorly crystalline iron comprises a small fraction of total iron in Rifle sediments (~1 %) of total iron with phyllosilicate iron accounting for about 56% of the total iron with the remainder crystalline iron oxides (Komlos *et al.*, 2008b). The abundance of reducible iron, including phyllosilicate iron, well exceeds the extent of iron reduction measured in these column experiments. Thus, iron reduction likely continued throughout the duration of the biostimulation either directly by dissimilatory metal reducing microbes or indirectly through reaction of Fe(III) with dissolved sulfide. The formation of elemental S by reaction of free sulfide with Fe(III) solids results in oxidation of S^{-2} and reduction of Fe(III) to Fe(II) (Li *et al.*, 2009). This process is illustrated in the following reaction:

$$Fe(OH)_3(s) + 0.5\ H_2S \leftrightarrow Fe^{2+} + S^o + H_2O + 2\ OH^-.$$

This iron reduction pathway may also occur for phyllosilicate iron. Reduction of both Fe(III) oxides or phyllosilicate iron by sulfide or direct microbial reduction of phyllosilicate iron would result in little transport of dissolved iron from the columns after the onset of sulfate reduction.

4.2 Remobilization of Uranium during Oxic Elution

Combined the effluent and solid phase measurements from columns during and after the biostimulation stage suggests that stimulation and growth of the ambient microbial population in the aquifer sediments from the Rifle site by addition of electron donor and carbon source may be an effective means of removing dissolved uranium from contaminated groundwater. This conclusion is consistent with a number of both field and laboratory studies at Rifle (Anderson *et al.*, 2003; Williams *et al.*, 2011; Yabusaki *et al.*, 2010; Komlos *et al.*, 2008b; Sharp *et al.*, 2011) and at other sites (Gu *et al.*, 2005; Wu *et al.*, 2006). Because it well known that reduced uranium phases can undergo oxidative dissolution upon exposure to oxygen (Bi *et al.*, 2013; Komlos *et al.*, 2008b; Moon *et al.*, 2007; Moon *et al.*, 2009) many of these studies have stressed that the effectiveness of biostimulated reduction as a viable long-term remediation strategy requires evaluating the stability of the bioreduced uranium in response to changes in groundwater chemistry, such as presence of dissolved oxygen at suboxic levels. For example, Yabusaki *et al.* (2010) stated that "A key issue for uranium bioremediation is the stability of solid-phase reduction products, including U(IV)." The stability of bioreduced U(IV) is dependent on maintaining reducing conditions within the aquifer. The primary goal of this study was to evaluate the remobilization of U sequestered during biostimulated reduction under conditions in which biostimulation and concomitant U reduction extended well into sulfate reduction to enhance precipitation of reduced sulfur phases such as iron sulfides. The intent of producing these reduced phases was to test their effect on remobilization of the sequestered uranium, either serving as a redox buffer by competing for dissolved oxygen, or by armoring the reduced uranium. In particular, increased production of iron sulfide phases was attempted through addition of ferrous iron in the influent stream throughout biostimulation (column C).

The removal of dissolved U(VI) from the influent continued over the course of the 110 to 330 day biostimulation stage well after the onset of sulfate reduction at ~30 days. The resulting sequestered U was essentially all U(IV) consistent with the formation of nanoparticulate uraninite that may be associated with organic microbial biomass, and may in part be sorbed to C or P in the organic matter (Section 3.4.2). The speciation of U(IV) associated with sediments after oxic elution was essentially the same as that measured in samples recovered after biostimulation and prior to oxic elution. The reduced U(IV) formed coatings on sediment grains with thicknesses of a few 10s of microns (Figures 33, 34, 38). The coatings of U are largely contiguous with the coating infilling voids and cracks in the grain surface suggesting the coatings are formed in place as opposed to fine particles adhering to grains during sample drying.

4.2.1 Effect of U(IV) Form and Morphology

Nanoparticulate biogenic uraninite has been found to be on the order of 3 nm in diameter and tends to form aggregates (Burgos *et al.*, 2008; Schofield *et al.*, 2008). Because of the small particle size, Schofield *et al.* (2008) estimated that about 50% of the U is near the surface resulting in a lattice contraction compared with larger abiotic particles of bulk UO_2. Although the surface is distorted, the particle core remained highly ordered consistent with stoichiometric UO_2 (Burgos *et al.*, 2008; Schofield *et al.*, 2008; Singer *et al.*, 2009). The net effect, however, is that strain on the interior is negligible and likely does not enhance the solubility or stability (Schofield *et al.*, 2008). Nanoparticulate UO_2 has been shown to form aggregates with the size in part due to the rate of U reduction in some cases (Burgos *et al.*, 2008; Senko *et al.*, 2007). Although the ~3 nm UO_2 nanoparticles cannot be resolved by either μXRF mapping or SEM imaging, the U-

bearing coatings are likely comprised of aggregates of the UO_2 nanoparticles and perhaps may include U(IV) associated with the microbial biopolymers and microbes that attach to sediment surfaces (Bargar *et al.*, 2013). As noted above, the coatings in part appear to be comprised of smaller particles (e.g. Figure 35B), but these particles are well above the particle size inferred from fitting of EXAFS spectra. The fits to EXAFS spectra do suggest that U(IV) in the sediment may be present as both partially disordered nanoparticles and as monomeric U in association with organic matter. However, XRF does not measure all elements, in particular C and therefore do not provide information on other components comprising the grain coatings, for example microbial biomass. Thus, the coating morphology and accessibility of U within the coatings cannot be further constrained by the present measurements, but may influence the susceptibility of U(IV) to oxidative remobilization.

4.2.2 Competitive Oxidation Processes

Previous studies have reported oxidative remobilization of U(IV) under anaerobic conditions resulting from continued reduction of Fe and Mn oxides that serve as terminal electron acceptors for U oxidation coupled with increased dissolved carbonate shifting the redox state to more favorable conditions for U oxidation (Wan *et al.*, 2005). Remobilization of U has been studied following biostimulated reduction under low sulfate conditions in laboratory column experiments with aquifer sediments from the Rifle site inoculated with *Geobacter metallireducens*. These experiments showed about 88% and 97% remobilization of U within 54 days when 0.27 mM dissolved oxygen (saturation with respect to air) or 1.6 mM nitrate were added to the influent, respectively (Moon *et al.*, 2007). After 200 days of biostimulated reduction in similar column experiments under low sulfate conditions, re-oxidation of U(IV) resulted in the increase of effluent [U] to over 150 μM within 10 days of exposure to dissolved oxygen at saturation with air, with 60% of U remobilized after 60 days and nearly all by 120 days (Komlos *et al.*, 2008b). The extent of U remobilization in these experiments suggested little adsorption of U(VI) by iron oxides or other surfaces on the column sediments and that oxidation of ferrous iron provided negligible buffering of U(IV) oxidation. Cell decay and ferrous iron oxidation accounted for 43 and 23% of oxygen consumption, respectively, with U accounting for 12% (Komlos *et al.*, 2008b). In contrast, Sharp *et al.* (2011) observed little remobilization of biologically reduced U in columns with Rifle sediments under low sulfate conditions upon exposure to oxygen. Instead, the increase in the relative proportion of U(VI) in the middle and outflow end of the column was attributed to retention of U(VI) by sorption following re-oxidation of U(IV) near the inflow end of the column.

The presence of iron sulfides has been proposed to limit re-oxidation of U(IV) by serving as a redox buffer or armoring the U(IV) precipitate (Abdelouas *et al.*, 1999). The timing and extent of U remobilization following prolonged biostimulated reduction of sulfate, iron and U in column experiments with inoculated Rifle sediments show significantly less U re-oxidation and a delay in release of U upon addition of oxygen or nitrate to column influent (Moon *et al.*, 2009), compared to low sulfate experiments which had little or no iron sulfide precipitation (Moon *et al.*, 2007). The iron sulfides formed during biostimulation served to partially limit biogenic U(IV) oxidation by competing for dissolved oxygen. Less than 1% of U was remobilized by 0.27 mM dissolved oxygen and no oxidation at 0.03 mM dissolved oxygen was observed through 50 days of elution. Sulfide oxidation accounted for 85% of oxygen consumption. Mackinawite (FeS) has been shown to inhibit UO_2 oxidation provided that it is it is in physical proximity to the U(IV) phases and is in sufficient quantity to effectively scavenge oxygen to act as a redox buffer (Bi *et al.*, 2013).

4.2.3 Observed Rate and Extent of U(IV) Release

In the present study, the time dependence of U release in the absence of dissolved oxygen and subsequently during oxic elution provides a measure of the stability of the bioreduced U. Prior to introduction of dissolved oxygen to the column influent stream, column C effluent [U] averaged <0.1μM over 18 pore volumes after U(VI) and acetate were removed from the influent during the bromide tracer pulse prior to repacking for oxic elution. In contrast, effluent [U] in column A averaged 0.4 μM over 45 days (96 pore volumes) of flow under anoxic AGW without acetate or U(VI). It is not known If the release of U during these periods is from U(VI) desorption, oxidation of U(IV), or mobilization of U(IV) without oxidation. Dissolution and mobilization of uranium from reduced sediments has been observed previously in the absence of oxygen and was attributed in part to complexation by natural humic substances (Luo and Gu, 2009). The very low effluent [U] prior to introduction of dissolved oxygen combined with the predominance of U(IV) (>90%) in the sediment following biostimulation are consistent with negligible release of sorbed U(VI) from sediments prior to the introduction of oxygen.

After the first 15 days of oxic elution, effluent [U] for column A averaged 0.85±0.11 μM and was near constant over the duration of the 140 day (350 pore volume) elution (Figure 6). By comparison, column C effluent [U] averaged 0.34±0.07 μM over the first 30 days, then decreased slowly to 0.2 μM by the end of 120 day (300 pore volume) elution. Remobilization of uranium from column C during oxic elution resulted in about a factor of 3 lower integrated effluent dissolved [U] than was observed for column A (Table 3). The primary difference between column A and C was the inclusion of 15 μM ferrous iron to the influent of column C throughout biostimulated reduction.

The measured concentration in sediment samples was about a factor of 3 lower for the composite sediment from column C than the U concentration based on integrating the effluent profile (Figure 44). As noted in section 3.3.4, this disparity may be the result of incomplete sampling of sediment from column C at the end of biostimulation. Alternatively, U loss may have resulted upstream of the sediment in column C, perhaps from interaction of ferrous iron with U(VI) in the influent stream. The U mass released estimated by integrating effluent [U] during oxic elution, 2.5 μmol U, was comparable to the difference between measured sediment U before and after oxic elution, 2.3 μmol U (Figure 44). This comparison suggests the measured sediment U in the composite used to repack column C for oxic elution better represents the initial condition. The similarity in the measured U of intermediate depth intervals after oxic elution with the U concentration of the column C composite used for repacking (Figure 23) also supports the use of the measured sediment concentration of the composite to represent the whole column U at the start of oxic elution. In contrast, the total U at the start of oxic elution in column A based on the integrated effluent total U uptake was about 10% higher than the composite sediment U content (Figure 44). However, the total U remobilized from column A during oxic elution based on the integrated effluent, 10.6 μmol U, was about a factor of 3 greater than the sum of the uranium concentration of all sediment samples times their mass contribution, 3.4 μmol U. This discrepancy likely is the result of a greater uncertainty in the measured sediment U concentrations when a large number of sediment samples are summed to estimate changes in total U within a column (23 subsamples for column A). The uncertainty is in part from analysis of small sample masses, loss of fine grain material, and the poorly constrained contribution of the >2 mm size fraction (see sections 3.2.4 and 4.3.4), which all may have caused an underestimate of total U release from column A. As a result, this discussion of oxidative remobilization relies on effluent dissolved uranium. The effluent profiles also provide information on the time dependence of the release.

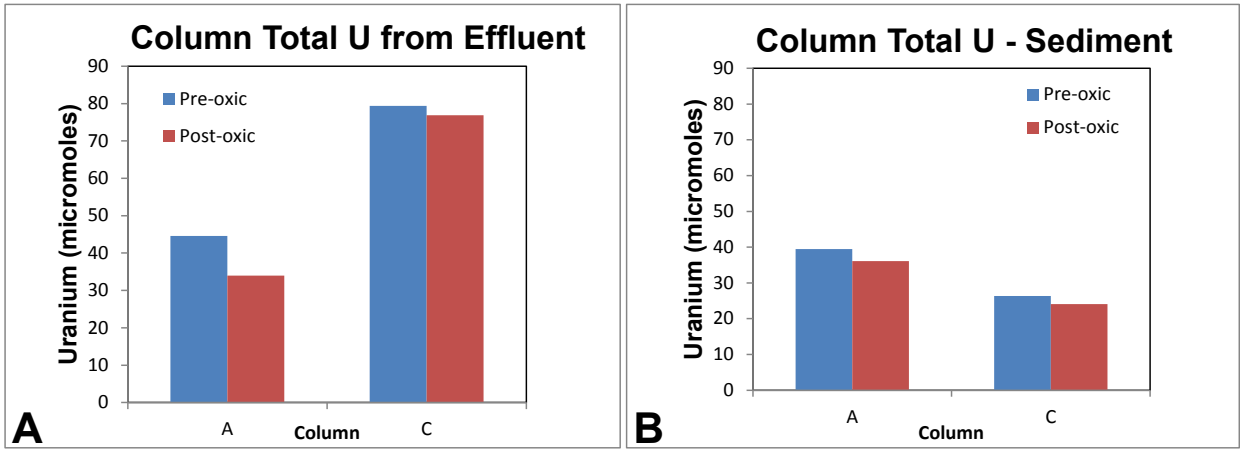

Figure 44. Total uranium on a whole column basis for oxic elution columns A and C, in micromoles, before and after oxic elution from (A) integrated effluent concentration profiles and (B) sediment U concentrations.

Previous studies of oxidative remobilization of reduced U report dissolution rates of synthetic and biogenic UO_2 in flow through or batch reactors in units of mol g^{-1} sec^{-1}, where g is the mass of reduced (or total) uranium (in grams) (Bi *et al.*, 2013; Sharp *et al.*, 2011; Ulrich *et al.*, 2009). Because the remobilization of U from both columns occurred at near constant rates, the linear slope of the change in sediment U per gram versus time (Figure 7A) yields release rates of 3.4E-10 and 1.2E-10 mol U/g sediment/day for column A and C, respectively. Normalizing to the initial mass of reduced U at the start of oxic elution yields dissolution rates of 6.5 E-11 and 3.4E-11 mol g-1 sec-1, respectively. The initial U mass is based on the measured U concentration of the composite sediment used to repack the columns and includes the fraction of U associated with the >2 mm particles. Because other processes, such as adsorption of U(VI) by sediment, can lower the effluent dissolved [U], calculated rates from column effluent data are considered net rates. The dominance of the solution speciation of dissolved U(VI) in the AGW as calcium carbonato complexes (>90%) likely limits adsorption or buildup of oxidized uranium on the sediments. Indeed, the U oxidation state from bulk XANES measurements of column sediments from intervals that appeared more oxidized also were dominated by U(IV) (Table 9). The calculated net release rates from the column effluent data are two orders of magnitude lower than the 1.5 to 4.7E-9 mol g^{-1} sec^{-1} rates reported for synthetic and biogenic UO_2 from flow through reactors (Ulrich *et al.*, 2009). The visual apparent channeling or preferential flow paths (Figures 8 and 9) combined with column samples which had little change in U concentration in response to oxic elution (Figures 20 and 23) suggest that release may not be not occurring uniformly from the whole column. Therefore, the actual mass of sediment U undergoing oxidation may be lower than the whole column U mass used to normalize the release rates. If so, the normalized rates would be higher if the actual mass of sediment U involved in the oxidative remobilization could be used instead of bulk sediment U concentrations.

4.2.4 Processes Affecting Uranium Remobilization in Column Experiments

A number of factors likely contributed to the observed lower rate and extent of U oxidative remobilization measured in column C compared to column A. The primary difference in the two column experiments was the 15 μM Fe(II) addition to the influent of column C throughout biostimulation. Differences in other constituents in the two columns may contribute to the observe difference in U remobilization. The μXRF maps and SEM-EDS measurements show co-association of U with Fe and S in some grain coatings, but not in others. In addition, thicker coatings would be expected for column C because of the longer biostimulation period and apparent greater rate of U reduction. Because of the few grains with U coatings that were found in thin sections of column sediments and imaged, no trend in coating thickness or composition between the two columns could be discerned. Column A went through a longer period without electron donor addition under low or zero oxygen conditions than column C. Decrease of biomass during this period would limit biomass contribution to oxygen consumption during oxic elution. For example, Komlos *et al.* (2008b) estimated that biomass decay accounted for 43% of oxygen consumption. However, the abundances of *Geobacter* and SRB based on cell numbers were substantially higher in column A compared to C (e.g Figures 41 and 42) suggesting biomass decay does not contribute to the observed trend. Column C had about 35% greater retention of S during biostimulation than column A (Figure 45), with the fraction of S as AVS about the same in both columns. The decrease in total sulfur during oxic elution was about 50% greater for column C than column A suggesting a greater consumption of oxygen by reduced sulfur species in column C perhaps limiting remobilization of U(IV) by buffering oxidation as proposed by Abdelouas *et al.* (1999) and observed in batch experiments (Bi *et al.*, 2013).

Although there was little loss from sediment intervals near the middle of column C, U was remobilized primarily from intervals nearest the column inlet and outlet (Figure 23). These intervals comprise 33% of the sediment mass but accounted for 75% of the U loss. Similarly these intervals accounted for most of the total S decrease with 70% of the decrease from loss of AVS, presumably oxidation. The decrease in extractable Fe(II) was primarily from these intervals (Figure 24). They also had a substantial increase in Fe(III) extracted by 0.5N HCl relative to the sediment at the start of oxic elution. U decrease generally was greater at the inlet end of column A, but occurred in subsamples throughout the column. Decrease in Fe(II) and in total S also occurred to a greater extent in column A subsamples with greater U loss but not consistently for all such subsamples. These variations illustrate the heterogeneity of flow within the columns during oxic elution which was also evident in the appearance of sediments at the exterior of the columns during the experiments (Figure 8) and on subsampling after oxic elution (Figure 9 and 10). Although the relative amount of reduced sediment exposed to preferential flow cannot be constrained, the difference in the fraction of sediments exposed to oxygen between the two columns may be the cause in the observed difference in uranium remobilization.

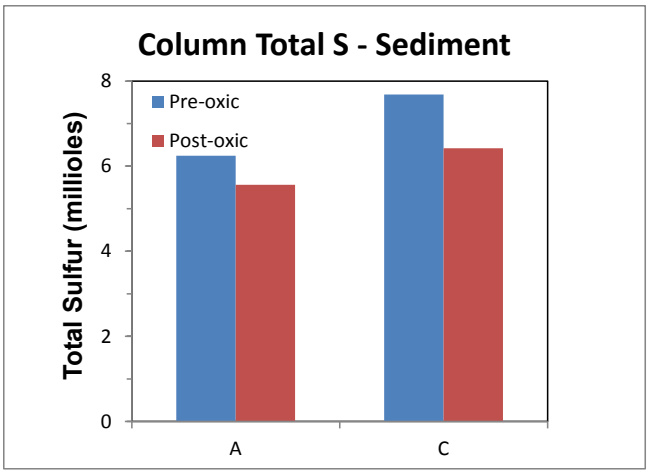

Figure 45. Total sulfur in columns A and C sediments, in millimoles, before and after oxic elution.

Overall, the release of U during oxic elution is a continuous process with dissolved uranium concentrations on the order of 0.8 and 0.2 μM for columns A and C, respectively (Figure 6). The effluent concentration from column C decreased over time indicative of a decreasing re-oxidation rate. In contrast, column A effluent [U] does not display this decreasing trend but is instead somewhat constant over 140 days. Overall, only about 9% of total uranium sequestered during biostimulation was remobilized. The prolonged period of biostimulation and concomitant sulfate reduction appears to limit the rate of U(IV) oxidative remobilization. The limited oxidative remobilization of U(IV) in the present column experiments is consistent with the decreased U remobilization where sulfate reduction occurred (Moon *et al.*, 2009) compared to large release from columns which had limited sulfate reduction (Moon *et al.*, 2007). Although continued sulfate reduction may cause a decrease in permeability resulting from precipitation of iron sulfide, as observed in column B, and a decrease in U(VI) removal in field studies (Anderson *et al.*, 2003; Williams *et al.*, 2011), the greater apparent stability of the sequestered U(IV) provided by the sustained biostimulation should be considered in design of field scale remediation efforts.

5 Reactive Transport Modeling of the Rifle Sediment Columns during Biostimulation

5.1 Introduction

5.1.1 Background

An important challenge identified in previous studies (Fang *et al.*, 2009; Williams *et al.*, 2011) is the impact of biologically-mediated reaction products (e.g., biomass, bicarbonate, Fe(II), U(IV), H_2S) on the behavior of uranium (Englert *et al.*, 2009; Li *et al.*, 2010; Li *et al.*, 2009). In particular, the sensitivity of uranium mobility to pH, Eh, alkalinity, calcium, and reactive surface area requires detailed biogeochemical process modeling to mechanistically simulate changes to the aqueous and solid phase chemistry induced by acetate biostimulation (Davis *et al.*, 2006; Dong *et al.*, 2005; Li *et al.*, 2009; Liu *et al.*, 2005; Luo *et al.*, 2007b). Biologically-mediated oxidation of acetate produces a large amount of bicarbonate that directly affects the alkalinity, and indirectly affects the pH, calcium and reactive surface area through precipitation of carbonate minerals (Li *et al.*, 2009). The dissolution of Fe(III) minerals and the precipitation of sulfides and elemental sulfur affects pH and reactive surface area (Poulton *et al.*, 2004). Ca–UO_2–CO_3 complexes (Dong and Brooks, 2006), which are predicted to be predominant under Rifle geochemical conditions, have been shown to affect U(VI) bioreduction (Brooks *et al.*, 2003) and adsorption (Zheng *et al.*, 2003). Furthermore, the calcium concentrations controlling uranium speciation can be altered through cation exchange with the sodium cation present in the dissolved acetate and bromide salts that comprise the injectate. Thus, the inclusion of a reaction network that accounts for uranium, terminal electron-accepting processes (TEAPs), biomass, major ion chemistry (Ca, Mg, K, Na, carbonate, sulfate, Cl), reduction products [Fe(II), U(IV), H_2S], aqueous complexation (e.g., Ca-UO_2-CO_3), surface complexation [Fe(II), U(VI)], and precipitation/dissolution (goethite, calcite, FeS, S, UO_2) is critical to capturing important biogeochemical interactions during biostimulation.

We describe the modeling of uranium biogeochemistry during the biostimulation stage of a set of laboratory column experiments that were performed by the USGS described in the preceding sections of this report. The experiments were motivated by work conducted at the Rifle Integrated Field Research Challenge (IFRC) site in western Colorado demonstrating that the stimulation of indigenous dissimilatory metal-reducing bacteria, via the addition of the electron donor acetate, can reduce soluble hexavalent uranium [U(VI)] to immobile solid-phase U(IV) (Anderson *et al.*, 2003; Vrionis *et al.*, 2005; Williams *et al.*, 2011). This biologically mediated reduction of U(VI) can decrease groundwater concentrations of U in the shallow unconfined aquifer below relevant standards.

We use the systematic and quantitative coupling of process models to describe the interplay between the saturated flow, microbiology, and geochemistry during acetate biostimulation of the Rifle sediment column experiments. Modeling of these experiments is used to understand and quantify uranium behavior in the context of 1) transient biostimulation with acetate electron donor, 2) functional microbial groups representing Fe(III)-reducing bacteria (FeRB, such as *Geobacter*) and sulfate-reducing bacteria (SRB) responding to the biostimulation, and 3) geochemical response to the biostimulation products.

The numerical model incorporates advection, diffusion with Fick's law modified for the inclusion of dispersion, and mixed kinetic and equilibrium reactions. An operator splitting solution method is used for flow, transport, and reactions, each of which employs implicit time-stepping

schemes. HYDROGEOCHEM was used to resolve the detailed coupled processes and large number of reactive components.

5.1.2 History

Previous 1-D saturated flow and multicomponent biogeochemical reactive transport modeling studies were performed to simulate the 2002, 2003, and 2007 field biostimulation experiments at the Rifle IFRC site (Fang *et al.*, 2009; Yabusaki *et al.*, 2007). A comprehensive reaction network was developed from these studies that included biologically-mediated TEAPs for solid phase Fe(III), aqueous U(VI), and aqueous sulfate; aqueous and non-electrostatic surface complexation for Fe(II) and U(VI); calcite, siderite, FeS, S secondary minerals; sulfide promoted dissolution of Fe(III) minerals, cation exchange, protonation/deprotonation of Fe(III) surfaces, and major ion chemistry.

The integration of the abiotic chemistry with the TEAPs in the modeling is necessary to account for the impact of biostimulation products on uranium behavior. For example, the TEAP reaction products affect the system pH and alkalinity, which are controls on uranium mobility (Davis *et al.*, 2004). In laboratory and field experiments, the bulk of the bicarbonate and reduced phases (e.g., Fe(II), sulfide) produced by the biologically-mediated reactions are not observed in solution. This underscores the importance of accurately representing the solid phase reactions (e.g., mineral reactions for carbonates, iron, and sulfur; iron and uranium surface complexation) that control the pH, Eh, alkalinity, and aqueous components of interest.

5.2 Model Components

5.2.1 HYDROGEOCHEM

All simulations were run with the HYDROGEOCHEM (HGC) simulator (Yeh *et al.*, 2004). It provides the framework for incorporating and coupling the flow and reactive transport process models in this investigation. In particular, the multicomponent biogeochemical solver technology (Fang *et al.*, 2006; Fang *et al.*, 2003) addresses the complexity of mixed kinetic and equilibrium reactions that describe the aqueous and surface complexation, redox, mineral precipitation and dissolution, and microbial mediated transformations.

5.2.2 Conceptualization of Processes

The biologically-mediated transfer of electrons to solid phase Fe(III) by FeRB and to aqueous sulfate by SRB provides the energy for cell maintenance, activity, and growth. Introducing acetate electron donor in solutions passing through the sediment stimulates FeRB that catalyze the reduction of Fe(III) minerals but also opportunistically catalyze the reduction of the trace amounts of aqueous U(VI) that are present (Lovley *et al.*, 1991). Reduced uranium [U(IV)] becomes part of the solid phase, most likely associated with surface coatings or overgrowths on existing grains. Increases in aqueous Fe(II) and decreases in aqueous U(VI) occur very soon after biostimulation is initiated. Conversely, the SRB are slow growing and initially low in abundance. Although the SRB actively respond to the acetate biostimulation, their initial impact on acetate consumption and sulfate reduction is negligible. With time, however, the SRB growth continues and sulfate reduction becomes the dominant process after about 30 to 40 days. At this point, the bulk of acetate is being consumed by the SRB. In the sulfate TEAP reaction, ~1

mole of sulfate is reduced and ~2 moles of bicarbonate are produced for each mole of acetate consumed. The increase in bicarbonate concentrations thermodynamically favors the formation of aqueous U(VI)- CO_3 complexes. The resulting desorption of U(VI) increases aqueous U(VI) concentrations although there is still a net reduction in aqueous U(VI) relative to the influent concentrations. In the presence of elevated alkalinity, Fe(II), and sulfide; and lowered redox potential, calcite and iron sulfide secondary mineral formation are thought to be the most important volumetrically (Li *et al.*, 2009). Lesser amounts of elemental sulfur, from the sulfide promoted dissolution of Fe(III) minerals (Fang *et al.*, 2009), and siderite should also form.

5.2.3 Model Description

The simulation of the 194-, 219-, and 185-day biostimulation periods of experimental observation for columns A, B, and C, respectively, used variable time stepping with a maximum time step of 30 min. The 1-D model domain used to represent the experimental field plot was 6 cm long, comprised of 15 grid cells with uniform 0.4 cm spacing. The influx of acetate was based on the flow rate and influent concentrations.

The initial reactive transport modeling of biostimulated reduction used a reaction network developed for the 2008 Big Rusty field experiment at the Rifle IFRC site (Fang *et al.*, 2009; Yabusaki *et al.*, 2007). In this case, the equilibrium and kinetic reactions in this reaction network (Tables 18-22) addressed 2 distinct functional microorganisms (i.e., FeRB and SRB), 4 TEAPs (i.e., phyllosilicate Fe(III), poorly crystalline Fe(III), U(VI), and sulfate), 102 biogeochemical species (including surface complexes, exchanged cations), and 7 minerals (i.e., FeOOH, Fe_3O_4, FeS, S, calcite, siderite, uraninite).

Key assumptions included: 1) FeRB are solely responsible for bioreduction of aqueous U(VI) that occurs throughout the biostimulation, 2) SRB are present and active throughout the biostimulation, 3) abiotic uranium reduction is negligible, and 4) geochemistry, including uranium surface complexation, is fully operative during biostimulation (e.g., biomass does not significantly alter geochemical reactivity).

The aqueous initial and boundary conditions were acetate, U(VI), pH, bicarbonate, calcium, magnesium, sodium, potassium, chloride, Fe(II), and sulfate. The initial sorbed U(VI) and Fe(II) were assumed to be in equilibrium with their aqueous counterparts through the respective surface complexation models (Tables 18 and 19). U(VI) minerals were not included in the reaction network as they have not been identified in sediment analyses and are undersaturated with respect to the solution chemistry. Other nonaqueous initial conditions include FeRB and SRB biomass, goethite, phyllosilicate iron and surface complexation sites.

Both functional microbial groups, FeRB and SRB, are present and active during the initial period of biostimulation (Callister *et al.*, 2010). The kinetics of the microbially mediated TEAP reactions is of the Monod type with thermodynamic control. The acetate consumption rate, R_C^{bio}, as described by Fang *et al.* (2009) is:

$$R_C^{bio} = -\sum_{eA}^{N_{eA}} \mu_{m,eA} s_C B \left(\frac{C_C}{K_{s,C} + C_C} \right) \left(\frac{C_{eA}}{K_{s,eA} + C_{eA}} \right) f(\Delta G_r)$$

where N_{eA} = number of terminal electron acceptors

s_C = stoichiometric coefficient of acetate in the TEAP reaction

C_c = acetate concentration

B = biomass concentration of microorganism mediating the TEAP reaction

C_{eA} = terminal electron acceptor concentration

$\mu_{m,eA}$ = acetate oxidation rate for the terminal electron acceptor

$K_{s,C}$ = half-saturation coefficient for acetate

$K_{s,eA}$ = half-saturation coefficient for the terminal electron acceptor

$f(\Delta G_r)$ = $1 - \exp[(\Delta G_r - \Delta G_{min})/RT]$

ΔG_r = free energy change of the corresponding TEAP reaction

ΔG_{min} = minimum free energy change required to drive ATP Synthesis

R = gas constant

T = absolute temperature.

The half-saturation coefficient is the substrate concentration at which the reaction rate occurs at half of its maximum rate. The FeRB and SRB are assumed to be attached populations whose biomass is a control on the rates of the TEAP reactions they catalyze. The initial FeRB and SRB biomass amounts are initially low (Table 24). As the FeRB and SRB biomass grow, the respective TEAP reaction rates increase commensurately. A first-order decay model (dB/dt = -kB) is used to describe the loss of biomass via decay. Over time (typically 20-30 days), the net growth of SRB biomass is sufficient for sulfate reduction to become the dominant TEAP reaction and principal consumer of acetate. A maximum rate is used to limit the biomass-dependent reduction rates.

Table 18. Uranium species and their formation constants

Reaction	logK (I = 0) [a]
Aqueous Species	
$UO_2^{2+} + H_2O = UO_2OH+ + H^+$	-5.25
$UO_2^{2+} + 2H_2O = UO_2(OH)_{2(aq)} + 2H^+$	-12.15
$UO_2^{2+} + 3H_2O = UO_2(OH)_3^- + 3H^+$	-20.25
$UO_2^{2+} + 4H_2O = UO_2(OH)_4^{2-} + 4H^+$	-32.40
$2UO_2^{2+} + H_2O = (UO_2)_2OH^{3+} + H^+$	-2.70
$2UO_2^{2+} + 2H_2O = (UO_2)_2(OH)_2^{2+} + 2H^+$	-5.62
$3UO_2^{2+} + 4H_2O = (UO_2)_3(OH)_4^{2+} + 4H^+$	-11.90
$3UO_2^{2+} + 5H_2O = (UO_2)_3(OH)_5^+ + 5H^+$	-15.55
$3UO_2^{2+} + 7H_2O = (UO_2)_3(OH)_7^- + 7H^+$	-32.20
$4UO_2^{2+} + 7H_2O = (UO_2)_4(OH)_7^+ + 7H^+$	-21.90
$UO_2^{2+} + CO_3^{2-} = UO_2CO_{3(aq)}$	9.94
$UO_2^{2+} + 2CO_3^{2-} = UO_2(CO_3)_2^{2-}$	16.61
$UO_2^{2+} + 3CO_3^{2-} = UO_2(CO_3)_3^{4-}$	21.84
$3UO_2^{2+} + 6CO_3^{2-} = (UO_2)_3(CO_3)_6^{6-}$	54.00
$2UO_2^{2+} + CO_3^{2-} + 3H_2O = (UO_2)_2CO_3(OH)_3^- + 3H^+$	-0.85
$3UO_2^{2+} + CO_3^{--} + 3H_2O = (UO_2)_3CO_3(OH)_3^+ + 3H^+$	0.66
$UO_2^{2+} + Cl^- = UO_2Cl^+$	0.17
$Ca^{2+} + UO_2^{2+} + 3CO_3^{2-} = CaUO_2(CO_3)_3^{2-}$	25.40 [b]
$2Ca^{2+} + UO_2^{2+} + 3CO_3^{2-} = Ca_2UO_2(CO_3)_3^0(aq)$	30.55 [b]
$UO_2^{2+} + 2Cl^- = UO_2Cl_{2(aq)}$	-1.10
$Mg^{2+} + UO_2^{2+} + 3CO_3^{2-} = MgUO_2(CO_3)_3^{2-}$	26.11 [c]
$UO_2^{2+} + SO_4^{2-} = UO_2(SO_4)_{(aq)}$	3.15
$UO_2^{2+} + 2SO_4^{2-} = UO_2(SO_4)_2^{2-}$	4.14

[a] Values from (Guillaumont *et al.*, 2003), unless otherwise indicated.
[b] (Bernhard *et al.*, 2001).
[c] (Dong and Brooks, 2006).

Table 19. Uranium surface complexation reactions and formation constants

Reaction	logK (estimated*)
Surface Species	
$SSOH + UO_2^{2+} = SSOUO_2^{+} + H^{+}$	12.28
$SOH + UO_2^{2+} = SOUO_2^{+} + H^{+}$	6.95
$WOH + UO_2^{2+} = WOUO_2^{+} + H^{+}$	2.74
$SSOH + UO_2^{2+} + H_2O = SSOUOOH + 2H^{+}$	0.033
$SOH + UO_2^{2+} + H_2O = SOUOOH + 2H^{+}$	-2.12
$WOH + UO_2^{2+} + H_2O = WOUOOH + 2H^{+}$	-5.01
SSOH denoting very strong binding sites: 0.01% of total sites	
SOH denoting strong binding sites: 0.1% of total sites	
WOH denoting weak binding sites: 99.89% of total sites	

*Values from (Fang *et al.*, 2009)

Table 20. Equilibrium Reactions

Reaction	LogK*
$CH_3COO^- + H^+ = AcH$	4.76
$Ca^{2+} + H_2O = CaOH^+ + H^+$	-12.60
$Ca^{2+} + CH_3COO^- = CaCH_3COO^+$	1.18
$Ca^{2+} + CO_3^{2-} + H^+ = CaHCO_3^+$	11.33
$Ca^{2+} + CO_3^{2-} = CaCO_3$	3.15
$Ca^{2+} + SO_4^{2-} = CaSO_4$	2.31
$CO_3^{2-} + 2H^+ = H_2CO_3$	16.68
$CO_3^{2-} + H^+ = HCO_3^-$	10.33
$Fe^{2+} + H_2O = FeOH^+ + H^+$	-9.50
$CH_3COO^- + Fe^{2+} = FeCH_3COO^+$	1.82
$Fe^{2+} + CO_3^{2-} + H^+ = FeHCO_3^+$	12.33
$Fe^{2+} + CO_3^{2-} = FeCO_3(aq)$	5.50
$Fe^{2+} + 2CO_3^{2-} = Fe(CO_3)_2^{2-}$	7.10
$Fe^{2+} + SO_4^{2-} = FeSO_4$	2.25
$Fe^{2+} + Cl^- = FeCl^+$	0.90
$Fe^{2+} + 2HS^- = Fe(HS)_2(aq)$	8.95
$Fe^{2+} + 3HS^- = Fe(HS)_3^-$	10.99
$HS^- + H^+ = H_2S(aq)$	6.99
$HS^- = H^+ + S^{2-}$	-12.92
$K^+ + SO_4^{2-} = KSO_4^-$	0.85
$Mg^{2+} + H_2O = MgOH^+ + H^+$	-11.79
$CH_3COO^- + Mg^{2+} = MgCH_3COO^+$	1.14
$CO_3^{2-} + Mg^{2+} + H^+ = MgHCO_3^+$	11.40
$CO_3^{2-} + Mg^{2+} = MgCO_3(aq)$	2.98
$Mg^{2+} + SO_4^{2-} = MgSO_4(aq)$	2.25
$Na^+ + CH_3COO^- = NaCH_3COO$	-0.18
$Na^+ + CO_3^{2-} + H^+ = NaHCO_3(aq)$	10.08
$CO_3^{2-} + Na^+ = NaCO_3^-$	1.27
$Na^+ + SO_4^{2-} = NaSO_4^-$	0.70
$NH_4^+ = NH_3(aq) + H^+$	-9.25
$NH_4^+ + SO_4^{2-} = NH_4SO_4^-$	1.11
$SO_4^{2-} + H^+ = HSO_4^-$	1.99
$H_2O = OH^- + H^+$	-14.00
$>FeOH + H^+ = >FeOH_2^+$	7.47
$>FeOH = >FeO^- + H^+$	-9.51
$>FeOH + Fe^{++} = >FeOFe^+ + H^+$	-5.00
$>FeOH + Fe^{++} + H_2O = >FeOFeOH + 2H^+$	-11.96

* Values from the EQ3/6 database.

Table 21. Kinetic Reactions

Calcite dissolution/precipitation
$Ca^{2+} + HCO_3^- = Calcite(s) + H^+$
Siderite dissolution/precipitation
$Fe^{2+} + HCO_3^- = Siderite(s) + H^+$
Iron sulfide dissolution/precipitation
$Fe^{2+} + HS^- = FeS(s) + H^+$
Silicate Iron(III) bioreduction
$0.125\ CH_3COO^- + Fe(III)(ls) + 0.5\ H_2O = 0.25\ HCO_3^- + 0.9\ Fe(II)(ls) + 0.1\ Fe^{++} + 1.125H^+$ where (ls) refers to phyllosilicate Fe
Goethite bioreduction
$0.125\ CH_3COO^- + FeOOH(s) + 1.875\ H^+ = Fe^{2+} + 1.5\ H_2O + 0.25\ HCO_3^-$
Uranium bioreduction
$0.125CH_3COO^- + 0.3538H_2O + 0.0113NH_4^+ + 0.3875UO_2^{2+} = 0.0113BM\_iron + 0.855H^+ + 0.1938HCO_3^- + 0.3875UO_2(s)$ where BM_iron is the FeRB biomass
Sulfate bioreduction
$0.125CH_3COO^- + 0.0057H^+ + 0.0038NH_4^+ + 0.1155SO_4^{2-} = 0.0038BM\_sulfate + 0.0114H_2O + 0.231HCO_3^- + 0.1155HS^-$ where BM_sulfate is the SRB biomass
Sulfide-promoted goethite dissolution
$2FeOOH(s) + HS^- + 5H^+ = 2Fe^{2+} + S^0 + 4H_2O$

Table 22. Rate Constants

Parameter	Value*
Precipitation rate for calcite	1.644×10^{-7} Md^{-1}
Dissolution rate for calcite	1.37×10^{-6} d^{-1}
Precipitation rate for siderite	1.37×10^{-6} Md^{-1}
Dissolution rate for siderite	1.37×10^{-7} d^{-1}
Precipitation rate for FeS(s)	5.11×10^{-6} Md^{-1}
Dissolution rate for FeS(s)	6.85×10^{-6} d^{-1}
Rate constant for phyllosilicate iron bioreduction	0.075 $M^{-1}d^{-1}$
Rate for Fe(III) bioreduction	0.016 d^{-1}
Half-Saturation for acetate	5.0×10^{-4} M
Threshold based on silicate iron Fe(III)	0.14 μMg^{-1}
Rate for sulfate bioreduction	1.22×10^{-3} Md^{-1}
Half-Saturation for sulfate bioreduction	10^{-5} M
Rate for U(VI) conversion by iron reducers	2.5×10^{-6} Md^{-1}
Half-Saturation for U(VI) conversion by iron reducers	10^{-7} M
Half-Saturation for U(VI) conversion by sulfate reducers	10^{-7} M
Dissolution rate of goethite by sulfide	20.8 $M^{-1}d^{-1}$

*Values from (Fang *et al.*, 2009)

5.2.4 UCODE

We used UCODE_2005 version 1.021 (Poeter *et al.*, 2008) with the HGC reactive transport simulator to calibrate model parameters for the simulation of the three Rifle IFRC sediment column experiments. The “black box” model application includes pre- and post-processing utilities that update the HGC input files using UCODE output and extract the HGC output to be used as UCODE input.

UCODE is invoked by executing a ~.bat file (e.g., ucode_HGCflowchem.bat). The principal input file is a ~.in file (e.g., ucode_HGCflowchem.in). We have created a separate input file (HGCflowchemupdate.dat) for the black box application that contains only the parameters that UCODE is updating. A template file (HGCflowchemupdate.dat.tpl) is used to guide the formatted updates.

The black box model is executed by a Linux script (runHGCflowchem) which

1) executes updateHGCflowcheminput, a utility program developed to take the changes UCODE has made to the HGCflowchemupdate.dat file and creates usgs_1d_fast.inp, the HGC input file

2) executes hgc_usgs.x, the HGC executable that creates the or1.bst binary output file

3) executes tecFLOWCHEM, which takes the or1.bst binary output file and creates HGCflowchem.out, the formatted output of selected concentrations (Ac, Fe(II), U(VI), sulfate) expected by UCODE.

UCODE then reads the HGCflowchem.out file using the HGCflowchem.out.ins instruction file to extract the model output that will be compared with the observation data in the UCODE input file, ucode_HGCflowchem.in.

5.3 Approach for Modeling Biostimulation Stage of Column Experiments

The goal is to interpret the observed behavior of the column experiments using the existing Rifle IFRC field-scale modeling reaction framework. The principal objective is to develop a single reactive transport modeling parameterization to simulate the bioreduction of sulfate, Fe(III), and U(VI) in the three acetate biostimulation column experiments using Rifle IFRC sediments.

5.3.1 General Approach

The starting point for the model development is the existing parameterization of the field-scale reactive transport model. The approach is based on the assumption that the modeled processes and reactions in the field-scale model are appropriate and sufficient for the modeling of the column experiments. The focus, therefore, is the adjustment of the reaction parameters in the existing model to reproduce the experimental observations.

It should be noted that the field-scale reactive transport model was designed for the suboxic Rifle IFRC aquifer conditions, where post-biostimulation oxidation of solid-associated U(IV) has not been observed. Since there is no process model support for U(IV) oxidation, the modeling scope for the Rifle sediment columns addresses the biostimulation and cessation of influent components but not the introduction of elevated concentrations of dissolved oxygen. The modeling also does not address columns that have been repacked. This is because of uncertainty regarding the alteration of the processes, properties, and conditions of the experiments. Accordingly, only the first 193.6, 220.9, and 186.3 days of the columns A, B, and C experiments, respectively, are modeled.

The approach was to first calibrate a set of model parameters for each of the three column experiments to make sure that the modeled processes were appropriate and sufficient to represent the observed behaviors. After assessing the three calibrated sets of parameters, a single set would be identified and applied to all three column experiments.

The sediments used in the column experiments represent the finer-grained subset of the field particle size distribution (Tables 4 and 25). This subset represents the most reactive component of the sediments with respect to adsorption. We use the calibration procedure to estimate the initial >FeOH site density, which is assumed to control the number of reactive sites in the surface complexation modeling.

5.3.2 Challenges

There were two significant challenges: 1) increasing uranium bioreduction rate with time that had not been observed in the field, and 2) data limitations and inconsistency between the initial component concentrations, influent concentrations, and effluent concentrations, described in detail below.

1) Increasing rate of U(VI) bioreduction. The observation of continuously decreasing aqueous U(VI) concentrations in the column experiment after the onset of significant sulfate removal indicated increasing U(VI) reactivity over the course of the column biostimulation experiments. This was a departure from the field behavior and the existing conceptualization of model processes had no mechanism to account for increasing consumption of U(VI) during dominantly sulfate reducing conditions. In the conceptualization of modeled processes, the FeRB are responsible for both the Fe(III) and U(VI) reduction. It was decided that the reactive transport

model would be modified to add Fe(III) reducing bacteria (FeRB) biomass to the goethite and layer silicate Fe(III) terminal electron accepting process (TEAP) reactions. This would allow FeRB biomass to be incorporated into the U(VI) TEAP rate law. With the growth in FeBR biomass concentration, the U(VI) bioreduction rate increases commensurately.

2) Limitations in observed concentrations. The predicted aqueous U(VI) is very sensitive to the initial water chemistry and surface complexation sites. While the initial aqueous component concentrations in the column are flushed out with the first pore volumes, the initial sorbed uranium and Fe(II) concentrations are determined by assuming initial equilibrium with their aqueous counterparts. Thus, the initial concentrations of sorbed components are dictated by the selection of initial concentrations, as well as the concentration of surface complexation sites. Since the Fe(II) and U(VI) dynamics during the experiment are tied to the reservoirs of their sorbed species, a consistent set of initial and influent conditions in the context of the reaction thermodynamics is necessary to avoid artificial transients. In the absence of initial component concentrations, it was found that using the influent water chemistry as the initial condition was superior to using the initial effluent concentrations.

Another issue was the variability in the monitored influent concentrations during experiments and between experiments. This was most obvious when effluent concentrations were higher than influent for acetate, sulfate, and uranium. We chose to honor the effluent values because there were more measurements and they were more consistent. Since the influent artificial groundwater composition was supposed to be the same for all three columns (with the exception of intentional cessation of acetate and uranium in column A, late Fe(II) addition in column B, and Fe(II) addition in column C, as well as an inadvertent period of lower Fe(II) and U in column C), we chose to use the artificial groundwater composition (Table 1) instead of the monitored influent concentrations. This also resolved an issue of sampling coverage for the Column C experiment, which was characterized by several long unmonitored periods for the influent solution including a 158 day interval between the initial and subsequent measurement of acetate and sulfate.

For all three column experiments, the effluent sulfate concentrations were higher than the influent concentration (1) before sulfate reducing conditions became dominant, and (2) after acetate input ceased in the column A experiment. We infer an uncharacterized sulfate source from the column sediments. Since the influent sulfate concentrations were low relative to the higher concentrations resulting from the internal source, there is a transient sulfate release of indeterminate duration and strength in all three experiments. After about 20 days in all three experiments, the sulfate TEAP reaction consumes the bulk of the influent acetate. Thus, there is considerable uncertainty in the predicted acetate and sulfate effluent concentrations as the model does not account for the internal sulfate source.

5.3.3 Parameter Estimation

Twenty three model parameters were initially targeted for calibration in the biostimulation modeling of the Rifle sediment columns:

- Physical parameters: darcy flux, porosity, dispersivity
- Sulfate TEAP: intrinsic sulfate TEAP reaction rate, initial SRB biomass, decay of SRB biomass, max sulfate rate (to control overall rate with biomass and monod terms). Note that the TEAP reactions includes biomass production as well as bioreduction.
- Fe(III) TEAP: layer silicate Fe(III) bioreduction rate, goethite bioreduction rate, initial FeRB biomass, decay of FeRB biomass
- U(VI) TEAP: aqueous U(VI) bioreduction rate, max uranium rate

- Surface complexation: initial >FeOH site density, log K for >FeOH + Fe^{+2} =>FeOFeOH + H^{+}
- Iron minerals: siderite reaction rate, FeS reaction rate, sulfide promoted goethite dissolution rate
- Major ions: calcite precipitation rate, cation exchange capacity, log K_s for Ca^{+2}, Mg^{+2}, K+, Na^{+} ion exchange

We initially included Darcy flux, porosity, and dispersivity in the calibration of the reactive transport models but found that we could specify the measured Darcy flux and porosity (Table 23) without significant loss of fidelity. UCODE determined that the calibration was generally insensitive to dispersivity and the initial 6 cm value was maintained. The modeled aqueous species acetate, Fe(II), U(VI), and sulfate were relatively insensitive to changes in the calcite and cation exchange reaction parameters. Consequently, they were omitted from the UCODE application, leaving 13 estimated parameters.

Table 23. Hydrologic parameters for columns A, B, and C.

		Column A	Column B	Column C
Darcy Flux (cm/min)		**0.00237**	**0.00237**	**0.00257**
Porosity	**(-)**	**0.269**	**0.286**	**0.302**
Dispersivity	**(cm)**	**6.00**	**6.00**	**6.00**

A two-stage calibration approach was used. The first stage focused on sulfate related behaviors: intrinsic sulfate bioreduction rate, initial SRB biomass, decay of SRB biomass, and maximum total sulfate bioreduction rate. This is because the sulfate TEAP has the largest impact on the acetate and sulfate behavior. In the first stage, calibration of parameters was based only on the observed acetate and sulfate concentrations. In the second stage of the calibration approach, the calibrated parameters from the first stage were fixed and the rest of the parameters selected for estimation were calibrated. In the second stage, only the Fe(II) and U(VI) reaction parameters were targeted. To summarize, the approach is to fit the sulfate TEAP, then adjust the iron and uranium behaviors. This approach takes advantage of the multiprocessor option in UCODE where the sensitivity to each estimated parameter for each iteration can be determined through simultaneous HGC simulations.

We used the post-processing executable tecflowchem to create the HGCflowchem.out file that is used by UCODE. Weighting factors for the Fe(II) comparisons were lowered by a factor of 0.03 to adjust for concentrations that were 6 times higher than the other components (i.e., weighting is by the inverse square, $6^{-2} \approx 0.03$).

5.3.4 Calibration

It was determined that a biomass-dependent U(VI) bioreduction rate would conceptually address the increasing removal of U(VI) observed in the column experiments. Since the biomass for both the Fe(III) and U(VI) TEAPs are attributed to the FeRB, this required new TEAP reactions for both Fe(III) and U(VI):

Phyllosilicate Fe(III)

$$0.125Ac^{-} + Fe(III)(ls) = 0.25\ HCO_3^{-} + 0.9Fe(II)(ls) + 0.1Fe^{++} + 1.125H^{+} + 0.0043BM\_iron$$

Goethite

$0.125Ac^- + 0.6FeOOH + 1.155H^+ + 0.02NH_4^+ = 0.004BM\_iron + 0.6\ Fe^{++} + 0.15HCO_3^-$

U(VI)

$0.125Ac^- + 0.00113NH_4^+ + 0.3875\ UO_2^{++} = 0.0113BM\_iron + 0.855H^+ + 0.1938HCO_3^- + 0.3875UO_2(s)$

where,

(ls) denotes layer silicate

BM_iron is the FeRB biomass concentration based on the molecular formula $C_5H_7O_2N$.

New parameters were needed for the initial FeRB biomass, FeRB biomass decay rate, and maximum total rate for uranium bioreduction. It should be noted that the conversion of the Fe(III) and U(VI) rate laws to biomass dependence requires a much larger intrinsic rate to offset multiplication by the biomass concentration.

5.3.5 Initial Simulations

The three column experiments use sediments from a common sample with minor variations in packing and hydrologic forcing (Table 2). The influent solution is based on the artificial groundwater (AGW) recipe in Table 1 with the following variations:

- Column A simulation:
    - 111.5 days of AGW
    - 35.7 days without acetate
    - 35.5 days without both acetate and uranium
- Column B simulation:
    - 210.1 days of AGW
    - 10.9 days with the addition of 11.65 uM Fe(II)
- Column C simulation:
    - 135.3 days of AGW with the addition of 13.53 to 11.65 uM Fe(II)
    - 23.2 days with low 1.38 uM Fe(II) and low 0.13 to 0.57 uM U(VI)
    - 27.8 days with low iron but otherwise standard AGW

The column B experiment was conceptually the simplest (influent concentrations maintained for all but the last 11 days of the 221 day biostimulation) and, like column A, had good sampling coverage of influent concentrations. The addition of Fe(II) to the influent after 210 days did seem to have a subtle effect on the observed acetate, Fe(II), and U(VI) concentrations. The column C experiment was characterized by considerably less temporal sampling coverage, with

several long unmonitored periods for the influent. For example, after the initial measurement of acetate and sulfate, the next measurement was 158 days later. Consequently, we chose to use the calibrated reaction parameters from the column B experiment on columns A and C.

Table 24 summarizes the parameters calibrated for column B. Note that the intrinsic U(VI) bioreduction rate for the column is four orders of magnitude larger than the field modeling value because it is being multiplied by the biomass concentration, which is typically a small value, ~1E-6 M (Table 24). Nearly all the calibrated reaction parameters represent an increase in reactivity over the field-scale modeling. This may be explained to some degree by the use of the < 8 mm particle size fraction in the experiments (Table 4), which disproportionately contains the most reactive size fractions in the full particle size distribution (Table 25, unpublished data from A.L. Ward, Pacific Northwest National Laboratory). In this case, the <8 mm size fraction is 22% by weight of the total field sediment size distribution, which implies there could be 5 times higher reactivity if it is assumed that the > 8 mm size fraction is largely inert. Interestingly, the homogeneous sulfate bioreduction reaction also had a higher calibrated reaction rate, suggesting a potential linkage to the higher fraction of finer grained sediment.

Table 24. Calibrated model parameters for column B

Parameter	Field Modeling Value	Column B Value[a]
Intrinsic Crystalline Fe(III) Reduction Rate, d^{-1}	1.60E-02	3.80E-03
Intrinsic Sulfate Reduction Rate, Md^{-1}	80	2.54E+02
Intrinsic U(VI) Reduction Rate, Md^{-1}	2.50E-05	1.02E+00[b]
Initial Sulfate Reducing Bacteria Biomass, M	1.00E-07	2.17E-06
Sulfate Reducing Bacteria Decay Rate, d^{-1}	1.50E-02	7.48E-01
Maximum Total Sulfate Bioreduction Rate, Md^{-1}	3.26E+02	3.18E+02
Sulfide Promoted Goethite Dissolution Rate, $M^{-1}d^{-1}$	2.08E+02	4.17E+03
FeS(s) Rate, Md^{-1}	5.11E-05	6.07E-02
Initial >FeOH Site Concentration, M	3.28E-02	7.67E-02
Initial Fe(III) Reducing Bacteria Biomass, M	not included in field reaction network	3.51E-07
Fe(III) Reducing Bacteria Biomass Decay Rate, d^{-1}	not included in field reaction network	2.48E-06
Maximum Total U(VI) Bioreduction Rate, Md^{-1}	not included in field reaction network	2.36E+00
>FeOH + Fe^{+2} = H^{+} + >FeOFeOH log K	-1.196E+01	-9.84E+00

a. Magenta shading indicates parameter value decreased by greater than 25%. Green shading indicates parameter value increased by greater than 25%.
b. Parameter increased for biomass-dependent rate.

Table 25. Particle Size Distribution of Rifle Aquifer

sieve size (mm)	% of mass	% mass finer
256	**0.00**	**100.00**
64	**41.07**	**58.93**
32	**17.17**	**41.75**
16	**13.08**	**28.67**
8	**7.02**	**21.64**
4	**3.84**	**17.81**
2	**1.91**	**15.90**
1	**2.46**	**13.45**
0.5	**7.65**	**5.79**
0.25	**2.65**	**3.14**
0.125	**1.60**	**1.55**
0.063	**0.78**	**0.77**

5.4 Model Simulation Results

5.4.1 Column B Simulations

During the first ~20 days of all experiments, acetate-driven bioreduction by FeRB results in a ~70 uM peak in Fe(II) concentrations as well as a ~3 μM decrease in U(VI). Acetate consumption is relatively low because of (1) the general efficiency of the TEAP reactions (e.g., 5-8 moles of Fe(III) reduced for every mole of acetate consumed) and (2) the relatively small amounts of metal reduced (e.g., 10 μM U(VI)). From day ~20 to ~50, effluent acetate concentrations decrease sharply to ~3 mM before beginning to level off after 50 days (Figure 46). This generally coincides with the increase in sulfate bioreduction by SRB, which results in low effluent sulfate concentrations (1-1.5 mM) after ~50 days. Significant changes in the effluent acetate concentrations are thus dictated by the sulfate TEAP reaction, which has ~1:1 acetate to sulfate consumption ratio. This explains the similarity in the time-dependent acetate and sulfate effluent concentration behaviors. The model used 8 mM for the influent acetate, lower than the 10 mM acetate concentration measured in the effluent over the first 22 days of the column B experiment. This disparity between the model predicted and measured effluent acetate is the result of using the intended AGW recipe influent acetate concentration of 8 mM in the model whereas the experimental influent acetate concentration was 10 mM during the first 70 days of biostimulation of column B and for the entire biostimulation period of column A. The experimental acetate influent was 8 mM for the remainder of column B and all of column C. (see sections 2.1 and 3.1.2). The modeled effluent acetate generally captures the increasing consumption beginning 20 days into the biostimulation experiment (Figure 46). After 50 days, the rate of acetate consumption begins to level off leading to an asymptotic value of 2 mM, which is generally captured by the model.

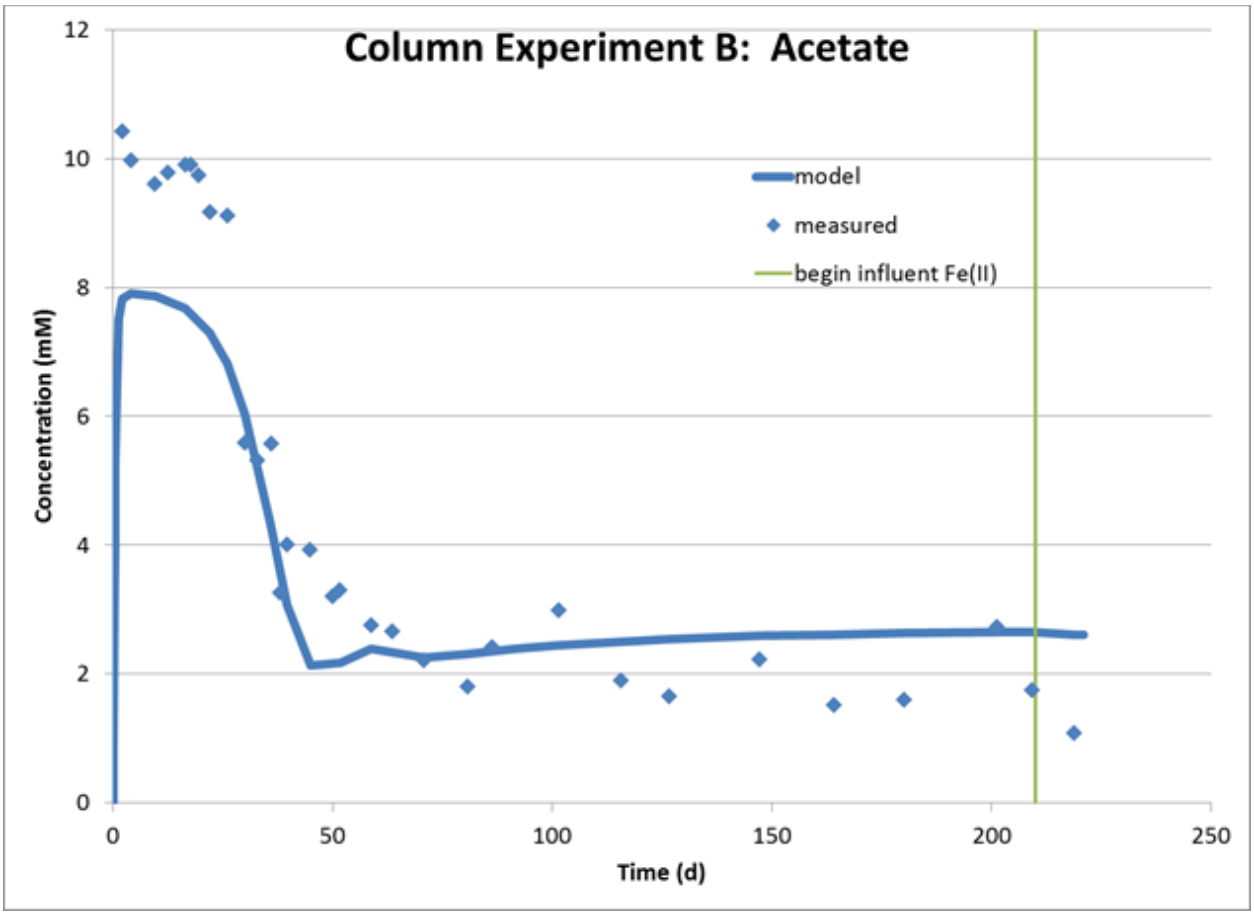

Figure 46. Model simulation column B effluent acetate.

The model adsorbed Fe(II) is increasing during the early buildup of aqueous Fe(II), which means the Fe(II) source is from mineral dissolution: Fe(III) bioreduction and/or goethite dissolution via biogenic sulfide. The model has two pools of bioavailable Fe(III), goethite and phyllosilicate. Since the biogenic Fe(II) from the phyllosilicate Fe(III) is largely reduced in place, the principal source of the aqueous Fe(II) is the goethite. As sulfate bioreduction ramps up after 20 days, Fe(II) and sulfide are consumed in the formation of FeS mineral, putatively mackinawite. This results in a fairly rapid and near-complete removal of aqueous Fe(II) (Figure 47). The addition of 11.65 μM Fe(II) at day 210 is completely consumed in the model result compared to the smaller spike that was observed.

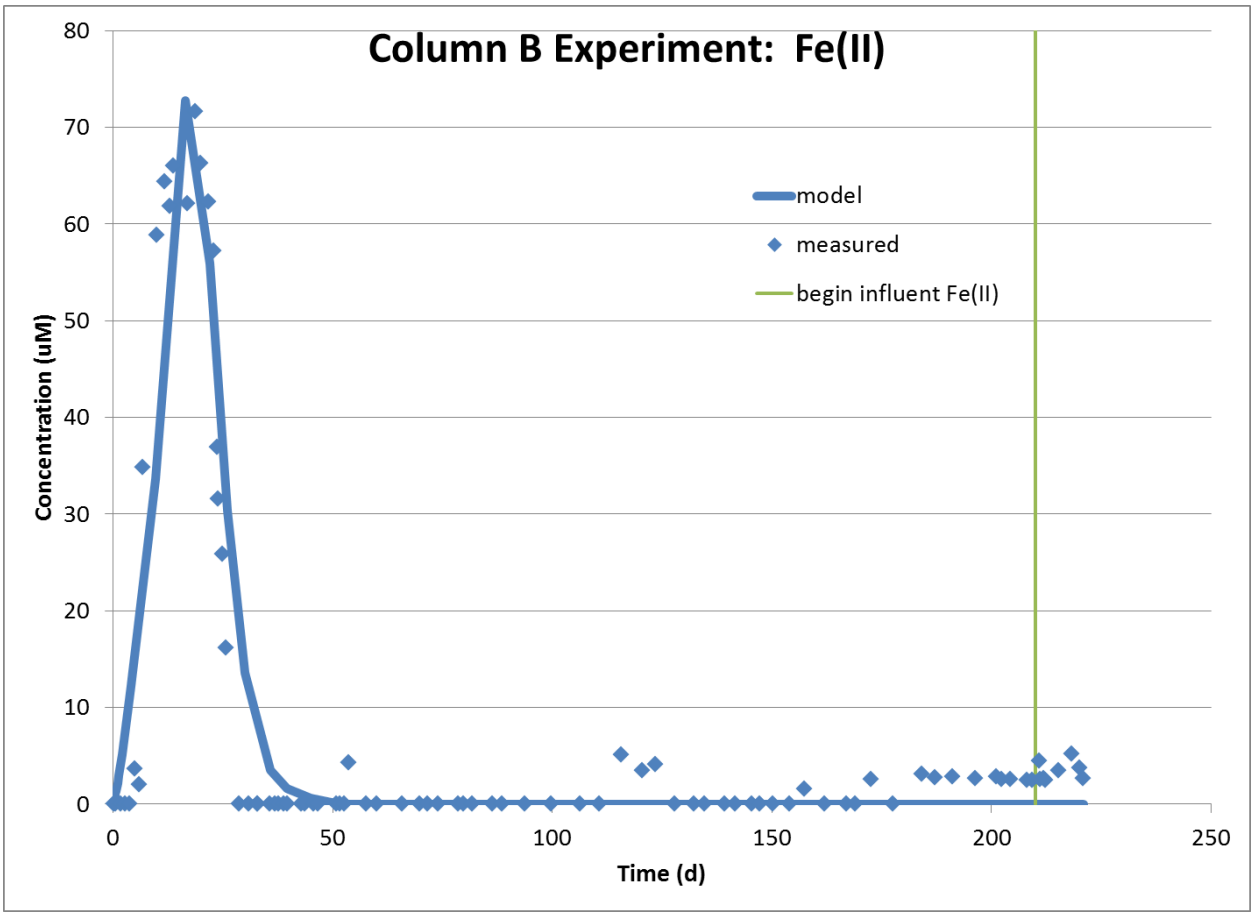

Figure 47. Model simulation column B effluent dissolved iron.

In the model, the decrease in aqueous U(VI) is described to occur primarily by bioreduction. This is because the other uranium reactions result in a net desorption over the first 35 days that largely depletes the initial pool of adsorbed U(VI). The initial drop in aqueous U(VI), which bottoms out after 20 days, coincides with the spike in aqueous Fe(II) concentrations from the reductive dissolution of Fe(III) mineral (Figure 48). The dominance of FeRB during the initial biostimulation with associated impacts on iron and uranium chemistry are consistent with observations from Rifle IFRC field experiments (Anderson *et al.*, 2003; Vrionis *et al.*, 2005; Williams *et al.*, 2011). In particular, U(VI) desorption begins to accelerate after 25 days, when increasing oxidation of acetate by the SRB significantly elevates the bicarbonate available for aqueous complexation with U(VI). This is consistent with the short-term increase in effluent aqueous U(VI) concentrations, peaking at 35 days, but still below the influent concentration. After 50 days, relatively low adsorbed U(VI) concentrations stabilize with the evolving water chemistry. The modeled rate of uranium bioreduction is slowly increasing over the duration of the experiment because of the biomass dependent rate law. The drop in observed U(VI) after day 210 appears to coincide with the addition of 11.65 μM Fe(II) to the influent. There was no similar impact to the modeled U(VI) behavior. This could be due to an uptake mechanism not included in the model such as abiotic U(VI) reduction. Similar experiments in the Rifle aquifer with the addition of 45 μM Fe(II) had minimal impact on aqueous U(VI) concentrations (unpublished, 2012 Rifle IFRC Annual Report).

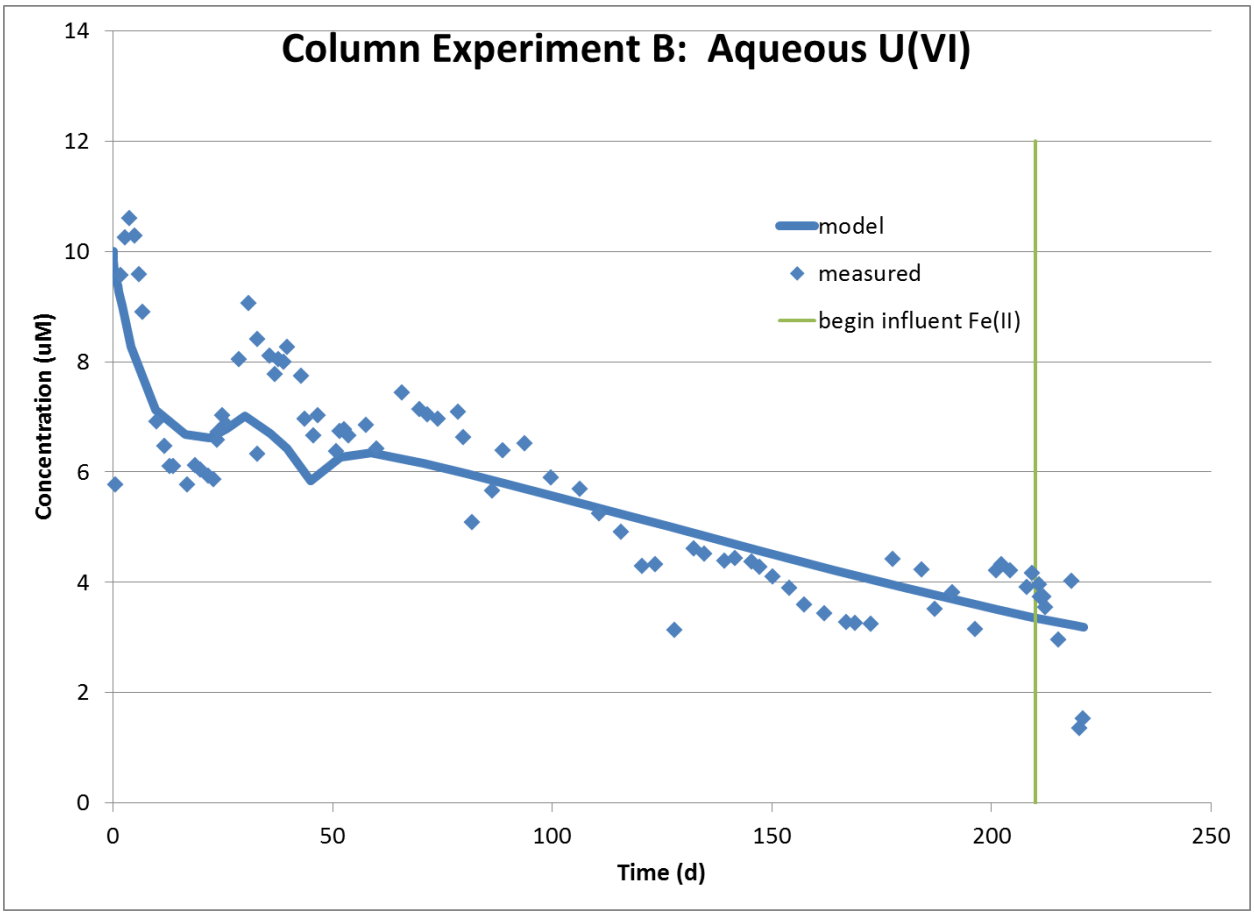

Figure 48. Model simulation column B effluent dissolved uranium.

Similar to the modeled acetate behavior, the presence of an uncharacterized internal source of sulfate from the column sediments leads to significant underprediction of the sulfate concentrations for the first 25 days of the experiment (Figure 49). During this time period, the millimolar sulfate concentrations are largely unaffected by the biogeochemical impacts of the stimulated FeRB. After this period, the time-dependent sulfate concentrations are a direct consequence of the acetate-oxidizing SRB, which accounts for the similarity with the acetate behavior (Figure 49). In this case, the biomass-dependent sulfate bioreduction rate becomes very high, before leveling off, yielding ~1 mM sulfate concentrations. In the model, there is initially a small amount of slow growing SRB that have minimal impact on sulfate concentrations. As the SRB biomass increases over time, the bioreduction rate increases commensurately until a maximum is reached at ~50 days. It should be noted that the rate-limited microbially-mediated sulfate reduction reactions result in the non-equilibrium coexistence of Fe(II), sulfide and sulfate. This behavior is always observed in the field biostimulation experiments, underscoring the kinetic control exerted by these TEAP reactions over the redox couples.

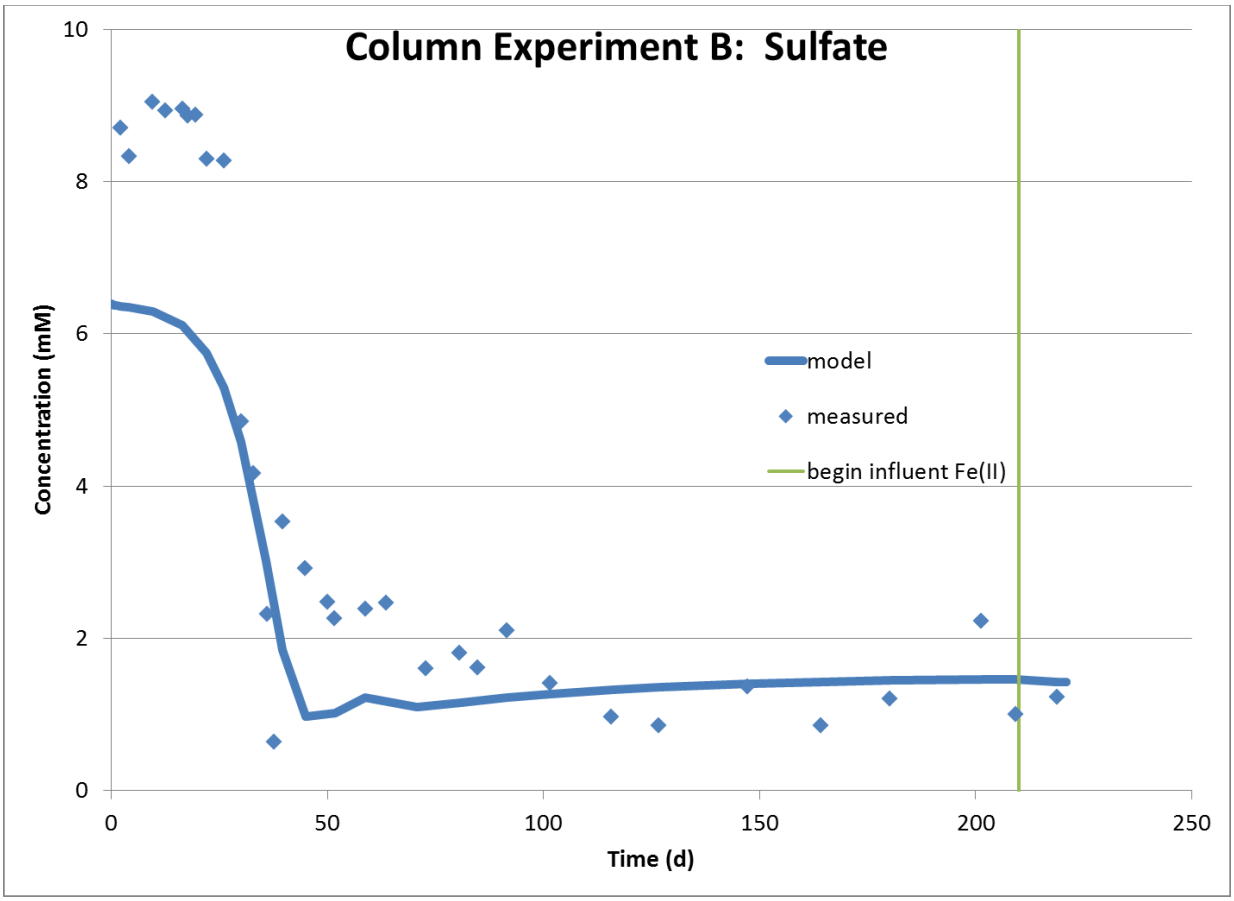

Figure 49. Model simulation column B effluent dissolved sulfate.

5.4.2 Simulation of Column A Effluent using Column B Parameters

We used the reaction parameters calibrated from the column B experimental observations to model the column A experiment. The column A experiment is run with the same flow rate, influent conditions and sediments as the column B experiments. After 111 days, influent acetate is stopped and after 147 days, influent uranium is stopped. Thus, for the first 111 days, the model results are the same as for the column B experiment and the comparison with experimental observations was also similar (Figure 50). The termination of influent acetate and then sulfate did result in model discrepancies, especially for the micromolar Fe(II) and U(VI) components. While acetate does behave similarly to Column B, there is a more gradual and sustained decrease in acetate concentrations after day 30 until influent acetate is stopped after 111 days. Unlike the column B experiment, acetate does not level off to a 2 mM concentration. Instead it appears that acetate would eventually be completely consumed if the cessation of acetate did not occur after 111 days. This implies a continuous increase in the sulfate bioreduction rate beyond that in the column B experiment. Acetate concentrations rapidly go to zero after acetate is eliminated from the influent solution, which the model reproduces.

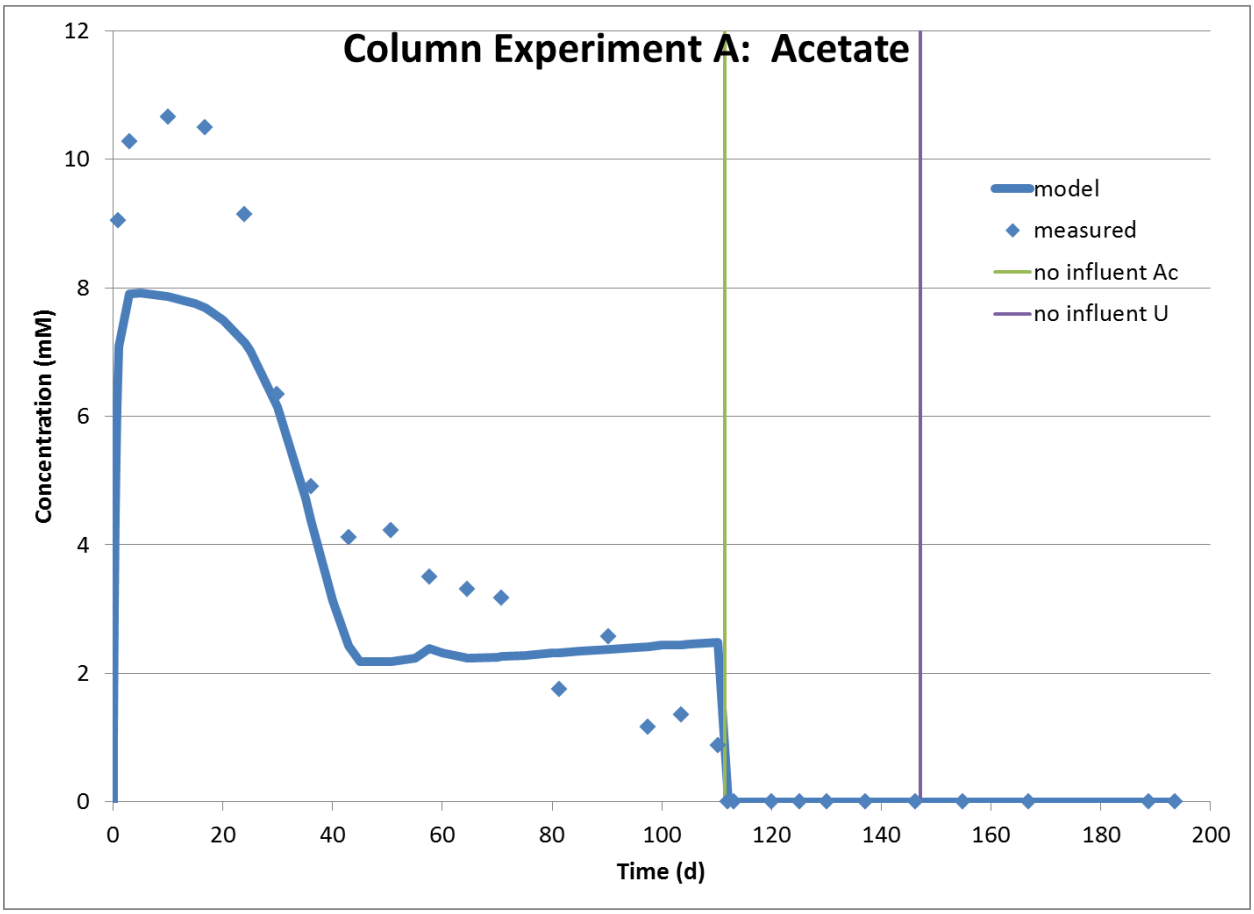

Figure 50. Model simulation column A effluent acetate.

As with the column B experiment, the model does a fairly good job capturing the peak Fe(II) concentration just before 20 days (Figure 51). In this case, there is a phase error in the timing of the Fe(II) peak arrival as the model is predicting a later breakthrough. The measured column A porosity was smaller than column B, 0.269 versus 0.286. A slightly smaller effective porosity might account for the observed behavior. For the 50 days prior to the end of biostimulation, aqueous Fe(II) is largely diminished by reaction with sulfide, forming an FeS mineral. When influent acetate is stopped at 111.5 days, Fe(II) concentrations are below detection, after which there is a steady increase in effluent Fe(II) to ~25 μM at the end of the 194 day simulation (Figure 51) While this behavior has never been observed in the field, ambient Fe(II) concentrations of that magnitude (10-50 μM) are typically present at the Rifle site under unstimulated conditions. Assuming these concentrations are in quasi-equilibrium with the sediments, the absence of Fe(II) in the influent solution creates disequilibria that results in desorption and/or dissolution from the sediments. This uncharacterized internal source of Fe(II) may have been occurring throughout the experiment but was not detectable because FeS solubility was limiting dissolved Fe(II). The cessation of influent U after 147 days has negligible impact on the Fe(II) behavior.

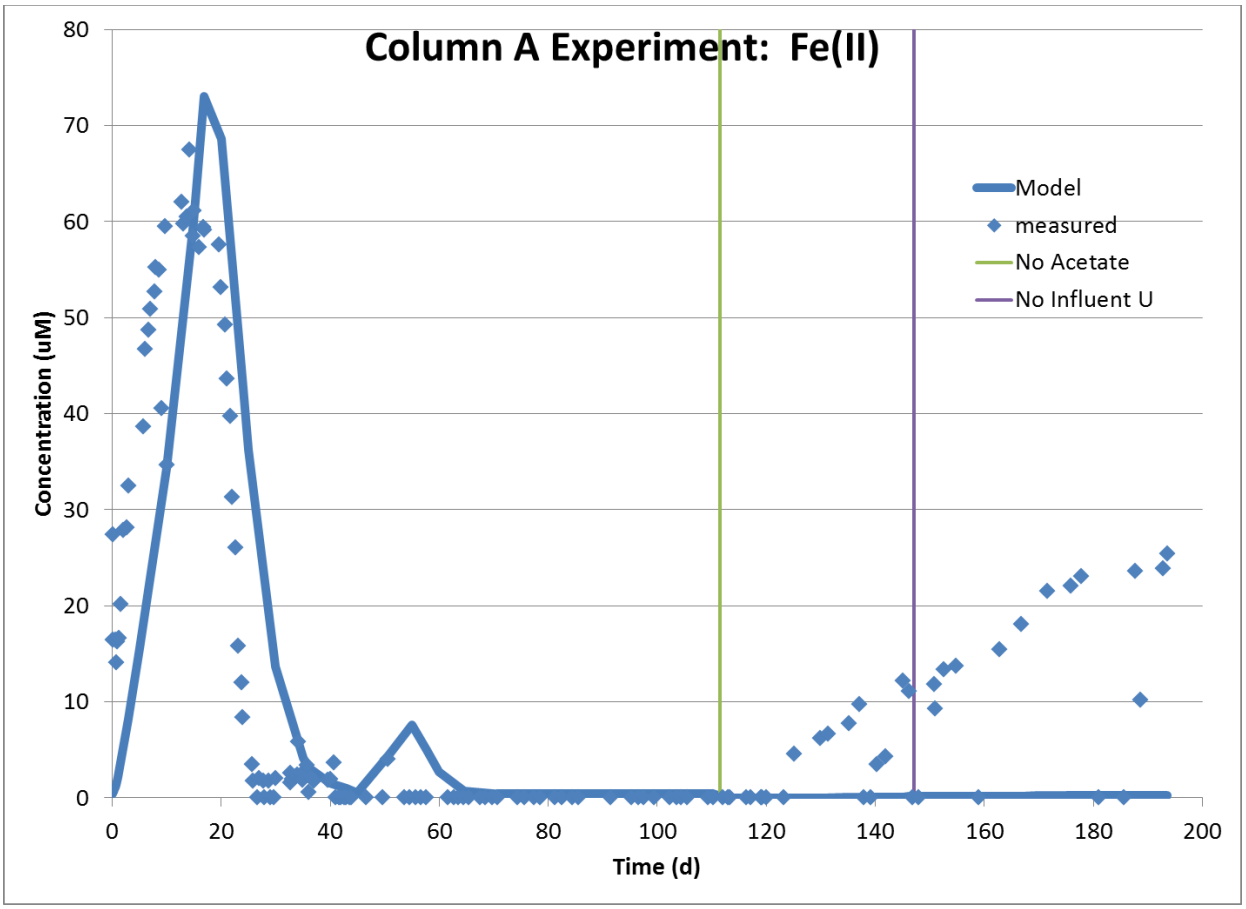

Figure 51. Model simulation column A effluent iron.

While there are some dynamics in the aqueous U(VI) concentrations, there is a general increase in U(VI) removal from solution until the influent acetate is stopped after day 111 (Figure 52). This behavior includes a slight rise in aqueous U(VI) concentrations at day 30 when higher bicarbonate concentrations from acetate oxidation in the sulfate TEAP reaction results in U(VI) desorption. The uranium behavior under biostimulation is generally captured by the model, but concentrations between 70 and 110 days are under predicted (Figure 52). This under prediction is difficult to explain since, up to this point, columns A and B should have been operating under the same conditions.

The post-biostimulation U(VI) behavior was not captured well by the modeled reaction network. Since there has been no evidence for substantial abiotic U(VI) reduction in the Rifle aquifer, the rapid drop in observed aqueous U(VI) concentrations when acetate loading stops is more consistent with adsorption that has been enhanced by 1) the cessation of bicarbonate production from acetate oxidation (i.e., lower bicarbonate concentrations thermodynamically favor U(VI) speciation that enhances adsorption), and 2) the availability of surface complexation sites vacated during biostimulation via bicarbonate-induced desorption. For the column water chemistry, the nominal model specification of >FeOH sites would have to be increased by a factor of 50 to match the post-biostimulation uptake. This assumes no abiotic reduction occurs. The consequence of increasing the >FeOH sites is that there would be significantly more initial U(VI) adsorbed on these sites and desorption during high sulfate reduction would result in a massive U(VI) peak after 35 days, which was not observed. The 50 times more surface complexation sites required seems excessive since the <4 mm size fraction accounts for 18% of the mass of the full particle size distribution (Table 25). The surface area contribution of the <4

mm fraction to the bulk sediment is not known. It would appear that the SCM we have been using is not consistent with the column geochemistry. One possible explanation is that the surface complexation model was developed from experiments on a sediment sample from a different part of the Rifle Site than the sediments in the column studies. If the sediments were physically and geochemically different, the selected surface complexation reactions and derived stability constants for those reactions may not be a good match. There could also be unresolved kinetic limitations controlling the uranium in the column studies, or that some other process, such as abiotic reduction of U(VI) by sulfide or Fe(II), results in the observed continued uptake, as discussed in section 5.1.2.

As the surface complexation sites are re-saturated with U(VI) after 110 days, the effluent concentrations begin to climb ostensibly toward the influent 10 uM U(VI) concentration. This process is interrupted when the influent U(VI) is terminated after 147 days and the U(VI) concentrations drop to the ~1 uM level, a pseudo-equilibrium driven by the absence of influent U(VI).

The comparison of the modeled and observed sulfate behavior prior to stopping the acetate loading after 111 days is similar to the column B analysis (Figure 53). As mentioned previously, there was an internal sulfate source that initially resulted in ~9 mM effluent sulfate concentrations (versus the 6.4 mM influent concentration) that could not be addressed by the modeling. The rebound of post-biostimulation (i.e., > 111 days) sulfate concentrations back up to the initial concentrations, implied that the initial sulfate release from the sediments was not a short transient but more likely continuous over the experiment duration. The uncharacterized source, however, is not a part of the modeled reactions. Consequently, the predicted post-biostimulation sulfate concentrations are significantly below the observations.

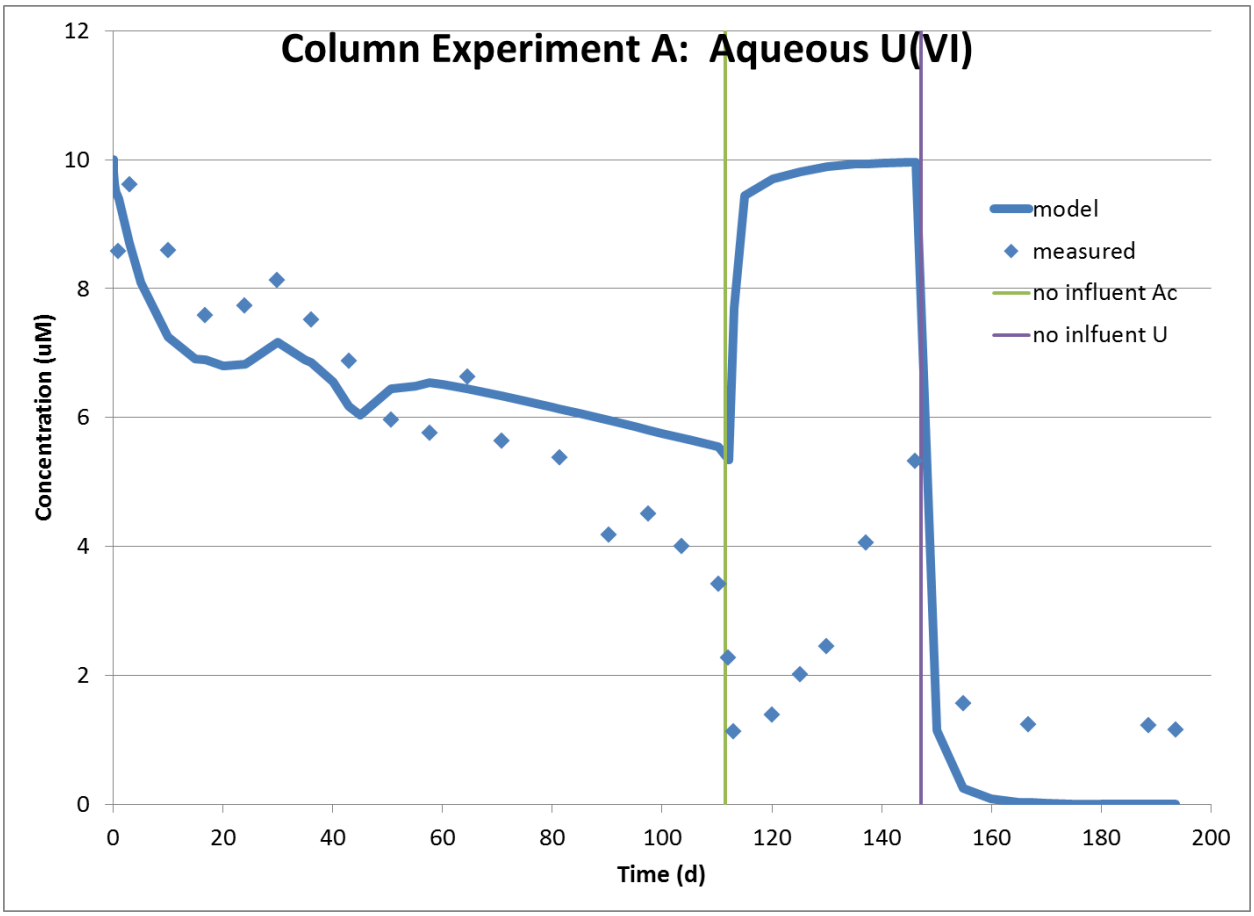

Figure 52. Model simulation column A effluent uranium.

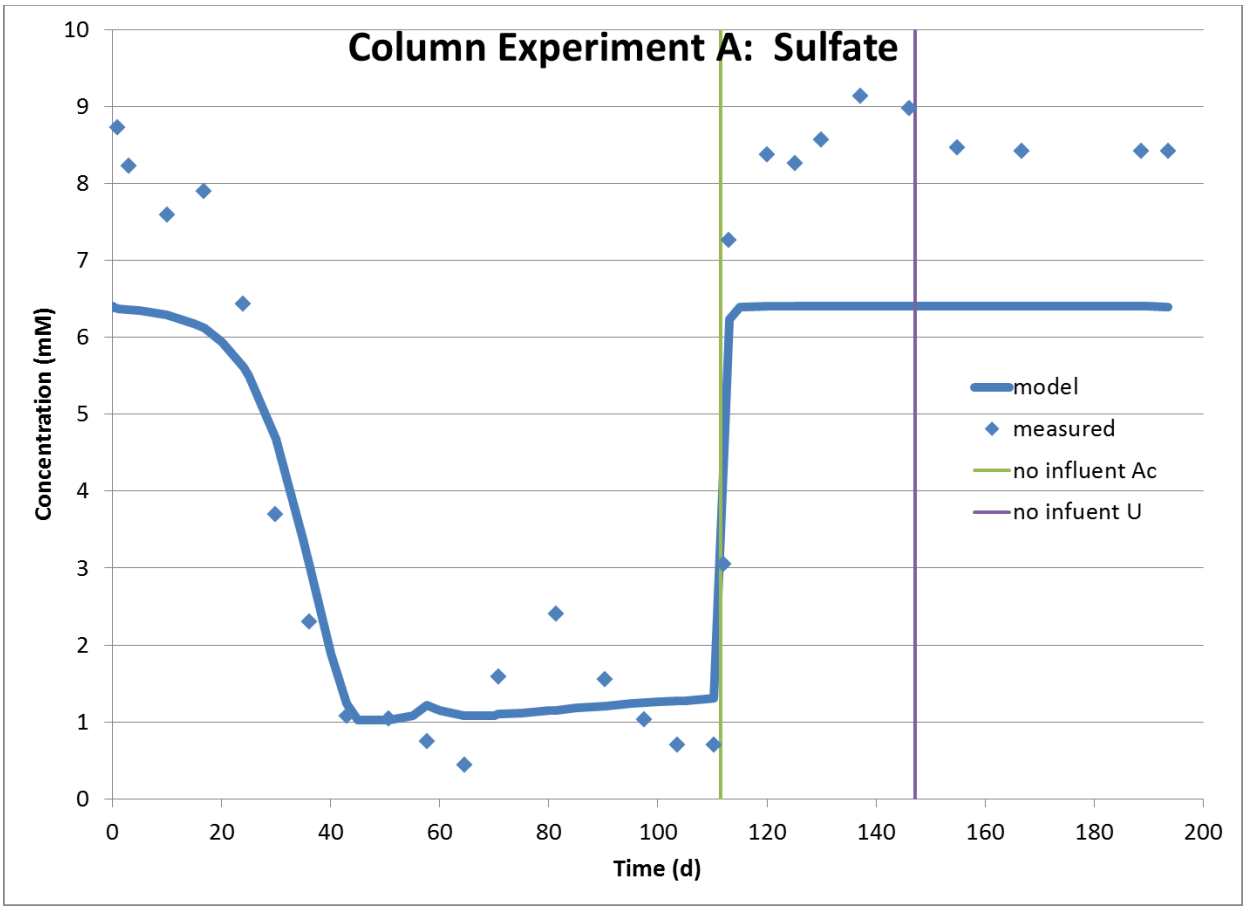

Figure 53. Model simulation column A effluent sulfate.

5.4.3 Simulation of Column C Effluent using Column B Parameters

The column B reactions parameters were next applied to the column C experiment. The flow rate in the column C experiment was 8% faster than columns A and B. With the exception of the Fe(II) that was added, the influent solution for the column C experiment was based on the same artificial groundwater recipe as the columns A and B experiments. Over the first 40 days, the three influent Fe(II) measurements were 13.53, 12.52, and 11.65 μM. Because of an error in the influent composition from day 135 to 159, the influent U(VI) was as low as 0.13 μM versus the 10 μM recipe and the only Fe(II) measurement was 1.38 μM. The column C experiment was characterized by considerably less temporal sampling coverage, with several long unmonitored periods for the influent. For example, after the initial measurement of acetate and sulfate, the next measurement was 158 days later.

The acetate behavior is similar to the other experiments in magnitude and timing with no obvious impact of the 8% faster flow rate. This might be explained by the pore velocity of 8.5 cm/min, which is between the 8.3 cm/min for column B and the 8.8 cm/min for column A. In this experiment, the effluent acetate measurements over the initial 20 days are only slightly higher than the 8 mM influent. After day 40, the model predicted acetate consumption is slightly greater than observed, which is stoichiometrically consistent with the slight over prediction of sulfate consumption (Figure 54). On day 135, there was a significant decrease in influent U(VI) (2 order of magnitude decrease) and Fe(II) (1 order of magnitude decrease). This coincided with an observed decrease in acetate, presumably from reaction. The modeled acetate, on the other

hand, was relatively unaffected. It's not clear why acetate consumption would increase when influent U(VI) and Fe(II) concentrations were significantly decreased. The model does not have a process that would account for enhanced acetate consumption under these conditions.

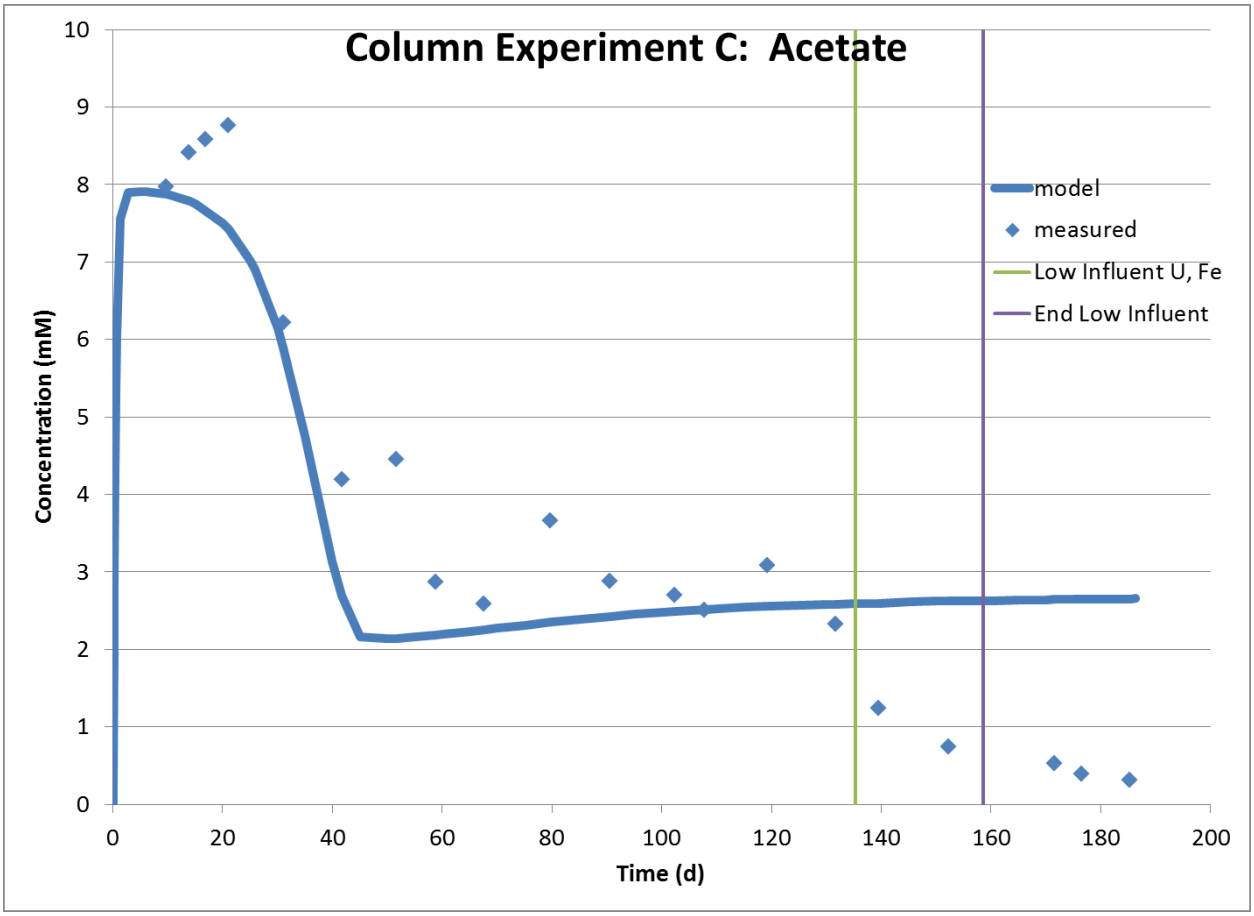

Figure 54. Model simulation column C effluent acetate.

The predicted column C Fe(II) peak magnitude and timing over the first 40 days was particularly good and similar to the other columns (Figure 55). While columns A and B exhibited Fe(II) concentrations below detection after the primary peak at 20 days, column C has a few periods with ~5 μM concentrations. The modeled Fe(II) is consistent with below detection concentrations, primarily due to precipitation of FeS. The observed Fe(II) concentrations seemed to be anti-correlated to the changes in influent Fe(II), increasing during the low influent Fe(II) period (days 135 to 159) to ~5 μM and decreasing after resumption of the design influent Fe(II) concentration.

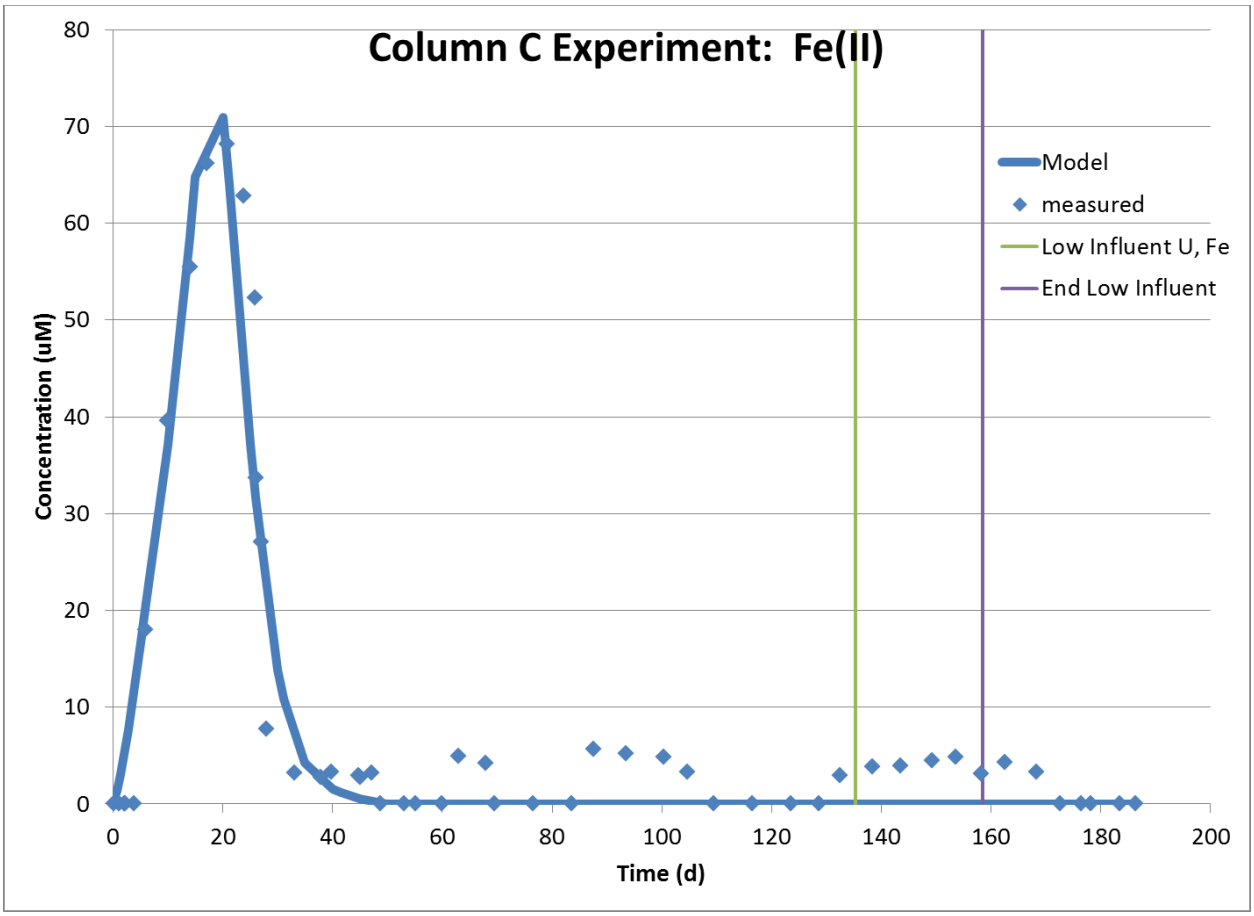

Figure 55. Model simulation column C effluent iron.

The observed U(VI) behavior in column C was a significant departure from columns A and B. The highest initial effluent U(VI) measurement was 7.8 μM versus 9.6 and 10.6 in columns A and B, respectively. From 40 to 100 days the observed U(VI) concentrations in column C were ~3 μM lower than column A and ~4 μM lower than column B, and significantly over predicted by the model (Figure 56). The unplanned drop in influent U(VI) after 135 days is captured by the model but the resumption of the design influent U(VI) concentration after 159 days results in even lower observed U(VI) concentrations. Column C had continuous ~12 μM influent Fe(II) whereas the other columns did not. When column B introduced a similar amount of Fe(II) at the end of the experiment, a ~3 μM drop in U(VI) was observed. The model does not have a mechanism (e.g., abiotic U(VI) reduction, enhanced U(VI) sorption) that would address the enhanced U(VI) removal; consequently, the U(VI) reactivity is significantly under predicted. As mentioned previously, a 45 μM Fe(II) injection was performed in the field with no significant impact on U(VI) concentrations. More recently, abiotic laboratory studies with up to 1.41 mM Fe(II) at pH 7.1 and 400 ppm CO_2 (similar conditions to the Rifle site) result in negligible additional U(IV) (unpublished, 2012 Rifle IFRC Annual Report).

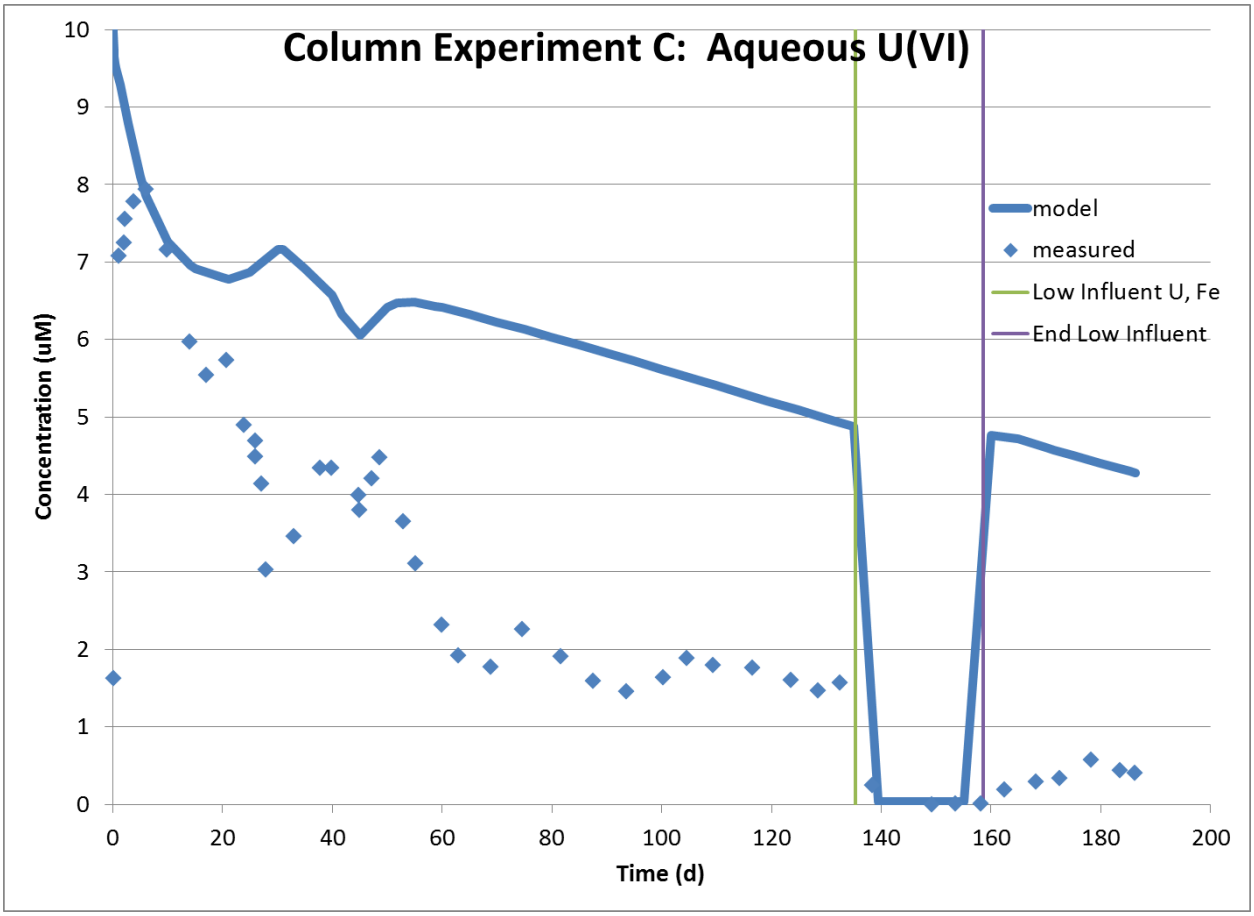

Figure 56. Model simulation column C effluent uranium.

The general trends of the observed and modeled sulfate behaviors are similar to the previous discussions for columns A and B where the influent 6.4 μM concentrations are considerably below the first 20 days of effluent measurements (Figure 57). The sulfate bioreduction is slightly over-predicted in the model, by an amount that is approximately stoichiometrically consistent with the over prediction of the acetate consumption. The drop in influent U(VI) and Fe(II) at day 135 coincided with decreasing observed sulfate concentrations. This sulfate concentration drop was not restored by the return to design influent Fe(II) and U(VI) after 158.5 days. The model has no mechanism that would account for this magnitude of sulfate concentration change from transients in trace components. As a result, the predicted sulfate concentrations are unaffected by the period of lower Fe(II) and U(VI).

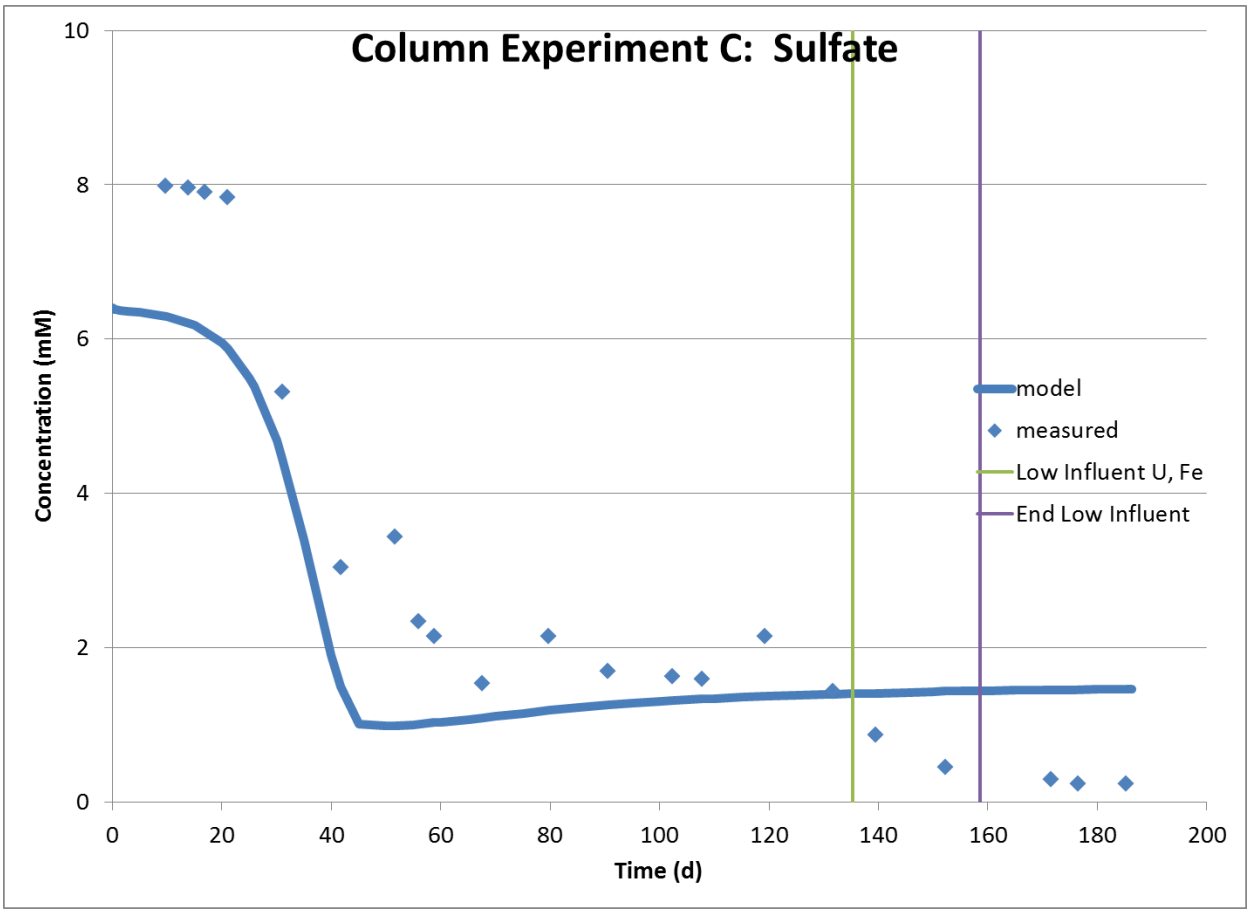

Figure 57. Model simulation column C effluent sulfate.

5.5 Discussion of Model Simulations

Uranium aqueous and surface complexation reactions are very important to the uranium behavior during acetate biostimulation. Prior to biostimulation in the field and assuming undersaturation of U(VI) minerals, dissolved U(VI) is controlled by adsorption and desorption with the majority of U(VI) adsorbed to the sediments. In the modeling of the column experiments, 70% of the U(VI) is initially sorbed. Acetate stimulates metal reducing bacteria to rapidly catalyze the reduction of U(VI) to solid-associated U(IV), effectively lowering aqueous U(VI) concentrations. The microbially-mediated oxidation of acetate leads to the production of bicarbonate which complexes with U(VI). U(VI) desorption is thermodynamically favored by the lower aqueous U(VI) concentrations and higher alkalinity. Consequently, the pool of initially adsorbed U(VI) is rapidly depleted over the initial 40 days of biostimulation. Figure 58 compares the adsorbed U(VI) and total solid phase U(IV) over time in the last model grid cell for column A. At the end of the three column experiments, the adsorbed U(VI) accounts for 0.15%, 0.16%, and 0.24% of the solid associated uranium in columns A, B, and C, respectively. The remainder is U(IV). This findings agrees well with the >95% U(IV) measured in column A sediments by XANES (Table 9). At the end of the simulated column experiments, the spatial variation from inlet to outlet of adsorbed U(VI), U(IV), FeS, elemental S, and phyllosilicate Fe(II) is generally small (Table 26). Higher concentrations of U(IV) are predicted near the influent end because progressive removal of U(VI) is sufficiently high to limit availability further down the column. The predicted trends in solid phase concentrations with position in column are in general agreement

with measured distribution of the constituents in sediments recovered after biostimulation (Figures 11-19).

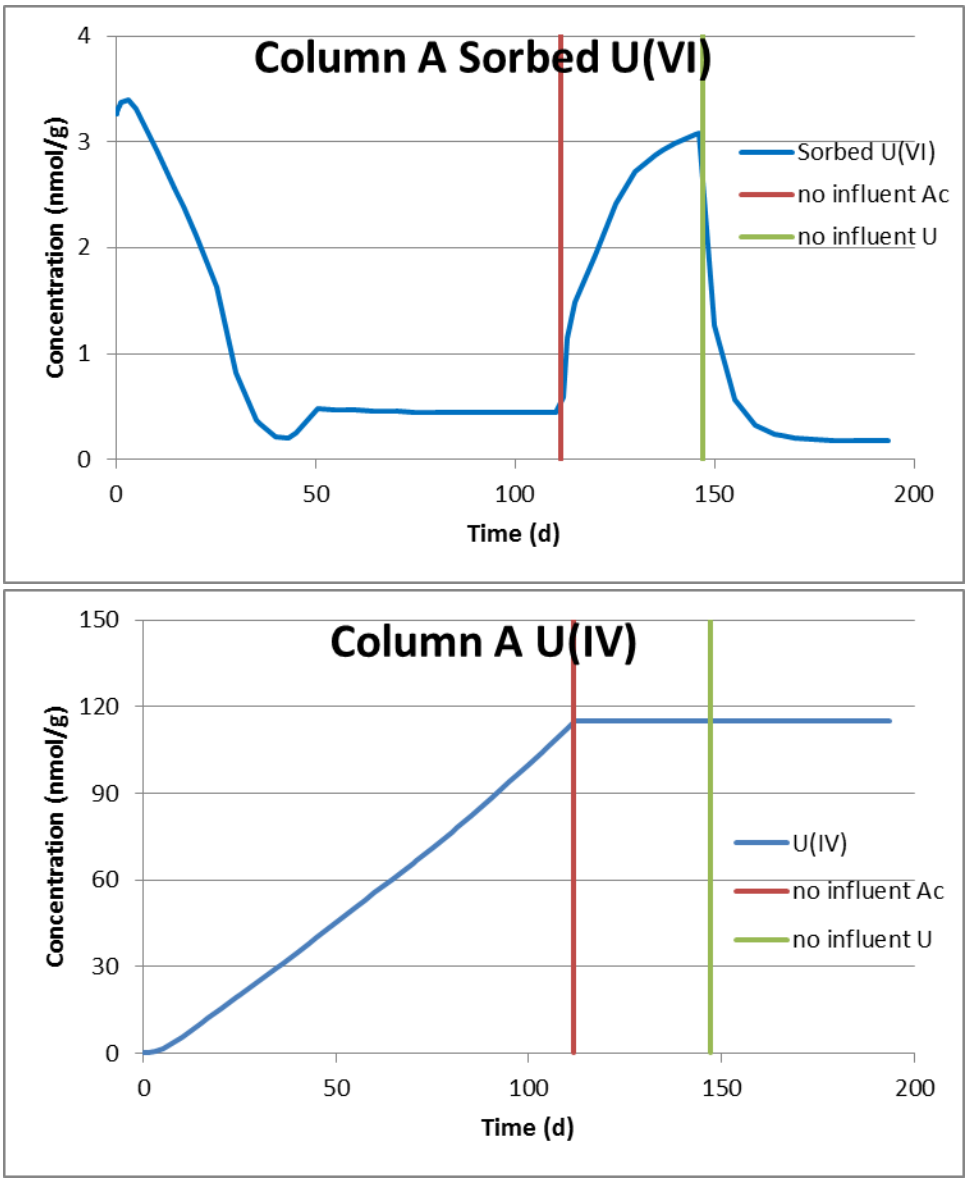

Figure 58. Time-dependent variation in adsorbed U(VI) (top) and U(IV) (bottom) for the grid cell closest to the column A effluent. Influent acetate was stopped after 111 days and influent U(VI) was stopped after 147 days.

Table 26. Simulated adsorbed U(VI), U(IV), FeS, elemental S, and phyllosilicate Fe(II) at the end of experiments in columns A, B, and C.

	Column A (nmol/g)		Column B (nmol/g)		Column C (nmol/g)	
	inlet	**outlet**	**inlet**	**outlet**	**inlet**	**outlet**
U(VI) Adsorbed	**0.172**	**0.173**	**0.460**	**0.439**	**0.517**	**0.499**
U(IV)	**126**	**114**	**353**	**281**	**248**	**212**
FeS	**1.42E+04**	**1.48E+04**	**1.50E+04**	**1.54E+04**	**1.85E+04**	**1.71E+04**
S	**7.43E+03**	**7.43E+03**	**7.73E+03**	**7.73E+03**	**8.57E+03**	**8.58E+03**
Fe(II) Layer Silicate	**6.37E+02**	**6.37E+02**	**6.63E+02**	**6.63E+02**	**7.35E+02**	**7.35E+02**

6 Summary

The primary goal of this study was to evaluate the remobilization of U sequestered during biostimulated reduction under conditions in which biostimulation and concomitant U reduction extended well into sulfate reduction to enhance precipitation of reduced sulfur phases such as iron sulfides. The intent of producing these reduced phases was to test their effect on remobilization of the sequestered uranium, either serving as redox buffer by competing for dissolved oxygen, or by armoring the reduced uranium. Increased production of iron sulfide phases was attempted through addition of ferrous iron in the influent stream throughout biostimulation in one column.

During biostimulation of the ambient microbial population with acetate, the removal of dissolved U(VI) from the influent continued over 110 to 330 days of biostimulation, well after the onset of sulfate reduction at ~30 days. Dissolved uranium was lowered from the influent 10 μM to <4 μM. The uranium sequestered during biostimulation was essentially all U(IV) resulting from the formation of nano-particulate uraninite that may be associated with organic microbial biomass. The sequestered U(IV) may in part be coordinated to C or P in the organic matter. The reduced U(IV) formed contiguous coatings on sediment grains with thicknesses of a few 10s of microns and was in association with S and Fe in some cases. Combined the effluent and solid phase measurements from columns during and after the biostimulation stage suggests that stimulation and growth of indigenous microbial population in the aquifer sediments from the Rifle site by addition of an electron donor and carbon source may be an effective means of removing dissolved uranium from contaminated groundwater, consistent with many field and laboratory studies.

Determining the stability of the bioreduced uranium in response to changes in groundwater chemistry after biostimulation has ceased, such as the return to oxic conditions, is needed to evaluate if the biostimulated reduction process would be an effective tool for long term remediation of U-contaminated shallow aquifers. Elution of bioreduced U(IV) associated with sediments from two columns (A and C) was conducted using AGW at equilibrium with atmospheric oxygen. This oxygen level was used to assess the upper limit of dissolved oxygen in recharge water. The difference between the two columns was the addition of 15 μM dissolved Fe(II) to column C during biostimulation to enhance formation of iron sulfides.

Release of U during oxic elution was a continuous process over 120 to 140 days (300 to 350 PV) with dissolved uranium concentrations on the order of 0.8 and 0.2 μM for columns A and C, respectively. The effluent concentration from column C decreased over time indicative of a decreasing rate of U(IV) oxidation. In contrast, column A effluent [U] was somewhat constant over 140 days. The prolonged period of biostimulation and concomitant sulfate reduction appears to limit the rate of U(IV) oxidative remobilization. The speciation of U(IV) associated with sediments after oxic elution was essentially the same as that measured in samples recovered after biostimulation and prior to oxic elution. The limited oxidative remobilization of U(IV) in the present column experiments is consistent with the decreased U remobilization where sulfate reduction occurred in contrast to large releases of U from columns which did not undergo sulfate reduction. Although continued sulfate reduction may cause decrease in permeability from precipitation of iron sulfide, the greater apparent stability of the sequestered U(IV) provided by the sustained biostimulation should be considered in design of field scale remediation efforts.

Specific Findings

1. The large extent of sequestration of dissolved uranium over the course of the biostimulation stage in all three columns indicates that stimulation of the ambient microbial population in the Rifle aquifer sediments may be an effective means of remediating dissolved uranium in groundwater at contaminated sites. The removal of dissolved uranium, which is in the +6 oxidation state, occurred predominantly by reduction and subsequent precipitation as U(IV).

2. The onset of U reduction was coincident with iron reduction, but the extent of U uptake increased overall throughout the duration of biostimulation with the greatest uptake occurring during sulfate reduction. The increased U removal by reduction may be the result of sufficient electron donor availability such that microbial processes are not limited in these columns. Thus, competition between sulfate reducing and metal reducing microbes is not sufficient to diminish uranium reduction by metal reducing microbes. Uranium reduction also could occur by other microbial processes such as reduction by sulfate reducing bacteria, which have been shown to reduce uranium directly through enzymatic mechanisms, or by abiotic processes.

3. About one third of the total U uptake in column A occurred after the acetate amendment was halted at 110 days and sulfate reducing bacterial activity stopped, and likely other microbial activity decreased. Because greater than 97% of the total U was determined to be U(IV), the observed continued uranium uptake is inferred to occur largely by abiotic reduction processes such as by interaction with iron sulfides produced during biostimulation. The increase of Fe(II) and reduced S in sediments are consistent with U reduction by interactions with iron sulfides. The co-association of U(IV) with Fe and S in some grain coatings support this conclusion.

4. Bioreduction resulted in precipitation and accumulation of U in each column, with between 62 and 104 µmoles retained on the columns. In all three biostimulation columns, U uptake occurred primarily at or near the inlet end of the column. In contrast, iron reduction, as evidenced from the increase in extractable Fe(II), was relatively uniform over the entire column.

5. The column receiving dissolved Fe(II) in the influent throughout biostimulation (column C) had a greater removal rate of U(VI) from the influent as well as better retention of U during oxic elution.

6. Sulfate reduction was the dominant TEAP process for oxidation of acetate accounting for >75% of electron transfer from acetate oxidation. Acetate was oxidized primarily to CO_2. Total S increased 5-fold or more in all three columns with fully reduced S, measured as acid volatile sulfur (e.g. S^{-2}), contributing 50 to 75% of the total S increase. The remaining increase likely includes elemental sulfur and S^{-1} precipitated as FeS_2. The total S increase ranged from 50 to 120% of the increase in extractable Fe(II), with AVS equal to 50 to 70% of the sediment Fe(II) increase. Small fractionation factors of -0.2 to -5.1‰ $\delta^{34}S$ were observed indicative of microbial sulfate reduction in systems where sulfate and electron donor are not limiting.

7. Increases in extractable Fe(II) were about two orders of magnitude greater than the integrated effluent dissolved iron exported from the columns, indicating most of the iron reduced was retained within the column either as iron sulfide or as Fe(II) from in-place reduction of phyllosilicate Fe(III).

8. The sequestered U was essentially all in the +4 oxidation state (U(IV)) in sediments recovered after the biostimulation period. Fitting of U-EXAFS spectra of column sediments are consistent with U(IV) comprised of a mixture of both partially disordered nanoparticulate UO_2 and non-uraninite U(IV) species associated with biomass, NUSAB. The non-uraninite U(IV)-bearing phase may exist separately from the partially polymerized nano-UO_2-like U(IV). No measurable changes in speciation of U associated with sediments were observed as a result of oxic elution.

9. The 30-μm and 2-μm resolution XRF images of thin sections show a limited number of grains with distinct coatings of uranium. Sequestered U on sediment grain surfaces formed near-contiguous coatings ranging from 5 to 30 μm in thickness. Multi-energy 2-μm resolution U XANES map, as well as point XANES spectra, shows that U in these coatings is primarily U(IV). The U coatings overlay iron phases in some cases. Some U grain coatings have Fe and/or S intermixed with U. SEM-BSE images and EDS analysis show areas of high U that appear to be forming on the iron sulfide material. These findings are consistent with abiotic reduction of U(VI) by iron sulfides. In other grain coatings, little Fe or S was apparent in μXRF or SEM images.

10. Fine grained sediments (<63 μm) are abundant (~12% by mass) and contain 3 to 4 times higher U concentrations. However, discrete U-bearing particles of this size range were not evident in μXRF images. SEM images of U-bearing grain coatings do not appear to be comprised of fine grained sediments adhering to larger grains.

11. Microbial analysis of column sediments recovered following biostimulation show that *Geobacter* was higher in abundance than SRB in most samples. Clone analysis showed that sequences were not very diverse and were dominated by *Geobacteraceae*, previously described as important in U(VI) reduction in aquifers. Sequences of sulfate reducing bacteria also have relatively little diversity and were dominated by *Desulfobulbaceae* and *Desulfobacteraceae* with *Desulfotomaculum* and *Syntrophobacteraceae* present in some samples but at lower abundance.

12. Multicomponent biogeochemical reactive transport model simulation of column effluents during biostimulation generally described the acetate oxidation, iron, sulfate, and uranium reduction for all three columns using parameters derived from simulations of field scale biostimulation experiments.

13. The increasing rate of U reduction over the course of biostimulation, previously not observed in field experiments, required a rate law with dependency on the growing biomass of metal reducing bacteria to simulate column effluent. Continued uranium uptake after cessation of acetate was not captured by the model.

14. Remobilization of uranium during the re-oxidation phase of the experiments was four times higher in column A compared to column C with near constant effluent dissolved uranium concentrations of about of 0.8 and 0.2 μM for the column A and C, respectively. However, even with the greater uranium stability caused by iron sulfide precipitation the effluent uranium concentration of approximately 0.2 μM did exceed EPA's uranium MCL of 30 μg/L (0.126 μM).

15. The U(IV) retained by the sediments and not remobilized was largely still reduced indicating that U oxidized during oxic elution was primarily transported out of the columns with little U(VI) retained by surface complexation to sediment surfaces such as iron oxides.

7 References Cited

Abdelouas, A., Lutze, W., Nuttall, H.E., 1999. Oxidative dissolution of uraninite precipitated on Navajo sandstone. J. Contam. Hydrol. 36, 353-375.

Alessi, D.S., Uster, B., Veeramani, H., Suvorova, E.I., Lezama-Pacheco, J.S., Stubbs, J.E., Bargar, J.R., Bernier-Latmani, R., 2012. Quantitative separation of monomeric U(IV) from UO2 in products of U(VI) reduction. Environ. Sci. Technol. 46, 6150-6157.

Anderson, R.T., Rooney-Varga, J.N., Gaw, C.V., Lovley, D.R., 1998. Anaerobic benzene oxidation in the Fe(III) reduction zone of petroleum- contaminated aquifers. Environ. Sci. Technol. 32, 1222-1229.

Anderson, R.T., Vrionis, H.A., Ortiz-Bernad, I., Resch, C.T., Long, P.E., Dayvault, R., Karp, K., Marutzky, S., Metzler, D.R., Peacock, A., White, D.C., Lowe, M., Lovley, D.R., 2003. Stimulating the In Situ Activity of Geobacter Species to Remove Uranium from the Groundwater of a Uranium-Contaminated Aquifer. Appl. Environ. Microbiol. 69, 5884-5891.

Ankudinov, A.L., Rehr, J.J., 1997. Relativistic calculations of spin-dependent x-ray-absorption spectra. Phys. Rev. B 56, R1712-R1715.

Bargar, J.R., Williams, K.H., Campbell, K.M., Long, P.E., Stubbs, J.E., Suvorova, E.I., Lezama-Pacheco, J.S., Alessi, D.S., Stylo, M., Webb, S.M., Davis, J.A., Giammar, D.E., Blue, L.Y., Bernier-Latmani, R., 2013. Uranium redox transition pathways in acetate-amended sediments. Proc. Natl. Acad. Sci. 110, 4506-4511.

Bernhard, G., Geipel, G., Reich, T., Brendler, V., Amayri, S., Nitsche, H., 2001. Uranyl(VI) carbonate complex formation: Validation of the $Ca_2UO_2(CO_3)_3$(aq.) species. Radiochim. Acta 89, 511-518.

Bernier-Latmani, R., Veeramani, H., Vecchia, E.D., Junier, P., Lezama-Pacheco, J.S., Suvorova, E.I., Sharp, J.O., Wigginton, N.S., Bargar, J.R., 2010. Non-uraninite products of microbial U(VI) reduction. Environ. Sci. Technol. 44, 9456-9462.

Bi, Y., Hyun, S.P., Kukkadapu, R., Hayes, K.F., 2013. Oxidative dissolution of UO2 in a simulated groundwater containing synthetic nanocrystalline mackinawite. Geochim. Cosmochim. Acta 102, 175-190.

Boyanov, M.I., Fletcher, K.E., Kwon, M.J., Rui, X., O'Loughlin, E.J., Laffler, F.E., Kemner, K.M., 2011. Solution and Microbial Controls on the Formation of Reduced U(IV) Species. Environ. Sci. Technol. 45, 8336-8344.

Brooks, S.C., Fredrickson, J.K., Carroll, S.L., Kennedy, D.W., Zachara, J.M., Plymale, A.E., Kelly, S.D., Kemner, K.M., Fendorf, S., 2003. Inhibition of bacterial U(VI) reduction by calcium. Environ. Sci. Technol. 37, 1850-1858.

Brunk, C.F., Avaniss-Aghajani, E., Brunk, C.A., 1996. A computer analysis of primer and probe hybridization potential with bacterial small-subunit rRNA sequences. Appl. Environ. Microbiol. 62, 872-879.

Burgos, W.D., McDonough, J.T., Senko, J.M., Zhang, G., Dohnalkova, A.C., Kelly, S.D., Gorby, Y., Kemner, K.M., 2008. Characterization of uraninite nanoparticles produced by *Shewanella oneidensis* MR-1. Geochim. Cosmochim. Acta 72, 4901-4915.

Callister, S.J., Wilkins, M.J., Nicoral, C.D., Williams, K.H., Banfield, J.F., VerBerkmoes, N.C., Hettich, R.L., N'Guessan, A.L., Mouser, P.J., Elifantz, H., Smith, R.D., Lovley, D.R., Lipton, M.S., Long, P.E., 2010. Analysis of Biostimulated Microbial Communities from Two Field Experiments Reveals Temporal and Spatial Differences in Proteome Profiles. Environ. Sci. Technol. 44, 8897-8903.

Campbell, K.M., Gallegos, T.J., Landa, E.R., 2013. Biogeochemical aspects of uranium mineralization, mining, milling, and remediation, In: Seal, R. (Ed.), The Environmental Geochemistry of Mineral Deposits, Society of Economic Geology Reviews in Economic Geology.

Campbell, K.M., Veeramani, H., Ulrich, K.-U., Blue, L.Y., Giammar, D.E., Bernier-Latmani, R., Stubbs, J.E., Suvorova, E., Yabusaki, S., Lezama-Pacheco, J.S., Mehta, A., Long, P.E., Bargar, J.R., 2011. Oxidative dissolution of biogenic uraninite in groundwater at Old Rifle, CO. Environ. Sci. Technol. 45, 8748-8754.

Cardenas, E., Wu, W.-., Leigh, M.B., Carley, J., Carroll, S., Gentry, T., Luo, J., Watson, D., Gu, B., Ginder-Vogel, M., Kitanidis, P.K., Jardine, P.M., Zhou, J., Criddle, C.S., Marsh, T.L., Tiedje, J.M., 2008. Microbial communities in contaminated sediments, associated with bioremediation of uranium to submicromolar levels. Appl. Environ. Microbiol. 74, 3718-3729.

Chang, Y., Long, P.E., Geyer, R., Peacock, A.D., Resch, C.T., Sublette, K., Pfiffner, S., Smithgall, A., Anderson, R.T., Vrionis, H.A., Stephen, J.R., Dayvault, R., Ortiz-Bernad, I., Lovley, D.R., White, D.C., 2005. Microbial Incorporation of 13C-Labeled Acetate at the Field Scale: Detection of Microbes Responsible for Reduction of U(VI). Environ. Sci. Technol. 39, 9039-9048.

Chao, T.T., Zhou, L., 1983. Extraction techniques for selective dissolution of amorphous iron oxides from soils and sediments. Soil Sci. Soc. Am. J. 47, 225-232.

Cline, J.D., 1969. Spectrophotometric Determination of Hydrogen Sulfide in Natural Waters. Limnol. Oceanogr. 14, 454-458.

Davis, J.A., Meece, D.E., Kohler, M., Curtis, G.P., 2004. Approaches to surface complexation modeling of uranium(VI) adsorption on aquifer sediments. Geochim. Cosmochim. Acta 68, 3621-3641.

Davis, J.A., Curtis, G.P., Wilkins, M.J., Kohler, M., Fox, P., Naftz, D.L., Lloyd, J.R., 2006. Processes affecting transport of uranium in a suboxic aquifer. Phys. Chem. Earth 31, 548-555.

Dong, W., Brooks, S.C., 2006. Determination of the formation constants of ternary complexes of uranyl and carbonate with alkaline earth metals (Mg^{2+}, Ca^{2+}, Sr^{2+}, and Ba^{2+}) using anion exchange method. Environ. Sci. Technol. 40, 4689-4695.

Dong, W.M., Ball, W.P., Liu, C.X., Wang, Z.M., Stone, A.T., Bai, J., Zachara, J.M., 2005. Influence of calcite and dissolved calcium on uranium(VI) sorption to a Hanford subsurface sediment. Environ. Sci. Technol. 39, 7949-7955.

Englert, A., Hubbard, S.S., Williams, K.H., Li, L., Steefel, C.I., 2009. Feedbacks Between Hydrological Heterogeneity and Bioremediation Induced Biogeochemical Transformations. Environ. Sci. Technol 43, 5197-5204.

Fang, Y., Yabusaki, S.B., Morrison, S.J., Amonette, J.P., Long, P.E., 2009. Multicomponent reactive transport modeling of uranium bioremediation field experiments. Geochim. Cosmochim. Acta 73, 6029-6051.

Fang, Y.L., Yeh, G.T., Burgos, W.D., 2003. A general paradigm to model reaction-based biogeochemical processes in batch systems. Water Res. Research 39(4).

Fang, Y.L., Yabusaki, S.B., Yeh, G.T., 2006. A general simulator for reaction-based biogeochemical processes. Comput. Geosci. 32, 64-72.

Fox, P.M., Davis, J.A., Kukkadapu, R., Singer, D.M., Bargar, J., Williams, K.H., 2013. Abiotic U(VI) reduction by sorbed Fe(II) on natural sediments. Geochim. Cosmochim. Acta 117, 266-282.

Fuller, C.C., Van Geen, A., Baskaran, M., Anima, R., 1999. Sediment chronology in San Francisco Bay, California, defined by ^{210}Pb, ^{234}Th, ^{137}Cs, and ^{239,240}Pu. Mar. Chem. 64, 7-27.

Gallegos, T.J., Fuller, C.C., Webb, S.M., Betterton, W., 2013. Uranium(VI) interactions with mackinawite in the presence and absence of bicarbonate and oxygen. Environ. Sci. Technol. 47, 7357-7364.

Geets, J., Borremans, B., Diels, L., Springael, D., Vangronsveld, J., van der Lelie, D., Vanbroekhoven, K., 2006. DsrB gene-based DGGE for community and diversity surveys of sulfate-reducing bacteria. J. Microbiol. Meth. 66, 194-205.

Ginder-Vogel, M., Stewart, B., Fendorf, S., 2010. Kinetic and mechanistic constraints on the oxidation of biogenic uraninite by ferrihydrite. Environ. Sci. Technol. 44, 163-169.

Gorby, Y.A., Lovley, D.R., 1992. Enzymatic uranium precipitation. Environ. Sci. Technol. 26, 205-207.

Gu, B., Wu, W.-., Ginder-Vogel, M.A., Yan, H., Fields, M.W., Zhou, J., Fendorf, S., Criddle, C.S., Jardine, P.M., 2005. Bioreduction of uranium in a contaminated soil column. Environ. Sci. Technol. 39, 4841-4847.

Guillaumont, R., Fanghanel, T., Fugen, J., Grenthe, I., Neck, V., Palmer, D.A., Rand, M.H., 2003. Chemical Thermodynamics 5. Update on the Chemical Thermodynamics of Uranium, Neptunium, Plutonium, Americium, and Technetium. Elsevier, Amsterdam.

Habicht, K.S., Canfield, D.E., 1997. Sulfur isotope fractionation during bacterial sulfate reduction in organic-rich sediments. Geochim. Cosmochim. Acta 61, 5351-5361.

Holmes, D.E., O'Neil, R.A., Vrionis, H.A., N'Guessan, L.A., Ortiz-Bernad, I., Larrahondo, M.J., Adams, L.A., Ward, J.A., Nicoll, J.S., Nevin, K.P., Chavan, M.A., Johnson, J.P., Long, P.E., Lovley, D.R., 2007. Subsurface clade of *Geobacteraceae* that predominates in a diversity of Fe(III)-reducing subsurface environments. ISME Journal 1, 663-677.

Hsieh, Y.P., Yang, C.H., 1989. Diffusion methods for the determination of reduced inorganic sulfur species in sediments. Limnol. Ocean. 34, 1126-1130.

Hsieh, Y.-., Chung, S.-., Tsau, Y.-., Sue, C.-., 2002. Analysis of sulfides in the presence of ferric minerals by diffusion methods. Chem. Geol. 182, 195-201.

Hua, B., Deng, B., 2008. Reductive immobilization of uranium(VI) by amorphous iron sulfide. Environ. Sci. Technol. 42, 8703-8708.

Hyun, S.P., Davis, J.A., Sun, K., Hayes, K.F., 2012. Uranium(VI) reduction by iron(II) monosulfide mackinawite. Environ. Sci. Technol. 46, 3369-3376.

Jimenez-Lopez, C., Romanek, C.S., 2004. Precipitation kinetics and carbon isotope partitioning of inorganic siderite at 25°C and 1 atm. Geochim. Cosmochim. Acta 68, 557-571.

Jones, E.J.P., Voytek, M.A., Lorah, M.M., Kirshtein, J.D., 2006. Characterization of a microbial consortium capable of rapid and simultaneous dechlorination of 1,1,2,2-tetrachloroethane and chlorinated ethane and ethene intermediates. Bioremediation J. 10, 153-168.

Kelly, S.D., Kemner, K.M., Brooks, S.C., 2007. X-ray absorption spectroscopy identifies calcium-uranyl-carbonate complexes at environmental concentrations. Geochim. Cosmochim. Acta 71, 821-834.

Komlos, J., Kukkadapu, R.K., Zachara, J.M., Jaffé, P.R., 2007. Biostimulation of iron reduction and subsequent oxidation of sediment containing Fe-silicates and Fe-oxides: Effect of redox cycling on Fe(III) bioreduction. Water Res. 41, 2996-3004.

Komlos, J., Moon, H.S., Jaffé, P.R., 2008a. Effect of sulfate on the simultaneous bioreduction of iron and uranium. J. Environ. Qual. 37, 2058-2062.

Komlos, J., Peacock, A., Kukkadapu, R.K., Jaffé, P.R., 2008b. Long-term dynamics of uranium reduction/reoxidation under low sulfate conditions. Geochim. Cosmochim. Acta 72, 3603-3615.

Lane, D.J., 1991. 16S/23S rRNA sequencing, In: Stackebrandt, E. and Goodfellow, M. (Eds.), *Nucleic Acid Techniques in Bacterial Systematics*. Wiley, New York, pp. 115-148.

Lee, J.-., Fredrickson, J.K., Kukkadapu, R.K., Boyanov, M.I., Kemner, K.M., Lin, X., Kennedy, D.W., Bjornstad, B.N., Konopka, A.E., Moore, D.A., Resch, C.T., Phillips, J.L., 2012. Microbial reductive transformation of phyllosilicate Fe(III) and U(VI) in fluvial subsurface sediments. Environ. Sci. Technol. 46, 3721-3730.

Li, L., Steefel, C.I., Williams, K.H., Wilkins, M.J., Hubbard, S.S., 2009. Mineral transformation and biomass accumulation associated with uranium bioremediation at Rifle, Colorado. Environ. Sci. Technol. 43, 5429-5435.

Li, L., Steefel, C.I., Kowalsky, M.B., Englert, A., Hubbard, S.S., 2010. Effects of physical and geochemical heterogeneities on mineral transformation and biomass accumulation during biostimulation experiments at Rifle, Colorado. J.Contam.Hydrol. 112, 45-63.

Liger, E., Charlet, L., Van Cappellen, P., 1999. Surface catalysis of uranium(VI) reduction by iron(II). Geochim. Cosmochim. Acta 63, 2939-2955.

Liu, C.X., Zachara, J.M., Zhong, L.R., Kukkadupa, R., Szecsody, J.E., Kennedy, D.W., 2005. Influence of sediment bioreduction and reoxidation on uranium sorption. Environ. Sci. Technol. 39, 4125-4133.

Locock, A.J., Burns, P.C., 2003. The crystal structure of synthetic autunite, $Ca[(UO_2)(PO_4)]_2(H_2O)_{11}$. Am. Mineral. 88, 240-244.

Lovley, D.R., Phillips, E.J.P., 1987. Rapid Assay for Microbially Reducible Ferric Iron in Aquatic Sediments. Appl. Environ. Microbiol. 53, 1536-1540.

Lovley, D.R., Phillips, E.J.P., Gorby, Y.A., Landa, E.R., 1991. Microbial reduction of uranium. Nature 350, 413-416.

Lovley, D.R., Phillips, E.J.P., 1992. Bioremediation of uranium contamination with enzymatic uranium reduction. Environ. Sci. Technol. 26, 2228-2234.

Lovley, D.R., Roden, E.E., Phillips, E.J.P., Woodward, J.C., 1993. Enzymatic iron and uranium reduction by sulfate-reducing bacteria. Mar. Geol. 113, 41-53.

Luo, J., Weber, F.-., Cirpka, O.A., Wu, W.-., Nyman, J.L., Carley, J., Jardine, P.M., Criddle, C.S., Kitanidis, P.K., 2007a. Modeling in-situ uranium(VI) bioreduction by sulfate-reducing bacteria. J. Contam. Hydrol. 92, 129-148.

Luo, J., Wu, W.M., Carley, J., Ruan, C.M., Gu, B.H., Jardine, P.M., Criddle, C.S., Kitanidis, P.K., 2007b. Hydraulic performance analysis of a multiple injection-extraction well system. J. Hydrol. 336, 294-302.

Luo, W., Gu, B., 2009. Dissolution and mobilization of uranium in a reduced sediment by natural humic substances under anaerobic conditions. Environ. Sci. Technol. 43, 152-156.

Maurer, M., Rittmann, B.E., 2004. Modeling intrinsic bioremediation for interpret observable biogeochemical footprints of BTEX biodegradation: The need for fermentation and abiotic chemical processes. Biodegradation 15, 405-417.

Mayhew, L.E., Webb, S.M., Templeton, A.S., 2011. Microscale imaging and identification of fe speciation and distribution during fluid-mineral reactions under highly reducing conditions. Environ. Sci. Technol. 45, 4468-4474.

Mereiter, K., 1982. The crystal structure of Liebigite, $Ca_2UO_2(CO_3)_3 \cdot \sim 11H_2O$. Tscher. Miner. Petrograp. 30, 277-288.

Miletto, M., Williams, K.H., N'Guessan, A.L., Lovley, D.R., 2011. Molecular analysis of the metabolic rates of discrete subsurface populations of sulfate reducers. Appl. Environ. Microbiol. 77, 6502-6509.

Moon, H.S., Komlos, J., Jaffé, P.R., 2007. Uranium reoxidation in previously bioreduced sediment by dissolved oxygen and nitrate. Environ. Sci. Technol. 41, 4587-4592.

Moon, H.S., Komlos, J., Jaffé, P.R., 2009. Biogenic U(IV) oxidation by dissolved oxygen and nitrate in sediment after prolonged U(VI)/Fe(III)/SO_4^{2-} reduction. J. Contam. Hydrol. 105, 18-27.

Muyzer, G., Stams, A.J.M., 2008. The ecology and biotechnology of sulphate-reducing bacteria. Nature Reviews Microbiology 6, 441-454.

O'Loughlin, E.J., Kelly, S.D., Kemner, K.M., 2010. XAFS investigation of the interactions of UVI with secondary mineralization products from the bioreduction of FeIII oxides. Environ. Sci. Technol. 44, 1656-1661.

Poeter, E.P., Hill, M.C., Banta, E.R., Mehl, S., Christensen, S., 2008. UCODE_2005 and Six Other Computer Codes for Universal Sensitivity Analysis, Calibration, and Uncertainty Evaluation, U.S. Geological Survey Techniques and Methods 6-A11, U.S. Geological Survey, pp. 283.

Poulton, S.W., Krom, M.D., Raiswell, R., 2004. A revised scheme for the reactivity of iron (oxyhydr)oxide minerals towards dissolved sulfide. Geochim. Cosmochim. Acta 68, 3703-3715.

Sani, R.K., Peyton, B.M., Dohnalkova, A., Amonette, J.E., 2005. Reoxidation of reduced uranium with iron(III) (Hydr)oxides under sulfate-reducing conditions. Environ. Sci. Technol. 39, 2059-2066.

Schofield, E.J., Veeramani, H., Sharp, J.O., Suvorova, E., Bernier-Latmani, R., Mehta, A., Stahlman, J., Webb, S.M., Clark, D.L., Conradson, S.D., Ilton, E.S., Bargar, J.R., 2008. Structure of biogenic uraninite produced by *Shewanella oneidensis* strain MR-1. Environ. Sci. Technol. 42, 7898-7904.

Senko, J.M., Istok, J.D., Suflita, J.M., Krumholz, L.R., 2002. In-situ evidence for uranium immobilization and remobilization. Environ. Sci. Technol. 36, 1491-1496.

Senko, J.M., Kelly, S.D., Dohnalkova, A.C., McDonough, J.T., Kemner, K.M., Burgos, W.D., 2007. The effect of U(VI) bioreduction kinetics on subsequent reoxidation of biogenic U(IV). Geochim. Cosmochim. Acta 71, 4644-4654.

Sharp, J.O., Lezama-Pacheco, J.S., Schofield, E.J., Junier, P., Ulrich, K.-U., Chinni, S., Veeramani, H., Margot-Roquier, C., Webb, S.M., Tebo, B.M., Giammar, D.E., Bargar, J.R., Bernier-Latmani, R., 2011. Uranium speciation and stability after reductive immobilization in aquifer sediments. Geochim. Cosmochim. Acta 75, 6497-6510.

Sim, M.S., Ono, S., Donovan, K., Templer, S.P., Bosak, T., 2011. Effect of electron donors on the fractionation of sulfur isotopes by a marine Desulfovibrio sp. Geochim. Cosmochim. Acta 75, 4244-4259.

Singer, D.M., Farges, F., Brown Jr., G.E., 2009. Biogenic nanoparticulate UO_2: Synthesis, characterization, and factors affecting surface reactivity. Geochim. Cosmochim. Acta 73, 3593-3611.

Singer, D.M., Chatman, S.M., Ilton, E.S., Rosso, K.M., Banfield, J.F., Waychunas, G.A., 2012. Identification of simultaneous U(VI) sorption complexes and U(IV) nanoprecipitates on the magnetite (111) surface. Environ. Sci. Technol. 46, 3811-3820.

Stoliker, D.L., Campbell, K.M., Singer, D.M., Kaviani, N., Carey, M., Peck, N.E., Bargar, J.R., Kent, D.B., Davis, J.A., 2013. Evaluating Chemical Extraction Techniques for the Determination of Uranium Oxidation State in Reduced Aquifer Sediments. Environ. Sci. Technol. 47, 9225-9332.

Stookey, L.L., 1970. Ferrozine - A new spectrophotometric reagent for iron. Anal. Chem. 42, 779-781.

Ulrich, K.-U., Ilton, E.S., Veeramani, H., Sharp, J.O., Bernier-Latmani, R., Schofield, E.J., Bargar, J.R., Giammar, D.E., 2009. Comparative dissolution kinetics of biogenic and chemogenic uraninite under oxidizing conditions in the presence of carbonate. Geochim. Cosmochim. Acta 73, 6065-6083.

Ulrich, K.-U., Veeramani, H., Bernier-Latmani, R., Giammar, D.E., 2011. Speciation-dependent kinetics of uranium(VI) bioreduction. Geomicrobiol. J. 28, 396-409.

Veeramani, H., Scheinost, A.C., Monsegue, N., Qafoku, N.P., Kukkadapu, R., Newville, M., Lanzirotti, A., Pruden, A., Murayama, M., Hochella, M.F., 2013. Abiotic reductive immobilization of U(VI) by biogenic mackinawite. Environ. Sci. Technol. 47, 2361-2369.

Vrionis, H.A., Anderson, R.T., Ortiz-Bernad, I., O'Neill, K.R., Resch, C.T., Peacock, A.D., Dayvault, R., White, D.C., Long, P.E., Lovley, D.R., 2005. Microbiological and geochemical heterogeneity in an in situ uranium bioremediation field site. Appl. Environ. Microbiol. 71, 6308-6318.

Wagner, M., Roger, A.J., Flax, J.L., Brusseau, G.A., Stahl, D.A., 1998. Phylogeny of dissimilatory sulfite reductases supports an early origin of sulfate respiration. J. Bacteriol. 180, 2975-2982.

Wan, J., Tokunaga, T.K., Brodie, E., Wang, Z., Zheng, Z., Herman, D., Hazen, T.C., Firestone, M.K., Sutton, S.R., 2005. Reoxidation of bioreduced uranium under reducing conditions. Environ. Sci. Technol. 39, 6162-6169.

Ward, B.B., Eveillard, D., Kirshtein, J.D., Nelson, J.D., Voytek, M.A., Jackson, G.A., 2007. Ammonia-oxidizing bacterial community composition in estuarine and oceanic environments assessed using a functional gene microarray. Environ. Microbiol. 9, 2522-2538.

Webb, S., 2004. SIXPACK: a graphical user interface for XAS analysis using IFEFFIT. Phys. Scripta T T115, 1011-1014.

Williams, K.H., Long, P.E., Davis, J.A., Wilkins, M.J., N'Guessan, A.L., Steefel, C.I., Yang, L., Newcomer, D., Spane, F.A., Kerkhof, L.J., Mcguinness, L., Dayvault, R., Lovley, D.R., 2011. Acetate availability and its influence on sustainable bioremediation of Uranium-contaminated groundwater. Geomicrobiol. J. 28, 519-539.

Wilson, T.A., Amirbahman, A., Norton, S.A., Voytek, M.A., 2010. A record of phosphorus dynamics in oligotrophic lake sediment. J. Paleolimnol. 44, 279-294.

Wu, T., Shelobolina, E., Xu, H., Konishi, H., Kukkadapu, R., Roden, E.E., 2012. Isolation and microbial reduction of Fe(III) phyllosilicates from subsurface sediments. Environ. Sci. Technol. 46, 11618-11626.

Wu, W.-., Carley, J., Gentry, T., Ginder-Vogel, M.A., Fienen, M., Mehlhorn, T., Yan, H., Caroll, S., Pace, M.N., Nyman, J., Luo, J., Gentile, M.E., Fields, M.W., Hickey, R.F., Gu, B., Watson, D., Cirpka, O.A., Zhou, J., Fendorf, S., Kitanidis, P.K., Jardine, P.M., Criddle, C.S., 2006. Pilot-scale in situ bioremedation of uranium in a highly contaminated aquifer. 2. Reduction of U(VI) and geochemical control of U(VI) bioavailability. Environ. Sci. Technol. 40, 3986-3995.

Wyckoff, R.W.G., 1963. *Crystal Structures*, Second Edition, Interscience Publishers, New York, New York, pp. 239-244.

Yabusaki, S.B., Fang, Y., Waichler, S.R., Long, P.E., 2010. Processes, properties, and conditions controlling in situ bioremediation of uranium in shallow, alluvial aquifers, NUREG/CR-7014, Nuclear Regulatory Commission, Office of Nuclear Regulatory Research, Washington, DC, pp. 111.

Yabusaki, S.B., Fang, Y., Long, P.E., Resch, C.T., Peacock, A.D., Komlos, J., Jaffe, P.R., Morrison, S.J., Dayvault, R.D., White, D.C., Anderson, R.T., 2007. Uranium removal from groundwater via in situ biostimulation: Field-scale modeling of transport and biological processes. J. Contam. Hydrol. 93, 216-235.

Yeh, G.T., Sun, J.T., Jardine, P.M., Burgos, W.D., Fang, Y., Li, M.H., Siegel, M.D., 2004. HYDROGEOCHEM 5.0: a threedimensional model of coupled fluid flow, thermal transport and

hydrogeochemical transport through variable saturated conditions – version 5.0, Oak Ridge National Laboratory, Oak Ridge, TN, USA.

Zheng, Z.P., Tokunaga, T.K., Wan, J.M., 2003. Influence of calcium carbonate on U(VI) sorption to soils. Environ. Sci. Technol. 37, 5603-5608.

Zhong, L., Liu, C., Zachara, J.M., Kennedy, D.W., Szecsody, J.E., Wood, B., 2005. Oxidative remobilization of biogenic uranium(IV) precipitates: Effects of iron(II) and pH. J. Environ. Qual. 34, 1763-1771.

NRC FORM 335
(12-2010)
NRCMD 3.7

U.S. NUCLEAR REGULATORY COMMISSION

BIBLIOGRAPHIC DATA SHEET

(See instructions on the reverse)

1. REPORT NUMBER
(Assigned by NRC, Add Vol., Supp., Rev., and Addendum Numbers, if any.)

NUREG/CR-7178

2. TITLE AND SUBTITLE

Uranium Sequestration during Biostimulated Reduction and in Response to the Return of Oxic Conditions in Shallow Aquifers

3. DATE REPORT PUBLISHED

MONTH	YEAR
December	2014

4. FIN OR GRANT NUMBER

N6651

5. AUTHOR(S)

C.C. Fuller, K.J. Johnson, K.C. Akstin, D.M. Singer, S.B. Yabusaki, Y. Fang, M. Fuhrmann

6. TYPE OF REPORT

Final

7. PERIOD COVERED (Inclusive Dates)

8. PERFORMING ORGANIZATION - NAME AND ADDRESS (If NRC, provide Division, Office or Region, U. S. Nuclear Regulatory Commission, and mailing address; if contractor, provide name and mailing address.)

U.S. Geological Survey,
345 Middlefield Rd
Menlo Park, CA 94025

9. SPONSORING ORGANIZATION - NAME AND ADDRESS (If NRC, type "Same as above", if contractor, provide NRC Division, Office or Region, U. S. Nuclear Regulatory Commission, and mailing address.)

NRC Division of Risk Analysis
Office of Nuclear Regulatory Research

10. SUPPLEMENTARY NOTES

11. ABSTRACT (200 words or less)

A key issue in the remediation of uranium (U) contamination in aquifers by biostimulated reduction is the long term stability of the sequestered uranium. Three flow-through column experiments using aquifer sediment were used to evaluate the remobilization of bioreduced U sequestered under conditions in which biostimulation extended well into sulfate reduction to enhance precipitation of reduced sulfur phases such as iron sulfides. One column received added ferrous iron, Fe(II), increasing production of iron sulfides, to test their effect on remobilization of the sequestered uranium. During biostimulation of the ambient microbial population with acetate, dissolved uranium was lowered by a factor of 2.5 or more with continued removal for over 110 days of biostimulation. Sequestered uranium was essentially all U(IV) resulting from the formation of nano-particulate uraninite that coated sediment grains to a thickness of a few 10's of microns, sometimes in association with S and Fe. A multicomponent biogeochemical reactive transport model simulation of column effluents during biostimulation was generally able to describe the acetate oxidation, iron, sulfate, and uranium reduction for all three columns. The prolonged period of biostimulation and concomitant sulfate reduction appears to limit the rate of U(IV) oxidative remobilization in contrast to a large release observed for columns in previous studies that did not undergo sulfate reduction.

12. KEY WORDS/DESCRIPTORS (List words or phrases that will assist researchers in locating the report.)

uranium, bioremediation, bioreduction, shallow aquifer,

13. AVAILABILITY STATEMENT

unlimited

14. SECURITY CLASSIFICATION

(This Page)

unclassified

(This Report)

unclassified

15. NUMBER OF PAGES

16. PRICE

Federal Recycling Program

UNITED STATES
NUCLEAR REGULATORY COMMISSION
WASHINGTON, DC 20555-0001

OFFICIAL BUSINESS

NUREG/CR-7178

Uranium Sequestration During Biostimulated Reduction and In Response to the Return of Oxic Conditions In Shallow Aquifers

December 2014